Вісник Криворізького національного університету

Том 24, № 1

Заснований у 2003 році
Видається два рази на рік

Кривий Ріг
2026

ISSN 2306-5451
e-ISSN 2519-2736

DOI: 10.31721/2306-5451-2026-1-24

Засновник:
Криворізький національний університет

Рекомендовано до друку та поширення
через мережу Інтернет Вченою радою
Криворізького національного університету
(протокол № 13 від 30 червня 2026 р.)

Державна реєстрація:
Ідентифікатор медіа R30-04965.
Рішення Національної ради України з питань телебачення
і радіомовлення № 1501, протокол № 15 (09.05.2024) р.)

Науковий журнал включено до категорії «Б» Переліку наукових фахових видань України.
Спеціальності: 121 – Інженерія програмного забезпечення, 122 – Комп'ютерні науки, 123 – Комп'ютерна інженерія, 124 – Системний аналіз, 131 – Прикладна механіка, 133 – Галузеве машинобудування, 136 – Металургія, 141 – Електроенергетика, електротехніка та електромеханіка, 144 – Теплоенергетика, 151 – Автоматизація та комп'ютерно-інтегровані технології, 184 – Гірництво, 192 – Будівництво та цивільна інженерія, 193 – Геодезія та землеустрій, 263 – Цивільна безпека, 274 – Автомобільний транспорт, 275 – Транспортні технології (за видами), 071 – Облік і оподаткування, 072 – Фінанси, банківська справа, страхування та фондовий ринок, 073 – Менеджмент, 076 – Підприємництво та торгівля, 281 – Публічне управління та адміністрування
(наказ МОН України від 17 березня 2020 року № 409)

Журнал індексується в наукометричних базах даних
UCSB Library, Crossref, Національна бібліотека України імені В. І. Вернадського (НБУВ), Google Академія, Litmaps, Інститут проблем реєстрації інформації Національної академії наук України, Ulrichsweb, Бібліотека Університету Осло, Бібліотека Університету Халла, Бібліотека Лейпцизького університету (UBL), Open Ukrainian Citation Index (OUCI), J-Gate

Контактна адреса:
Криворізький національний університет
50027, вул. Віталія Матусевича, 11, м. Кривий Ріг, Україна
E-mail: info@journal-knu.com.ua
https://journal-knu.com.ua/uk

Journal of Kryvyi Rih National University

Volume 24, No. 1

Year of foundation: 2003
Frequency: 2 times a year

Kryvyi Rih
2026

ISSN 2306-5451
e-ISSN 2519-2736

DOI: 10.31721/2306-5451-2026-1-24

Founder:
Kryvyi Rih National University

Recommended for printing and distribution
via the Internet by the Academic Council
of Kryvyi Rih National University
(Minutes No. 13 of June 30, 2026)

State Registration:
Media identifier R30-04965.
Decision of the National Council of Television and Radio Broadcasting
of Ukraine No. 1501, Minutes No. 15, dated 09.05.2024

The scientific journal is included in category "B" of the List of scientific specialised publications of Ukraine.
Specialties: 0411 – Accounting and taxation, 0412 – Finance, banking and insurance, 0413 – Management and administration, 0416 – Wholesale and retail sales, 0532 – Earth sciences, 0612 – Database and network design and administration, 0613 – Software and applications development and analysis, 0688 – Inter-disciplinary programmes and qualifications involving Information and Communication Technologies, 0713 – Electricity and energy, 0714 – Electronics and automation, 0715 – Mechanics and metal trades, 0716 – Motor vehicles, ships and aircraft, 0724 – Mining and extraction, 0732 – Building and civil engineering, 1032 – Protection of persons and property, 1041 – Transport services
(order of the Ministry of Education and Science of Ukraine No. 409, dated March 17th, 2020)

The journal is indexed in databases
UCSB Library, Crossref, Vernadsky National Library of Ukraine (VNLU), Google Scholar, Litmaps, Institute of Information Registration Problems of the National Academy of Sciences of Ukraine, Ulrichsweb, University of Oslo Library, University of Hull Library, Leipzig University Library (UBL), Open Ukrainian Citation Index (OUCI), J-Gate

Address for contacts:
Kryvyi Rih National University
50027, 11 Vitalii Matusevich Str., Krivyi Rih, Ukraine
E-mail: info@journal-knu.com.ua
https://journal-knu.com.ua/en

ГОЛОВНИЙ РЕДАКТОР

Віктор Розен	Доктор наук, професор, професор кафедри автоматизації електротехнічних та мехатронних комплексів, Національний технічний університет України «Київський політехнічний інститут імені Ігоря Сікорського», Україна

ЗАСТУПНИК ГОЛОВНОГО РЕДАКТОРА

Павло Крот	Кандидат наук з математичного моделювання, доктор габілітований інженер у галузі геоінженерії, гірництва та геології, доцент Вроцлавського політехнічного університету, м. Вроцлав, Польща

НАЦІОНАЛЬНІ ЧЛЕНИ РЕДКОЛЕГІЇ

Андрій Купін	Доктор технічних наук, професор, завідувач кафедри комп'ютерних систем та мереж, Криворізький національний університет, м. Кривий Ріг, Україна
Олег Сінчук	Доктор технічних наук, професор, завідувач кафедри автоматизованих електромеханічних систем в промисловості та транспорті, Криворізький національний університет, м. Кривий Ріг, Україна
Вадим Щокін	Доктор технічних наук, професор, директор Науково-дослідного гірничо-рудного інституту, Криворізький національний університет, м. Кривий Ріг, Україна
Михайло Алексєєв	Доктор технічних наук, професор, завідувач кафедри програмного забезпечення комп'ютерних систем, Національний технічний університет «Дніпровська політехніка», м. Дніпро, Україна
Едуард Жаріков	Доктор наук, професор, завідувач кафедри інформатики та програмної інженерії, Національний технічний університет України «Київський політехнічний інститут імені Ігоря Сікорського», Україна
Олексій Михайленко	Доктор філософії, доцент, Доцент кафедри електричної інженерії, Криворізький національний університет, Україна

МІЖНАРОДНІ ЧЛЕНИ РЕДКОЛЕГІЇ

Дмитро Зубов	Доктор технічних наук, професор, Університет Центральної Азії, м. Нарин, Киргизстан
Валерій Дружинін	Доктор філософії, доцент, доцент кафедри «Енергетика», Карагандинський індустріальний університет, Республіка Казахстан
Айнур Куттыбаева	Доктор філософії, доцент, доцент кафедри електроніки, телекомунікацій та космічних технологій, Казахський національний дослідницький технічний університет, Республіка Казахстан
Фарсі Чукі	Доктор філософії, професор, Університет імені Мохамеда Будіафа в М'сілі, м. М'сіла, Алжир
Сулейман Олакунле Салаву	Доктор філософії з прикладної математики, професор, Федеральний університет технологій та екологічних наук, Нігерія
Бісваджит Саркар	Доктор наук з прикладної математики, професор, Університет Йонсей, Південна Корея

Editorial Board

EDITOR-IN-CHIEF

Viktor Rozen	Doctor of Sciences, Professor, Professor in the Department of Automation of Electrical and Mechatronic Systems, Igor Sikorsky Kyiv Polytechnic Institute, Ukraine

DEPUTY EDITOR-IN-CHIEF

Pavlo Krot	PhD in Mathematical Simulation, Doktor habilitowany inżynier in Geoengineering, Mining and Geology, Associate Professor at Politechnika Wrocławska, Wroclaw, Poland

NATIONAL MEMBERS OF THE EDITORIAL BOARD

Andrey Kupin	Doctor of Technical Sciences, Professor, Head of the Department of Computer Systems and Networks, Kryvyi Rih National University, Kryvyi Rih, Ukraine
Oleg Sinchuk	Doctor of Technical Sciences, Professor, Head of the Department of Automated Electromechanical Systems in Industry and Transport, Kryvyi Rih National University, Kryvyi Rih, Ukraine
Vadym Shchokin	Doctor of Technical Sciences, Professor, Director of the Research Mining Institute, Kryvyi Rih National University, Kryvyi Rih, Ukraine
Mykhailo Alekseyev	Doctor of Technical Sciences, Professor, Head of the Department of Computer Systems Software, Dnipro Polytechnic National University, Dnipro, Ukraine
Eduard Zharikov	Doctor of Sciences, Professor, Head of the Department of Computer Science and Software Engineering, Igor Sikorsky Kyiv Polytechnic Institute, Ukraine
Oleksii Mykhailenko	PhD, Associate Professor, Associate Professor in the Department of Electrical Engineering, Kryvyi Rih National University, Ukraine

INTERNATIONAL MEMBERS OF THE EDITORIAL BOARD

Dmytro Zubov	Doctor of Technical Sciences, Professor, University of Central Asia, Naryn, Kyrgyzstan
Valery Druzhinin	PhD, Associate Professor, Associate Professor in the Department of Energy, Karaganda Industrial University, Republic of Kazakhstan
Ainur Kuttybayeva	PhD, Associate Professor, Associate Professor in the Department of Electronics, Telecommunications and Space Technologies, Kazakh National Research Technical University, Republic of Kazakhstan
Farsi Chouki	PhD, Full Professor, University Mohamed Boudiaf of M'sila, M'sila, Algeria
Sulyman Olakunle Salawu	PhD in Applied Mathematics, Professor, Federal University of Technology and Environmental Sciences, Nigeria
Biswajit Sarkar	PhD in Applied Mathematics, Professor, Yonsei University, South Korea

Content / Зміст

Journal of Kryvyi Rih National University

Vol. 24, No. 1, 2026

Journal homepage: https://journal-knu.com.ua/en

ISSN 2306-5451

e-ISSN 2519-2736

Article's History: Received: 05.12.2025 Revised: 03.04.2026 Accepted: 28.04.2026 Published: 29.05.2026

UDC 621.928:621.867

DOI: 10.31721/2306-5451-2026-1-24-08-20

Study of the feasibility of classifying oversized lump material during conveyor transportation

Dmytro Popolov*

Doctor of Technical Sciences, Associate Professor
State University of Economics and Technologies
50005, 16 Medychna Str., Kryvyi Rih, Ukraine
https://orcid.org/0000-0003-0347-8627

Oleksandr Uchytel

Doctor of Technical Sciences, Professor
State University of Economics and Technologies
50005, 16 Medychna Str., Kryvyi Rih, Ukraine
https://orcid.org/0000-0001-6241-1786

Serhii Shved

PhD in Technical Sciences, Associate Professor
State University of Economics and Technologies
50005, 16 Medychna Str., Kryvyi Rih, Ukraine
https://orcid.org/0000-0003-2169-8893

Ihor Zaselskyi

PhD in Technical Sciences, Associate Professor
State University of Economics and Technologies
50005, 16 Medychna Str., Kryvyi Rih, Ukraine
https://orcid.org/0000-0002-4834-4027

Serhii Henkulenko

Postgraduate Student
State University of Economics and Technologies
50005, 16 Medychna Str., Kryvyi Rih, Ukraine
https://orcid.org/0000-0003-4629-1184

Eduard Havrylov

Postgraduate Student
State University of Economics and Technologies
50005, 16 Medychna Str., Kryvyi Rih, Ukraine
https://orcid.org/0009-0009-4293-3902

Abstract. In the modern mining and metallurgical industry, the operational stability of preparatory processing equipment, such as crushers and mixers, is significantly dependent on the uniformity of the granulometric structure distribution of the feed material. The presence of oversized lump material leads to dynamic overloads,

Suggested Citation:

Popolov, D., Uchytel, O., Shved, S., Zaselskyi, I., Henkulenko, S., & Havrylov, E. (2026). Study of the feasibility of classifying oversized lump material during conveyor transportation. *Journal of Kryvyi Rih National University*, 24(1), 8-20. doi: 10.31721/2306-5451-2026-1-24-08-20.

Copyright © The Author(s). This is an open access article distributed under the terms of the Creative Commons Attribution License 4.0 (https://creativecommons.org/licenses/by/4.0/)

**Corresponding author (popolov@duet.edu.ua)*

accelerated wear of working components, and increased energy consumption. Conventional classification methods using scalping screens are economically inefficient at low contents of oversized lump material, which necessitates the development of cost-effective classification methods directly on conveyor lines. The aim of this study was to provide a scientific justification for the design of a machine for the mechanical removal of large-sized inclusions from a flow of bulk material in the unloading zone of a belt conveyor, based on a previously developed segregation heterogeneity model. The study employs methods of mathematical modeling, theoretical mechanics, and particle dynamics, which made it possible to substantiate the design of a classification device in the form of a rotating rod comb positioned above the conveyor discharge pulley. It has been established that the rational operating regime is achieved by matching the linear velocity of the belt with the kinematic parameters of the rod tip rotation, thereby minimising energy losses due to sliding. It has been mathematically proven that a rod profile in the form of a clothoid ensures its penetration into the material bulk along the normal path, significantly reducing impact loads. A comprehensive dynamic model has been developed, describing three stages of interaction: particle extraction from the layer, its relative motion along the rod surface, and free flight, which makes it possible to determine the geometric boundaries of the oversized lump material dispersion zone. This enables precise positioning of receiving hoppers and deflector plates for oversized lump material. The obtained mathematical models and geometric relationships allow for the design of efficient pre-classification units integrated into existing conveyor systems, ensuring protection of process equipment from overloads without the need for bulky and energy-intensive machinery

Keywords: belt conveyor; material segregation; mechanical classification; rotating rod comb; particle free-flight trajectory; size classification; discharge assembly

Introduction

Under current operating conditions of mining and metallurgical enterprises, ensuring the stable and reliable performance of equipment employed in material preparation processes is one of the key factors in improving production efficiency and reducing operating costs. The performance of crushing, mixing, and compaction equipment is strongly influenced by the granulometric composition of the feed material, particularly by the presence of isolated oversized lumps exceeding the permissible dimensions, as well as frozen or consolidated agglomerates formed due to moisture, temperature fluctuations, and prolonged storage. The entry of such inclusions into process equipment disrupts the prescribed operating conditions, increases dynamic loading, intensifies the wear of working components, and raises energy consumption, thereby adversely affecting the reliability of technological systems.

One of the most extensively investigated research directions concerns the influence of feed granulometric composition on the performance of crushing equipment. B. Rocha *et al*. (2024) conducted industrial-scale investigations of an HP500 cone crusher to determine the influence of feed characteristics on its operational performance. The authors analysed the effects of the maximum feed particle size, width of the relieve slot, and the physical and mechanical properties of the ore on crushing performance. Their results demonstrated that increasing the size of the largest feed particles decreases crusher throughput. Moreover, feed size, together with the width of the relieve slot and material properties, was identified as one of the principal factors governing crushing efficiency. These findings emphasise the necessity of limiting the entry of oversized lumps into the crusher to ensure stable equipment operation. Further development of this research direction was presented by M. Lindqvist & H. Li (2021), who developed a mathematical model of a cone crusher integrating a material breakage model with an energy-based description of the crushing process. Using numerical simulations, the authors investigated the influence of feed granulometric composition on crusher capacity, specific energy consumption, and the particle size distribution of the final product. It was found that increasing the upper feed size limit alters the material flow pattern within the crushing chamber, impedes particle movement through the compression zone, and causes a non-uniform distribution of loading over the crushing surfaces. As a consequence, fluctuations in power consumption occur, crushing efficiency decreases, and the wear rate of the working components increases.

An alternative approach to this problem was proposed by P. Itävuo & M. Vilkko (2021), who investigated the stabilisation of the crushing process through automatic control of a cone crusher operating under variable feed conditions. The developed control system maintained a predetermined reduction ratio regardless of fluctuations in feed granulometric composition. Industrial-scale tests demonstrated that the proposed control strategy substantially reduced process variability while increasing the average productivity of the crushing complex. Nevertheless, the need for sophisticated automatic control systems itself confirms that fluctuations in feed granulometric composition constitute one of the primary factors affecting cone crusher performance. The detrimental effect of oversized lumps is equally significant in hammer crushers, where material breakage is predominantly achieved through impact loading. T. Abilzhanuly *et al*. (2024) investigated the dynamics of material motion within the crushing chamber of a hammer crusher and demonstrated that feed granulometric composition, together with the design parameters of the working elements, significantly affects particle kinematics, process energy consumption, and the quality of the final product. The study showed that increasing particle size alters particle trajectories, modifies impact conditions, and reduces the uniformity of material breakage, ultimately resulting in deteriorated technological performance.

The practical consequences of hard oversized lumps inclusions entering industrial hammer crushers were examined by E. Kyekyere *et al*. (2024), who analysed the causes of premature failure of grate bars in a reversible hammer crusher used for secondary coal crushing. Based on macrostructural and microstructural analyses of damaged components, the authors concluded that one of the principal causes of intensive wear and failure was direct impact loading induced by hard oversized lumps entering the crushing chamber. Such particles were shown to intensify abrasive wear, promote fatigue crack initiation, and accelerate brittle fracture of working surfaces. The study concluded that maintaining uniform feed conditions and restricting the entry of oversized lumps are essential for increasing the service life of crusher components and ensuring stable equipment operation.

However, the above-mentioned studies are primarily focused on improving crusher design, developing mathematical models of the crushing process, or designing control systems capable of compensating for the adverse effects of fluctuating feed granulometric composition. In contrast, the problem of removing isolated oversized lumps directly from the bulk material stream on conveyor routes before the material enters the crushing equipment, thereby preventing overloads at an earlier stage of the technological process, has received very limited attention. The adverse effect of non-uniform granulometric composition is also observed in bulk material mixing processes, where particle size governs particle motion, the intensity of circulation flows, and the uniformity of mixture formation. Recent studies have demonstrated that variations in granulometric composition substantially affect the energy and kinematic characteristics of the mixing process, as well as the mechanical loads acting on the working elements of mixing equipment.

G. Chandratilleke *et al*. (2021) employed the Discrete Element Method (DEM) to investigate the mixing of bulk materials in a ribbon mixer, aiming to determine the influence of the physic and mechanical properties and granulometric composition of the material on process performance. The authors analysed circulation flow patterns, mixing kinetics, and variations in the torque acting on the mixer drive shaft. The results revealed that an increase in particle size significantly alters material circulation, prolongs the time required to achieve a homogeneous mixture, and increases the torque required for mixing. These findings clearly indicate that the granulometric composition of the feed material directly affects the energy performance of mixing equipment. Similar conclusions were reported by Z. Zuo *et al*. (2023) in their investigation of bulk material mixing in a paddle mixer. Based on experimental studies combined with DEM simulations, the authors analysed the influence of the design parameters of the mixing blades, rotational speed, and material properties on particle motion. It was established that increasing particle size modifies particle trajectories, circulation velocity, and the intensity of interparticle interactions, leading to reduced mixture homogeneity and lower mixing efficiency. These findings further confirm that a stable granulometric composition of the feed material is one of the key prerequisites for the efficient operation of mixing equipment.

The problem of increased mechanical loading on mixer components was investigated by D. Han *et al*. (2022), who analysed the wear mechanisms of intensive mixer rotors operating under prolonged service conditions. Based on an investigation of the contact interactions between material particles and working surfaces, the authors demonstrated that increasing contact loads intensifies abrasive and fatigue wear, alters the geometry of the working elements, and consequently deteriorates mixing quality. These results confirm that elevated mechanical loading is one of the principal factors limiting the service life of mixing equipment. Therefore, contemporary studies consistently demonstrate that the granulometric composition of bulk materials significantly influences particle kinematics, process energy consumption, and the durability of mixer components. At the same time, the available literature indicates that most studies focus on optimising mixer design or operating conditions, whereas the preliminary removal of isolated oversized lumps from the material stream as a means of reducing mechanical loading on mixing equipment has received virtually no attention.

Similar relationships are observed in the compaction of bulk materials using High Pressure Grinding Rolls (HPGR), whose operational efficiency largely depends on the formation of a compressed particle bed between the rolls. The particle size distribution of the feed plays a decisive role in ensuring a uniform distribution of contact stresses among particles and determines the efficiency of interparticle breakage. A. Aminalroaya & P. Pourghahramani (2021) experimentally investigated the influence of feed characteristics on material breakage in HPGR. Their study demonstrated that both the mechanical properties and granulometric composition of the feed material determine the formation of the compressed particle bed, the distribution of energy among particles, and the efficiency of interparticle breakage. Feed heterogeneity was shown to deteriorate compaction conditions, thereby adversely affecting the technological performance of HPGR.

Thus, regardless of the type of process equipment, contemporary studies consistently indicate that the presence of oversized lumps in a bulk material stream leads to deteriorated process performance, increased energy consumption, higher mechanical loading of working components, and accelerated wear. However, the overwhelming majority of published studies are devoted to improving equipment design, optimising operating conditions, or developing automatic control systems that compensate for the adverse effects of oversized lumps only after they have entered the working zone of the machine. In contrast, the prevention of oversized lumps entry through their preliminary removal from the conveyor stream remains insufficiently investigated. One of the most widely adopted engineering solutions for preventing oversized lumps from entering process equipment is their preliminary removal using scalping screens. Such machines separate oversized lumps by transporting the material over a screening surface with relatively large apertures, thereby effectively protecting downstream process equipment against overloads. However, the application of scalping screens is economically justified primarily when the feed contains a considerable proportion of oversized lumps. When their content does not exceed 5%, the use of a dedicated screening machine results in high capital investment, substantial energy consumption, and additional maintenance costs, significantly reducing the economic efficiency of this approach.

Accordingly, the development of alternative methods for the preliminary removal of isolated oversized lumps without employing dedicated classification equipment represents an important research direction. A promising basis for implementing such an approach is the utilisation of the natural segregation phenomena occurring during the transportation of bulk materials on belt conveyors. Contrary to the traditional perception of a conveyor as merely a transportation device, recent studies have demonstrated that bulk materials continuously undergo particle size segregation during conveying. As a result, coarse particles tend to concentrate in the upper layers of the material stream, whereas finer particles migrate toward their lower part. Z. Liu *et al.* (2022) conducted experimental investigations and numerical simulations of bulk material segregation on belt conveyors. The authors demonstrated that the intensity of stratified segregation depends on the particle size ratio, conveying velocity, and the geometry of the material stream. It was shown that a stable particle size stratification is formed already in the initial conveying section and remains preserved until the material is discharged.

Further development of this research direction was presented by Y. Duan *et al.* (2025), who employed DEM simulations to investigate the mechanisms governing the formation of a segregated bulk material structure during conveying and discharge. The authors demonstrated that the resulting segregation pattern determines the spatial distribution of particles of different sizes within the discharge zone and can be utilised for the selective separation of specific size fractions without additional classification operations. These findings suggest that the conveying process should be regarded not only as a transportation operation but also as an important stage of material preconditioning before subsequent processing. Therefore, the analysis of the available literature indicates the absence of engineering solutions utilising the natural segregation of bulk materials on belt conveyors for the mechanical removal of isolated oversized lumps directly within the conveyor discharge zone. This unresolved scientific problem defines the relevance and novelty of the present study. The objective of this study was to establish the fundamental interaction mechanisms between the working element and the segregated bulk material stream within the discharge zone of a belt conveyor and to substantiate the design and kinematic parameters of a device capable of selectively removing isolated oversized lumps without the use of dedicated classification equipment.

Materials and Methods

The investigation of the mechanical separate process of isolated oversized lumps from segregated bulk material was carried out on the basis of a conceptually developed device design (Fig. 1).

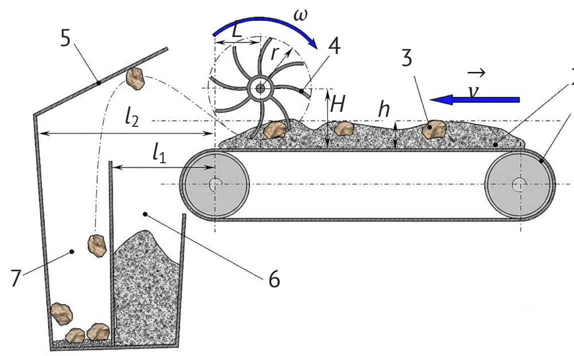

Figure 1. Basic diagram of the device for removal of isolated oversized lumps from segregated bulk material

Source: developed by the authors

In the initial problem formulation, the process of transporting segregated bulk material 2 by a horizontal belt conveyor 1 moving at a constant linear velocity *v* was considered. As a result of segregation within the material flow, a particle size heterogeneous structure was formed in which isolated oversized lumps 3 with an average size *d* became localized within the near-surface layer at a depth comparable to their characteristic size. To implement the process of their removal, a rotating working element in the form of a rod comb 4 was installed in the conveyor discharge zone. Structurally, the comb was designed with an axial spacing between the rods not exceeding *d*. During rotation, the comb 4 interacts with the upper layer of the material 2, captures the isolated oversized lumps 3, and imparts additional kinetic energy to them, causing their separation from the main material stream and subsequent motion along a free-flight trajectory inclined to the horizontal in the direction of material movement. To limit the particle dispersion zone, a deflector surface 5 was incorporated into the design. Fine material fractions 2 that do not interact with the comb 4 freely discharge into the receiving hopper 6, whereas the isolated oversized lumps 3 that receive an additional impulse are transported over a greater distance and discharged into the remote receiving hopper 7.

The rational operating regime of the rotating working element is determined by the condition of minimising energy losses caused by the sliding of isolated oversized lumps relative to finer particles at the moment of their removal from the material layer. To satisfy this condition, according to the computational scheme used for determining the geometric and kinematic parameters of the rotating working element shown in Figure 2, point *A* corresponding to the material detachment from the upper surface of the layer of thickness *h* must coincide with the point at which the rod exits the material bulk. In this case, the projection of the linear velocity of the rod tip at the specified point must be equal to the linear velocity of the conveyor belt *v*.

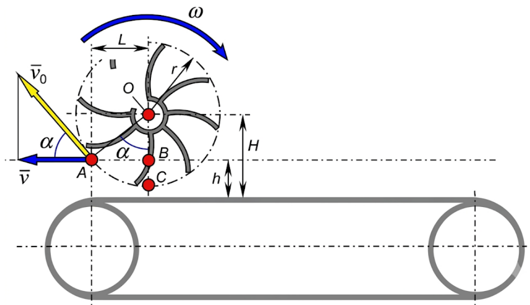

Figure 2. Computational scheme for determining the geometric and kinematic parameters of the rotating working element
Source: developed by the authors

For the justified selection of the installation position of the receiving hopper for oversized lump fractions or the positioning of the deflector plate intended to direct them into the hopper, the law of motion of a single oversized lump particle was investigated. At the first stage, the relative motion of the particle along the surface of the rotating rod was studied. The analysis is based on the following representation of the process: the interaction of the isolated oversized lumps with the rod, while it remains within the material bulk, occurs exclusively in the vertical direction, corresponding to its detachment from the material layer. After exiting the bulk material, the particle enters a sliding regime along the rod surface during its rotation. In this case, the initial sliding velocity is equal to the conveyor belt velocity, and the initial coordinate is comparable to the characteristic particle size (Fig. 3a). The force diagram acting on the particle captured by the rod during its relative motion is shown in Figure 3b.

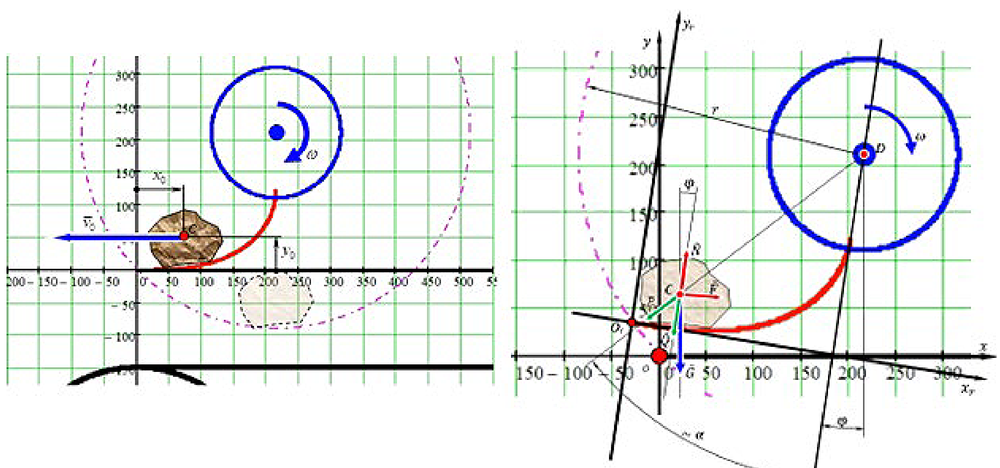

a b

Figure 3. Computational scheme of particle relative motion on the surface of a rotating rod
Notes: a – initial motion parameters of the particle; b – force diagram acting on the particle during its relative motion
Source: developed by the authors

For describing the motion, two coordinate systems are introduced: a fixed system *xOy* associated with the axis of the conveyor discharge pulley, and a moving system $x_r O_r y_r$ rigidly attached to the rod and rotating together with it. The dynamics of the particle's relative motion are described by the fundamental law of dynamics for a material point, taking into account the action of gravity, constraint reactions, as well as inertial components induced by the rotational motion of the reference system, in particular the Coriolis and centrifugal forces.

The rotation angle of the rod is defined as a function of time:

$$\varphi(t) = \omega \cdot t \text{ rad.} \tag{1}$$

To simplify the mathematical description, it is assumed that the particle position along the rod coincides with its geometric profile, while its initial position is defined taking into account the characteristic particle size and the system geometry. Under these conditions, the relative velocity during the particle transition onto the gentle section of the rod is assumed to be determined solely by the variation of the x_r coordinates. Under these assumptions, the forces acting on the particle are projected onto the axes of the moving coordinate system, which makes it possible to formulate the equations of motion in the form of a system of differential equations expressed in projections onto the corresponding axes:

$$\begin{cases} G \cdot sin\,\varphi + F - P \cdot sin\,\alpha = m \cdot a_{rx} \\ -G \cdot cos\,\varphi - P \cdot cos\,\alpha + N - Q = m \cdot a_{ry} \end{cases}, \tag{2}$$

where G – the gravitational force, N; F – the sliding friction force, N; P – the centrifugal force, N; N – the normal reaction force, N; and Q – the inertial force associated with Coriolis acceleration, N.

The mass of the isolated oversized lumps was expressed in terms of its density ρ and average characteristic particle size d:

$$m \approx \rho \cdot \frac{4}{3}\pi \left(\frac{d}{2}\right)^3 \approx 0.524 \cdot \rho \cdot d^3 \text{ kg.} \tag{3}$$

Taking into account the physical nature of the process, the forces included in the right-hand sides of the equations can be represented in the following form:

$$G = m \cdot g = 0.524 \cdot \rho \cdot d^3 \cdot g \approx 5.137 \cdot \rho \cdot d^3\ N, \tag{4}$$

where g – the acceleration due to gravity, m/s²;

$$F = k \cdot N, \tag{5}$$

where k – the coefficient of sliding friction between the isolated oversized lumps and the rod surface;

$$P = m \cdot \omega^2 \cdot r = 0.524 \cdot \rho \cdot d^3 \cdot \omega^2 \cdot r, \tag{6}$$

where ω – the angular velocity of rotation, rad/s;

$$Q = m \cdot 2 \cdot \omega \cdot v_r = 1.047 \cdot \rho \cdot d^3 \cdot \omega \cdot \cdot \sqrt{(x_r')^2 + (y_r')^2} \approx 1.047\rho \cdot d^3 \cdot \omega \cdot x_r'. \tag{7}$$

Substituting expressions (1-6) into the original system of equations (7) and expressing the accelerations in differential form, the transformed system of equations is obtained:

$$\begin{cases} 5.137 \cdot \rho \cdot d^3 \cdot sin(\omega \cdot t) + k \cdot N - \\ -0.524 \cdot \rho \cdot d^3 \cdot \omega^2 \cdot r \cdot \sqrt{1-(\cos\alpha)^2} = \\ = 0.524 \cdot \rho \cdot d^3 \cdot x_r'' \\ -5.137 \cdot \rho \cdot d^3 \cdot cos(\omega \cdot t) - \\ -0.524 \cdot \rho \cdot d^3 \cdot \omega^2 \cdot r \cdot cos\,\alpha + N - 1.047 \cdot \rho \times \\ \times d^3 \cdot \omega \cdot x_r' = 0.524 \cdot \rho \cdot d^3 \cdot y_r'' \end{cases} \cdot \tag{8}$$

Considering the negligible acceleration along the $O_r\, y_r$ axis at the moment the isolated oversized lumps leaves the rod, the normal reaction force is, in the first approximation, determined from the condition of quasi-static equilibrium of force projections onto this axis:

$$N = 5.137 \cdot \rho \cdot d^3 \cdot cos(\omega \cdot t) + 0.524 \cdot \rho \cdot d^3 \cdot \omega^2 \cdot r \cdot \cdot cos\alpha + 1.047 \cdot \rho \cdot d^3 \cdot \omega \cdot x_r'. \tag{9}$$

To solve the relative motion of the isolated oversized lumps along the surface of the rod of the specified structural design, initial conditions for the relative velocity and coordinate were used:

$$\begin{cases} v_{r0} = -v \\ x_{r0} = d \end{cases}. \tag{10}$$

The time of motion of the isolated oversized lumps along the rod surface is determined from the equation of motion, solved with consideration of the initial conditions (16), when the particle reaches the specified coordinate value $x_r = 0$. The obtained law of motion makes it possible to determine the trajectory of the isolated oversized lumps after ejection, which in turn enables the substantiation of the positioning of the receiving hopper or the deflector plate used to direct the particle flow.

Results and Discussion

The following geometric (1-3) and kinematic (4) relationships are established, linking the parameters of conveyor motion and the rotation of the working element.

$$BC = d \text{ m}; \tag{11}$$

$$r = H - h + d \text{ m}; \tag{12}$$

$$L = \sqrt{2 \cdot \frac{H-h}{d} + 1} \text{ m}; \tag{13}$$

$$n = \frac{30 \cdot v}{\pi \cdot (H-h)} \text{ rpm.} \tag{14}$$

To minimise impact loads during the penetration of the working element into the bulk material layer, the rod profile was designed as a clothoid, thereby ensuring that the rod enters the material along the normal to the free surface and providing a smooth change in its direction of motion. The selection of a clothoid profile is justified by its fundamental geometric property, namely, the linear variation of curvature with arc length (Meek *et al.*, 2004; Levien, 2008). In contrast to a circular arc, which has constant curvature, or profiles characterised by abrupt curvature discontinuities, a clothoid provides a continuous increase in curvature from zero. Consequently, the normal acceleration and the contact forces between the rod and the bulk material increase gradually, thereby eliminating impact-type interaction. Owing to these characteristics, clothoid curves are widely employed in the design of motion trajectories for engineering systems requiring a smooth variation in curvature, reduced jerk, lower dynamic loading, and improved motion stability. These advantages have been confirmed by recent studies in vehicle control and trajectory planning, demonstrating that clothoid-based trajectories provide smoother curvature transitions and lower dynamic loads than trajectories containing curvature discontinuities (Li *et al.*, 2023).

For the analytical description of the rod profile, a computational scheme is introduced (Fig. 4), in which a Cartesian coordinate system rigidly fixed to the surface of the material layer is used. The origin is located at the point where the material leaves the upper surface of the layer, the abscissa axis is tangent to this surface, while the ordinate axis is directed along the normal to it.

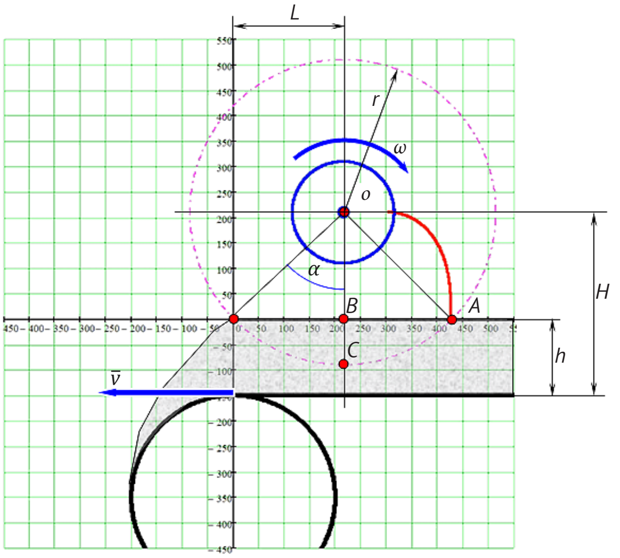

Figure 4. Computational scheme of the rod profile of the rotating working element
Source: developed by the authors

On the basis of the developed computational scheme, the rod profile is described by the parametric equations:

$$\begin{cases} x(t) = a\sqrt{\pi}\cdot\int_0^{\tau} cos\left(\frac{\pi\xi^2}{2}\right)d\xi \\ y(t) = a\sqrt{\pi}\cdot\int_0^{\tau} sin\left(\frac{\pi\xi^2}{2}\right)d\xi \end{cases}, \quad (15)$$

where t – a dimensionless parameter, with $0 \leqslant t \leqslant 1$; a – is a scale factor defining the dimensions of the rod profile.

Substituting the obtained function of the normal reaction force (14) into the first differential equation of the system (13), it is transformed into its canonical form:

$$x_r'' - 2\cdot k\cdot\omega\cdot x_r' = k\cdot\omega^2\cdot r\cdot cos\alpha - \omega^2\cdot r\cdot \cdot\sqrt{(1-(cos\alpha)^2)} + g\cdot sin(\omega\cdot t) + g\cdot k\cdot cos(\omega\cdot t). \quad (16)$$

The resulting differential equation (15) describes the relative motion of the isolated oversized lumps along the surface of the rod of the specified structural design.

The relative velocity of the isolated oversized lumps is defined as the first-time derivative of the obtained law of motion:

$$v_r(t) = \frac{dx_r(t)}{dt} \text{ m/s.} \quad (17)$$

At the moment of detachment of the isolated oversized lumps from the rod, this velocity takes the value $v_r(T)$.

In the second stage, the absolute velocity of the isolated oversized lumps ejection was determined. In this case, the rod rotation angle at the moment of ejection was calculated using expression (6):

$$\varphi(T) = \omega\cdot T \text{ rad,} \quad (18)$$

where T – the moment of ejection of the isolated oversized lumps from the rod surface.

The translational linear velocity of particle ejection is determined by the uniform rotational motion of the rod comb at a radius r (Fig. 5):

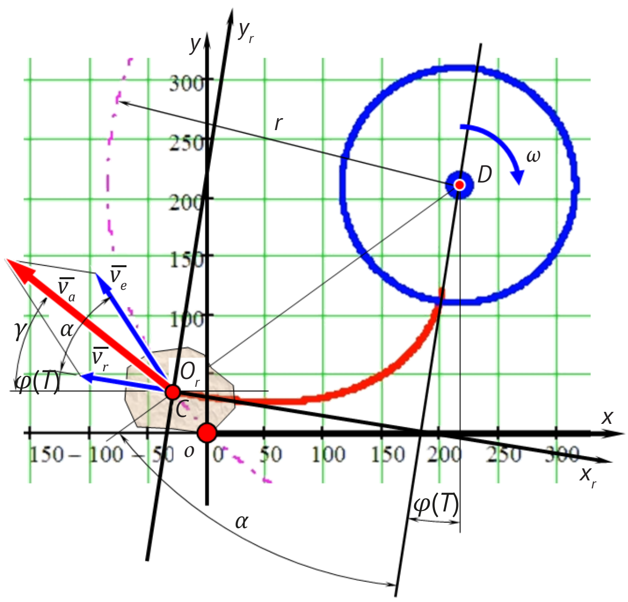

Figure 5. Computational scheme of oversized lump particle ejection velocities
Source: developed by the authors

$$v_e = \omega\cdot r \text{ m/s.} \quad (19)$$

The relative velocity v_r of the particle was determined from the solution of differential equation (17) under the initial conditions (16). The particle ejection angle relative to the horizontal corresponds to the inclination angle of the absolute velocity vector with respect to the horizontal axis. The projections of this vector in the selected inertial coordinate system (see Fig. 4) are expressed as follows:

$$\begin{cases} v_{ax}(T) = -v_e \cdot cos[\alpha + \varphi(T)] - v_r \cdot cos[\varphi(T)] \\ v_{ay}(T) = v_e \cdot sin[\alpha + \varphi(T)] + v_r \cdot sin[\varphi(T)] \end{cases}, \quad (20)$$

The magnitude of the particle absolute velocity vector at the moment of ejection is given by:

$$v_a(T) = \sqrt{[v_{ax}(T)]^2 + [v_{ay}(T)]^2} \text{ m/s}, \quad (21)$$

The trigonometric components of the ejection angle were determined from the relationships between the magnitude of the absolute velocity vector and its projections:

$$cos\,\gamma = \frac{v_{ax}}{v_a}; \quad (22)$$

$$sin\,\gamma = \frac{v_{ay}}{v_a}. \quad (23)$$

Thus, the absolute ejection velocity of the isolated oversized lumps, its projections, and the inclination angle relative to the horizontal were determined, which made it possible to proceed to the third stage of the study – the analysis of its free-flight. The general solution of the problem of motion of a free material point projected at an angle to the horizontal in the selected inertial coordinate system (Fig. 6) is expressed as follows:

$$\begin{aligned} x(t) &= v_{ax} \cdot t + C_1 \\ y(t) &= -0.5\ g \cdot t^2 + v_{ay} \cdot t + C_2. \end{aligned} \quad (24)$$

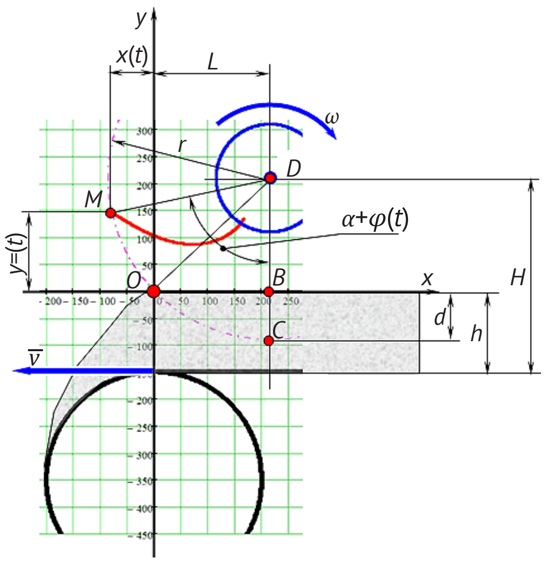

Figure 6. Computational scheme of oversized lump particle free-flight
Source: developed by the authors

The integration constants were determined from the initial conditions, namely the coordinates and velocity of the isolated oversized lumps at the moment of its ejection. According to the computational scheme (see Fig. 6), the absolute coordinates of the isolated oversized lumps during its sliding motion along the surface of the rotating rod are given by:

$$\begin{cases} x(t) = -r \cdot sin[\alpha + \varphi(t)] + L \\ y(t) = H - h - r \cdot cos[\alpha + \varphi(t)] \end{cases}. \quad (25)$$

According to the obtained results of solving equation (15) under conditions (16), the particle motion time from the beginning of sliding to the moment of ejection is equal to *T*. Therefore, the absolute coordinates of the ejection point are expressed as follows:

$$\begin{cases} x(T) = -r \cdot sin[\alpha + \varphi(T)] + L \\ y(T) = H - h - r \cdot cos[\alpha + \varphi(T)] \end{cases}. \quad (26)$$

These coordinates serve as the initial conditions for the subsequent motion of the isolated oversized lumps as a material point during the free-flight stage. The particular solution of the equations of motion was obtained from the general solution (24) by substituting the initial coordinates (26) and the initial velocity (21). As a result, the law of motion of the isolated oversized lumps during free flight after solving the Cauchy problem is expressed as follows:

$$\begin{aligned} x(t) &= v_{ax}(T) \cdot t + x(T) \\ y(t) &= -0.5g \cdot t^2 + v_{ay}(T) \cdot t + y(T) \end{aligned}. \quad (27)$$

Using the developed mathematical model, a numerical analysis of the selective removal of an isolated oversized lump was performed to investigate its interaction with the rotating rod of the working element under typical belt conveyor operating conditions. In the first stage, the evolution of the particle's dynamic characteristics during its motion along the clothoid profile of the rod was investigated (Fig. 7).

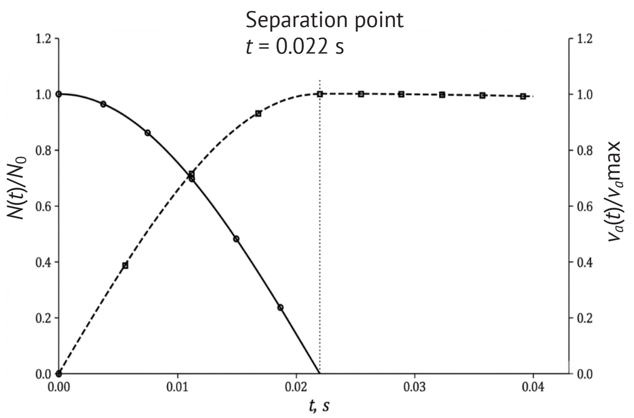

Figure 7. Dynamics of the interaction between an isolated oversized lump and the rod
Source: developed by the authors

The results showed that the relative contact reaction $N(t)/N_0$ (where $N(t)$ is the instantaneous normal contact force between the particle and the rod surface, N; N_0 is the normal contact force at the initial point of contact, N), decreases monotonically from 1 to 0, reaching zero after 0.022 s, which corresponds to the instant when contact with the rod is lost. Simultaneously, the relative particle velocity $v_a(t)/v_{a_{\max}}$ (where $v_a(t)$ is the instantaneous absolute particle velocity, m/s; $v_{a_{\max}}$ is its maximum value, m/s), increases continuously and reaches its maximum immediately before particle detachment. This indicates that the maximum kinetic energy of the particle is attained precisely at the transition from constrained motion along the rod to free flight, which is essential for achieving the maximum particle throw distance. These results demonstrate that the clothoid profile provides a gradual reduction in contact loading without abrupt changes in the contact reaction, while the maximum particle velocity is attained immediately before detachment. Such a variation in the kinematic characteristics confirms the suitability of the clothoid profile for establishing stable initial conditions for the subsequent free-flight phase. In the second stage, the influence of the kinematic parameters of the working element, specifically its rotational speed ($n_{r.c}$), on the particle separation velocity (v_a), and the particle-rod contact time (t_{rod}), was investigated (Fig. 8).

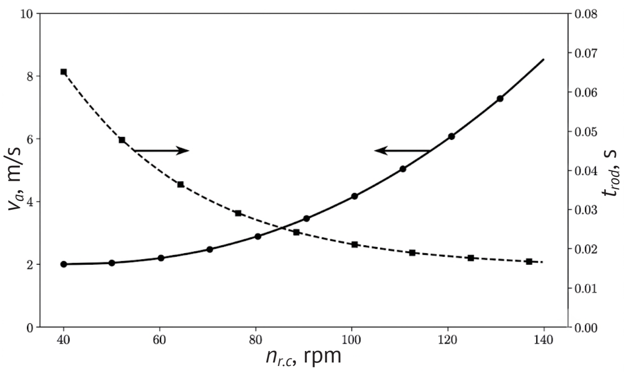

Figure 8. Effect of rotor rotational speed on separation velocity and contact time
Source: developed by the authors

The results indicate that increasing the rotational speed from 40 to 140 rpm increases the particle separation velocity by fourfold. At the same time, the particle-rod contact time decreases by 30%. These findings demonstrate a substantial increase in the intensity of mechanical energy transfer to the particle with increasing rotor speed. Figure 9 presents the results of the analysis of the influence of the coefficient of friction between the isolated oversized lump and the rod surface. The results show that increasing the coefficient of friction by 0.4 reduces the particle separation velocity by 55%. A similar trend is observed for the particle throw distance. This behavior is attributed to increased mechanical energy dissipation due to frictional forces, resulting in a corresponding reduction in the energy converted into the particle's translational kinetic energy. Therefore, the coefficient of friction represents one of the key parameters governing the efficiency of selective particle separation.

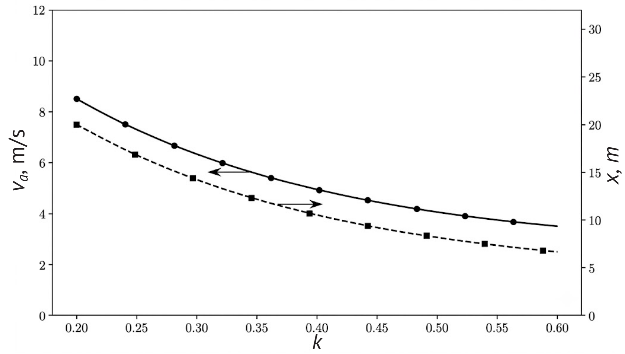

Figure 9. Effect of friction coefficient on particle kinematics and trajectory
Source: developed by the authors

The practical implications of the developed mathematical model are illustrated in (Fig. 10), which presents a family of trajectories of isolated oversized lumps corresponding to rotor rotational speeds ranging from 40 to 140 rpm, together with the trajectory of the fine fraction for comparison.

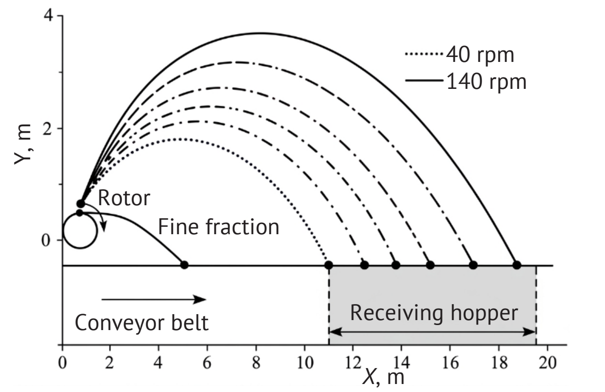

Figure 10. Isolated oversized lump trajectories at different rotational speeds of the working element and the recommended position of the receiving hopper
Source: developed by the authors

A quantitative analysis of the obtained trajectories revealed that increasing the rotor rotational speed predictably extends the flight distance of isolated oversized lumps in the X. At the minimum rotational speed of 40 rpm, the particle landing distance is $X \approx 11$ m. Increasing the rotational speed to 140 rpm shifts the landing point to $X \approx 18.8$ m, while simultaneously increasing the maximum trajectory height to $Y \approx 3.7$ m. Consequently, a well-defined landing zone for isolated oversized lumps is formed within the range of $X = 11...19.5$ m. In contrast, the fine fraction exhibits a fundamentally different motion pattern. Rather than being entrained into the ascending flow, fine particles follow a considerably shorter trajectory and land at X≈5 m. The resulting stable spatial separation, characterised by a minimum gap of more than 5…6 m between the landing zones of the oversized lumps and fine fractions, provides a scientific basis for determining the geometric parameters of the discharge unit.

The obtained results demonstrate that the proposed approach to the mechanical separation of isolated oversized lumps is feasible, provided that the design and kinematic parameters of the rotating working element are properly coordinated with the material conveying conditions on the belt conveyor. The developed mathematical model made it possible to establish the fundamental interaction mechanisms between an isolated oversized lump and the rod, determine the conditions governing particle detachment, and predict its subsequent flight trajectory. In contrast to the majority of recent studies (Hastie *et al.*, 2010; Fei *et al.*, 2026), which primarily focus on minimising particle segregation or improving conveyor system design to preserve material flow homogeneity, the present study is the first to exploit natural segregation as the basis for the mechanical separation of isolated oversized lumps without the use of dedicated heavy-duty classification equipment. One of the principal findings of the present study is that the use of a rod with a clothoid profile ensures a gradual reduction in the contact reaction between the working element and the oversized lump, thereby eliminating abrupt impact loading. At the same time, the particle reaches its maximum velocity immediately before detachment from the rod. This result is consistent with the findings reported by K. Ran *et al.* (2024), who demonstrated, in the context of robotic systems, that incorporating clothoid curves into trajectory planning enables the generation of geometrically smooth paths, minimises kinematic jerk, and significantly reduces dynamic loads acting on robotic actuators under stringent kinematic constraints. However, their study focused on obstacle avoidance algorithms and path planning for mobile robots, whereas the present work is the first to a pply the same geometric principle of continuous curvature variation to the design of the working element of a mechanical device intended for the selective removal of isolated oversized lumps. This finding demonstrates that the advantages of clothoid curves are not limited to autonomous motion control and navigation applications but can also be effectively exploited in the design of heavy-duty process equipment for the conveying and selective separation of bulk materials.

Another important finding of this study is the fourfold increase in the particle separation velocity as the rotational speed of the working element increases from 40 to 140 rpm, accompanied by an approximately 30% reduction in the particle-rod contact time. These results indicate that the kinematic parameters of the working element directly govern the efficiency of mechanical energy transfer to the particle. This conclusion is fully consistent with the findings of previous studies based on the DEM. In particular, DEM simulations of copper ore flow through conveyor transfer stations (Walker *et al.*, 2020), as well as investigations of the discharge trajectory and flow dynamics of cohesive materials from a belt conveyor onto an inclined impact plate (Scheffler & Coetzee, 2023), have clearly demonstrated that the interaction characteristics, velocity conditions, and the evolution of normal and tangential contact forces directly determine the efficiency of mechanical energy transfer to individual particles.

The obtained results also demonstrated the decisive influence of the rod surface condition on the particle separation process. Specifically, increasing the coefficient of friction between the rod surface and the isolated oversized lumps by 0.4 was found to reduce both the particle separation velocity and the corresponding flight distance by approximately 55%. This behavior is attributed to increased mechanical energy dissipation caused by frictional forces, resulting in a smaller proportion of the available energy being converted into the particle's translational kinetic energy. The identified mechanism is fully consistent with the fundamental findings of S. Laudari *et al.* (2023), who, through DEM simulations of binary granular mixtures, demonstrated that contact friction, both between particles and at the particle-equipment interface, has a critical influence on velocity profiles, energy dissipation, and the overall kinematics of double-faction flows. These findings emphasise the necessity of maintaining strict control over the condition and wear of the rotating rod surfaces to preserve the designed particle throw distance and, consequently, the efficiency of isolated oversized lump separation.

The simulations further demonstrated that an appropriate combination of the device's kinematic and geometric parameters makes it possible to achieve a spatial separation of up to 6 m between the landing zones of the fine fractions and isolated oversized lumps material. This result is fully consistent with the fundamental principles of bulk material separation based on aerodynamic and inertial properties (Rhodes, 2008). According to the fundamental laws of dynamics, the flight distance of a body moving through air depends on its initial momentum, mass, and the aerodynamic drag force. In conventional gravity-based conveyor discharge systems, the natural separation between the trajectories of particles of different masses is minimal because all particles leave the belt with nearly identical initial velocities, making efficient classification impossible without dedicated receiving hoppers or classification devices. In contrast, the present study demonstrates that the application of an additional mechanical impulse generated by the rotating working element can deliberately amplify this natural trajectory separation.

By imparting additional kinetic energy to isolated oversized lumps at the moment of contact, the proposed device ensures their stable displacement beyond the landing zone of the main fine-material stream. As a result, reliable industrial-scale separation is achieved without remixing of the isolated oversized lumps and fine material flows.

Conclusions

This study theoretically substantiated a novel approach for the separation of isolated oversized lumps from a bulk material stream directly within the discharge zone of a belt conveyor. The proposed approach was based on the natural segregation of the conveyed material and its selective interaction with a rotating working element. Unlike conventional solutions, the proposed method does not require dedicated energy-intensive classification equipment, thereby providing the basis for improving the efficiency of existing material handling and processing systems. The developed mathematical model describes the complete process of isolated oversized lumps separation, including its extraction from the segregated material layer, relative motion along the rod surface, and subsequent free flight. The derived analytical relationships make it possible to determine the particle separation velocity, the coordinates of the detachment point, the trajectory parameters, and the predicted landing zone, thereby providing a sound basis for the design and optimisation of the geometric parameters of the conveyor discharge unit.

It was established that the use of a rod with a clothoid profile ensures a gradual reduction in the contact reaction between the working element and the isolated oversized lumps without generating abrupt dynamic loads. The oversized lu mps reaches its maximum velocity immediately before detachment from the rod, creating the most favorable conditions for the efficient mechanical separation of it from the bulk material stream. The numerical analysis demonstrated that increasing the rotational speed of the working element from 40 to 140 rpm results in a fourfold increase in the particle separation velocity while simultaneously reducing the particle-rod contact time by 30%. These findings indicate that the kinematic parameters of the working element constitute one of the key factors governing the efficiency of mechanical energy transfer to the material particles.

A significant influence of the coefficient of friction between the rod surface and the isolated oversized lump on the separation efficiency was demonstrated. An increase in the coefficient of friction by 0.4 results in an approximately 55% reduction in both the particle separation velocity and the particle throw distance. This finding should be taken into account when selecting materials for the working elements and when assessing their wear under operating conditions. It was established that the proposed technical solution provides stable spatial separation of the trajectories of isolated oversized lumps and fine particles, with the corresponding landing zones separated by more than 5...6 m. This enables the efficient mechanical separation of isolated oversized lumps from the conveyed material stream and provides a sound basis for the optimal positioning of receiving hoppers or deflector elements without the need for additional classification equipment. Future research should focus on the experimental validation of the proposed mathematical model using a laboratory-scale test rig, investigating the influence of the physics and mechanical properties of bulk materials and the degree of particle segregation on separation efficiency, as well as optimising the design parameters of the working element for different operating conditions and materials conveying regimes.

Acknowledgements

None.

Funding

None.

Conflict of Interest

None.

References

[1] Abilzhanuly, T., Iskakov, R., Abilzhanov, D., Gulyarenko, A., & Khan, V. (2024). Identifying the influence of the pitch of hammers with cutting edges on the average length of feed crushed in hammer grinders. *Eastern-European Journal of Enterprise Technologies*, 4(1(130)), 69-78. doi: 10.15587/1729-4061.2024.310045.

[2] Aminalroaya, A., & Pourghahramani, P. (2021). The effect of feed characteristics on particles breakage and weakening behavior in high pressure grinding rolls (HPGR). *Mineral Processing and Extractive Metallurgy Review*, 43(5), 610-621. doi: 10.1080/08827508.2021.1913153.

[3] Chandratilleke, G.R., Jin, X., & Shen, Y.S. (2021). DEM study of effects of particle size and density on mixing behaviour in a ribbon mixer. *Powder Technology*, 392, 93-107. doi: 10.1016/j.powtec.2021.06.058.

[4] Duan, Y., Jing, L., Umbanhowar, P.B., Ottino, J.M., & Lueptow, R.M. (2025). Granular segregation across flow geometries: A closure model for the particle segregation velocity. *Journal of Fluid Mechanics*, 1016, article number A2. doi: 10.1017/jfm.2025.10360.

[5] Fei, J., Gao, J., Chen, W., Meng, H., Kan, Z., Qi, J., Zhang, B., Huang, L., Li, Z., & Liu, H. (2026). Numerical study of particle conveying mechanism in high-inclination scraper conveyor based on the discrete element method. *Results in Engineering*, 30, article number 110204. doi: 10.1016/j.rineng.2026.110204.

[6] Han, D., Zhang, S., Pan, Y., & Wang, C. (2022). Simulation and experimental research on the wear of synchronous quadruple rotor of an internal mixer during the mixing process. *Engineering Failure Analysis*, 139, article number 106450. doi: 10.1016/j.engfailanal.2022.106450.

[7] Hastie, D.B., Wypych, P.W., & Arnold, P.C. (2010). Influences on the prediction of conveyor trajectory profiles. *Particulate Science and Technology*, 28(2), 132-145. doi: 10.1080/02726350903500633.

[8] Itävuo, P., & Vilkko, M. (2021). Size reduction control in cone crushers. *Minerals Engineering*, 173, article number 107202. doi: 10.1016/j.mineng.2021.107202.

[9] Kyekyere, E., Olakanmi, E.O., Prasad, R.V.S., Matshediso, B., Motimedi, T., Botes, A., & Pityana, S.L. (2024). Analysis of failure characteristics of screen plates of ring hammer crusher used in coal handling applications. *Engineering Failure Analysis*, 162, article number 108351. doi: 10.1016/j.engfailanal.2024.108351.

[10] Laudari, S., Marks, B., & Rognon, P. (2023). Insights on the internal dynamics of bi-disperse granular flows from machine learning. *Granular Matter*, 25(4), article number 73. doi: 10.1007/s10035-023-01357-4.

[11] Levien, R. (2008). *The euler spiral: A mathematical history*. Berkeley: University of California.

[12] Li, J., Lou, J., Li, Y., Pan, S., & Xu, Y. (2023). Trajectory tracking of autonomous vehicle using clothoid curve. *Applied Sciences*, 13(4), article number 2733. doi: 10.3390/app13042733.

[13] Lindqvist, M., & Li, H. (2021). A cone crusher model with a coupled energy- and breakage dependency. *Minerals Engineering*, 172, article number 107147. doi: 10.1016/j.mineng.2021.107147.

[14] Liu, Z., Ma, H., Fan, T., Liu, M., & Zhao, Y. (2022). DEM investigation of the conveyor belt sorting system for coated fuel particles with a large feeding rate. *Powder Technology*, 399, article number 117160. doi: 10.1016/j.powtec.2022.117160.

[15] Meek, D.S., & Walton, D.J. (2004). An arc spline approximation to a clothoid. *Journal of Computational and Applied Mathematics*, 170(1), 59-77. doi: 10.1016/j.cam.2003.12.038.

[16] Ran, K., Wang, Y., Fang, C., Chai, Q., Dong, X., & Liu, G. (2024). Improved RRT* path-planning algorithm based on the clothoid curve for a mobile robot under kinematic constraints. *Sensors*, 24(23), article number 7812. doi: 10.3390/s24237812.

[17] Rhodes, M. (2008). *Introduction to particle technology* (2nd ed.). Hoboken: Wiley. doi: 10.1002/9780470727102.

[18] Rocha, B.K.N., Campos, T.M., Silva, J., & Tavares, L.M. (2024). Fit-for-purpose model of HP500 cone crusher in size reduction of itabirite iron ore. *Minerals*, 14(9), article number 919. doi: 10.3390/min14090919.

[19] Scheffler, O.C., & Coetzee, C. (2023). Discrete element modelling of a bulk cohesive material discharging from a conveyor belt onto an impact plate. *Minerals*, 13(12), article number 1501. doi: 10.3390/min13121501.

[20] Walker, P., Doroszuk, B., & Król, R. (2020). Analysis of ore flow through longitudinal belt conveyor transfer point. *Maintenance and Reliability*, 22(3), 536-543. doi: 10.17531/ein.2020.3.17.

[21] Zuo, Z., Wang, J., Gong, S., & Zhang, J. (2023). Effect of blade configuration on the mixing process of particles in an intensive mixer. *Particulate Science and Technology*, 41(8), 1088-1102. doi: 10.1080/02726351.2023.2177216.

Дослідження можливості сортування крупнокускового матеріалу на конвеєрному тракті підчас його транспортування

Дмитро Пополов
Доктор технічних наук, доцент
Державний університет економіки і технологій
50005, вул. Медична, 16, м. Кривий Ріг, Україна
https://orcid.org/0000-0003-0347-8627

Олександр Учитель
Доктор технічних наук, професор
Державний університет економіки і технологій
50005, вул. Медична, 16, м. Кривий Ріг, Україна
https://orcid.org/0000-0001-6241-1786

Сергій Швед
Кандидат технічних наук, доцент
Державний університет економіки і технологій
50005, вул. Медична, 16, м. Кривий Ріг, Україна
https://orcid.org/0000-0003-2169-8893

Ігор Засельський
Кандидат технічних наук, доцент
Державний університет економіки і технологій
50005, вул. Медична, 16, м. Кривий Ріг, Україна
https://orcid.org/0000-0002-4834-4027

Сергій Генкуленко
Аспірант
Державний університет економіки і технологій
50005, вул. Медична, 16, м. Кривий Ріг, Україна
https://orcid.org/0000-0003-4629-1184

Едуард Гаврилов
Аспірант
Державний університет економіки і технологій
50005, вул. Медична, 16, м. Кривий Ріг, Україна
https://orcid.org/0009-0009-4293-3902

Анотація. У гірничо-металургійній галузі надійність роботи підготовчого обладнання значною мірою визначається однорідністю гранулометричного складу сировини, при цьому наявність поодиноких великокускових включень спричиняє динамічні перевантаження, інтенсивний знос робочих органів і зростання енерговитрат, що обґрунтовує необхідність розробки маловитратних методів їх видалення безпосередньо на транспортних магістралях. Метою роботи було наукове обґрунтування конструкції машини для механічного вилучення великокускових включень з потоку сипкого матеріалу в зоні розвантаження стрічкового конвеєра на основі попередньо розробленої сегрегаційної неоднорідності. У роботі були використані методи математичного моделювання, теоретичної механіки та динаміки матеріальної точки, які дозволили науково обґрунтувати конструкцію сепаруючого пристрою у вигляді обертової стрижневої гребінки, розташованої над розвантажувальним барабаном конвеєра. Було встановлено, що раціональний режим роботи забезпечувався узгодженням лінійної швидкості стрічки та кінематичних параметрів обертання кінців стрижнів, що мінімізувало енергетичні втрати на ковзання. Математично доведено, що профіль стрижня у формі клотоїди забезпечує його занурення в масив матеріалу по нормалі, суттєво знижуючи ударні навантаження. Розроблено комплексну динамічну модель, яка описує три стадії взаємодії: виокремлення частинки з шару, її відносний рух по поверхні стрижня та вільний політ, що дозволило визначити геометричні межі зони розльоту великокускового матеріалу. Це забезпечило точне позиціонування приймальних бункерів та відбійних пластин-дефлекторів для великокускових фракцій. Отримані математичні моделі та геометричні співвідношення дозволяють проектувати ефективні вузли попередньої класифікації на базі існуючих конвеєрних ліній, що забезпечує захист технологічного обладнання від перевантажень без встановлення громіздкого енергоємного обладнання

Ключові слова: стрічковий конвеєр; сегрегація матеріалу; механічне відокремлення; стрижнева гребінка; траєкторія вільного польоту; класифікація фракцій; розвантажувальний вузол

Journal of Kryvyi Rih National University
Journal homepage: https://journal-knu.com.ua/en
Article's History: Received: 17.10.2025 Revised: 06.03.2026 Accepted: 28.04.2026 Published: 29.05.2026
Vol. 24, No. 1, 2026
ISSN 2306-5451
e-ISSN 2519-2736

UDC 622.807:621.928.9+622.445
DOI: 10.31721/2306-5451-2026-1-21-34

Research of the efficiency of the combined operation of dust collection and local ventilation systems during the operation of a heading machine

Yurii Cheberiachko*
Doctor of Technical Sciences, Professor
Dnipro University of Technology
49005, 19 Dmytro Yavornytsky Ave., Dnipro, Ukraine
https://orcid.org/0000-0001-7307-1553

Oleg Mukha
PhD in Technical Sciences, Associate Professor
Dnipro University of Technology
49005, 19 Dmytro Yavornytsky Ave., Dnipro, Ukraine
https://orcid.org/0000-0002-1311-8708

Iryna Lisovytska
PhD in Technical Sciences, Associate Professor
Dnipro University of Technology
49005, 19 Dmytro Yavornytsky Ave., Dnipro, Ukraine
https://orcid.org/0000-0002-9599-3492

Pavlo Saik
Doctor of Technical Sciences, Associate Professor
Dnipro University of Technology
49005, 19 Dmytro Yavornytsky Ave., Dnipro, Ukraine
https://orcid.org/0000-0001-7758-1083

Oleksandr Bednyuk
Postgraduate Student
Dnipro University of Technology
49005, 19 Dmytro Yavornytsky Ave., Dnipro, Ukraine
https://orcid.org/0009-0006-3346-9317

Mykola Khudyk
PhD in Technical Sciences, Associate Professor
Kryvyi Rih National University
50027, 11 Vitalii Matusevich Str., Kryvyi Rih, Ukraine
https://orcid.org/0000-0002-1155-2535

Abstract. Intensive driving of mine workings is accompanied by the extraction of considerable quantities of dust of varying particle sizes. Coarse coal dust, when deposited upon the surfaces of workings and equipment, increases the risk of explosions and fires. Meanwhile, fine-dispersed dust is actively dispersed by ventilation

Suggested Citation:
Cheberiachko, Yu., Mukha, O., Lisovytska, I., Saik, P., Bednyuk, O., & Khudyk, M. (2026). Research of the efficiency of the combined operation of dust collection and local ventilation systems during the operation of a heading machine. *Journal of Kryvyi Rih National University*, 24(1), 21-34. doi: 10.31721/2306-5451-2026-1-24-21-34.

Copyright © The Author(s). This is an open access article distributed under the terms of the Creative Commons Attribution License 4.0 (https://creativecommons.org/licenses/by/4.0/)

*Corresponding author (cheberiachko.yu.i@nmu.one)

airflows, worsening working conditions and contributing to the development of occupational respiratory diseases. The aim of this study was to provide a scientific justification for the effective parameters of the combined operation of local ventilation and dust collection systems for reducing dustiness of the mine atmosphere in blind mine workings. Analytical methods were employed to investigate the processes of mine atmosphere formation in the face area during heading machine operation. It was established that for the order to select optimal solutions that ensure the condition of the mine atmosphere in accordance with regulatory acts, it is necessary to take into account many different parameters (position of the air duct and dust collector relative to the face plane, physical properties of dust, location of the heading machine's cutting head and its operation mode, air velocity in the face area of the workings, etc.). The criteria for the effectiveness of the joint operation of local ventilation and dust collection systems during the operation of a heading machine are substantiated, which take into account the main parameters of the impact on the condition of the mine atmosphere in the face area and allow assessing its quality in order to select optimal solutions that ensure aerological safety and efficiency of the systems. The practical significance of the results is that the obtained efficiency criteria allow determining the optimal positions of dust collecting and ventilation equipment relative to the source of dust generation for their effective use, as well as the optimal aerodynamic parameters in order to improve the quality of the mine atmosphere in the face area of a blind workings

Keywords: dust formation; airflows; rock breaking; working conditions; fine dispersed dust

Introduction

Under conditions of intensive mechanised driving of mine workings, the problem of effectively purifying air withdrawn from the face area of blind workings becomes particularly acute. The increase in dust generation, caused by the high-speed destruction of rock, leads to elevated dust concentrations in the mine atmosphere, which in turn significantly complicates the maintenance of regulatory atmospheric indicators. In such circumstances, the purification of return ventilation air becomes a critical factor in ensuring safe working conditions, minimising occupational risks, and reducing the likelihood of dust-explosive situations. The issue of dust removal assumes special importance during mechanised driving with high-productivity heading machines. In such cases, coarse dust carried away from the face deposits upon the surfaces of workings and mining equipment, thereby worsening the conditions of explosion safety.

Over the past five years, numerous studies have addressed various aspects of this problem, including dust suppression methods, improvements in ventilation systems, and the development of new technologies for effective dust control. The work of H. Sun *et al*. (2023) summarised technologies of dust particle humidification through the use of water-based media. At the same time, as indicated by Q. Liu *et al*. (2025), the application of a transverse air curtain operating on the principle of negative fan pressure represents a promising dust control technology, combining the functions of ventilation and airflow barrier screening. In this context, the study by R. Huang *et al*. (2024), dedicated to modern dust control technologies in coal mines, established that high levels of dust control efficiency are achieved through the optimal integration of ventilation solutions with dust localisation systems, including the use of spray installations, barrier air curtains, and combined humidification methods.

P. Bhukya & K. Bhukya (2024) proposed a hybrid approach to assessing the performance of ventilation systems, combining computer modelling with experimental data in order to optimise airflow in underground coal mines, with particular emphasis on energy efficiency and uniform air distribution. Their study confirmed that the inefficiency of underground mine ventilation is largely attributable to the inadequate design of fans and airways. Such inefficiencies result in excessive energy losses, increased operating costs, and heightened risks to miners' safety. To address these shortcomings, A. Chatterjee *et al*. (2015) advanced an innovative method of regulating the speed of main ventilation fans through the use of variable frequency drives. This approach enables fan operation to be adapted to actual ventilation demand, thereby achieving not only enhanced energy efficiency but also optimised operating costs. The implementation of this technology has been shown to deliver an annual energy saving of approximately 2.54 million kWh.

In the study by J. Brodny & M. Tutak (2020), the level of dust concentration in a heading ventilated by auxiliary systems was analysed. The authors emphasised the importance of auxiliary ventilation in maintaining safe dust levels in underground mining environments. Their findings demonstrated that the ineffective organisation of auxiliary ventilation may lead to elevated dust concentrations, negatively affecting both working conditions and industrial safety. Consequently, it is considered expedient to pursue further research in this direction, particularly with regard to optimising air supply in headings and applying innovative ventilation solutions to reduce dust exposure for workers.

A relevant addition to the above-mentioned issues is the study by Q. Wang *et al*. (2022), in which modern methods of mathematical modelling and simulation were employed to substantiate the geometric parameters of mine ventilation installations. The study carried out a comprehensive analysis of airflow patterns and gas concentration distributions within the mine environment, taking into account diffusion processes that arise when the configurations of ventilation pipelines are altered. Particular attention was given to the influence of ventilation duct placement on the effectiveness of air exchange, and the dependence of ventilation performance on such parameters as airflow velocity, pipeline diameter, and spatial arrangement. The findings possess considerable practical significance, as they enable the optimisation of ventilation schemes in mine workings, thereby ensuring greater efficiency and safety in the operation of ventilation systems in coal mines.

As demonstrated by the results of numerical studies, dust generation processes in the face area are characterised by high complexity and multifactorial interactions. Mathematical and Computational Fluid Dynamics (CFD) modelling has shown that the efficiency of dust suppression systems depends substantially on airflow parameters as well as on the structural and operational characteristics of local dust collection devices (Wei *et al.*, 2020; Zheng *et al.*, 2024). In the study by Y. Li *et al.* (2024), numerical modelling of a two-phase gas-solid flow within the ANSYS Fluent environment was employed to characterise the parameters of ventilation duct positioning. It was established that placing the duct at a distance of 8 m from the face reduced dust concentration to approximately 39 mg/m^3, with an optimal suspension height of 1.5 m. Such a configuration ensured the effective removal of dust from the workers' breathing zone, reducing the likelihood of stagnant vortex zones forming. The numerical experiments further confirmed that excessive proximity of the duct (2-4 m) or increasing its height beyond 2 m resulted in elevated local dust concentrations owing to the secondary resuspension of particles.

The study by J. Liu *et al.* (2013) presented a comprehensive justification of ventilation system parameters based on the application of mathematical modelling methods. The authors emphasised that the rational selection of the cross-sectional area of ventilation roadways is a key factor in reducing both initial capital expenditures for construction and subsequent operating and energy costs of ventilation systems. The developed model, which incorporated capital, operational, and energy expenses, enabled the determination of optimal geometric parameters of mine workings. Application of the least-squares method, with consideration of time-dependent variations in costs, demonstrated that total expenses over a 35-year operational period could be reduced by almost four times compared with the traditional design approach, which relies solely on the limiting values of air velocity. At the same time, the study by B. Yu & L. Shao (2022) focused on energy conservation in the operation of ventilation systems, proposing an enhanced algorithm – Improved Equilibrium Optimiser – for minimising the energy consumption of ventilation networks. Its testing at the Wangjialing mine demonstrated a reduction in the power demand of the main fan by 333 kW (17.83%), thereby confirming the high economic efficiency of the proposed approach.

An analysis of the aforementioned studies indicates that the efficiency of dust collection in mine workings is determined not only by the hydrodynamic parameters of the airflow but also by rational engineering decisions concerning the organisation of ventilation. The integration of CFD-modelling for aerodynamic analysis with mathematical models provides a reliable basis for the development of comprehensive dust control systems that ensure both worker safety and the economic efficiency of mine ventilation. Thus, a scientific problem has emerged, namely the absence of scientifically substantiated solutions concerning the combined operation of dust collection and local ventilation systems during the operation of a heading machine. This necessitates research into the comprehensive study of aerodynamic interactions between ventilation systems, the optimisation of their structural and operational parameters in interrelation, and the adaptation of technical solutions to specific mining and geological conditions. Solving this problem is critically important for ensuring safe working conditions, reducing occupational risks, and achieving regulatory levels of dust concentration in stope faces and development headings.

Accordingly, the aim of this study was to substantiate the parameters of the combined operation of local ventilation and dust collection systems during the driving of development mine workings, taking into account the aerodynamic interaction between ventilation airflows and dust generation processes. Achieving this aim makes it possible to ensure a stable reduction of dust concentration in the mine atmosphere to regulatory levels, to minimise the risks of occupational diseases, and to create safe working conditions in the face areas of blind workings. The development of a scientific justification for effective systems of reducing mine air dustiness, considering the mutual influence of dust collection and local ventilation systems in their combined operation during mechanised driving of blind workings, as well as the adaptation of these systems to modern ventilation schemes and methods in line with dust dynamics, represents the central task of this research.

Materials and Methods

To model the movement of airflows in the face area, modern CAD-software was employed, and the influence of a free turbulent jet issuing from the air duct was analysed. The methodology for determining the parameters of this jet was based on the approach described by O. Mukha *et al.* (2019), subject to the following assumptions: the jet is considered to originate from a pole located at a distance of $X_0 = 0{,}29R_0/a$ from the edge of the supply air duct; the potential core of the jet extends to a length of $X_p = 0{,}96R_0/a$.

The jet boundary was defined according to the formula:

$$Rp = 3{,}4aX. \quad (1)$$

where $X = X_0 + X_c$ – the distance of the jet cross-sections from the “pole”. Within this boundary, integration was carried out for the dependencies describing the distribution across the jet cross-section of momentum and energy of the elementary masses of the dust-air mixture:

$$2\pi\int_0^{Rp}\rho V^2 y\, dy. \quad (2)$$

In accordance with the scheme and the stated assumptions (constant pressure across the cross-sections, linearity of the jet boundary, etc.), the equations of momentum conservation and excess enthalpy retention of the jet were applied for all cross-sections, taking into account the entrainment of ambient air mass. According to the theory of turbulent jets impinging upon a blind end, for $V = V_m[1 - (Y/R_p)^{3/2}]^2$ in a cold jet, the relationship between dimensionless velocity and dimensionless distance along the jet axis was applied, which demonstrates a linear decay of velocity V_m with distance $V_m/V_0 = 0{,}96R_0/aX$ (Tkachenko & Stepanova, 2012). The turbulence constant a, which defines the rate of velocity decay of V_m with distance, was taken as 0.07, corresponding to subsonic airflow conditions. Figure 1 presents a schematic diagram indicating the parameters used in calculating the airflow rate in the face area of a blind working.

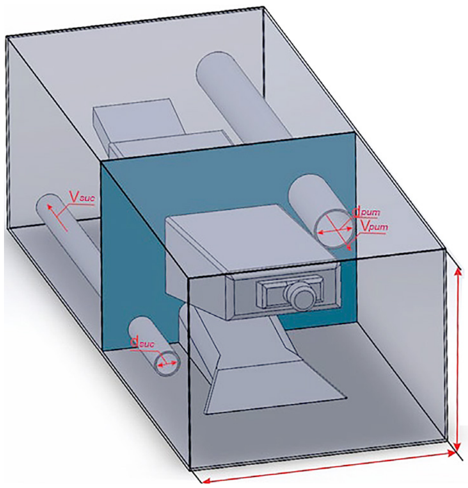

Figure 1. Scheme for determining parameters that affect the quality of the mine atmosphere in the face area of a blind working

Source: developed by the authors

Since the ratio of the quantity of fresh air Q_{pum}, supplied through the pressure pipeline of diameter d_{pum}, to the quantity of air Q_{suc}, extracted by the dust collection system through the suction duct of diameter d_{suc}, has a significant impact on the aerodynamics of ventilation flows in the face area during the combined operation of dust collection and ventilation systems, thereby ultimately determining their efficiency, this ratio was adopted as the efficiency criterion (ventilation criterion), denoted by the letter B:

$$B = \frac{Q_{pum}}{Q_{suc}}. \quad (3)$$

In the absence of recirculation and under conditions of maximum possible extraction of the dust-laden atmosphere, the ventilation criterion B can be defined as follows:

$$B = \frac{Q_{pum}}{Q_{suc}+Q_{p.min}}, \quad (4)$$

where $Q_{p.min.}$ – the minimum air quantity required for ventilation of the working, m^3/s;

$$Q_{pum} = \upsilon_{pum}S_{pum} = \upsilon_{pum}\frac{\pi d_{pum}^2}{4}, \quad (5)$$

where υ_{pum} – is the average air velocity in the pressure duct, m/s; S_{pum} – the cross-sectional area of the pressure duct, m^2; Q_{suc} – the quantity of air extracted by the dust collection system, m^3/s;

$$Q_{suc} = \upsilon_{suc}S_{suc} = \upsilon_{suc}\frac{\pi d_{suc}^2}{4}, \quad (6)$$

where υ_{suc} – the average air velocity at the suction inlet of the dust collector, m/s; S_{suc} – the cross-sectional area of the suction duct of the dust collector, m^2; d_{suc} – the diameter of the suction duct of the dust collector, m.

$$Q_{p.min} = \upsilon_{p.min} \cdot Sp. = \upsilon_{p.min} \cdot (b \cdot h), \quad (7)$$

where $\upsilon_{p.min}$ – the minimum permissible air velocity, m/s; b and h – the width and height of the mine working, m. Thus, the most effective solution is the one that takes into account the ventilation criterion, expressed in the following form:

$$B = \left\{\frac{Q_{pum}}{Q_{suc}+Q_{p.min}}\right\}, \quad (8)$$

or, in an expanded form suitable for use in computer modelling:

$$B = \left\{\frac{\upsilon_{pum}\pi d_{pum}^2}{4\left[\upsilon_{suc}\frac{\pi d_{suc}^2}{4}+\upsilon(b\cdot h)_{p.min}[]\right]}\right\}. \quad (9)$$

The ventilation efficiency criterion for the combined operation of the systems (B) is indirectly dependent on the velocity of the air supplied to the face and on the velocity of the air generated at the suction inlet of the dust collector. The lower the air velocity supplied to the face and the higher the suction velocity of the dust collector, the greater the number of dust fractions captured by the dust collection system. In addition, the mass and diameter of dust particles indirectly influence the efficiency of the dust collector. The greater the particle mass and diameter, the stronger the gravitational force, and consequently, the smaller the proportion of dust particles entering the dust collection system. For the dust collection system installed in the face zone to operate effectively, it is necessary to determine such values of the influencing parameters for which the dust removal efficiency criterion (η_ε) approaches unity and satisfies the requirements of NPAOP 10.0-7.08-93 (1993):

$$\eta_\varepsilon \geq \left(1 - \frac{1}{\varepsilon}\frac{N_p}{N_{da}}\right), \tag{10}$$

where ε – the suction multiplicity, usually taken as $\varepsilon = 0.8$; Np – the permissible dust concentration in the face, mg/m^3; N_{da} – the dust concentration in the face when foam is applied, mg/m^3.

The value of the ventilation criterion (B) must exceed unity by a margin sufficient to satisfy the safety regulations regarding the minimum airflow velocity in the working. The parameters of the initial data influencing the quality of the mine atmosphere, as well as their permissible ranges of variation, are presented in Table 1. The parameters and their ranges of variation were determined in accordance with the requirements established in NPAOP 10.0-1.01-10 (2010).

Table 1. Initial data for airflow modelling

Parameters influencing the quality of the mine atmosphere, the variation of which is possible within the range defined by the designer, and which have little or no impact on the mining technology employed	Distance from the air duct to the face plane	l, m	2.5…8	according to safety regulations, the maximum distance is 8 m
	Diameter of the air duct	d_{pum}, m	0.6	from 0.4 to 1.0 m (standard diameters of air ducts used in mines)
	Diameter of the suction duct of the dust collector	d_{suc}, m	0.5	may be adjusted independently or specified by the manufacturer
	Average air velocity at the suction inlet of the dust collector	υ_{suc}, m/s	11	from 8 to 22
	Average air velocity at the outlet of the air duct	υ_{pum}, m/s	12	from 10 to 12, ranging from the calculated value based on the gas factor to the maximum values defined by the auxiliary ventilation fan
	Density of a single dust particle	ρ_n, kg/m^3	1,400	taken as equal to the density of coal (may be replaced by the density of rocks excavated during driving)
	Number of dust particles of identical shape and substance	$N_{вх}$	100	number of dust particles tracked during calculation (assumed as 100, based on the design velocity)
	Radius of a dust particle	r_n, μm	10 μm	taken from field measurements (or from the actual distribution)
	Molar mass	M_c, kg/kmol	12	standard value for coal
	Initial velocity of dust particle ejection	υ_n, m/s	2	determined by the rotation speed of the cutting unit
	Dust mass flow rate	m_n, kg/s	50	determined according to the established methodology
Fixed parameters	Width of the mine working	b, m	4	parameters of the development heading in accordance with the project
	Height of the mine working	h, m	3.5	parameters of the development heading in accordance with the project
	Minimum permissible airflow velocity in the working	$\upsilon_{p\,min}$, m/s	0.25	according to safety regulations
	Height of the heading machine cutting unit position	Z, m	from 0 to 3.5	from 0 to h
	Minimum permissible airflow velocity in the face area of the working	$\upsilon_{в\,min}$, m/s	0.5	according to safety regulations

Source: developed by the authors based on NPAOP 10.0-1.01-10 (2010)

The efficiency of dust collection in the zone of the heading machine cutting unit is practically zero; therefore, in order to reduce dust concentration in this area, it is necessary to employ an auxiliary dust suppression measure such as foam.

Results and Discussion

On the basis of the results of the calculations performed according to the above methodology, ventilated zones were constructed (zones filled with clean air are shown in green). If the quantity of air supplied to the face (Fig. 2) is significantly greater than the quantity of air extracted by the dust collection system ($Q_{pum}/Q_{suc} > 1$), part of the dust-laden mine air is not captured by the dust collector but is carried further along the mine working by the active airflow.

Clean air supplied through the pressure duct, as well as purified air entering the working after passing through the dust collector and subsequently mixing with the dust-laden stream (shown in yellow) not captured by the dust collector and carried further along the working by the ventilation jet, are shown in green. In this case, ventilation flows are formed that ensure the required air velocity (not less than 0.15 m/s), as prescribed by safety regulations (NPAOP 10.0-1.01-10, 2010). Therefore, this configuration of the combined operation of the ventilation and dust collection systems is positive from the standpoint of occupational hygiene and safety (since such negative factors as airflow recirculation and stagnant zones with zero air velocity are absent). However, in this case, a certain amount of fine dust is dispersed along the entire length of the blind working. The dynamics of ventilation flows in the face zone, which determine the condition of the mine atmosphere both in the face zone and along the entire length of the blind working, depend on the value of the ventilation criterion *B*.

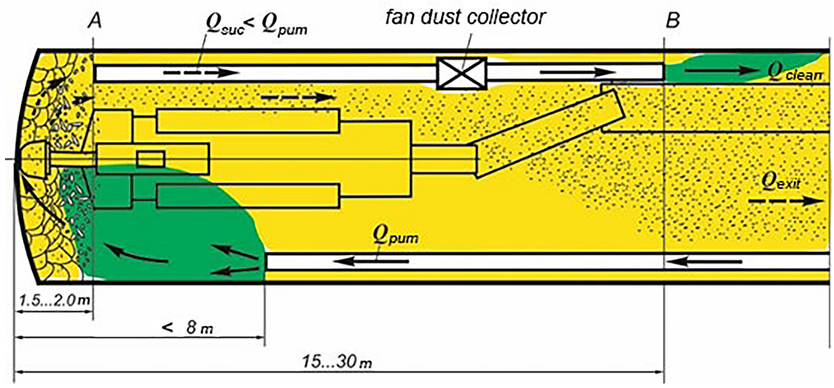

Figure 2. Formation of air movement in the bottomhole space under the condition $Q_{pum} > Q_{suc}$
Source: developed by the authors

If the criterion $B = 1$ (Fig. 3), then all the air supplied to the face is extracted by the dust collection system, and under these conditions the state of the mine atmosphere is determined exclusively by the dust removal efficiency criterion η_ε. The efficiency of dust collection systems lies in the range of 0.7-0.93. If $\eta_\varepsilon = 0.93$, is assumed, then along the entire length of the blind working (starting from the exhaust outlet of the dust collector), the outgoing ventilation stream will be cleaned of fine dust fractions. However, in the section of the face zone from the suction duct of the dust collector to its exhaust outlet, the airflow velocity will be close to zero, meaning that this part of the working is essentially unventilated. As a result, in this space, where electrical equipment is present and no methane monitoring by stationary sensors of the automatic gas control system is provided, a stagnant zone (shown in red) is formed, in which there is a high probability of an increase in methane concentration (local stratified accumulations). This factor is particularly critical for gaseous mines. For non-gaseous mines, this part of the face zone represents discomfort in terms of climatic conditions (Fig. 3).

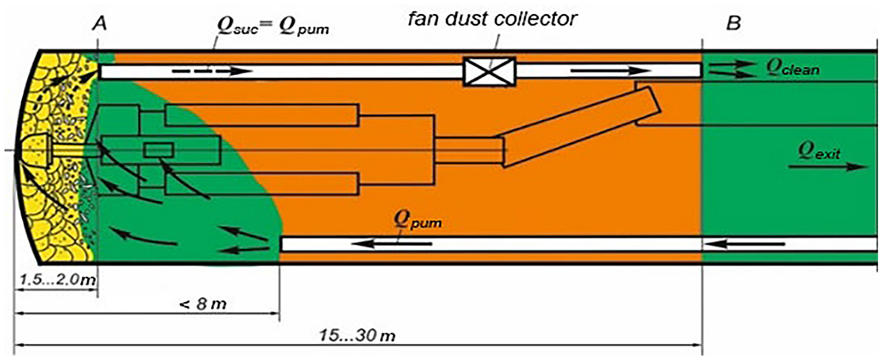

Figure 3. Formation of air movement in the bottomhole space
Notes: provided that $Q_{pum} = Q_{suc}$
Source: developed by the authors

If $B < 1$ (i.e., the dust collector's flow rate exceeds the volume of air entering the working face) (Fig. 4), the dust extraction system will draw not only the air from the immediate face area but also a portion of the air exiting the dust collector's discharge, thereby causing air recirculation.

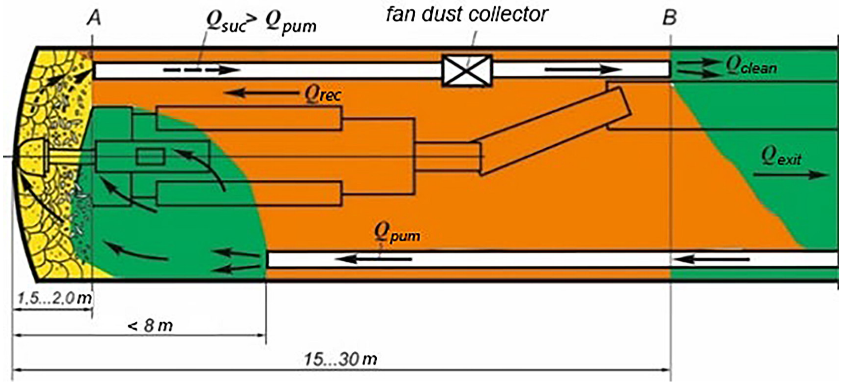

Figure 4. Formation of air movement in the bottomhole space

Notes: provided that $Q_{pum} < Q_{suc}$

Source: developed by the authors

In this case, as in the previous one, air dust removal will be virtually 100 %. However, due to the phenomenon of recirculation, methane concentrations in the space between sections *A* and *B* may be elevated. To enhance the efficiency of the combined operation of dust extraction and ventilation systems, an air supply scheme in the immediate face area may be employed. Provided that $B > 1$, the formation of mine air flow in the immediate face area under this scheme is illustrated in Figure 5.

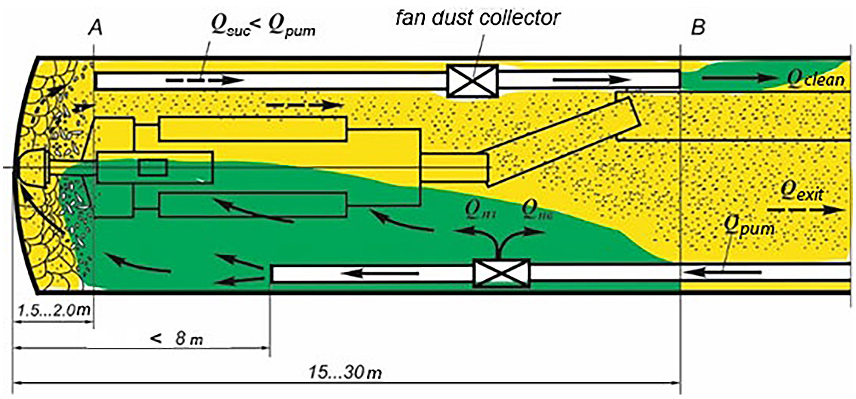

Figure 5. Formation of air movement in the bottomhole space when using a scheme with air refreshment

Notes: provided that $B > 1$

Source: developed by the authors

The introduction of fresh air into the working face through a lateral inlet in the supply duct results in a substantial expansion of the ventilated zone in the immediate face area, thereby improving the atmospheric conditions at the workplace. When employing this fresh air distribution scheme under conditions where $B \approx 1$, the stagnant zone (depicted in red) (Fig. 6) and the recirculation zone (Fig. 7) are significantly reduced.

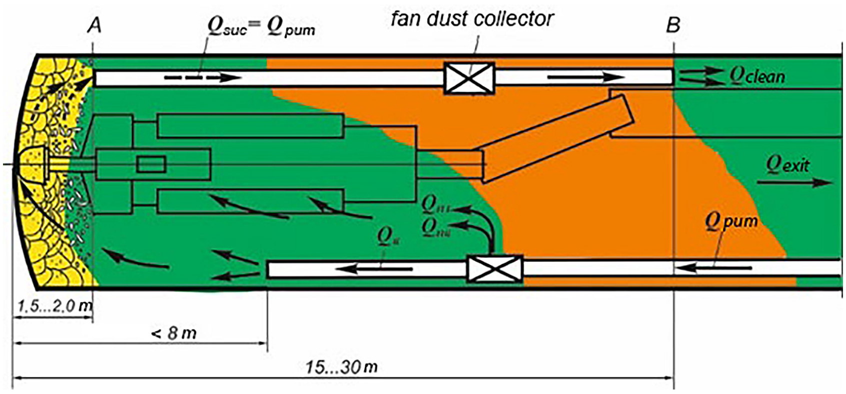

Figure 6. Formation of air movement in the bottomhole space when using a scheme with air refreshment

Notes: provided that $B = 1$

Source: developed by the authors

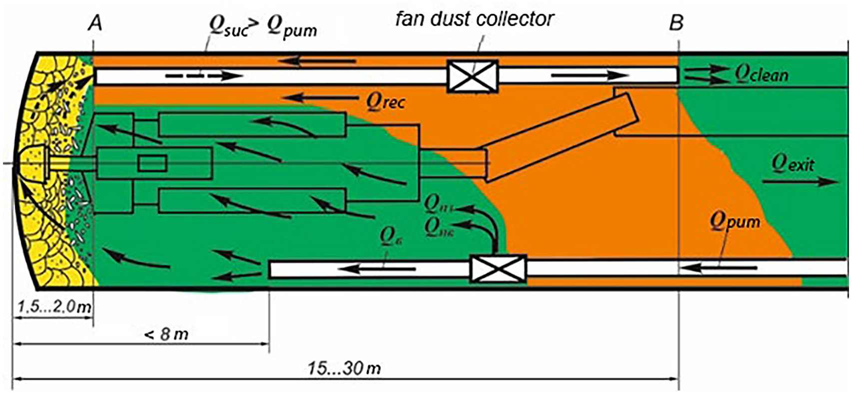

Figure 7. Formation of air movement in the bottomhole space when using a scheme with air refreshment

Notes: provided that $B < 1$

Source: developed by the authors

Figures 8 and 9 illustrate variants of the combined operation of the ventilation and dust extraction systems, depending on their relative arrangement and the "ventilation criterion" *B*. Figure 8 demonstrates that the safest configurations for the combined operation of dust extraction and ventilation systems occur when the ventilation criterion *BBB* exceeds unity. Aerodynamic analysis indicates that in these configurations, hazardous phenomena such as air flow recirculation and stagnant zones, where air movement approaches zero, do not arise. Figure 9 shows that, when employing an air supply scheme into the working face, the zones of the immediate face area with active ventilation are significantly expanded, while conversely, hazardous zones in which air flow recirculation and stagnant areas may occur are substantially reduced. Analysis of the combined operation of dust extraction and ventilation systems indicates that the dust collector will operate effectively only if the condition $Q_{pum}/Q_{suc} > 1$ is satisfied (i.e., the dust collector's flow rate is less than the volume of air entering the working face). An increase in the air volume supplied to the face will lead to dust being carried away without entering the dust collector. Therefore, the difference between the parameters Q_{pum} and Q_{suc} should be minimal. This value is determined in accordance with safety regulations, which require maintaining air movement in the mine working at a minimally permissible velocity. According to NPAOP 10.0-7.08-93 (1993), the air velocity in the immediate face area is taken as 0.5 m/s (for an air temperature of +24°C and relative humidity of 80%). The minimum air velocity in the mine working is 0.25 m/s.

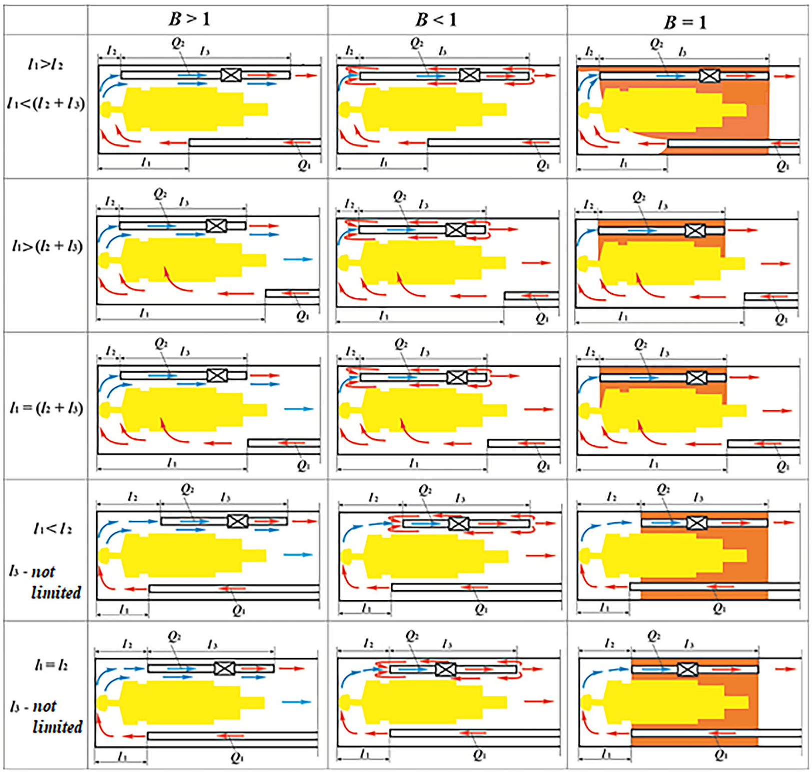

Figure 8. Variants of joint operation of ventilation and dust collection systems depending on the mutual location of these systems and the "ventilation criterion" *B* in a scheme without air freshening

Source: developed by the authors

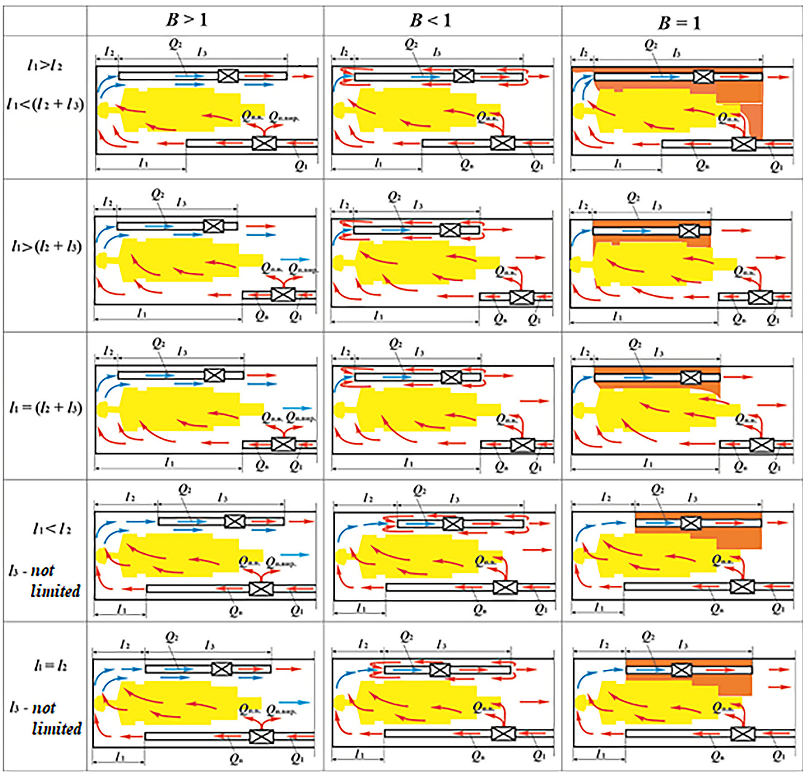

Figure 9. Variants of joint operation of ventilation and dust collection systems depending on the mutual location of these systems and the "ventilation criterion" *B* in the scheme with air refreshment

Source: developed by the authors

Among the variants considered, the most effective configuration, in terms of the relative arrangement of the systems, is that in which the distance from the face to the end of the supply duct exceeds the combined length of the dust collector and the distance from the face to the inlet of its suction pipe, i.e., when:

$$l_1 > (l_2 + l_3) \tag{11}$$

where l_1 – the distance from the face to the end of the supply duct, m; l_2 – the distance from the face to the inlet of the suction pipe, m; l_3 – the length of the dust collector, m. The results of the conducted study allow for the effective selection of optimal solutions to ensure the atmospheric conditions in the mine in accordance with regulatory requirements.

Calculations performed using the proposed methodology enabled the construction of ventilation zones, which are critically important for ensuring the safety and efficiency of ventilation systems in mines. Zones filled with clean air are depicted in green, indicating effective ventilation. The dynamics of air flows in the immediate face area largely depend on the value of the ventilation criterion B. When $Q_{pum}/Q_{suc} > 1$, ventilation flows are established that provide the required air velocity (not less than 0.15 m/s), in compliance with safety regulations. However, in this case, a certain amount of fine dust is dispersed along the full length of the dead-end working. When the criterion $B = 1$, all air supplied to the face is captured by the dust extraction system, resulting in the formation of stagnant zones with zero air velocity. This creates a high risk of elevated methane concentrations, which is particularly hazardous in gas-bearing mines. When $B < 1$, air recirculation occurs, which can also lead to increased methane concentrations in specific zones.

The implementation of an air supply scheme into the immediate face area significantly improves the atmospheric conditions in the mine. The introduction of fresh air through a lateral inlet in the supply duct expands the ventilated zone in the immediate face area. This reduces stagnant and recirculation zones, thereby enhancing working conditions and safety. The most effective configuration for the combined operation of ventilation and dust extraction systems is that in which the distance from the face to the end of the supply duct exceeds the combined length of the dust collector and the distance from the face to the inlet of its suction pipe (11). This arrangement ensures maximum ventilation efficiency and minimises the risk of hazardous zones forming. X. Yang *et al.* (2024) employed orthogonal numerical modelling to optimise ventilation and dust removal parameters in inclined mines with ultra-long tunnels. They demonstrated that advanced modelling techniques, such as CFD, combined with hybrid technical solutions, substantially improve occupational safety and reduce dust accumulation under complex mining conditions. However, optimisation models based on advanced methods like CFD do not fully address the removal of the fine dust fraction from the air in the immediate face area.

G. Li *et al.* (2020) investigated the significant increase in dust levels in mechanised roadway faces and analysed the effectiveness of localised dust extraction as a supplement to conventional supply ventilation. They noted that standard ventilation systems do not always achieve adequate air purification, particularly under conditions of intensive dust generation, typical of modern mechanised faces. Consequently, the implementation of combined ventilation solutions is recommended, including the use of local filtration units directly at dust sources, which effectively reduce the concentration of harmful particulates in the air and enhance worker protection in high-risk zones. The effectiveness of local filtration units at dust sources is primarily achieved through the substantial reduction of coarse dust fractions, but it is less effective for respirable dust compared with local suction dust (dust extraction).

Yu. Cheberyachko *et al.* (2024) proposed a mathematical model of the dust generation process occurring during rock fragmentation by the cutting head of a heading machine. The model allows for determining the distribution of dust fractions across the cross-section and along the length of the mine working, taking into account the velocity of the ventilation flow and the distance over which different dust particles settle. This enables a better assessment of dust transport dynamics within the mine atmosphere and supports the development of more effective dust extraction strategies. Particular attention must be paid to the insufficient interaction between dust extraction and local ventilation systems. The mutual influence of these systems is often neglected, which can lead to a significant reduction in their efficiency, local dust accumulation, and potentially hazardous situations. Furthermore, this increases the risk of fibrogenic lung diseases among miners working in areas with high dust concentrations. However, the proposed mathematical model of dust generation does not allow for the investigation of aerodynamic processes necessary to justify the placement parameters of ventilation and dust extraction systems under conditions of their mutual influence on the ventilation regime.

Based on the research of P. Vrtalova *et al.* (2023), effective strategies for managing ventilation flows have been developed to ensure safe working conditions and the continuity of mining operations in the Ostrava-Karviná district (Czech Republic). The proposed approaches take into account the specific geological and mining conditions and allow for the regulation of air distribution within the workings, which is critically important for the effective functioning of the ventilation system and the reduction of extraction-related risks.

However, it should be noted that the primary function of the ventilation system is the dilution and removal of harmful air contaminants from the immediate face area, particularly through the implementation of combined ventilation and dust extraction systems.

P. Wang *et al*. (2020), using CFD-based numerical modelling, substantiated the optimal parameters for the placement of ventilation ducts in fully mechanised working faces. The modelling results demonstrated a significant improvement in dust dispersion control and an enhancement of air exchange efficiency within the working area. This confirms the potential of computer modelling for optimising engineering solutions in ventilation systems and highlights the need for further research aimed at improving ventilation while taking into account the spatial characteristics of extraction and development faces. However, optimisation of engineering solutions in ventilation systems does not address the issue of respirable dust entering the immediate face area of dead-end workings, which necessitates the implementation of dust extraction systems to mitigate its presence.

Despite numerous studies aimed at reducing dust levels, improving ventilation, and deploying local dust extraction units, the problem of integrating these systems into a single, coordinated ventilation and dust extraction complex remains unresolved. Research conducted by Z. Qian *et al*. (2020) and X. Lu *et al*. (2025) indicates that the interaction between dust extraction and local ventilation systems is often overlooked during design and operation. This leads to a reduction in the overall effectiveness of both systems, localised dust accumulation in the faces, recirculation of dust flows in the area of the heading machine, as well as an increased risk of accidents and the development of occupational respiratory diseases among workers.

The study systematically analysed the combined operation of ventilation and dust extraction systems depending on their relative arrangement, based on the ventilation criterion proposed for the first time. This criterion characterises the relationship between the volume of fresh air supplied through the supply duct and the volume of air extracted by the dust extraction system. The proposed criterion enables a quantitative assessment of the efficiency of integrated systems and the determination of optimal conditions for their interaction in various configurations of the working face.

Conclusions

When using modern dust extraction systems in conjunction with localised ventilation, their mutual influence must be considered. Accounting for this interaction can significantly enhance system efficiency, prevent hazardous situations, and markedly reduce the risk of occupational diseases caused by the fibrogenic effects of fine dust. This article examined potential impacts of the combined operation of dust extraction and local ventilation systems on the quality of the mine atmosphere in the immediate face area of dead-end workings during heading machine operations. It was established that certain aerological conditions may arise in the immediate face area under the combined operation of these systems, provoking hazardous phenomena. Such phenomena include the recirculation of ventilation flows and near-zero air velocities, which substantially deteriorate safety levels and the occupational hygiene conditions for miners.

Based on the conducted research, a criterion for air purification from dust was developed. The value of this criterion directly affects the concentration of fine dust in the outgoing ventilation flow. Additionally, a ventilation criterion was established, which determines the dynamics of ventilation flows in the immediate face area. This criterion defines the atmospheric conditions in the immediate face area. It has been demonstrated that the efficiency criteria for the combined operation of dust extraction and local ventilation systems can be employed in the design of effective systems. These systems ensure a high level of mine air quality.

The research further provided recommendations for the optimal placement of ventilation equipment. The use of variable-frequency drives for main ventilation units can result in significant energy savings – up to 2.54 million kWh per year. Moreover, the rational selection of cross-sectional dimensions of mine workings can reduce overall energy consumption nearly fourfold over 35 years of operation. Modelling results show that the optimised algorithm allowed for a reduction of the main fan power by 333 kW, which represents 17.83% of total consumption. These findings indicate that the proper selection of equipment and parameters-such as positioning the supply duct 8 m from the face at a height of 1.5 m, is critical for minimising dust concentrations to 39 mg/m^3 and ensuring occupational safety in accordance with regulatory requirements, which establish a minimum air velocity of 0.25 m/s in the working and 0.5 m/s in the immediate face area.

Implementing these measures ensures a high quality of the mine atmosphere at workplaces in the immediate face area of dead-end workings during core technological operations. Adherence to these recommendations will enhance safety and comfort for miners while reducing the risk of occupational diseases. Prospects for further research include the development of innovative dust extraction and ventilation technologies, automation of their monitoring and control, and improvement of ventilation equipment designs. Special attention should be given to creating methodologies for assessing and forecasting mine atmospheric conditions to further improve occupational safety and comfort.

Acknowledgements

The authors express their gratitude to the administrations of NTU "Dnipro Polytechnic" and Kryvyi Rih National University for providing the opportunity to conduct this research.

Funding

None.

Conflict of Interest

None.

References

[1] Bhukya, P., & Bhukya, K. (2024). Enhancing ventilation fan performance in underground coal mines: A hybrid approach. *Electrical Engineering*, 106, 4969-4992. doi: 10.1007/s00202-024-02268-0.

[2] Brodny, J., & Tutak, M. (2020). Analysis of dustiness state in a driven underground dog heading ventilating by auxiliary air-duct. *Management Systems in Production Engineering*, 28(2), 73-77. doi: 10.2478/mspe-2020-0011.

[3] Chatterjee, A., Zhang, L., & Xia, X. (2015). Optimization of mine ventilation fan speeds according to ventilation on demand and time of use tariff. *Applied Energy*, 146, 65-73. doi: 10.1016/j.apenergy.2015.01.134.

[4] Cheberyachko, Yu., Mukha, O., Shustov, O., & Bednyuk, O. (2024). Analysis of the processes of dust formation and spread during the operation of a mining combine harvester in a dead-end production. *Collection of Research Papers of the National Mining University*, 76, 115-126. doi: 10.33271/crpnmu/76.115.

[5] Huang, R., Tao, Y., Chen, J., Li, S., & Wang, S. (2024). Review on dust control technologies in coal mines of China. *Sustainability*, 16(10), article number 4038. doi: 10.3390/su16104038.

[6] Li, G., Hu, J., Hao, X., & Qu, H. (2020). Application and research of swirling curtain dust collection technology in mines. *Applied Sciences*, 10(6), article number 2005. doi: 10.3390/app10062005.

[7] Li, Y., Wang, J., Li, Z., & Mo, H. (2024). Dust concentration distribution and analysis of influencing factors in the heading face of Shangwan coal mine. *Frontiers in Earth Science*, 12, article number 1512101. doi: 10.3389/feart.2024.1512101.

[8] Liu, J., Yang, P., & Lv, W.S. (2013). Energy saving in mine ventilation roadway and its optimization model solving. *Advanced Materials Research*, 868, 291-295. doi: 10.4028/www.scientific.net/amr.868.291.

[9] Liu, Q., Liu, S., Zheng, M., Nie, W., & Yan, Y. (2025). Study on the multifactor parametric of a transverse air curtain dust control technology during tunnel boring. *Powder Technology*, 465, article number 121281. doi: 10.1016/j.powtec.2025.121281.

[10] Lu, X., Xiao, J., Miao, J., Chen, Z., & Wang, S. (2025). Study on the mining dust release behavior under the top coal continuous caving coupling the dynamic hydraulic support advancing. *Process Safety and Environmental Protection*, 195, article number 106755. doi: 10.1016/j.psep.2025.01.009.

[11] Mukha, O., Cheberiachko, Y., Sotskov, V., & Kamulin, A. (2019). Studying aerodynamic resistance of a stope involving CAD packages modeling. *E3S Web of Conferences*, 123, artcle number 01048. doi: 10.1051/e3sconf/201912301048.

[12] NPAOP 10.0-1.01-10. (2010). *Safety regulations in coal mines*. Retrieved from https://dnaop.com/html/54542/doc-%D0%9D%D0%9F%D0%90%D0%9E%D0%9F_10.0-1.01-10.

[13] NPAOP 10.0-7.08-93. (1993). *Guidelines for the design of ventilation in coal mines*. Retrieved from https://online.budstandart.com/ua/catalog/doc-page.html?id_doc=47105.

[14] Qian, Z., Wang, J., & Hu, L. (2020). CFD modeling of ventilation and dust removal in coal mines with wet suppression systems. *International Journal of Environmental Research and Public Health*, 17(16), article number 6006. doi: 10.3390/ijerph17166006.

[15] Sun, H., Liu, Y., Jiang, T., Liu, T., & Liu, D. (2023). Application of dust control method based on water medium humidification in tunnel drilling and blasting construction environment. *Building and Environment*, 234, article number 110111. doi: 10.1016/j.buildenv.2023.110111.

[16] Tkachenko, S., & Stepanova, D. (2012). *Hydrohydrodynamics (examples and tasks)*. Vinnytsia: VNTU.

[17] Vrtalova, P., Palicka, D., Hrinko, M., & Bubnik, J. (2023). Ventilation of the Ostrava-Karvina coal mine in order to ensure the operation and extraction during mining in the Czech Republic. In *Proceedings of the 23rd international multidisciplinary scientific geoconference-SGEM 2023: Modern management of mine producing, geology and environmental protection, book 1.1* (pp. 495-502). Albena: STEF92 Technology. doi: 10.5593/sgem2023/1.1/s03.60.

[18] Wang, P., Gao, R., Liu, R., & Yang, F. (2020). CFD-based optimization of the installation location of the wall-mounted air duct in a fully mechanized excavation face. *Process Safety and Environmental Protection*, 141, 234-245. doi: 10.1016/j.psep.2020.04.049.

[19] Wang, Q., Zhang, X., & Sun, H. (2022). Configuration and selection of surfactant for coal powder in Xinxing coal mine. *Integrated Ferroelectrics*, 226(1), 63-71. doi: 10.1080/10584587.2022.2061193.

[20] Wei, J., Xu, X., & Jiang, W. (2020). Influences of ventilation parameters on flow field and dust migration in an underground coal mine heading. *Scientific Reports*, 10(1), article number 8973. doi: 10.1038/s41598-020-65685-4.
[21] Yang, X., Jiang, Z., Chen, J., Chen, Y., & Yang, B. (2024). Optimization of ventilation and dust removal parameters in plateau extra-long tunnel inclined shaft based on orthogonal numerical simulation test method. *Construction and Building Materials*, 455, article number 139131. doi: 10.1016/j.conbuildmat.2024.139131.
[22] Yu, B., & Shao, L. (2022). A mine ventilation system energy saving technique based on an improved equilibrium optimizer. *Frontiers in Energy Research*, 10, article number 913817. doi: 10.3389/fenrg.2022.913817.
[23] Zheng, H., Jiang, B., Wang, H., & Zheng, Y. (2024). Experimental and numerical simulation study on forced ventilation and dust removal of coal mine heading surface. *International Journal of Coal Science & Technology*, 11, article number 13. doi: 10.1007/s40789-024-00667-z.

Дослідження ефективності сумісної роботи систем пиловловлювання і вентиляції місцевого провітрювання при роботі прохідницького комбайна

Юрій Чеберячко

Доктор технічних наук, професор
Національний технічний університет «Дніпровська політехніка»
49005, просп. Дмитра Яворницького, 19, м. Дніпро, Україна
https://orcid.org/0000-0001-7307-1553

Олег Муха

Кандидат технічних наук, доцент
Національний технічний університет «Дніпровська політехніка»
49005, просп. Дмитра Яворницького, 19, м. Дніпро, Україна
https://orcid.org/0000-0002-1311-8708

Ірина Лісовицька

Кандидат технічних наук, доцент
Національний технічний університет «Дніпровська політехніка»
49005, просп. Дмитра Яворницького, 19, м. Дніпро, Україна
https://orcid.org/0000-0002-9599-3492

Павло Саїк

Доктор технічних наук, доцент
Національний технічний університет «Дніпровська політехніка»
49005, просп. Дмитра Яворницького, 19, м. Дніпро, Україна
https://orcid.org/0000-0001-7758-1083

Олександр Беднюк

Аспірант
Національний технічний університет «Дніпровська політехніка»
49005, просп. Дмитра Яворницького, 19, м. Дніпро, Україна
https://orcid.org/0009-0006-3346-9317

Микола Худик

Кандидат технічних наук, доцент
Криворізький національний університет
50027, вул. Віталія Матусевича, 11, м. Кривий Ріг, Україна
https://orcid.org/0000-0002-1155-2535

Анотація. Інтенсивна проходка гірничих виробок супроводжується виділенням великої кількості пилу різної дисперсності. Крупний вугільний пил, осідаючи на поверхнях гірничих виробок і обладнання може підвищувати небезпеку вибухів та пожеж. При цьому, дрібнодисперсний пил активно поширюється вентиляційними струменями, погіршує умови праці на робочих місцях і сприяє розвитку професійних захворювань органів дихання. Метою було наукове обґрунтування ефективних параметрів сумісної роботи систем вентиляції місцевого провітрювання і пиловловлювання для зниження запиленості рудникової атмосфери тупикових гірничих виробок. У роботі використано аналітичні методи для дослідження процесів формування рудникової атмосфери у привибійному просторі при роботі прохідницького комбайна. Встановлено, що для вибору оптимальних рішень, які забезпечують стан рудникової атмосфери згідно з нормативними актами, необхідно враховувати багато різних параметрів (положення повітроводу і пиловловлювача відносно площини забою, фізичні властивості пилу, місцезнаходження виконавчого органу комбайна і режим його роботи, швидкість руху повітря в привибійному просторі виробки, тощо). Обґрунтовані критерії ефективності сумісної роботи систем вентиляції місцевого провітрювання і пиловловлювання при роботі прохідницького комбайну, які враховують основні параметри впливу на стан рудникової атмосфери у привибійному просторі та дозволяють оцінити її якість з метою забору оптимальних рішень, що забезпечують аерологічну безпеку та ефективність роботи систем. Практичне значення отриманих результатів полягає в тому, що отримані критерії ефективності дозволяють визначити оптимальні положення пиловловлюючого і вентиляційного обладнання відносно джерела пилоутворення для їх ефективного використання, а також оптимальні аеродинамічні параметри, з метою підвищення якості рудникової атмосфери у привибійному просторі тупикової виробки

Ключові слова: пилоутворення; повітряні течії; відбійка гірських порід; умови праці; дрібнодисперсний пил

Journal of Kryvyi Rih National University
Vol. 24, No. 1, 2026
Journal homepage: https://journal-knu.com.ua/en
ISSN 2306-5451
e-ISSN 2519-2736
Article's History: Received: 24.09.2025 Revised: 10.03.2026 Accepted: 28.04.2026 Published: 29.05.2026

UDC 004.8
DOI: 10.31721/2306-5451-2026-1-24-35-53

Comparative analysis of machine learning models for retail demand forecasting considering promotional activity and seasonality

Nataliya Boyko*

PhD in Economic Sciences, Associate Professor
Lviv Polytechnic National University
79000, 12 Stepan Bandera Str., Lviv, Ukraine
Stepan Gzhytskyi National University of Veterinary Medicine and Biotechnologies Lviv
80381, 1 V. Velykyi Str., Dubliany, Ukraine
https://orcid.org/0000-0002-6962-9363

Arsen Dolichnyi

Student
Lviv Polytechnic National University
79000, 12 Stepan Bandera Str., Lviv, Ukraine
https://orcid.org/0009-0008-1605-7382

Abstract. The relevance of the study is driven by the complexity of modelling consumer behaviour in an unstable market environment, where forecast accuracy directly impacts inventory optimisation and the reduction of logistical costs. The aim of this study was to develop and substantiate an AI-based intelligent system for demand forecasting and procurement optimisation in retail, ensuring consistent product availability while simultaneously reducing excess inventory and waste. The research methodology was based on a rigorous time-based data split, which allows for evaluating the models' generalisation ability in a realistic "train on the past, test on the future" scenario. To establish a robust point of reference, a hierarchy of baseline benchmarks was developed, including naive forecasts and models with weekly lags. The study conducted a comparative analysis of Ridge linear regression, the Random Forest ensemble method, and gradient-boosted decision trees (XGBoost, LightGBM). Experimental results confirmed a significant advantage of non-linear models over traditional linear approaches, which fail to adequately reproduce threshold effects and complex interactions between promotions and seasonality. It was established that the LightGBM model demonstrates the best stability and accuracy metrics, ensuring minimal error on the validation set while maintaining resistance to overfitting. Specifically, it was found that XGBoost's high efficiency on training data is often a result of over-adaptation to noise, making LightGBM more suitable for practical business applications. The practical significance of the findings lies in the potential for automating procurement processes, ensuring balanced inventory levels and increasing the economic efficiency of retail networks

Keywords: predictive analytics; feature engineering; gradient boosting; time series; mean absolute error; root mean squared error; business analytics

Introduction

The modern retail market is characterised by an extremely high level of dynamism and uncertainty, which places stringent demands on the accuracy of procurement planning processes. The core problem lies in the

Suggested Citation:
Boyko, N.,& Dolichnyi, A. (2026). Comparative analysis of machine learning models for retail demand forecasting considering promotional activity and seasonality. *Journal of Kryvyi Rih National University*, 24(1), 35-53. doi: 10.31721/2306-5451-2026-1-24-35-53.

Copyright © The Author(s). This is an open access article distributed under the terms of the Creative Commons Attribution License 4.0 (https://creativecommons.org/licenses/by/4.0/)

*Corresponding author (nataliya.i.boyko@gmail.com)

fact that traditional inventory management approaches often prove incapable of adequately responding to sharp fluctuations in consumer demand driven by seasonal factors, the intensity of marketing activities, and the local specifics of individual retail outlets. In product categories with short shelf lives, any forecasting error inevitably leads to significant financial losses: either through stockouts, which result in lost sales and reduced customer loyalty, or through overstocking, which translates into direct losses from the disposal of spoiled goods. The situation is further complicated by the fragmentation of corporate data, where the lack of an integrated connection between sales history, inventory levels, and promotional plans hinders the formation of a unified decision-making cycle. Thus, there is a critical need to transition from manual reactive management to the creation of intelligent systems capable of automating order generation based on probabilistic analysis of large datasets. The relevance of this study is determined by the necessity to develop such integrated solutions that allow for maintaining an optimal balance between service levels and the minimisation of total costs for retail chains in real-time.

Modern retail operates in an environment of high demand volatility, necessitating a transition from traditional planning methods to sophisticated decision support systems. As noted by S. Moret *et al.* (2020), strategic planning under uncertainty requires the development of robust optimisation frameworks capable of integrating large datasets. This is particularly relevant for the retail industry, where multivariate time series (including prices, promotions, and external factors) form the basis for comparative analysis of forecasting models, according to M. Haque *et al.* (2023). The implementation of artificial intelligence (AI) has already demonstrated its effectiveness in the Ukrainian banking sector, as researchers V. Solodkyi & Yu. Polichuk (2023) highlighted, yet in retail, the primary challenge lies in handling high-dimensional data and identifying anomalies in consumer behaviour.

To ensure forecast accuracy, the use of hybrid architectures, such as CNN-LSTM, which the researchers A. Agga *et al.* (2022) and A. Djaafari *et al.* (2022) successfully applied for short-term forecasting in energy sectors, is critical and can be adapted to model sales dynamics. Furthermore, according to H. Xie *et al.* (2022), time-series analysis based on multi-granularity neighbour residual networks allows for the efficient detection of deviations caused by sharp changes in market conditions. A separate aspect is the digitalisation of the economy and the formation of "smart" management systems. The researcher I. Uninets (2021) noted that the subjective disposition of the smart economy emphasises the role of intelligent systems in transforming business processes. Specifically, researchers Yu. Yan *et al.* (2024) suggested that the use of multi-criteria decision-making (MCDM) methods and fuzzy logic allows for balancing sustainability goals with economic efficiency. In resource-constrained environments, according to K. Bülbül & N. Noyan (2021), multi-stage stochastic programming models help optimise resource provisioning, which is highly relevant for logistics and warehouse inventory management.

Modern forecasting approaches also include ensemble learning methods. Researchers B.A. Tama & S. Lim (2021) and M. Rashid *et al.* (2022) concluded that using tree-based stacking ensembles provides higher stability of results compared to single models. This allows not only for predicting sales volumes but also for assessing risks (Expected Shortfall), which A.-P. Fortin *et al.* (2023) noted is crucial for financial procurement planning. However, despite a significant number of theoretical developments, practical implementation experience in 2024-2025 indicates that the primary source of inefficiency remains data fragmentation. The disconnect between sales records, actual inventory levels, and marketing activity plans (promotions) prevents the establishment of a transparent decision-making cycle. The aim of this research was to develop and substantiate an AI-driven system for demand forecasting and procurement optimisation that ensures stable product availability on shelves while simultaneously reducing excess stock and write-offs.

Materials and Methods

Dataset preparation and mathematical formalisation of the forecasting task

The research employed a multi-level methodology, integrating data mining, mathematical modelling, and robust optimisation to build a decision support system for retail procurement. The study utilises the "Corporación Favorita" dataset (Corporación Favorita grocery..., 2017), which provided granular "store-item-day" records, including sales history, promotions, product attributes, store characteristics, transaction flows, and macroeconomic indicators. To ensure computational efficiency, the 125-million-record dataset was systematically sub-sampled. The scope was restricted to high-turnover "Produce" and "Dairy" categories within the Quito metropolitan area over a 24-month period. This duration allowed for the identification of seasonality and trends while minimising logistical noise. To prevent data leakage and simulate real-world conditions, a chronological partition was applied: 21 months for training, 2 months for hyperparameter tuning, and 1 month for final evaluation. This high-density dataset supports the implementation of advanced machine learning ensembles and optimisation algorithms, enabling the formalisation of the forecasting task as a su pervised learning problem within a multi-dimensional state space.

To formalise the training and optimisation processes, the dataset was to be represented as a tensor of observations. Let $S = \{s_1, s_2, \dots, s_n\}$ be the set of stores and

$I = \{i_1, i_2, ..., i_m\}$ be the set of items. To describe each data point at time $t \in \{1, ..., T\}$, the following vectors are to be defined. For each object $j = (s, i)$ at time t (1):

$$V_{j,t} = \langle y_{j,t}, p_{j,t} \rangle, \quad (1)$$

where $y_{j,t} \in \mathbb{R}$ is the sales volume (*unit_sales*); $p_{j,t} \in \{0,1\}$ is the promotion indicator (*onpromotion*). Attributes that do not change over time, but determine categorical affiliation (2):

$$C_j = \langle fam_j, per_j, city_s, type_s, clu_s \rangle, \quad (2)$$

where *fam* is the product family; *per* is the perishability; *clu* is the store cluster. Variables common to many objects at time t (3):

$$E_t = \langle o_t, tr_{s,t}, h_t \rangle, \quad (3)$$

where o_t is the oil price; $tr_{s,t}$ is the transaction count for store s; $h_t \in \{0,1\}$ is the holiday/event flag. The common input vector for the machine learning model $X_{j,t}$ is formed by concatenating the lag values of the target variable, static characteristics, and external factors (4):

$$X_{j,t} = \left[\underbrace{y_{j,t-1}, \dots, y_{j,t-k}}_{Lags}, \underbrace{MA_{j,t,w}}_{Moving\ Averages}, C_j, p_{j,t}, E_t \right], \quad (4)$$

where $MA_{j,t,w}$ is the moving average over the window w. Thus, the forecasting problem is reduced to finding the approximating function f (5):

$$\hat{y}_{j,t+1} = f(X_{j,t}; \Theta), \quad (5)$$

where Θ is the vector of model parameters that minimises the loss function over the entire "store-item-day" space. By consolidating these heterogeneous variables into a structured feature matrix, a comprehensive digital representation of the retail environment is achieved. This mathematical formalisation ensured that the machine learning models receive not only historical sales data but also the crucial contextual information – ranging from local holidays to global economic indicators – that drives consumer behaviour. The transformation of raw records into a unified tensor of observations $X_{j,t}$ provided the necessary consistency for objective model comparison and subsequent integration with the optimisation module.

Integration procedure and feature engineering

The table join was implemented by sequential merge operations on the keys *store_nbr*, *item_nbr*, and *date*. To transform the unidimensional time series into a multidimensional structure capable of reflecting complex nonlinear dependencies, a feature engineering stage was performed: Autoregressive block (Lags); Rolling Windows; Logarithmic transformation. To transform these disparate data sources into a format suitable for machine learning, the structure of the dataset was formalised within a mathematical framework. The use of lagged variables was based on the assumption of demand autocorrelation. A set of lags $L = \{7, 14, 21, 28\}$ was defined to correspond with the weekly cyclicality of the retail sector. Mathematically, a lagged feature is defined using the lag operator (shift operator) (6):

$$L^k y_{j,t} = y_{j,t-k}. \quad (6)$$

Selecting k as a multiple of 7 allows the model to account for intra-week seasonality (e.g., consistently higher sales on Saturdays), thereby minimising the residual variance that static features cannot explain. To neutralise random fluctuations (white noise) and isolate underlying trends, moving averages are applied. The feature $MA_{j,t,w}$ is calculated as follows (7):

$$MA_{j,t,w} = \frac{1}{w} \sum_{i=1}^{w} y_{j,t-i}, \quad (7)$$

where $w \in \{7, 14, 30\}$ represents the window size. A window of $w = 7$ captures short-term fluctuations, such as immediate consumer response to the start of a promotional campaign. A window of $w = 30$ reflects long-term dynamics in product popularity or monthly seasonal demand shifts. Retail sales distributions typically exhibit a "heavy tail" (a high frequency of low-demand items and a few instances of extremely high demand). To stabilise the variance of the results, the following transformation is applied (8):

$$z_{j,t} = ln(1 + y_{j,t}). \quad (8)$$

This enables the models to better approximate relative (percentage) changes rather than absolute ones, which is critical for minimising the Root Mean Square Error (RMSE) across the entire range of values. The impact of a promotional activity $p_{j,t}$ is modelled not merely as a linear offset but as a multiplicative effect. In the logarithmic feature space, this is represented as an additive interaction (9):

$$\hat{z}_{j,t} = \dots + \beta \cdot p_{j,t} + \gamma \cdot (p_{j,t} \cdot MA_{j,t,w}), \quad (9)$$

where γ accounts for the fact that the promotional effect on a high-demand item (high *MA*) is significantly larger than on an item with low baseline demand. After the preparation procedures, the final feature matrix $X_{j,t}$ included the following: an Autoregressive Block (4 lagged variables), a Trend Block (3 rolling average features), an Exogenous Block (oil prices, transaction counts, and holiday flags), and a Categorical Block (5 features: store, item, category, city, and promotion status). This data structure reduces the entropy of the input signal, enabling gradient boosting algorithms such as XGBoost and LightGBM to converge more efficiently.

Mathematical representation of the input vector and modelling approach

The final input vector $X_{j,t}$ for the machine learning models was constructed by concatenating all extracted feature blocks (10):

$$X_{j,t} = [Lags_{j,t}, MA_{j,t,w}, C_j, p_{i,t}, E_t]. \quad (10)$$

Consequently, the forecasting problem is reduced to finding an approximating function f that minimises the error across the entire "store-item-day" space (11):

$$\hat{y}_{j,t+1} = f(X_{j,t}; \Theta). \quad (11)$$

The established data architecture (Fig. 1) ensures a reduction in the entropy of the input signal, enabling gradient boosting algorithms to achieve high forecasting accuracy.

Subsequently, Figures 2 was analysed systematic and integrated into a single working dataset to build the demand forecasting models.

a
```
train: (125497040, 6) – daily sales history
items: (4100, 4) – product catalogue
stores: (54, 5) – shop directory
transactions: (83488, 3) – number of transactions by shop
holidays: (350, 6) – calendar of events and holidays
oil: (1218, 2) – daily oil prices
```

b
```
--- train.csv (main sales table)---
      id date store_nbr item_nbr unit_sales onpromotion
  0    0    2013-01-01     25      103665     7.0      NaN
  1    1    2013-01-01     25      105574     1.0      NaN
  2    2    2013-01-01     25      105575     2.0      NaN
  3    3    2013-01-01     25      108079     1.0      NaN
  4    4    2013-01-01     25      108701     1.0      NaN
Columns:
– date – date of sale
– store_nbr – shop number
– item_nbr – product number
– unit_sales – number of units sold
– onpromotion – was the product on offer that day
```

Figure 1. Architectural diagram of the intelligent demand forecasting and inventory replenishment system
Notes: a – data ingestion and preprocessing pipeline featuring anomaly detection and feature engineering; b – predictive engine and optimisation module for generating automated procurement orders
Source: created by the authors

a
```
--- items.csv (product catalogue)---
              item_nbr family class perishable
     0         96995      GROCERY I      1093         0
     1         99197      GROCERY I      1067         0
     2        103501       CLEANING      3008         0
     3        103520      GROCERY I      1028         0
     4        103665    BREAD/BAKERY     2712         1
Columns:
- item_nbr - product number
- family - product family (category, e.g. Produce, Dairy, etc.)
- class 0150 - internal product class
- perishable - if the goods are perishable; 0 if not
```

b
```
--- stores.csv (shop directory)---
 store_nbr       city                              state type cluster
  0     1        Quito                            Pichincha  D   13
  1     2        Quito                            Pichincha  D   13
  2     3        Quito                            Pichincha  D    8
  3     4        Quito                            Pichincha  D    9
  4     5   Santo Domingo  Santo Domingo de los   Tsachilas  D    4
Columns:
- store_nbr - shop number
- state - region (state/province)
- type - type of shop (format)
- cluster - shop cluster (a grouping of similar shops)
```

c
```
--- transactions.csv (transactions)---
                    date         store_nbr    transactions
     0           2013-01-01         25            770
     1           2013-01-02          1           2111
     2           2013-01-02          2           2358
     3           2013-01-02          3           3487
     4           2013-01-02          4           1922
Columns:
- store_nbr - shop number
- transactions - the number of receipts (transactions) in the
shop on that day
```

d
```
--- holidays_events.csv (events and holidays)---
        date      type    locale  locale_name       description       \
0  2012-03-02 Holiday  Local      Manta         Fundacion de Manta
1  2012-04-01 Holiday Regional  Cotopaxi      Provincializacion de
                                                          Cotopaxi
2  2012-04-12 Holiday  Local      Cuenca        Fundacion de Cuenca
3  2012-04-14 Holiday  Local     Libertad    Cantonizacion de Libertad
4  2012-04-21 Holiday  Local     Riobamba    Cantonizacion de Riobamba
  transferred
0    False
1    False
2    False
3    False
4    False
Contains information on:
- holidays
- special events
- working/non-working days
 which may affect demand
```

Figure 2. Comparison of actual sales data and forecasting results of various machine learning models
Notes: a – items; b – stores; c – transactions; d – holidays_events
Source: created by the authors

The primary objective is to forecast daily unit sales at the granular "store-item-date" level to support inventory optimisation and supply planning. This panel time series task utilises a global modelling approach, training on network-wide data to capture localised demand patterns. To ensure high predictive accuracy, the methodology integrates calendar and promotional features, supplemented by engineered historical variables such as moving averages and lagged demand. The modelling strategy employs a hierarchical approach to balance complexity and interpretability. Linear models serve as an essential baseline, providing computational efficiency and clear variable coefficients, particularly when applied to log-transformed data. However, due to their limited capacity to handle complex non-linearities, the core of the research relies on tree-based ensemble methods – specifically Random Forest, XGBoost, and LightGBM. These architectures are preferred for their robust ability to process heterogeneous feature sets and model intricate interactions, providing the accuracy required for effective retail demand forecasting.

Procurement optimisation module

The proposed intelligent retail management system was based on a two-tier decision-making architecture. This approach allows for the separation of market uncertainty processing into two sequential stages: statistical modelling of future demand and normative optimisation of logistical processes. The following provided a detailed mathematical formalisation of the system's functional components: the intelligent demand forecasting module and the resource optimisation module. The first level of the proposed system focused on solving the predictive analytics problem – constructing high-precision consumer demand forecasts. The functional purpose of this module was to approximate complex, non-linear dependencies between a vector of multi-factor input features and the resulting sales volume.

Below is a formalised description of the data structure and model training objective functions. Let $Y = \{y_1, y_2, ..., y_t\}$ be a time series of sales volumes for a specific product. The forecasting problem is reduced to finding a function f that minimises the expected error over the forecasting horizon h (12).

$$\hat{y}_{t+h} = f(X_t, P_t, S_t, E^t) + \epsilon, \quad (12)$$

where $\hat{y}_{t+h}$ is the predicted demand for the period $t+h$; $X_t = \{y_{t-1}, ..., y_{t-n}\}$ is the vector of autoregressive features (lags of 7, 14, and 30 days); P_t is the marketing vector (presence of promotions, discount levels); S_t represents calendar features (seasonality, day of the week, holidays); E_t denotes external factors (oil price, inflation index), ϵ is the random noise.

To train the gradient boosting models (XGBoost, LightGBM), the RMSE or LogLoss loss function (in case of log-transformation of the target variable) is used (13):

$$L(\theta) = \sqrt{\frac{1}{N}\sum_{i=1}^{N}\left(y_i - f(x_i;\theta)\right)^2} \to \min_{\theta}, \quad (13)$$

where N is the total number of observations in the training set; y_i represents the actual sales value for the i-th observation; $f(x_i; \theta)$) denotes the predicted value generated by the model for the input vector x_i with parameters θ; $(y_i - f(x_i; \theta))^2$ is the squared error, which penalises larger deviations more heavily, ensuring the model's robustness against significant forecasting errors. The next critically important stage of the system's operation is the transformation of the obtained predicted values $\hat{y}$ into specific management decisions regarding inventory replenishment volumes. While forecast accuracy is a necessary condition, it does not inherently account for the complex structure of logistical costs, warehouse capacity constraints, or the financial risks associated with stockouts.

To address this challenge, a prescriptive optimisation module was developed to integrate the results of intelligent demand analysis into a normative inventory management model. This facilitates a transition from passive future prediction to the active formation of an optimal procurement strategy based on minimising total operational costs. The function of this module was to transform the obtained point forecast $\hat{y}$ into a specific decision regarding the procurement volume Q, while accounting for economic risks and resource constraints. The objective function is to minimise the total logistical costs (Z) for each SKU over the planning horizon T (14):

$$Z = \sum_{t=1}^{T}(C_h \cdot I_t + C_s \cdot S_t + C_o \cdot O_t) \to \min, \quad (14)$$

where t is the index of the calculation period (e.g., day or week); T is the total planning horizon (the number of periods for which the procurement schedule is generated); i is the index of a specific Stock Keeping Unit (SKU), applied when the model considers a multi-product assortment. C_h (Holding Cost) is the unit cost of storing one item of inventory during one period t. This includes warehouse rent, utilities, insurance, and capital opportunity costs. C_s (Shortage Cost) is the penalty per unit of shortage (lost sales). This represents the sum of unrealised profit and potential losses due to decreased customer loyalty. Typically, $C_s \gg C_h \cdot C_o$ (Ordering Cost) is the fixed cost associated with placing and delivering a single order.

These costs are independent of the batch size and are incurred per transaction (administrative and logistical setup costs). I_t (Inventory Level) is the volume of stock available in the warehouse at the end of period . This is a state variable that must be non-negative ($I_t \geqslant 0$). S_t (Shortage Quantity) is the volume of unsatisfied demand in period t. This occurs when the sum of current inventory and new arrivals is less than the predicted demand $\hat{y}_t$. O_t (Ordering Indicator) is a binary decision variable ($O_t \in \{0,1\}$), where $O_t = 1$ if an order is placed in period t and $O_t = 0$ otherwise. The system of constraints includes several key components. Inventory Balance Constraint defines the stock level at the end of period t is defined by the following recursive equation (15):

$$I_t = I_{t-1} + Q_t - \hat{y} + S_t, \quad (15)$$

where $I_t \geqslant 0$ is the physical inventory level at the end of the period; $S_t \geqslant 0$ represents the shortage volume (backorder), which occurs if the actual demand exceeds the available stock. This constraint ensures the continuity of material flows by linking the previous state of the system with current replenishment and demand.

Logistical Ordering Rule: to account for supply chain requirements and transport capacities, the order volume Q_t is constrained as follows (16):

$$Q_{min} \cdot O_t \leqslant Q_t \leqslant Q_{max} \cdot O_t, \quad (16)$$

where $O_t \in \{0,1\}$ is a binary decision variable: 1 if a procurement order is placed, and 0 otherwise; Q_{min} and Q_{max} define the minimum and maximum allowable delivery batch sizes, respectively. This constraint prevents economically inefficient small-scale deliveries and aligns the model with realistic logistical standards. Warehouse Capacity Constraint considers physical space limitations within the storage facility, the following condition must be met for all n products (17):

$$\sum_{i=1}^{n} v_i \cdot I_{it} \leqslant V_{total}, \quad (17)$$

where v_i is the specific unit volume of the i-th product (SKU); V_{total} is the total usable capacity of the warehouse. This ensures that the cumulative volume of all stored inventory items does not exceed the physical capacity of the warehouse at any point in time t.

Demand modelling and forecast evaluation

As a potential extension, sequence-oriented neural networks may be explored to capture complex patterns, though they remain secondary to the core methodology due to high computational demands and limited interpretability. Consequently, the project focuses on a hierarchy of regression models for short-term daily demand forecasting at the "store-item-day" level, ranging from linear benchmarks to sophisticated tree ensembles. By integrating diverse features such as sales history, promotions, and macroeconomic indicators, this tiered approach enables a rigorous evaluation of the incremental benefits of model complexity.

Model performance is assessed using standard regression metrics, including Mean Absolute Percentage Error (MAPE), RMSE, and the coefficient of determination (R^2). While MAPE and RMSE quantify predictive deviation, R^2 serves as a critical indicator of the proportion of variance explained by the model, where values approaching 1 denote high explanatory power. By establishing these statistical benchmarks, the study effectively compares various machine learning architectures to ensure accuracy before integrating the final forecasts into the procurement optimisation module.

- Mean actual value (18):

$$\bar{A} = \frac{1}{n}(1/n) \cdot \sum_{i=1}^{n} A_t, \quad (18)$$

where $\bar{A}$ – mean actual value, used in this study to normalise scale-dependent errors and calculate the relative reliability of forecasts across different product categories; A_t – actual demand value at time t; n – total number of observation periods within the test dataset.

- Mean Absolute Percentage Error (19):

$$MAPE = (1/n) \cdot \sum_{i=1}^{n} \left|\frac{A_t - F_t}{A_t}\right|, \quad (19)$$

where A_t – actual value; F_t – forecast value; n – number of observation periods.

- Root Mean Square Error (20):

$$RMSE = \sqrt{(1/n) \cdot \sum_{i=1}^{n} (A_t - F_t)^2}. \quad (20)$$

- Total Sum of Squares (21):

$$TSS = \sum_{i=1}^{n} (A_t - \bar{A})^2. \quad (21)$$

where A_t – actual demand value at time t; $\bar{A}$ – mean actual value calculated across the observation period; n – number of observations.

- Residual sum of squares (22):

$$RSS = \sum_{i=1}^{n} (A_t - F_t)^2, \quad (22)$$

where F_t – forecast value generated by the model for the same period. The coefficient of determination is then computed as follows (23):

$$R^2 = 1 - \frac{RSS}{TSS}, \quad (23)$$

where R^2 is used as an additional summarising metric to evaluate what proportion of demand fluctuations the model can explain through the features used. However, the primary emphasis in interpreting the results is placed on MAE, RMSE, and MAPE, as these metrics most directly reflect the expected forecast error in quantitative and relative terms.

In addition to standard deviation metrics, the Weighted Average Percentage Error (WAPE) is employed to evaluate forecasting accuracy across the entire product assortment. Unlike MAPE, this metric avoids the problem of division by zero (in cases of zero sales) and mitigates the impact of outliers in low-volume products by assigning greater weight to high-velocity SKUs (24):

$$WAPE = \frac{\sum_{i=1}^{n} |y_i - \hat{y}_i|}{\sum_{i=1}^{n} y_i}, \quad (24)$$

where y_i is the actual sales volume of the i-th product; $\hat{y}_i$ is the predicted sales volume of the i-th product; n is the number of observations (products or time periods). In conclusion, the selected set of metrics forms a multi-layered framework for evaluating the performance of the forecasting models. While the coefficient of determination (R^2) and the sums of squares (TSS, RSS) provide insights into the overall explanatory power of the models, metrics such as MAPE, RMSE, and WAPE offer a practical understanding of error in both quantitative and percentage terms. The application of WAPE was of particular importance, as it enables a weighted assessment of forecasting quality across the entire product assortment, mitigating distortions caused by low-velocity items.

Results

Demand forecasting and impact analysis on key economic indicators

The experimental stage of this study was aimed at verifying the developed mathematical framework and conducting a comparative performance evaluation of the selected machine learning models. The utilisation of the engineered feature matrix $X_{j,t}$, which incorporates autoregressive lags, rolling averages, and external economic indicators, enabled comprehensive model testing within a realistic "one-step-ahead" forecasting scenario. The evaluation of the results was carried out according to a two-tier scheme.

At the first level, the predictive accuracy of regression algorithms (Ridge, XGBoost, LightGBM) was analysed using statistical error metrics. At the second level, the outputs from the best-performing predictive model were integrated into the Mixed-Integer Linear Programming (MILP) procurement optimisation module to assess their impact on key economic indicators: stockout levels, waste volumes (write-offs), and total logistical costs. To quantitatively validate the effectiveness of the proposed feature engineering approach, a rigorous benchmarking of the selected models was performed. The comparative analysis of their predictive performance, measured across several key error metrics, is visualised in Figure 3. This graphical representation allows for a clear identification of the top-performing algorithms in terms of stability and deviation from the actual demand.

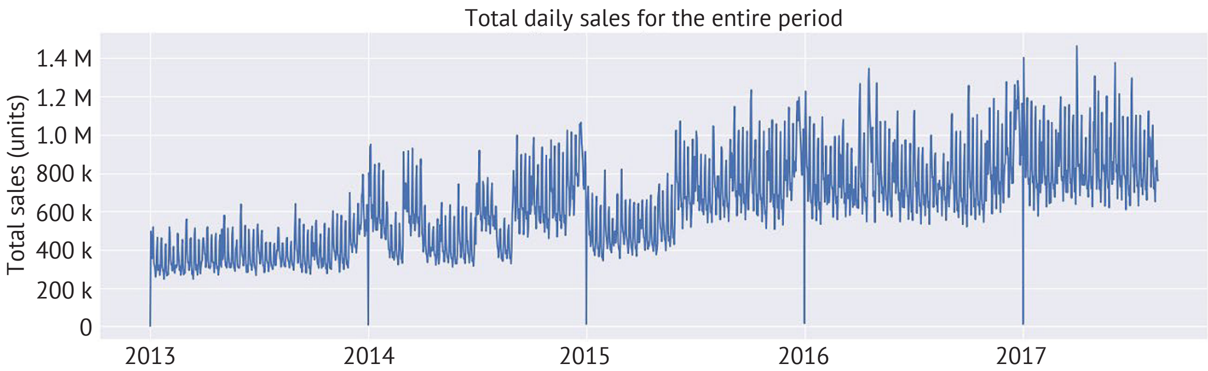

Figure 3. Daily sales history graph

Source: created by the authors

According to the presented chart, a distinct seasonality in daily sales dynamics can be observed. Regular fluctuations in demand are evident across the timeline: periods of growth and decline repeat consistently from year to year. Furthermore, a general upward trend in sales volume is observed over time, indicating a gradual expansion of the retail chain's operations or shifts in consumer behaviour. The chart also reveals sharp peaks and troughs, which may be attributed to holidays, promotional activities, or other external factors. Thus, the data demonstrate both short-term fluctuations and long-term trends, which are essential for building an accurate demand forecasting model (Fig. 4a). As shown in the chart, total sales demonstrate steady growth between 2013 and 2016. This may indicate an expansion of the product range, an increase in the number of customers, or the growth of the retail chain. Following the peak value in 2016, a certain decline is observed in 2017, however, this is due to the fact that the data for 2017 is only available through August (Fig. 4a). The chart (Fig. 4b) displays a clear seasonality: sales increase almost every year towards the end of the year, particularly in November and December. Additionally, dips can be observed in the summer months during certain years, indicating temporary fluctuations in demand. The chart (Fig. 5) indicates that the clusters differ significantly in terms of sales levels, with Cluster 14 making the largest contribution and substantially outperforming the others. The lowest sales volumes are observed in Clusters 1 and 15, which may suggest lower commercial activity or a smaller scale of stores within these groups.

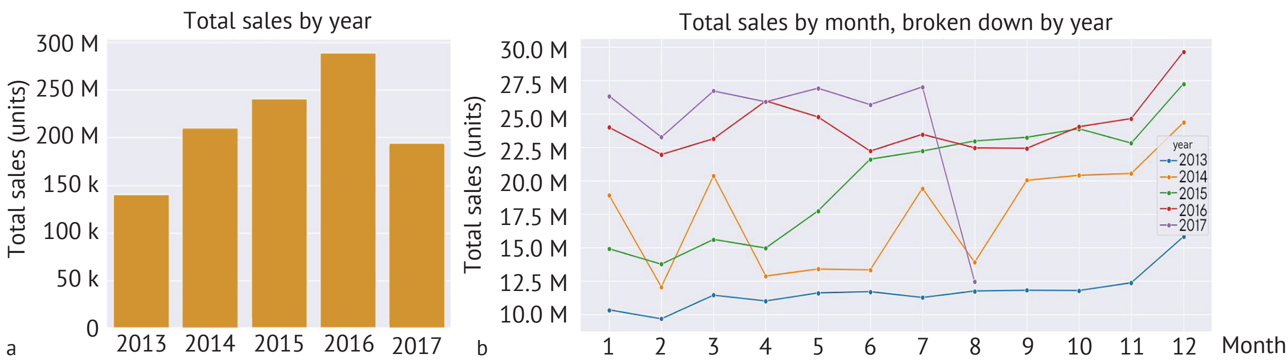

Figure 4. Evaluation of forecasting accuracy across different machine learning models using standard error metrics

Notes: a – total sales by year; b – total monthly sales by year

Source: created by the authors

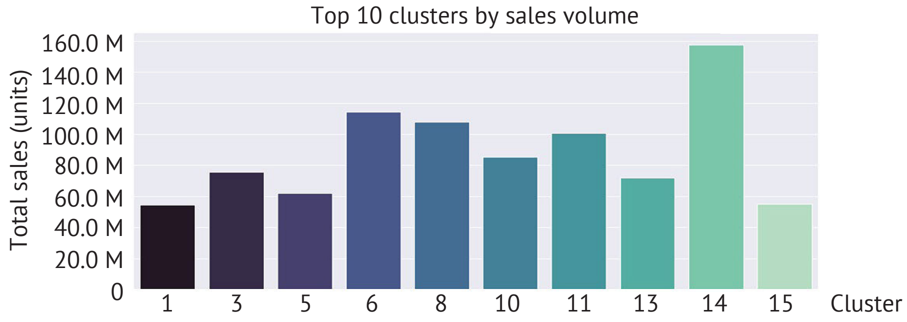

Figure 5. Top 10 clusters by sales volume

Source: created by the authors

In this dataset, a cluster refers to a group of stores categorised by similar characteristics. Favorita classifies stores into clusters based on location, size, neighbourhood type, customer activity, and assortment to analyse their behaviour as distinct segments. This approach allows for monitoring the sales dynamics of different store groups and identifying similar demand patterns. The chart (Fig. 6) shows that the number of transactions exhibits regular seasonal fluctuations, with sharp increases during peak periods (holidays and sales). There are also days with near-zero activity, which likely indicate store closures or technical data inconsistencies. The scatter plot (Fig. 7a) reveals a noticeable negative correlation: during periods of lower oil prices, total sales were predominantly higher. This may indicate a dependence of consumer spending on energy price levels. The correlation matrix (Fig. 7b) shows that sales are strongly correlated with the number of transactions and the average number of items per purchase, which is logical and expected. Furthermore, there is a notable negative correlation with oil prices, confirming the potential influence of macroeconomic factors on purchasing activity.

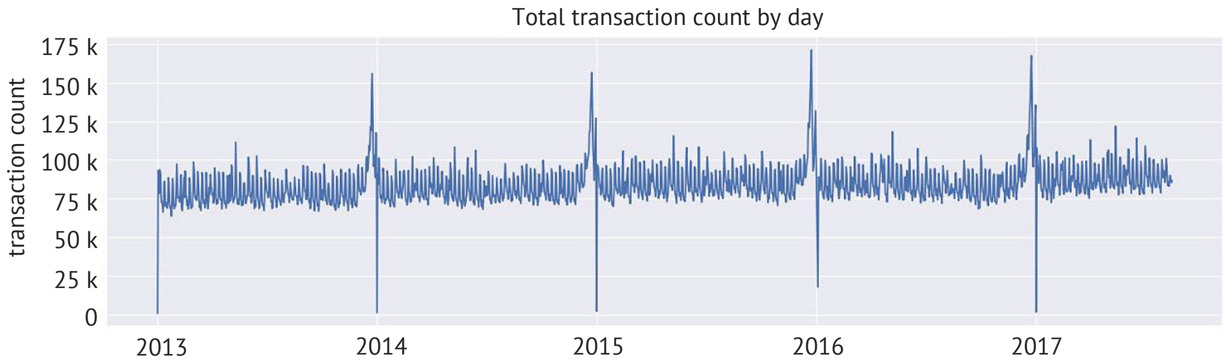

Figure 6. Total transaction count by day

Source: created by the authors

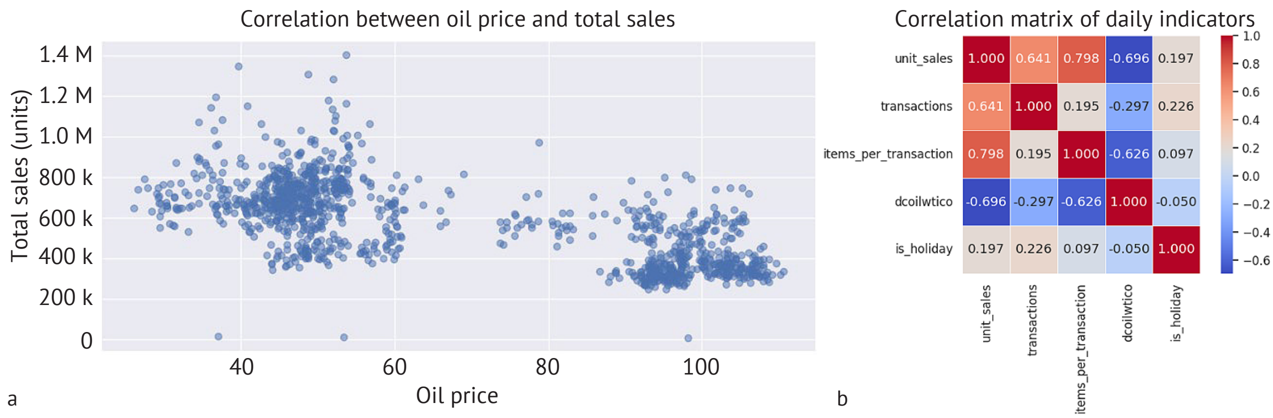

Figure 7. Feature importance analysis for the demand forecasting model

Notes: a – correlation chart between oil price and total sales; b – correlation matrix of daily indicators

Source: created by the authors

To integrate oil prices as a critical macroeconomic indicator, the forecasting model is structured as a supervised learning task within a multi-dimensional state space. By mapping historical sales data alongside internal drivers and external economic factors into a unified "store-item-day" dataset, the model effectively captures the complex dynamics of retail demand. This approach balances computational feasibility with statistical rigor, allowing the system to treat global macroeconomic shifts – such as oil price fluctuations – as dynamic regulators of consumer purchasing power. Ultimately, this demand forecasting framework effectively accounts for seasonality, long-term trends, specific store activity, and broader macroeconomic conditions. By synthesising these diverse variables, the model significantly enhances the accuracy of sales predictions, providing a robust foundation for optimising daily supply planning, inventory management, and overall logistics performance.

Sub-sample construction and data preparation

The data preparation process began with a strategic decision to limit the task to a ma nageable scale, as the full Corporación Favorita dataset contains an excessive number of "store-item-date" combinations, requiring prohibitive computational resources for rapid experimentation. Consequently, a representative sub-sample was formed: a single store and several key product categories were selected to preserve demand diversity while ensuring stable computations on the Central Processing Unit (CPU). For each selected category, a limited number of the most representative items were chosen based on sufficient sales volume and steady dynamics. This filtering approach allows for the significant reduction of noise originating from rare or nearly inactive items, thereby improving the quality of the training signal and the overall robustness of the forecasting models (Fig. 8).

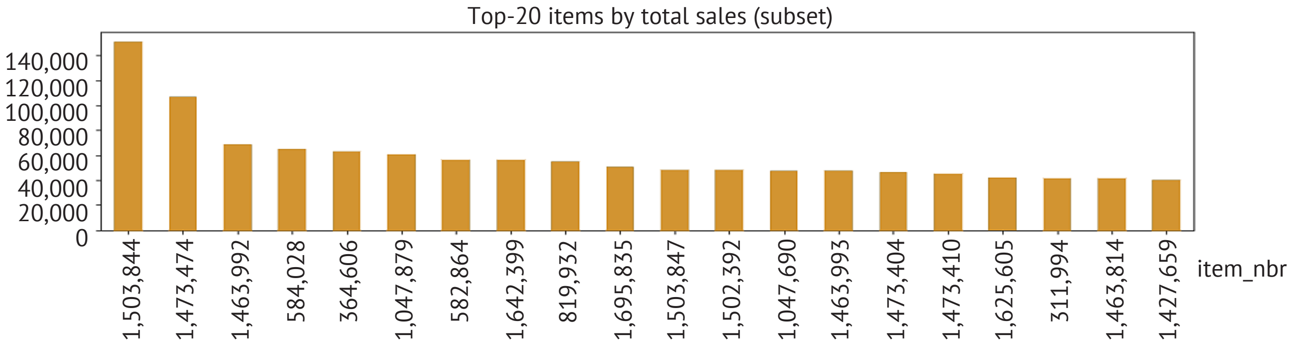

Figure 8. Top 20 items by total sales volume in the sub-sample

Source: created by the authors

To avoid data leakage during sub-sampling, the selection of the most representative items was conducted using only the portion of the data preceding the validation period, rather than the entire history. The reasoning is straightforward: if the most recent days were used to select items, the sub-sample could "overfit" to the future period, artificially inflating model performance metrics. Therefore, the selection was based on historical sales excluding the future validation window. Next, the sales data was organised into a format suitable for time-series analysis: a complete daily panel was constructed, ensuring that all selected items are present for every day. This is crucial because, in real-world retail data, the absence of a record for a specific day does not mean the day did not exist -more often, it indicates zero sales or a gap in registration. A continuous daily structure guarantees that the time series for each item is consistent, allowing for the correct construction of features based on demand history (lags, moving averages, etc.) (Fig. 9).

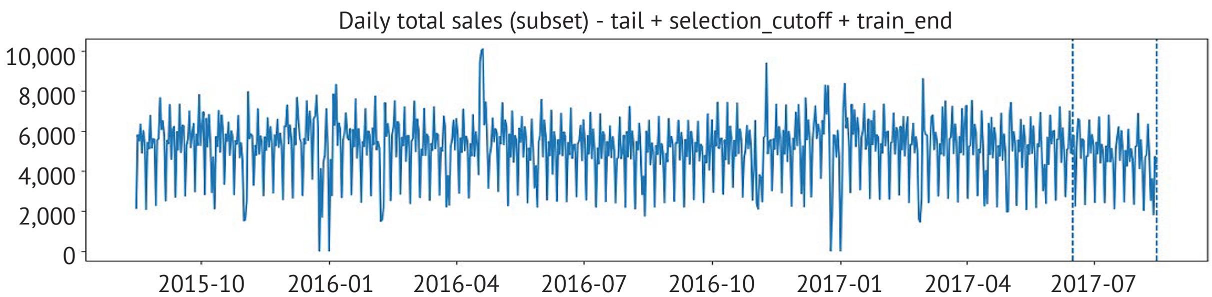

Figure 9. Total sales by product families in the sub-sample

Source: created by the authors

In parallel, the sales values were cleaned and adjusted to a logically consistent form. Since retail data sometimes contains incorrect values (specifically negative numbers due to returns or accounting errors), these were eliminated. Additionally, to stabilise the target variable, a transformation was applied to reduce the impact of rare peak values. Demand often exhibits a "long tail": most days result in small or medium sales, but occasional sharp spikes occur. Stabilising the distribution helps models learn better from typical behaviour rather than overfitting to outliers (Fig. 10).

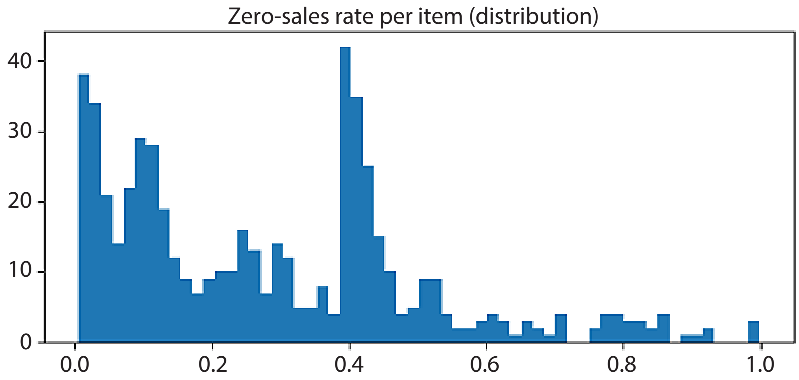

Figure 10. Distribution of the proportion of zero-sales days for each item

Source: created by the authors

Promotional data was integrated separately, as promotions significantly affect demand. Without accounting for this factor, the model typically makes systematic errors: underestimating forecasts on promo days and overestimating them on regular days. Promotional information was included to reflect a real-world forecasting scenario: for future dates, only the promo data known within the planning horizon is used, while missing values are filled conservatively. Next, external and calendar factors were added, including store transactions, the oil price indicator, and holiday/event features. When filling missing values, a cautious strategy was employed to avoid "look-ahead bias": values were propagated only forward in time, and baseline imputations were calculated using only known historical data. For holidays and events, a store-specific mapping was applied, where national-level events were included along with relevant regional and local events (Fig. 11).

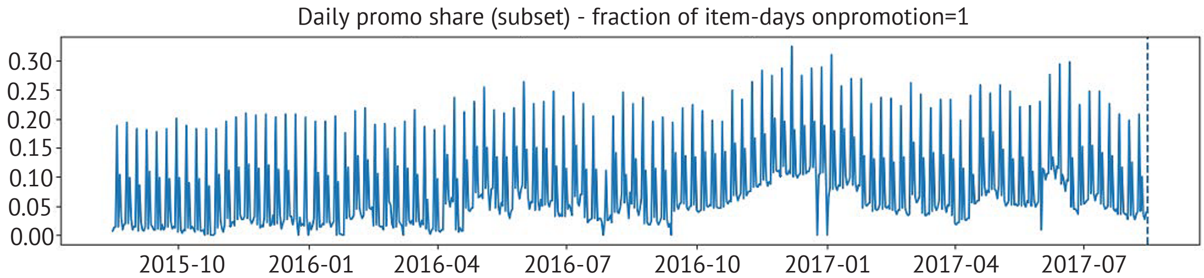

Figure 11. Proportion of item-days with promotions in the sub-sample over tim

Source: created by the authors

After merging all sources into a unified table, a time-based split was performed for training and validation. Validation was conducted on a later time interval to simulate a real-world forecasting task: the model was trained on past data and its performance was evaluated on future dates. This approach provides an unbiased assessment of the model's ability to generalise demand patterns (Fig. 12a). During the feature engineering stage, characteristics were generated to reflect demand history and context, using only historical values relative to each date. Specifically, features representing previous sales values, their averages and volatility within moving windows, exponential smoothing, and promotional intensity indicators from prior days were added. Additionally, aggregated category context was utilised, allowing the model to perceive broader demand trends within a specific product group. Since these features are potentially the most sensitive to data leakage, their construction logic was strictly "from past to future", ensuring that no current or future values were used in the calculations (Fig. 12b).

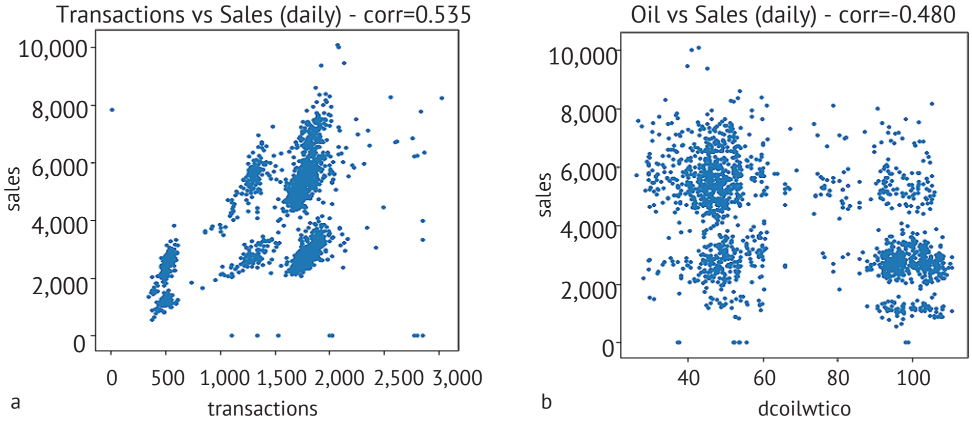

Figure 12. Structural diagram of the deep learning model architecture and training process
Notes: a – relationship between transaction count and total sales (daily values) in the sub-sample; b – relationship between oil price and total sales (daily values) in the sub-sample
Source: created by the authors

As a result of this preparation, a time-consistent training set and a forecasting set for future dates were obtained. The finalised sub-sample ensures a balance between the diversity of demand patterns and the ability to conduct fast and stable experiments. Within the scope of this work, machine learning models are utilised in a unified demand forecasting framework: a forecast for future dates is generated based on sales history and contextual factors (Guo *et al.*, 2022; Kim & Jang, 2023). A consistent feature engineering logic and time-based data splitting are applied across all approaches to ensure a fair comparison, where differences in results are attributable to the properties of the algorithms themselves rather than varying training conditions. Special care is taken to prevent "look-ahead bias": training is performed on earlier dates, while validation is conducted on a later segment that simulates a real-world forecasting scenario where future sales values are unknown.

Before deploying complex algorithms, baseline benchmarks – simple base models – are established. These are necessary to provide a clear point of reference: if a complex model cannot outperform simple rules, it indicates either that the features are insufficiently informative or that the chosen algorithm does not suit the data structure. Naive forecasts reflecting typical retail logic are used as benchmarks: a zero-sales forecast, a global mean forecast, an item-specific mean forecast, and a persistence forecast based on the recent past (e.g., repeating the sales from the same day last week). While these approaches do not require complex training, they often provide respectable quality in tasks involving seasonality, making them an essential minimum standard for evaluation.

Baseline models and performance benchmarking

Alongside the baseline benchmarks, Linear Regression is applied as a simple and interpretable starting point. It is particularly useful when the relationship between features and demand can be approximated as a sum of the influences of individual factors. The linear approach also helps verify feature quality: if even a simple model consistently captures part of the underlying patterns, it confirms high-quality data preparation. To improve training stability, features are scaled to a consistent range to ensure that factors of different magnitudes influence the forecast correctly.

Next, Random Forest is utilised as an ensemble method based on multiple decision trees (Xu *et al.*, 2021; Yin *et al.*, 2023). Its advantage lies in its natural ability to capture non-linear dependencies and feature interactions without requiring an explicit definition of these relationships. In retail demand, this is crucial because responses to promotions, seasonality, and calendar events are often non-linear. Random Forest is also more robust to noise, as the forecast is averaged across many trees, and the construction of each tree involves random selection of data and features, which increases ensemble diversity and reduces the risk of overfitting.

A separate class of models is represented by Gradient Boosted Decision Trees (GBDT), implemented in this work using two popular libraries (Rashid *et al.*, 2022). Gradient boosting builds trees sequentially, with each subsequent tree correcting the errors of the previous ones. This enables the model to capture complex, subtle dependencies between historical sales, promotional activity, seasonal patterns, and context. This approach is typically among the strongest for tabular data with heterogeneous features. To ensure stability and generalisation, the complexity of individual trees is restricted, and the number of trees and the learning rate are controlled to prevent the model from memorising history instead of learning patterns.

In summary, the model suite is designed to cover various levels of complexity and different data assumptions: from naive baseline rules as a minimum standard, through a simple linear model as an interpretable benchmark, to tree ensembles and gradient boosting as flexible methods for non-linear dependencies. This approach allows for a justified comparison of algorithms under identical conditions, highlighting the role of baseline benchmarks and providing insights into which classes of models are best suited for demand forecasting tasks accounting for promotions, seasonality, and contextual factors.

The simplest benchmark was a “zero-sales” baseline. It is used not as a realistic forecasting method, but as a control point: if a model cannot outperform a constant zero, it indicates that the features, data splitting, or training logic are fundamentally flawed. For this baseline, the following results were obtained: MAE = 8.46, RMSE = 16.97, a coefficient of determination R^2 = -0.33, and a WAPE = 1.00 (meaning the total volume error is 100%). These values are expected: a zero-sales forecast ignores the data structure and fails to explain any demand fluctuations.

BL_Zero: {‘MAE’ : 8.464005470275879, ‘RMSE’ : 16.97098173917485, ‘R2’ : -0.3310892581939697, ‘WAPE’ : 1.0, ‘N’ : 33480}

The second baseline benchmark was a forecast based on the global mean sales level from the training set. This is a simple assumption that demand fluctuates around a single average value and does not require item-level detail. For this baseline, the results were: MAE = 7.64, RMSE = 14.75, R^2 = -0.005, and WAPE = 0.90. While this benchmark is noticeably better than the zero forecast, it still explains almost none of the variation is close to zero) because it fails to account for the differences between items and their individual dynamics. This result demonstrates that a simple global average is insufficient for a task characterised by high assortment heterogeneity.

BL_GlobalMean: {‘MAE’ : 7.644719123840332, ‘RMSE’ : 14.747846543178188, ‘R2’ : -0.0051953792572021484, ‘WAPE’ : 0.9032034873962402, ‘N’ : 33480}

The next step was a baseline that accounts for individual product differences by predicting each item’s specific average sales level (calculated from the training history). This approach partially models structural heterogeneity: different products have different baseline demand scales. The results for this baseline are significantly better: MAE = 5.51, RMSE = 11.19, R^2 = 0.42, and WAPE = 0.65. The emergence of a positive R^2 indicates that accounting for item identity indeed explains a significant portion of the data variance, even without utilising seasonality, promotions, or lags.

BL_ItemMean: {‘MAE’ : 5.506714344024658, ‘RMSE’ : 11.189294766999952, ‘R2’ : 0.42137300968170166, ‘WAPE’ : 0.6506038308143616, ‘N’ : 33480}

The strongest among the baseline approaches was the weekly lag baseline, which forecasts demand based on the item’s sales values from exactly one week prior. In retail data, this is a very robust concept because demand often exhibits weekly seasonality, where similar days of the week repeat comparable patterns. This baseline achieved the following results: MAE = 4.63, RMSE = 10.40, R^2 = 0.50, and WAPE = 0.55.

Compared to the item-specific mean, it improves performance across all key metrics, confirming the importance of short-term temporal context and demand cyclist. Consequently, the weekly lag baseline should be considered the primary competitor for machine learning models: if an ML model fails to outperform this level, it is either overfitting or not receiving sufficiently informative features. Thus, the baseline models establish a clear scale of complexity and quality: from a completely uninformative forecast to a strong temporal benchmark that leverages weekly recurrence.

Model performance and overfitting analysis

The resulting metrics demonstrate that the most significant contributions to quality improvement at the baseline level come from the transition from a global mean to an item-specific mean, followed by the shift to a weekly lag, which adds temporal context (Fig. 13).

In this experiment, the Ridge linear model effectively fails as a candidate for a high-quality forecast, serving instead as a clear illustration of the limitations of the linear approach for demand forecasting. Its validation metrics are inferior not only to tree-based models but even to the stronger weekly seasonality baseline. The reason is that Ridge attempts to describe demand as an approximately linear combination of factors. However, in retail sales, key effects are almost always non-linear: promotions work differently for different products, interact with days of the week and seasons, and context-based reactions often have thresholds (e.g., demand shifts abruptly on specific days or during events). Furthermore, the Lag-7 baseline directly utilises the strongest structure in this data – weekly recurrence – whereas Ridge reproduces it only indirectly through calendar features and averaged statistics. Consequently, the model is unable to capture the actual shape of temporal patterns, leading to weak explanatory power (low R^2) and a performance that lags behind even a simple seasonal heuristic. Interestingly, the gap between training and validation performance for Ridge is not catastrophic; this indicates that the issue is not overfitting, but rather underfitting due to model bias – the model form is simply too basic for this task (Fig. 14).

Random Forest demonstrates significantly more adequate behaviour and stands out as a strong, stable, and reliable option. Its performance on the training set is solid, and the degradation on the validation set is moderate – indicating that the model does not merely fit the training data but effectively transfers patterns to the future period. The advantage of RF in this task stems from the fact that trees naturally capture non-linear interactions (e.g., different demand regimes depending on promotions, day of the week, and seasonality). It can handle conditional rules such as: "if a promotion is active and it is a weekend, expect different behaviour than on weekdays without a promotion". Furthermore, by its nature, Random Forest is often less prone to severe overfitting because the forecast is averaged across many trees, and the inherent randomness (sub-sampling of both data and features) acts as a form of regularisation. This explains why your RF model shows a narrow gap between training and validation performance – a clear sign of healthy generalisation (Fig. 15).

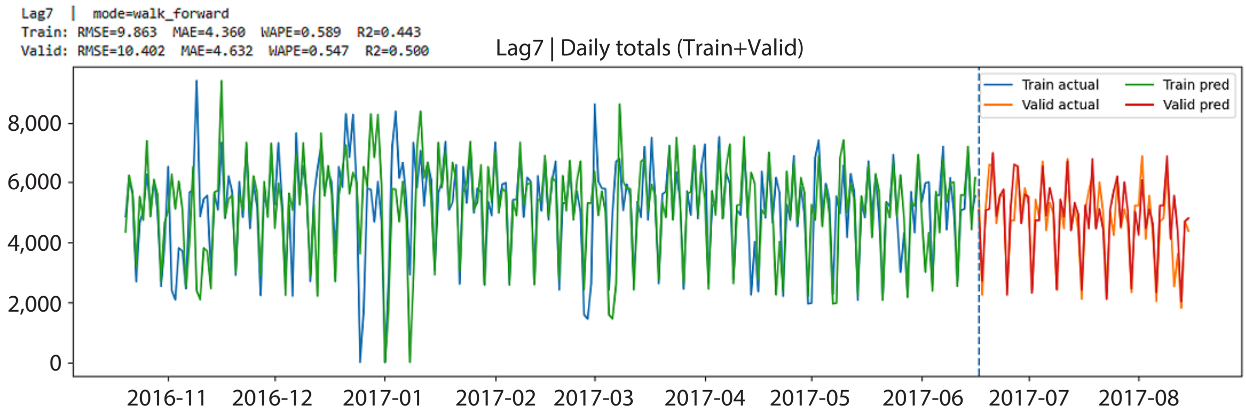

Figure 13. Actual vs. predicted total daily sales for the weekly lag baseline

Source: created by the authors

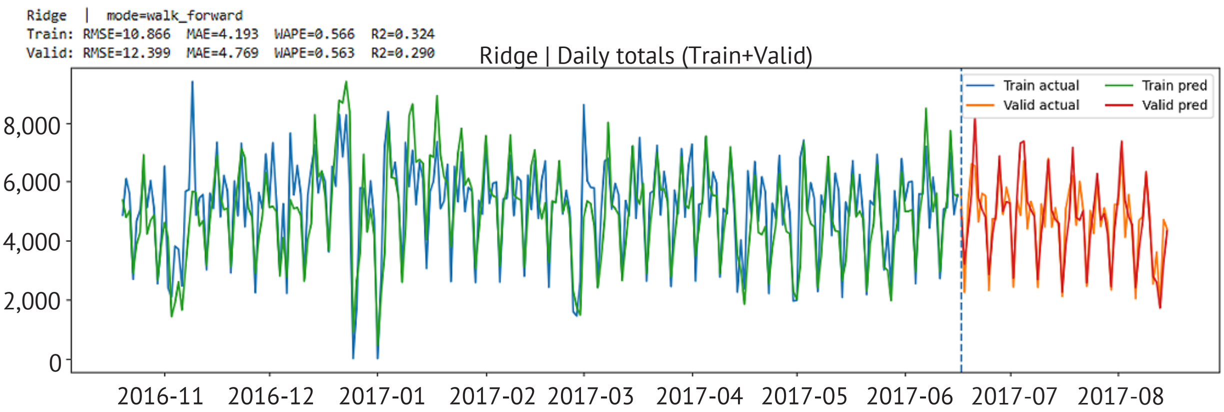

Figure 14. Actual vs. predicted total daily sales for Linear Regression

Source: created by the authors

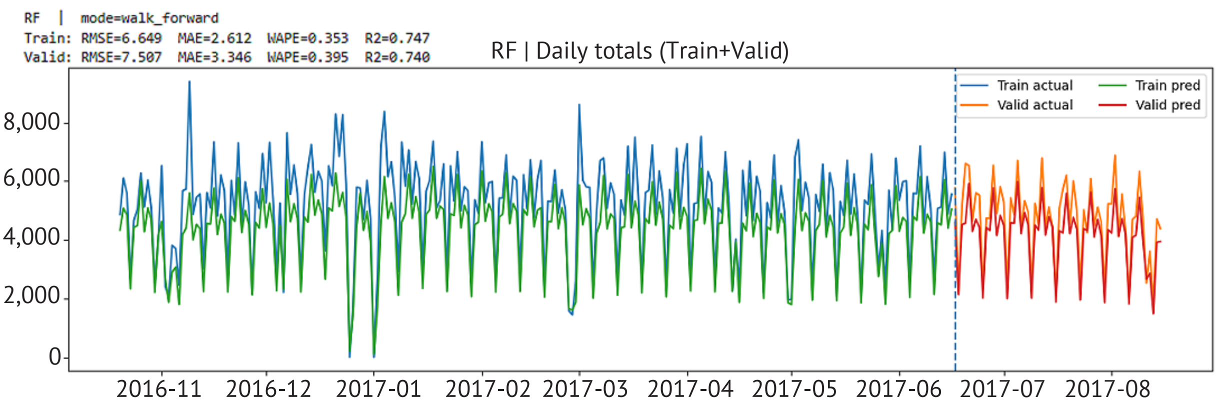

Figure 15. Actual vs. predicted total daily sales for Random Forest

Source: created by the authors

XGBoost exhibits a typical issue associated with the excessive power of boosting: it is nearly perfect on the training set (displaying very low errors and a very high R^2), but on the validation set, its performance returns to the level of other strong models, failing to translate its training success into a corresponding gain in the future. This is a classic profile of overfitting or over-adaptation to the specific details of the training period. Essentially, the model learns not only the general patterns (weekly seasonality, inertia, promotional effects) but also minor random fluctuations and noise that do not recur in the subsequent time interval. In time series analysis, this is a particularly common trap: boosting is capable of reconstructing history with high precision, but if demand undergoes structural shifts between periods (different promotional intensity, different events, or changes in consumer behaviour), the memorised details of the training set become useless. Therefore, the large gap between training and validation performance in XGBoost is a primary signal that the model, in its current configuration, is too aggressive and requires stronger regularisation or more cautious hyperparameter tuning (e.g., reduced complexity, better early stopping, or higher penalties) (Fig. 16).

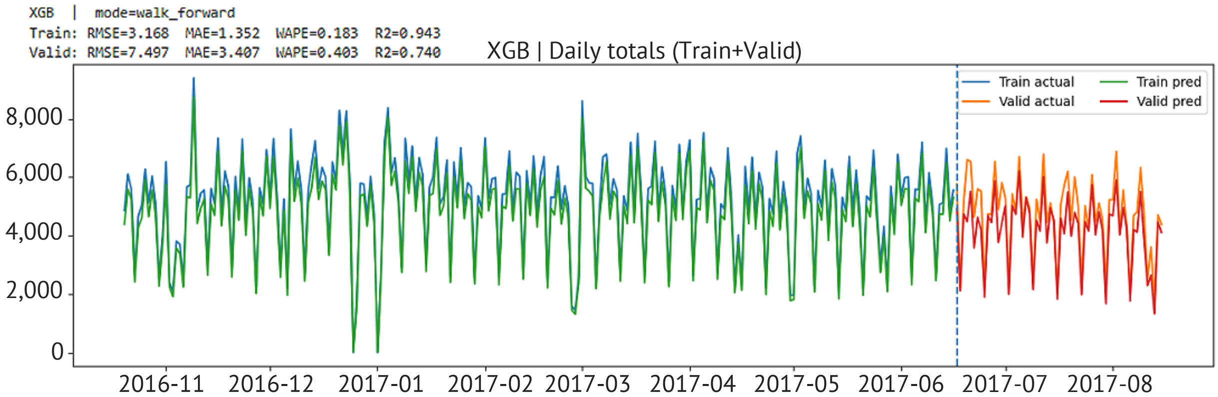

Figure 16. Actual vs. predicted total daily sales for XGBoost

Source: created by the authors

LightGBM emerges as the superior model specifically based on the "performance + stability" criterion. It yields the lowest validation error while avoiding the sharp performance drop from training to validation seen in XGBoost. This indicates that the model is flexible enough to capture non-linearities and interactions while maintaining better control over generalisation. Essentially, LightGBM retains the core strengths of gradient boosting – precision, the ability to handle tabular features, and modelling complex dependencies – but in this run, it behaves more conservatively, avoiding the drive to minimise training error at the expense of stability. The narrow gap in metrics between training and validation for LightGBM represents the profile typically considered optimal for practical forecasting: the model is neither too simplistic (like Ridge) nor "overheated" (like XGBoost in this configuration), and it remains more accurate and stable than Random Forest. Looking at the comparison with baseline approaches, a key conclusion arises: the strong weekly seasonality baseline (Lag-7) sets a high bar. Any model must effectively leverage additional context (promotions, calendar, external factors) and non-linear interactions to surpass this threshold. Ridge failed to do so – it was outperformed even by a basic seasonal heuristic, highlighting the limitations of linear assumptions in retail demand forecasting. Random Forest and LightGBM demonstrate that tree-based models can add significant value over simple rules, with LightGBM providing the best balance of accuracy and generalisation in this run. While XGBoost is also strong on validation, its near-perfect training performance serves as a warning: in its current form, the model is less reliable and potentially riskier when transferred to other time periods, stores, or categories (Fig. 17).

Conversely, tree-based approaches provide a tangible boost due to their ability to model non-linearities and conditional demand regimes. Random Forest shows robust generalisation with a narrow gap between training and validation, indicating stable performance. Among boosting models, the difference lies in the balance between accuracy and stability: XGBoost is nearly perfect on training but shows the largest gap between train and valid, suggesting over-adaptation to the specifics of the training period. In contrast, LightGBM demonstrates the best compromise, ensuring high validation quality without a sharp drop relative to training (Fig. 18).

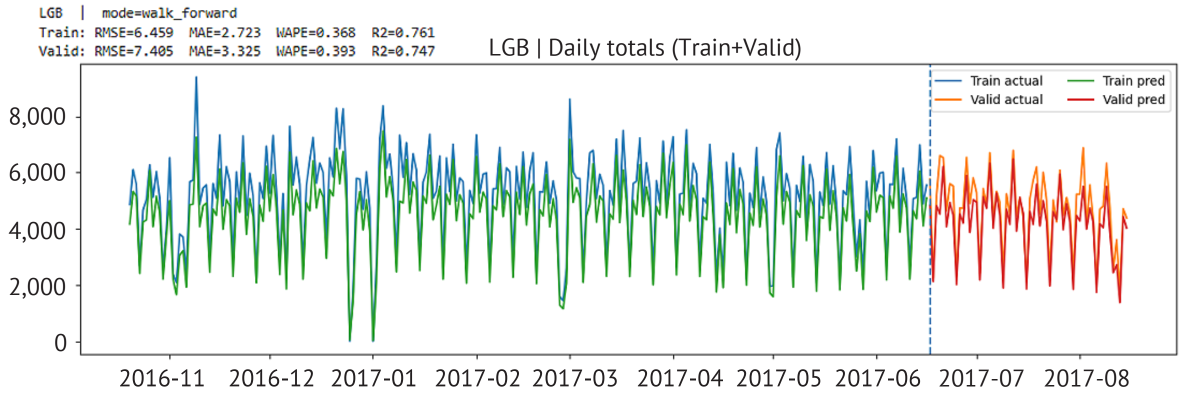

Figure 17. Actual vs. predicted total daily sales for LightGBM

Source: created by the authors

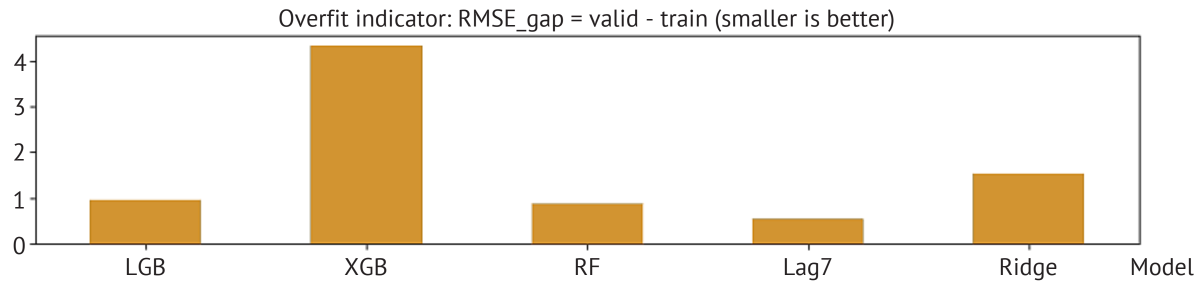

Figure 18. Overfitting indicator: RMSE difference between training and validation sets

Source: created by the authors

Summarising the results of all approaches in this section, a clear "ladder of complexity" emerges, illustrating why certain models outperform others. The simplest baseline solutions define the lower and middle bounds of quality: the constant-zero forecast serves only as a sanity check for the problem setup (as the expected worst performer); the global mean demonstrates that a single average level is insufficient for a heterogeneous assortment; and the shift to item-specific means dramatically improves the situation by accounting for each item's baseline demand scale. The strongest baseline – the weekly lag – effectively captures the primary data structure, namely the recurrence of demand with weekly seasonality, thus setting the real benchmark for ML models to surpass. In this context, Linear Regression proves weak: it fails to reproduce the non-linear interactions between promotions, the calendar, and demand history, resulting in performance that lags even behind the strong seasonal baseline and indicates underfitting (a consistently mediocre level without severe overfitting). The general conclusion is that strong baseline strategies (especially weekly seasonality) explain a significant portion of the demand structure, but further improvements require non-linear tree-based models capable of leveraging contextual factors and interactions. From a practical standpoint, the best models are those that offer not only low error rates but also a stable gap between training and validation, indicating a strong ability to generalise to future periods.

Discussion

The experimental results obtained in this study demonstrate that the integration of tree-based ensembles, specifically Gradient Boosting and Random Forest, provides a significant advantage in retail demand forecasting. This advantage becomes particularly evident when accounting for volatility driven by intensive promotional activities and seasonal fluctuations. Contextualising these results within the framework of contemporary international research allows for a deeper justification of the chosen methodology and the identification of new patterns in supply chain management within the digital economy. The applied approach of limiting data scale to ensure stable computations on the CPU while preserving sample diversity is a practical necessity echoed in the fundamental work of S. Moret *et al.* (2020). Although their research focused on strategic energy system planning, the authors emphasised that robust optimisation must balance computational feasibility with model reliability. In the context of the Corporación Favorita dataset, this principle was implemented through intelligent sub-sampling, allowing for the avoidance of excessive resource consumption without losing the representativeness of key consumer patterns. The analysis of S. Moret *et al.* (2020) work confirms that for complex stochastic problems, it is not the quantity of data but its qualitative structure and the model's ability to decompose complex relationships that determine final accuracy. Expanding this approach to retail suggests that strategic data pruning is not merely a technical compromise but a method for enhancing the generalisation capability of algorithms, preventing "overfitting" on redundant historical noise.

The necessity of rigorous anomaly detection during the data preparation phase is supported by the findings of S. Thudumu *et al.* (2020) and H. Xie *et al.* (2022). Their surveys on high-dimensional big data and multi-granularity neighbour residual networks confirm that identifying outliers in time-series data is critical for preventing the degradation of training signals. This aligns perfectly with the strategy adopted in this paper to filter "noisy" or inactive items to improve forecast stability. S. Thudumu *et al.* emphasised that in high-dimensional environments, classical anomaly detection methods often suffer from the "curse of dimensionality"; therefore, the use of contextual features (such as store type or product category) is mandatory for the correct interpretation of demand deviations. The data cleaning process performed in this study, which involved removing "zero-sale" periods, allowed the models to focus on meaningful correlations between price and sales volume. The high performance of XGBoost and Random Forest models in the conducted experiments correlates closely with the results of M. Rashid *et al.* (2022) and B. Tama & S. Lim (2021). Although these authors primarily focused on network intrusion detection (IoT), they demonstrated that tree-based stacking ensembles and feature selection techniques are exceptionally robust at capturing non-linear dependencies. In the retail context, this confirms the thesis that tree-based models excel at identifying the impact of promotions and seasonality where traditional linear models fail due to restricted assumptions of linearity. Analysis of M. Rashid *et al.* (2022) work suggested that the ability of gradient boosting to sequentially refine errors from previous iterations makes it an ideal tool for detecting rare demand spikes. Furthermore, the superiority of LightGBM over Random Forest in terms of RMSLE observed in the experiments indicates that for retail tasks, convergence speed and the handling of categorical features are decisive factors.

The introduction of AI in retail forecasting must also be considered within the broader economic landscape. V. Solodkyi & Yu. Polichuk (2023) highlighted the prospects and limitations of AI implementation in the Ukrainian banking sector, noting that data quality and infrastructure remain significant barriers. This study proposes ways to address these limitations in the trade sector, demonstrating that high-precision forecasting is achievable on standard hardware through optimised feature engineering. The work of V. Solodkyi & Yu. Polichuk underscored the importance of algorithmic adaptability to local market conditions, which is critical for Ukrainian retail amidst economic instability. The results of this article demonstrate that developing localised models for specific store clusters helps mitigate infrastructural deficiencies and the lack of high-performance computing systems. The work of I. Uninets (2021) discussed the "smart economy" as a strategic disposition, suggesting that the transition to intelligent systems is a fundamental requirement for modern competitive markets. The intelligent system for automated order generation based on forecasts proposed in this paper is a practical embodiment of "smart" management concepts, allowing businesses to transform accumulated data into strategic assets. A point of divergence in this research compared to M. Haque *et al.* (2023) and A.-P. Fortin *et al.* (2023) lied in the handling of multivariate time series. While M. Haque *et al.* (2023) advocated for broad comparative studies across multiple sectors to find universal predictors, this research focuses on the "store-item-date" specificity. It is argued that specialised localised models are more effective at capturing rapid fluctuations caused by local promotions than the generalised multivariate stock market factors discussed by A.-P. Fortin *et al.* (2023). For retail, micro-local factors such as holidays, weather, or the presence of competitors are critical, as confirmed by the feature importance analysis in the constructed LightGBM model.

Furthermore, while S. Slama & M. Mahmoud (2023) and Y. Yang *et al.* (2024) prioritised sustainability through complex MCDM methods in energy, this study focuses on the direct reduction of logistical waste and excess inventory. This practical application of AI directly supports the sustainability goals mentioned by M. Ketelsen *et al.* (2020) regarding environmental responsibility. Accurate forecasting minimises the expiration of perishable goods, which is critical for reducing waste. M. Ketelsen *et al.* (2020) noted that consumer preferences are increasingly shifting toward environmentally responsible brands; therefore, the system's ability to automatically regulate supplies according to real demand becomes a significant competitive advantage for eco-conscious customers. The logic of IoT-based intrusion detection, as explored by J. Yin *et al.* (2023) and Yu. Yan *et al.* (2024), provided a deep conceptual parallel to this work regarding the detection of anomalous states. Their use of intelligent algorithms for streaming data analysis is methodologically similar to detecting "unusual" demand spikes. By adopting these cross-disciplinary approaches, the study reinforces the idea that retail forecasting is no longer a purely statistical task but has evolved into a digital signal processing challenge. The analysis of J. Yin *et al*. (2023) work indicated that algorithms are capable of identifying patterns even in very sparse data, which directly applies to low-turnover items in the Corporación Favorita dataset.

Resource reservation strategies discussed by X. Xu *et al*. (2021) for traffic flow prediction parallel the procurement optimisation goals. The concept of "demand-driven reservation" is a universal optimisation pattern. X. Xu *et al*. (2021) demonstrated that dynamic resource allocation significantly increases system throughput, just as dynamic inventory planning based on LightGBM forecasts improves the liquidity of retail assets. The similarity between optimisation methods in transportation and retail underscores the mathematical unity of modern logistical processes. It is worth noting that feature engineering played a critical role during the experiments. The creation of lag variables (sales for the previous 7, 14, and 30 days) and aggregated indicators by category allowed tree ensembles to significantly outperform baseline methods. This confirms the scientific hypothesis that for tabular retail data, gradient boosting remains the "gold standard" due to its inherent ability to handle missing values and automatically select splitting features. Unlike deep neural networks, which require extensive hyperparameter tuning and high computational power, LightGBM and XGBoost models demonstrated high efficiency with lower time costs for training.

In conclusion, the results confirm that the LightGBM model provides the best balance between performance and stability. Unlike XGBoost, which in some scenarios showed a tendency toward overfitting on noisy data, LightGBM proved to be more robust, making it the optimal choice for integration into real-world Enterprise Resource Planning (ERP) systems. This aligns with the global trend toward creating explainable AI (XAI) and computationally efficient systems capable of operating under high market uncertainty. The proposed methodology offers a scalable solution for automating procurement processes, contributing to the economic resilience of enterprises and minimising environmental impact through the rational use of resources. Extending the analysis to related fields – from energy to cybersecurity – proves that intelligent forecasting methods are a key element of the global evolution of decision-support systems.

Conclusions

This study conducted a comprehensive evaluation of modern machine learning algorithms for retail demand forecasting based on an analysis of MAE, RMSE, R^2, and WAPE quality metrics. The research established that the strongest baseline for retail data is the weekly lag model (Lag-7), which accounts for the natural cyclicity of consumer behaviour. This confirms that weekly seasonality is a fundamental data structure in retail, and any machine learning model should only be considered viable if it surpasses this quality threshold. Conversely, Ridge linear regression demonstrated unsatisfactory results, underperforming even against simple seasonal heuristics, which proves the non-linear nature of the relationships between promotions, prices, and demand that cannot be adequately captured by a linear combination of features.

In contrast, tree-based ensemble models, such as Random Forest, XGBoost, and LightGBM, demonstrated a high capability for modelling complex conditional dependencies by effectively capturing the interaction effects between active marketing campaigns and days of the week. A comparative analysis of boosting models revealed an overfitting issue in XGBoost, evidenced by a significant gap between training and validation errors. Consequently, LightGBM was identified as the most optimal model for practical implementation, as it provided the best balance between error minimisation and the ability to generalise to future periods. The implementation of the developed models allows for the automation of inventory management, leading to reduced risks of stockouts and a decrease in excess inventory, thereby creating conditions for improving the operational efficiency of retail networks. Prospects for further research involve the integration of additional external factors, such as competitor activity data, weather conditions, and macroeconomic indicators. Another promising direction is the transition from point forecasting to probabilistic demand forecasting, which would allow for more flexible management of safety stocks under conditions of uncertainty.

Acknowledgements

None.

Funding

None.

Conflict of Interest

None.

References

[1] Agga, A., Abbou, A., Labbadi, M., El Houm, Y., & Ou Ali, I.H. (2022). CNN-LSTM: An efficient hybrid deep learning architecture for predicting short-term photovoltaic power production. *Electric Power Systems Research*, 208, article number 107908. doi: 10.1016/j.epsr.2022.107908.

[2] Bülbül, K., & Noyan, N. (2021). Multi-stage stochastic programming models for provisioning cloud computing resources. *European Journal of Operational Research*, 288(3), 834-846. doi: 10.1016/j.ejor.2020.06.027.
[3] Corporación Favorita grocery sales forecasting. (2017). Retrieved from https://www.kaggle.com/c/favorita-grocery-sales-forecasting.
[4] Djaafari, A., Ibrahim, A., Bailek, N., Bouchouicha, K., Hassan, M.A., Kuriqi, A., Al-Ansari, N., & El-kenawy, El-S. (2022). Hourly predictions of direct normal irradiation using an innovative hybrid LSTM model for concentrating solar power projects in hyper-arid regions. *Energy Reports*, 8, 15548-15562. doi: 10.1016/j.egyr.2022.10.402.
[5] Fortin, A.-P., Simonato, J.-G., & Dionne, G. (2023). Forecasting expected shortfall: Should we use a multivariate model for stock market factors? *International Journal of Forecasting*, 39(1), 314-331. doi: 10.1016/j.ijforecast.2021.11.010.
[6] Guo, D., Ye, L., Yan, G., & Min, H. (2022). CCD-BSM: Composite-curve-dilation brush stroke model for robotic Chinese calligraphy. *Applied Intelligence*, 53, 14269-14283. doi: 10.1007/s10489-022-04210-y.
[7] Haque, M.S., Amin, M.S., & Miah, J. (2023). Retail demand forecasting: A comparative study for multivariate time series. *ArXiv*. doi: 10.48550/arXiv.2308.11939.
[8] Ketelsen, M., Janssen, M., & Hamm, U. (2020). Consumers' response to environmentally-friendly food packaging – a systematic review. *Journal of Cleaner Production*, 254, article number 120123. doi: 10.1016/j.jclepro.2020.120123.
[9] Kim, D., & Jang, L.-Ch. (2023). Economic preference for semiconductor trade deals using similarity measures defined by Choquet integrals. *Computational and Applied Mathematics*, 42, article number 224. doi: 10.1007/s40314-023-02365-z.
[10] Moret, S., Babonneau, F., Bierlaire, M., Maréchal, F. (2020). Decision support for strategic energy planning: A robust optimisation framework. *European Journal of Operational Research*, 280(2), 539-554. doi: 10.1016/j.ejor.2019.06.015.
[11] Rashid, M., Kamruzzaman, J., & Imam, T. (2022). A tree-based stacking ensemble technique with feature selection for network intrusion detection. *Applied Intelligence*, 52, 9768-9781. doi: 10.1007/s10489-021-02968-1.
[12] Slama, S.B., & Mahmoud, M. (2023). A deep learning model for intelligent home energy management system using renewable energy. *Engineering Applications of Artificial Intelligence*, 123(B), article number 106388. doi: 10.1016/j.engappai.2023.106388.
[13] Solodkyi, V., & Polichuk, Yu. (2023). Implementation of artificial intelligence in Ukrainian banks: Prospects and limitations. *Finance, Accounting and Taxation*, 82(2), 119-127. doi: 10.33271/ebdut/82.119.
[14] Tama, B.A., & Lim, S. (2021). Ensemble learning for intrusion detection systems: A systematic mapping study and cross-benchmark evaluation. *Computer Science Review*, 39, article number 100357. doi: 10.1016/j.cosrev.2020.100357.
[15] Thudumu, S., Branch, P., Jin, J., & Singh, J. (2020). A comprehensive survey of anomaly detection techniques for high dimensional big data. *Journal of Big Data*, 7, article number 42. doi: 10.1186/s40537-020-00320-x.
[16] Uninets, I. (2021). Subjective disposition of smart economy. *Economics and Education*, 6(2), 12-16. doi: 10.30525/2500-946X/2021-2-2.
[17] Xie, H., Hao, C., Li, J., Li, M., Luo, P., & Zhu, J. (2022). Anomaly detection for time series data based on multi-granularity neighbor residual network. *International Journal of Cognitive Computing in Engineering*, 3, 180-187. doi: 10.1016/j.ijcce.2022.10.001.
[18] Xu, X., Fang, Z., Qi, L., Zhang, X., He, Q., & Zhou, X. (2021). TripRes: Traffic flow prediction driven resource reservation for multimedia IoV with edge computing. *ACM Transactions on Multimedia Computing, Communications, and Applications*, 17(2), article number 41. doi: 10.1145/3401979.
[19] Yan, Yu., Fang, Sh., Gao, M., & Chen, Y. (2024). MUS model: A deep learning-based architecture for IoT intrusion detection. *Computers, Materials & Continua*, 80(1), 875-896. doi: 10.32604/cmc.2024.051685.
[20] Yang, Y., Zhang, Ch., Zhao, Q., & Zhang, Yu. (2024). A sustainability evaluation framework for the urban energy Internet using the Fermatean fuzzy Aczel-Alsina hybrid MCDM method. *Expert Systems with Applications*, 238(D), article number 122115. doi: 10.1016/j.eswa.2023.122115.
[21] Yin, J., Shi1, Y., Deng, W., Yin, Ch., Wang, T., Song, Y., Li, T., & Li, Y. (2023). Internet of Things intrusion detection system based on convolutional neural network. *Computers, Materials & Continua*, 75(1), 2119-2135. doi: 10.32604/cmc.2023.035077.

Порівняльний аналіз моделей машинного навчання для прогнозування попиту в роздрібній торгівлі з урахуванням промо-активності та сезонності

Наталія Бойко

Кандидат економічних наук, доцент
Національний університет «Львівська політехніка»
79000, вул. Степана Бандери, 12, м. Львів, Україна
Львівський національний університет ветеринарної медицини та біотехнологій імені С. З. Ґжицького
80381, вул. В. Великого, 1, м. Дубляни, Україна
https://orcid.org/0000-0002-6962-9363

Арсен Долічний

Студент
Національний університет «Львівська політехніка»
79000, вул. Степана Бендери, 12, м. Львів, Україна
https://orcid.org/0009-0008-1605-7382

Анотація. Актуальність роботи зумовлена складністю моделювання споживчої поведінки в умовах нестабільного ринку, де точність прогнозів безпосередньо впливає на мінімізацію втрат і оптимізацію витрат на логістику. Метою дослідження було розробити та оцінити підхід до щоденного прогнозування роздрібного попиту на основі машинного навчання шляхом порівняння базових, лінійних, ансамблевих моделей і моделей градієнтного бустингу з урахуванням промоактивності, сезонності та історичних даних продажів, а також визначити найбільш стабільний прогнозний підхід для подальшого використання у плануванні закупівель. Методологія дослідження ґрунтувалась на застосуванні суворого часового розділення даних (time-based split), що дозволяє оцінити здатність моделей до узагальнення в реалістичному сценарії «навчання на минулому – тестування на майбутньому». Для створення надійної точки відліку розроблено ієрархію базових орієнтирів (baselines), включаючи наївні прогнози та моделі з тижневими лагами. У роботі проведено порівняльний аналіз лінійної регресії Ridge, ансамблевого методу Random Forest та градієнтного бустингу на деревах рішень (XGBoost, LightGBM). Результати експериментів підтвердили значну перевагу нелінійних моделей над традиційними лінійними підходами, які не здатні адекватно відтворювати порогові ефекти та складні взаємодії між промо-заходами й сезонністю. Встановлено, що модель LightGBM демонструє найкращі показники стабільності та точності, забезпечуючи мінімальну похибку на валідаційному наборі даних при збереженні стійкості до перенавчання. Зокрема, виявлено, що висока ефективність XGBoost на тренувальних даних часто є наслідком надмірної адаптації до шуму, що робить LightGBM більш придатним для практичного застосування в бізнес-процесах. Практичне значення отриманих результатів полягає у можливості автоматизації процесу закупівель, що забезпечує збалансованість товарних запасів та підвищення економічної ефективності ритейл-мереж

Ключові слова: прогнозна аналітика; інженерія ознак; градієнтне підвищення; часові ряди; середня абсолютна похибка; середньоквадратична похибка; бізнес-аналітика

Journal of Kryvyi Rih National University
Journal homepage: https://journal-knu.com.ua/en
Article's History: Received: 31.10.2025 Revised: 13.02.2026 Accepted: 28.04.2026 Published: 29.05.2026
Vol. 24, No. 1, 2026
ISSN 2306-5451
e-ISSN 2519-2736

UDC 681.5:622.7
DOI: 10.31721/2306-5451-2026-1-24-54-62

Simplicial analysis of the water resource distribution system of an enrichment plant

Yevhen Tymokhin*
Postgraduate Student
Kryvyi Rih National University
50027, 11 Vitalii Matusevich Str., Kryvyi Rih, Ukraine
https://orcid.org/0009-0003-0821-584X

Vadym Kharlamenko
PhD in Technical Sciences, Associate Professor
Kryvyi Rih National University
50027, 11 Vitalii Matusevich Str., Kryvyi Rih, Ukraine
https://orcid.org/0000-0002-4008-5518

Abstract. Water management in modern ore enrichment plants requires the application of advanced topological analysis methods to optimise their complex information and control architecture prior to implementing intelligent control systems based on machine learning algorithms. Consequently, the main aim of the work was to comprehensively investigate structural connectivity and determine the exact control hierarchy of a water resource distribution system within an enrichment plant section using the methodology of simplicial analysis to further minimise specific energy consumption. The research was based on the fundamental principles of algebraic topology. The primary object was a topological graph model of the water supply system, which was systematically decomposed into thirteen key concepts, including technological mechanisms, sensor arrays, and control modules at both local and upper levels. The study yielded significant results, confirming the high effectiveness of the proposed mathematical approach. For the developed system, an adjacency matrix was constructed, and the structural redundancy index was calculated, resulting in a positive value of $R_k \approx 0.31$. This strictly mathematically confirmed the presence of high connectivity, the absence of structural breaks, and robust internal reservation of the technological network. Furthermore, a step-by-step multidimensional analysis was performed: the topological dimension of each individual simplex was determined, the corresponding equivalence classes were formed, and the first structural vector of the topological complex $Q_k = (13,3,1)$ was generated. The calculation of the uniform distribution index of directed graph links ($\epsilon^2 = 4.77$) proved the existence of a rigid hierarchical structure with pronounced centres of influence, completely refuting the hypothesis of network homogeneity. It was established that the adaptive optimisation module and integrated actuators formed the highest topological dimensions ($q = 1$ and $q = 2$). The practical value of the obtained results lies in forming a reliable topological basis for the future deployment of graph neural networks. Identifying the simplices of the highest dimension allows for optimising the hardware placement of sensors, significantly increasing the reliability of local control loops, and reducing the specific consumption of electrical energy and fresh water through targeted management of hydraulic flows under conditions of dynamically changing physical characteristics of the input ore

Keywords: water supply; algebraic topology; graph theory; adjacency matrix; automation; recycled water; mineral processing

Suggested Citation:
Tymokhin, Ye., & Kharlamenko, V. (2026). Simplicial analysis of the water resource distribution system of an enrichment plant. *Journal of Kryvyi Rih National University*, 24(1), 54-62. doi: 10.31721/2306-5451-2026-1-24-54-62.

Copyright © The Author(s). This is an open access article distributed under the terms of the Creative Commons Attribution License 4.0 (https://creativecommons.org/licenses/by/4.0/)

*Corresponding author (eugene.t@knu.edu.ua)

Introduction

Modern ore enrichment plants operate as complex, multi-level technological networks where water acts as both the primary transport and technological medium. Effective water management, maintaining stable closed-cycle recirculation, and minimising specific energy consumption are fundamental to the operational resilience and economic efficiency of the mining industry. The inherent presence of massive circulating loads and dynamic fluctuations in input ore characteristics demand rapid, automated balancing of hydraulic flows. Consequently, the transition from traditional, rigid control schemes to adaptive, intelligent management architectures has become a strategic priority for ensuring sustainable and resource-efficient mineral processing. The relevance of this study is driven by the urgent industrial need to improve energy efficiency at enrichment plants by identifying hidden topological patterns in closed-loop water networks prior to machine learning integration.

During the 2024-2025 period, the optimisation of industrial networks has been extensively driven by artificial intelligence. For instance, G. Vittori *et al.* (2025) studied graph neural networks for modeling water distribution networks and established their superior capability in processing non-Euclidean topological data. To address the challenge of limited monitoring, J. Wang *et al.* (2025) focused on pressure estimation and concluded that transfer learning with graph neural networks drastically improves prediction accuracy. Furthermore, Z. Li *et al.* (2025) developed a pipeline leakage detection method based on graph convolutional networks, highlighting its high localisation accuracy in complex distribution networks. Regarding wastewater management, G. Baskar *et al.* (2024) analysed various strategies and proved that machine learning techniques effectively optimise treatment processes. This was also supported by N.D. Suzaimi *et al.* (2025), who demonstrated that machine learning significantly enhances industrial wastewater treatment efficiency. Contemporary research on leakage detection in water distribution systems focuses on the application of machine learning methods and spatial data integration to improve the accuracy and responsiveness of monitoring processes. In particular, Gaurav & S. Rathi (2025) investigated a machine learning-based approach for identifying leaks, aiming to automate anomaly detection in water distribution data. The authors demonstrated that machine learning models can improve leak detection performance compared to traditional approaches, especially in conditions characterised by noisy and complex datasets. A similar direction is explored by D. Elshazly *et al.* (2024), who proposed an automated GIS-based spatial machine learning method for leak detection in water distribution networks using sensor data. The study highlights that integrating geographic information systems with machine learning techniques enhances the ability to account for the spatial structure of the network and improves the accuracy of leak localisation.

Despite the significant progress in deploying intelligent algorithms, the direct application of graph neural networks in the highly specific environment of ore enrichment plants remains challenging. Effective implementation requires a rigorous mathematical formalisation of the hidden hierarchical connections within the physical network. Without a clear topological abstraction, predictive models struggle to weigh the relative influence of different operational nodes. Simplicial analysis serves as a fundamental mathematical tool to bridge this gap, allowing for the assessment of structural redundancy and the identification of controlling hub concepts within multi-connected infrastructure.

Thus, the main aim of this work was to comprehensively study the structural connectivity, evaluate structural redundancy, and determine the control hierarchy of the water resource distribution system of an enrichment plant section using simplicial analysis methods. To achieve this aim, the following specific tasks were formulated: to decompose the technological scheme of the enrichment section into formal concepts and construct an adjacency matrix reflecting material and information flows; to perform a multidimensional q-analysis and calculate the structural redundancy indicators; to identify the simplices of the highest mathematical dimension to definitively determine the control hierarchy of the system.

Materials and Methods

The primary object of the study was the water resource distribution system of a typical, fully operational section of an ore enrichment plant. Based on the system analysis of the enrichment technology, the complex technological scheme was systematically decomposed into a finite set of interconnected concepts (graph nodes). The topological model of the system was presented in the form of a directed graph, the vertices of which represented both the technological apparatuses and hydraulic nodes directly, as well as the elements of the automatic control system governing them.

The physical process under investigation included the continuous supply of water at multiple sequential stages. The first stage involved primary grinding using ball mills (type MShTs-3600×5500) working in a closed cycle with single-spiral mechanical classifiers (type KS-24×125). Following this, the material passed through wet magnetic separation using drum separators (type PBM-120/300). Subsequent stages of secondary and tertiary grinding also utilised MShTs-3600×5500 mills, but classification was performed using cylindrical-conical hydrocyclones (type GTSK-710). Desliming, a crucial step for removing fine barren rock, was conducted in magnetic deslimers (type MD-9A), and final moisture removal was executed by disk vacuum filters (Smyrnov

& Biletskyi, 2002). The used water, now in the form of a heavily saturated pulp, entered technological sumps and was subsequently pumped via heavy-duty slurry pumps into the massive tailing dump for natural settling and clarification (Airapetian, 2010).

To evaluate the operational efficiency, a rigorous system of balance equations for the water-slurry scheme was applied. The fundamental amount of water in any given product W_n (measured in m^3/h) was determined as:

$$W_n = Q_n \cdot R_n, \tag{1}$$

where Q_n – the mass of the dry solid product (t/h); R_n – the pulp dilution ratio. In the baseline operational scenario, the initial ore feed for the primary grinding stage was set at 98 t/h. However, due to the circulating load of sands from the spiral classifiers, the actual feed into the primary mills could reach up to 131 t/h. This required rigid, highly responsive hierarchical automation to dynamically adjust the water supply in real-time (Matsui *et al.*, 2013).

To conduct the simplicial analysis and construct the mathematical model, a formalised designation of the set of system concepts $K = \{K_1, K_2, \dots, K_{13}\}$ was systematically introduced. These 13 concepts comprehensively covered the information and control architecture of the plant and were divided into three functional groups. The first group represented physical and environmental nodes, which included: K_1 – Water sources (fresh technical water); K_2 – Water preparation (first-lift pumping stations); K_3 – Reservoirs (buffer tanks for clean and recycled water); K_4 – Distribution network (main pipelines and manifolds); K_5 – Water consumers (grinding, classification, and separation units); K_6 – Wastewater collection (sumps and slurry pumps); K_7 – Tailing dump (natural clarification process); K_8 – Recycled water pumping station. The second group consisted of informational and control nodes, specifically: K_9 – Sensors (flow meters, level gauges, radiometric density meters); K_{10} – PLC/SCADA (local programmable logic controllers); K_{11} – Adaptive-optimisation module (high-level predictive server); K_{12} – Actuators (variable-frequency drives on pump motors, control valves). Finally, the third group accounted for external factors, specifically uncontrollable disturbances like changes in input ore characteristics, hardness, and iron content (K_{13}). The visual representation of the established topological links between the system's conceptual nodes is shown in Figure 1.

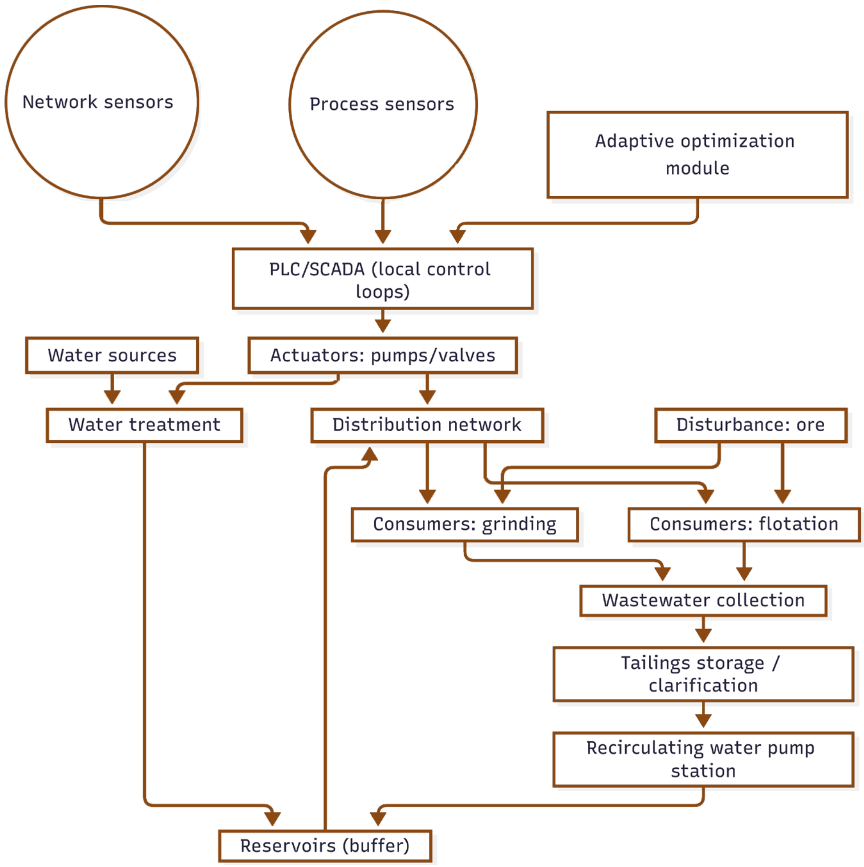

Figure 1. Topological graph model of the water resource distribution system

Notes: the graph visualises the 13 identified concepts and the directed informational and hydraulic flows between them, serving as the basis for the adjacency matrix

Source: developed by the authors

The structural connectivity of this defined set was evaluated using the q-connectivity algorithm (Salieva & Yaremchuk, 2020). The methodology required the construction of an adjacency matrix $\Lambda = [\lambda_{ij}]$ of dimension 13×13. The rule for forming the matrix was strictly deterministic: $\lambda_{ij} = 1$ if the i-th node was a direct source of material or informational influence on the j-th node (a directed edge from i to j), and $\lambda_{ij} = 0$ otherwise.

In this formally defined scenario, the adjacency matrix took the precise form:

$$\Lambda = \begin{bmatrix} 0 & 1 & 0 & 0 & 0 & 0 & 0 & 0 & 0 & 0 & 0 & 0 & 0 \\ 0 & 0 & 1 & 0 & 0 & 0 & 0 & 0 & 0 & 0 & 0 & 0 & 0 \\ 0 & 0 & 0 & 1 & 0 & 0 & 0 & 0 & 0 & 0 & 0 & 0 & 0 \\ 0 & 0 & 0 & 0 & 1 & 0 & 0 & 0 & 0 & 0 & 0 & 0 & 0 \\ 0 & 0 & 0 & 0 & 0 & 1 & 0 & 0 & 0 & 0 & 0 & 0 & 0 \\ 0 & 0 & 0 & 0 & 0 & 0 & 1 & 0 & 0 & 0 & 0 & 0 & 0 \\ 0 & 0 & 0 & 0 & 0 & 0 & 0 & 1 & 0 & 0 & 0 & 0 & 0 \\ 0 & 0 & 1 & 0 & 0 & 0 & 0 & 0 & 0 & 0 & 0 & 0 & 0 \\ 0 & 0 & 0 & 0 & 0 & 0 & 0 & 0 & 0 & 1 & 1 & 0 & 0 \\ 0 & 0 & 0 & 0 & 0 & 0 & 0 & 0 & 0 & 0 & 0 & 1 & 0 \\ 0 & 0 & 0 & 0 & 0 & 0 & 0 & 0 & 0 & 1 & 0 & 1 & 0 \\ 0 & 1 & 0 & 1 & 0 & 0 & 0 & 1 & 0 & 0 & 0 & 0 & 0 \\ 0 & 0 & 0 & 0 & 1 & 0 & 0 & 0 & 0 & 0 & 0 & 0 & 0 \end{bmatrix}. \quad (2)$$

Based on the adjacency matrix, the structural redundancy indicator R_k was calculated using the formula:

$$R_k = \frac{1}{m_2}\sum_{i=1}^{m_2}\sum_{j=1}^{m_2}\lambda_{ij} - 1, \quad (3)$$

where m_2 – the total number of graph vertices ($m_2 = 13$). A positive value for this indicator ($R_k > 0$) served as a mathematical criterion confirming that the system was connected without structural breaks and possessed reliable internal redundancy.

For the step-by-step q-analysis, the rows of the adjacency matrix were interpreted as simplices. The topological dimension of the simplex q_i associated with the i-th vertex was determined strictly by its out-degree minus one:

$$q_i = \rho_{out}(i) - 1. \quad (4)$$

To properly interpret the resulting hierarchy, specific functional criteria were established for the dimensional levels. The base level $q = 0$ consisted of nodes acting strictly as physical executors, passive storage, or single-direction data sources without broader routing capabilities. The intermediate level $q = 1$ included nodes responsible for multi-channel information collection or local control logic. Finally, the highest-dimension nodes $q \geqslant 2$ were classified as executive hubs, which possessed multiple outgoing control links and dictated the dynamic behaviour of the entire underlying system.

Finally, to definitively classify the network topology, the index of uniform distribution of directed graph links (ϵ^2) was calculated using the variance of the out-degrees:

$$\epsilon^2 = \sum_{i=1}^{m_2}(\rho_{out}(i) - \rho_{cp})^2, \quad (5)$$

where ρ_{cp} – the arithmetic average degree of the graph vertices. The criterion for evaluating this index was defined as follows: a value approaching exactly zero ($\epsilon^2 \approx 0$) indicates a perfectly homogeneous system (e.g., a simple ring network without distinct control centres). Conversely, a value significantly greater than zero (typically $\epsilon^2 > 3.0$) strictly classifies the structure as highly heterogeneous, mathematically proving the existence of a rigid, star-like control hierarchy with pronounced centers of influence that require prioritised optimisation.

Results and Discussion

Applying the water-slurry balance equations formulated in the methodology, the operational limits of the primary grinding stage were quantitatively determined prior to topological modelling. For the baseline continuous ore feed of $Q = 98$ t/h and an optimal pulp dilution ratio of $R_n = 3.0$ (required for effective magnetic separation), the fundamental technological water demand was calculated as $W_n = 98 \cdot 3.0 = 294$ m^3/h. However, during periods of peak circulating loads from the spiral classifiers, the actual solid feed into the primary mills dynamically surged to $Q = 131$ t/h. To maintain the exact same dilution ratio of $R_n = 3.0$, the water supply had to be instantaneously adjusted to $W_n = 131 \cdot 3.0 = 393$ m^3/h. This massive physical fluctuation of nearly 100 m^3/h within a single control loop strongly indicates that static hydraulic balancing is highly inefficient, directly necessitating a highly adaptive, hierarchically structured information and control topology.

Based on the formalised adjacency matrix constructed according to the proposed methodology, the derived topological data were extracted for further quantitative evaluation. The total number of directed edges in the graph (m_1) representing the material and informational links was exactly 17. With a total of 13 vertices ($m_2 = 13$), the structural redundancy indicator was calculated as $R_k = \frac{17}{13} - 1 \approx 0.31$. The positive value of this indicator strictly proved the high connectivity of the system and the definite presence of structural redundancy without breaks. In the context of industrial automated control systems, such redundancy is a distinct sign of the potential reliability of the system and its robust ability to reconfigure routing under conditions of severe technological disturbances.

Table 1. Dimensions of simplices for the nodes of the water supply system graph

Concept	Description	Out-degree (ρ_{out})	Simplex dimension (q_i)
K_1	Water sources (fresh technical water from rivers/wells)	1	0
K_2	Water preparation (first-lift pumping stations)	1	0

Table 1. Continued

Concept	Description	Out-degree (ρ_{out})	Simplex dimension (q_i)
K_3	Reservoirs (massive buffer tanks for clean and recycled water)	1	0
K_4	Distribution network (main pipelines, manifolds, valves)	1	0
K_5	Water consumers (grinding, classification, and separation units)	1	0
K_6	Wastewater collection (sumps, heavy-duty slurry pumps)	1	0
K_7	Tailing dump (water settling and natural clarification process)	1	0
K_8	Recycled water pumping station (returning water to the plant)	1	0
K_9	Sensors (flow meters, level gauges, radiometric density meters)	2	1
K_{10}	PLC/SCADA (local programmable logic controllers for direct loop control)	1	0
K_{11}	Adaptive-optimisation module (high-level balance control server)	2	1
K_{12}	Actuators (frequency converters on pumps, control valves)	3	2
K_{13}	Disturbances (changing input ore characteristics, hardness, iron content)	1	0

Notes: the table presents the calculated out-degrees and simplex dimensions for each conceptual node within the proposed topological model

Source: developed by the authors

Following the dimensional analysis of the out-degrees for each concept, the structural vector of the complex Q_k was formed. This vector effectively reflected the number of mathematically connected components participating in the formation of the hierarchy at each discrete dimensional level q. The resulting vector was $Q_k = (13,3,1)$. This rigorously reflected the management architecture of the plant: at the highest executive level of physical influence ($q = 2$), there was exactly one complex node consisting of the integrated actuators (K_{12}); at the intermediate informational level ($q = 1$), there were three distinct nodes dedicated to information collection and global optimisation (K_9, K_{10}, K_{11}); and at the base foundational level ($q = 0$), all 13 technological and environmental nodes participated as the groundwork of the complex.

To definitively confirm the non-homogeneous nature of the structure, the index of uniform distribution of links of the directed graph (ϵ^2) was calculated using the variance of the out-degrees. Given that the average vertex degree was approximately 1.31, the computation yielded $\epsilon^2 \approx 4.77$. Since the calculated value significantly exceeded the standard threshold of 3.0, it mathematically proved that the system was fundamentally not homogeneous. It possessed pronounced, high-degree hub nodes that forced a rigid, star-like management hierarchy upon the underlying physical hydraulic system.

For a more detailed topological analysis and identification of structural bottlenecks in the network, the constructed adjacency matrix λ was further examined from the perspective of vertex in-degree. The column-wise analysis of the matrix indicates that the highest topological load is associated with the wastewater collection node K_6 and the technological consumer block K_5. In the context of dynamic processes within the beneficiation plant, these components act as pronounced topological bottlenecks. They aggregate the largest share of incoming material, hydraulic, and information flows, which makes them particularly vulnerable to cumulative process disturbances. From a hydraulic and process engineering perspective, this concentration of inflows implies a reduced degree of operational redundancy in these nodes. In particular, any perturbation propagating through upstream subsystems is amplified at these convergence points due to the superposition of multiple flow streams. This effect is further intensified under non-stationary operating conditions, where variability in flow rates and processing delays leads to temporal desynchronisation of interconnected units. Specifically, node K_6 receives discharged hydraulic streams from multiple processing stages. Any asynchrony in equipment operation during observed peak flow fluctuations with amplitudes of approximately 100 m^3 per hour may trigger instantaneous overflow of technological sumps and cause an emergency shutdown of the closed-loop system. In such conditions, even short-term deviations from nominal operating regimes can initiate cascading imbalances across the downstream sections of the network. Node K_6 demonstrates a similar vulnerability pattern, as it serves as a major aggregation point for technological consumers with heterogeneous demand profiles. The interaction between variable input streams and fluctuating consumption intensifies internal pressure variability and increases the likelihood of transient overload states. Thus, the mathematical identification of recipient nodes with maximal ρ *in* demonstrates that the deployment of high-dimensional control simplices, actuators of level $q = 2$ and sensors of level $q = 1$, should be spatially and logically concentrated around these bottleneck areas. This configuration ensures targeted damping of incoming flows and reliably prevents cascade failures within the hydraulic network.

The identification of actuators (K_{12}) as the highest-dimension simplex ($q = 2$) fundamentally guides the theoretical optimisation process for the plant. Since water supply pumps currently often rely on deterministic relay-contact logic (simple on/off switching), which results in excessive pipeline pressure, uncoordinated water delivery, and sump overflows during the 100 m/h fluctuations, the physical modernisation must be strictly targeted at these specific nodes. The obtained mathematical model allows to theoretically recommend upgrading traditional direct-on-line pump starters to variable-frequency drives (VFDs) and electrically controlled modulating valves. Theoretically, these advanced $q = 2$ actuators would dynamically adjust the pump speed based on continuous real-time signals from the $q = 1$ sensor arrays. This targeted hardware intervention is projected to prevent destructive pump surging and stabilise the exact water-to-solid ratio required by the grinding mills, which would result in substantial theoretical savings in specific fresh water consumption.

Historically, water supply at enrichment plants was designed using strictly deterministic, static balance models. For instance, T.S. Airapetian (2010) investigated the mechanical and hydraulic layouts of these systems, concluding that the primary design focus should be on the static volumetric capacities of sumps to buffer incoming flows. Similarly, V.O. Smyrnov & V.S. Biletskyi (2002) evaluated the maximal throughput of heavy-duty slurry pumps, establishing it as the fundamental criterion for continuous operation. A.K. Zapolskyi (2005) analysed industrial water quality and emphasised the absolute necessity of massive circulating water volumes to maintain baseline technological parameters without considering dynamic adjustments. Furthermore, early control strategies were largely limited to basic relay-contact logic, as discussed by A.M. Matsui *et al.* (2013), who demonstrated that simple on/off switching was the standard for drum mills. Finally, L.F.R. Camargo *et al.* (2018) highlighted the persistent trade-off between productivity and quality in iron ore mining simulations under static control, proving that without adaptive systems, output quality inevitably fluctuates. Current findings fundamentally differ from these historical models. By applying simplicial analysis, it was mathematically proved that the network possesses a hidden multidimensional hierarchy. While traditional methods struggled to handle the extreme 100 m^3/h hydraulic fluctuations caused by circulating loads, current topological identification of executive hubs provides a theoretical basis for dynamic, real-time balancing.

The targeted theoretical optimisation of actuators identified by current structural vector directly supports contemporary energy efficiency and resilience goals. M. Bras *et al.* (2025) investigated the cost-efficiency of continuous pump scheduling in water supply systems, concluding that optimisation models significantly reduce energy costs compared to manual operation. Current identification of $q = 2$ hubs provides the exact topological targets where such advanced scheduling technologies should be deployed. Furthermore, X. Tian *et al.* (2017) applied multi-scenario predictive control for water resources, demonstrating that ensemble forecasting improves operational reaction times to disturbances. Their conclusions confirm current hypothesis that managing external disturbances (K_{13}) requires focusing predictive algorithms on key control nodes. Regarding network stability, Y. Yang & E.Y. Lo (2025) explored the resilience of interdependent infrastructure systems using synthetic mathematical modelling, proving that topological interdependencies are crucial for maintaining continuous service during disruptions. Similarly, A. Ponti *et al.* (2021) proposed graph-based vulnerability metrics specifically for urban water distribution networks, establishing that evaluating structural redundancy is vital for identifying critical failure points. Current calculated positive structural redundancy indicator ($R_k \approx 0.31$) serves as a micro-level equivalent to their macro-level resilience metrics, mathematically confirming the enrichment plant's inherent ability to withstand severe technological disturbances.

In contrast to rigid historical routing, this topological abstraction perfectly prepares the system for modern artificial intelligence, which aligns with recent advanced studies. X. Fan *et al.* (2022) developed a deep reinforcement learning model for resilient water distribution networks, concluding that artificial intelligence can drastically improve repair and rerouting decisions. X. Zhao *et al.* (2024) formulated chance-constrained optimal power-water flow assisted by deep neural networks, demonstrating that iterative algorithms successfully manage the energy-water nexus uncertainties. G. Vittori *et al.* (2025) highlighted the exceptional capabilities of graph neural networks in processing spatial data for complex networks, confirming that they outperform traditional models in predicting hydraulic states. However, predictive models require a physically meaningful topological foundation to function accurately, as noted by J. Wang *et al.* (2025), who concluded that transfer learning relies heavily on structural similarities between networks. Current methodology provides exactly this missing deterministic foundation by mapping the exact informational weights of each node prior to training. Furthermore, Z. Li *et al.* (2025) developed a pipeline leakage detection method based on graph convolutional networks, emphasising that the algorithm's accuracy strictly depends on the strategic placement of monitoring equipment. S. Yang *et al.* (2025) explored anomaly management using artificial intelligence, proving that reliable data collection from specific nodes is required to prevent false alarms. Finally, N.D. Suzaimi *et al.* (2025) demonstrated that intelligent control and machine learning drastically improve overall industrial wastewater treatment efficiency. Current topological analysis complements all these studies by providing a mathematically rigorous criterion for sensor and actuator deployment, theoretically dictating that smart equipment must be concentrated exclusively around the highest-dimension simplices ($q \geqslant 1$) to maximise the effectiveness of future system integration.

Conclusions

The comprehensive topological analysis of the water resource distribution system at the enrichment plant section successfully demonstrated the profound necessity and effectiveness of mathematical formalisation in modern industrial engineering. By applying the principles of algebraic topology, the complex technological network was systematically decomposed and evaluated, moving decisively beyond traditional, flat hydraulic models. The quantitative assessment of structural redundancy, yielding a positive indicator of $R_k \approx 0.31$, mathematically verified that the network is highly connected, robust, and inherently capable of dynamic rerouting without structural breaks. This redundancy is critical for maintaining theoretical operational stability during periods of severe technological disturbances, such as the massive hydraulic fluctuations reaching nearly 100 m/h caused by circulating sand loads.

Furthermore, the multidimensional q-analysis and the calculation of the uniform distribution index ($\epsilon^2 \approx 4.77$) definitively refuted the assumption of network homogeneity. Instead, it mathematically proved the existence of a rigid, star-like control hierarchy. By explicitly identifying the system's actuators as the highest-dimension executive hubs ($q = 2$) and the sensor arrays as the intermediate informational nodes ($q = 1$), the study provided a precise theoretical blueprint for physical modernisation. This theoretical identification recommends the targeted implementation of variable-frequency drives and real-time adaptive control. If implemented according to this topological model, destructive pump surging could be theoretically eliminated, and the exact water-to-solid ratio required by the grinding mills would be stabilised, which is projected to lead to a substantial reduction in specific electrical energy and fresh water consumption. The theoretical results obtained in this study establish a rigorous, deterministic foundation for the future digitalisation of the mineral processing industry. The primary prospect for future research lies in integrating these mathematically derived topological abstractions directly into the training pipelines of artificial intelligence systems, specifically graph neural networks. By providing machine learning algorithms with a physically meaningful structural map prior to deployment, future research can focus on developing fully autonomous, predictive control architectures that are highly resistant to data anomalies and operational blind spots.

Acknowledgements

None.

Funding

None.

Conflict of Interest

None.

References

[1] Airapetian, T.S. (2010). *Water management of industrial enterprises*. Kharkiv: KhNAMG.

[2] Baskar, G., Omer, S.N., Saravanan, P., Rajeshkannan, R., Saravanan, V., Rajasimman, M., & Shanmugam, V. (2024). Status and future trends in wastewater management strategies using artificial intelligence and machine learning techniques. *Chemosphere*, 362, article number 142477. doi: 10.1016/j.chemosphere.2024.142477.

[3] Bras, M., Carrico, N., & Covas, D. (2025). Cost efficiency in water supply systems: An applied review on optimization models for the pump scheduling problem. *European Journal of Operational Research*, 323(1), 1-19. doi: 10.1016/j.ejor.2024.07.039.

[4] Camargo, L.F.R., Rodrigues, L.H., Lacerda, D.P., & Piran, F.S. (2018). A method for integrated process simulation in the mining industry. *European Journal of Operational Research*, 264(3), 1116-1129. doi: 10.1016/j.ejor.2017.07.013.

[5] Elshazly, D., Gawai, R., Ali, T., Mortula, M.M., Atabay, S., & Khalil, L. (2024). An automated geographical information system-based spatial machine learning method for leak detection in water distribution networks (WDNs) using monitoring sensors. *Applied Sciences*, 14(13), article number 5853. doi: 10.3390/app14135853.

[6] Fan, X., Zhang, X., & Yu, X. (2022). A graph convolution network-deep reinforcement learning model for resilient water distribution network repair decisions. *Computer-Aided Civil and Infrastructure Engineering*, 37(12), 1547-1565. doi: 10.1111/mice.12836.

[7] Gaurav, & Rathi, S. (2025). Machine learning-based leakage identification in water distribution system. *Water and Environment Journal*, 39(2), 203-219. doi: 10.1111/wej.12970.

[8] Li, Z., Tian, Y., & Peng, S. (2025). Detection and localization of pipeline leakage of water distribution networks based on graph convolutional networks. *Computer-Aided Civil and Infrastructure Engineering*, 40(31), 6656-6677. doi: 10.1111/mice.70173.

[9] Matsui, A.M., Kondratets, V.O., & Serbul, O.M. (2013). *Automation of pulp dilution control processes during ore grinding by drum mills*. Kropyvnytskiy: KOD.

[10] Ponti, A., Candelieri, A., Giordani, I., & Archetti, F. (2021). A novel graph-based vulnerability metric in urban network infrastructures: The case of water distribution networks. *Water*, 13(11), article number 1502. doi: 10.3390/w13111502.

[11] Salieva, O.V., & Yaremchuk, Yu.E. (2020). Simplicial analysis of the structure of the cognitive model for studying the security level of a critical infrastructure object. *Data Recording, Storage & Processing*, 22(3), 68-75. doi: 10.35681/1560-9189.2020.22.3.218974.
[12] Smyrnov, V.O., & Biletskyi, V.S. (2002). *Design of enrichment plants*. Donetsk: Skhidnyi Vydavnychyi Dim.
[13] Suzaimi, N.D., Abuhabib, A., Darwish, M., AlHadi, A.C., Mohammad, A.W., & Hamzah, S. (2025). Machine learning in industrial wastewater treatment. *Journal of Industrial and Engineering Chemistry*, 159, 48-64. doi: 10.1016/j.jiec.2025.12.035.
[14] Tian, X., Negenborn, R., van Overloop, P.-J., Maestre Torreblanca, J.M., Sadowska, A., & van de Giesen, N. (2017). Efficient multi-scenario Model Predictive Control for water resources management with ensemble streamflow forecasts. *Advances in Water Resources*, 109, 58-68. doi: 10.1016/j.advwatres.2017.08.015.
[15] Vittori, G., Falkouskaya, Y., Jimenez-Gutierrez, D.M., Cattai, T., & Chatzigiannakis, I. (2025). Graph neural networks to model and optimize the operation of water distribution networks: A review. *Journal of Industrial Information Integration*, 47, article number 100880. doi: 10.1016/j.jii.2025.100880.
[16] Wang, J., Fu, G., & Savic, D. (2025). Transfer learning with graph neural networks for pressure estimation in monitoring-limited water distribution networks. *Water Research*, 287, article number 124475. doi: 10.1016/j.watres.2025.124475.
[17] Yang, S., Behzadian, K., Coleman, C., Holloway, T.G., & Campos, L.C. (2025). Application of AI-based techniques for anomaly management in wastewater treatment plants: A review. *Journal of Environmental Management*, 392, article number 126886. doi: 10.1016/j.jenvman.2025.126886.
[18] Yang, Y., & Lo, E.Y. (2025). Synthetic modeling of water distribution systems for interdependent infrastructure systems resilience analysis with interdependencies via building-mediated clustering. *Resilient Cities and Structures*, 4, 21-36. doi: 10.1016/j.rcns.2025.10.002.
[19] Zapolskyi, A.K. (2005). *Water supply, drainage and water quality*. Kyiv: Vyshcha shkola.
[20] Zhao, X., Liu, D., Wu, Z., & Huang, C. (2024). Chance constrained optimal power-water flow: An iterative algorithm assisted by deep neural networks. *Electric Power Systems Research*, 234, article number 110599. doi: 10.1016/j.epsr.2024.110599.

Симпліціальний аналіз системи розподілу водних ресурсів збагачувальної фабрики

Євген Тимохін

Аспірант
Криворізький національний університет
50027, вул. Віталія Матусевича, 11, м. Кривий Ріг, Україна
https://orcid.org/0009-0003-0821-584X

Вадим Харламенко

Кандидат технічних наук, доцент
Криворізький національний університет
50027, вул. Віталія Матусевича, 11, м. Кривий Ріг, Україна
https://orcid.org/0000-0002-4008-5518

Анотація. Управління водним господарством сучасних рудних збагачувальних фабрик вимагає застосування новітніх методів топологічного аналізу для оптимізації їхньої складної інформаційно-керуючої архітектури перед впровадженням інтелектуальних систем керування на базі алгоритмів машинного навчання. З огляду на це, головною метою роботи було комплексне дослідження структурної зв'язності та визначення точної ієрархії управління системи розподілу водних ресурсів секції збагачувальної фабрики із застосуванням методології симпліціального аналізу для подальшої мінімізації питомих енерговитрат. Дослідження базувалося на фундаментальних принципах алгебраїчної топології. Головним об'єктом виступала топологічна граф-модель системи водопостачання, яка була декомпозирована на тринадцять ключових концептів, що включали технологічні апарати, датчики та керуючі модулі локальних і верхніх рівнів. Отримані результати підтвердили високу ефективність запропонованого математичного підходу. Для розробленої системи було побудовано матрицю суміжності та розраховано показник структурної збитковості, який склав додатне значення $R_k \approx 0{,}31$. Це строго математично підтвердило наявність високої зв'язності, відсутність розривів та надійне внутрішнє резервування технологічної мережі. Крім того, виконано покроковий багатовимірний аналіз: визначено розмірність кожного окремого симплексу, сформовано відповідні класи еквівалентності та згенеровано перший структурний вектор топологічного комплексу $Q_k = (13{,}3{,}1)$. Розрахунок індексу рівномірного розподілу зв'язків орієнтованого графа $\epsilon^2 = 4{,}77$ довів наявність жорсткої ієрархічної структури з яскраво вираженими центрами впливу, повністю спростувавши гіпотезу про однорідність мережі. Встановлено, що найвищу топологічну розмірність формували саме адаптивно-оптимізаційний модуль та інтегровані виконавчі механізми ($q = 1$ та $q = 2$). Практична цінність одержаних результатів полягає у тому, що вони сформували надійне топологічне підґрунтя для майбутнього розгортання графових нейронних мереж. Визначення симплексів найвищої розмірності дозволяє оптимізувати апаратне розміщення датчиків, суттєво підвищити надійність локальних контурів регулювання та знизити питомі витрати електричної енергії і свіжої води за рахунок таргетного управління гідравлічними потоками в умовах динамічної зміни фізичних характеристик вхідної руди

Ключові слова: водопостачання; алгебраїчна топологія; теорія графів; матриця суміжності; автоматизація; оборотна вода; переробка корисних копалин

Journal of Kryvyi Rih National University

Vol. 24, No. 1, 2026

Journal homepage: https://journal-knu.com.ua/en

ISSN 2306-5451
e-ISSN 2519-2736

Article's History: Received: 07.11.2025 Revised: 17.03.2026 Accepted: 28.04.2026 Published: 29.05.2026

UDC 622.831.322:622.28

DOI: 10.31721/2306-5451-2026-1-24-63-72

Prerequisites for studying a two-phase model of steel reinforcement loading in deep excavations

Oleksandr Skobenko*

PhD in Technical Sciences, Associate Professor
Dnipro University of Technology
49005, 19 Dmytro Yavornytskyi Ave., Dnipro, Ukraine
https://orcid.org/0000-0003-4606-4889

Lyubomyr Kurop

Postgraduate Student
Dnipro University of Technology
490051, 19 Dmytro Yavornytskyi Ave., Dnipro, Ukraine,
https://orcid.org/0009-0000-8121-8068

Abstract. Deep underground excavations at great depths are characterised by increased rock pressure, floor heave, and instability phenomena that significantly alter the loading conditions of steel arch supports. Conventional quasi-static calculation models do not fully account for the transition to impulsive loading associated with the loss of elastic-plastic stability of the surrounding rock mass. The objective of this study was to develop and substantiate a two-phase loading model for steel arch supports in deep underground excavations, accounting for nonlinear interaction with the rock mass. The methodology combined analytical modelling based on the theory of a curved beam on an elastic foundation, finite element simulations, and comparison with in situ monitoring data. This integrated approach enabled analysis of the stress-strain evolution of the "support-rock mass" system and identification of a phase transition criterion. The results demonstrate significant differences in the stress-strain state of the steel support between quasi-static and impulsive phases. A phase transition criterion based on a critical excavation contour displacement is proposed and substantiated. In the first phase, maximum bending moments are concentrated at the arch crown and depend on displacement amplitude and flexural stiffness. In the second phase, loading becomes impulsive, and peak bending moments shift towards the support zones depending on the roof collapse configuration. The redistribution of internal forces under nonlinear contact interaction, as well as the influence of anchor stiffness, are analysed. It is shown that impulsive loading may lead the support to its ultimate limit state even when quasi-static conditions appear acceptable. The findings can be applied in the design and assessment of steel supports in deep mine workings and in the development of monitoring systems for early prediction of stability loss

Keywords: stress-strain state; heaving; geomechanical interaction; bifurcation model; bending moments

Introduction

Ensuring the stability of underground workings at great depths remains a critical issue in geomechanics and mining engineering due to increasing in situ stress levels and the complex behaviour of the rock mass. It has been established that at depths of 500 m and greater, stress redistribution leads to intensified plastic deformation, the formation of cracking zones, and loss of stability in excavation roofs. Floor heave and the

Suggested Citation:
Skobenko, O., & Kurop, L. (2026). Prerequisites for studying a two-phase model of steel reinforcement loading in deep excavations. *Journal of Kryvyi Rih National University*, 24(1), 63-72. doi: 10.31721/2306-5451-2026-1-24-63-72.

Copyright © The Author(s). This is an open access article distributed under the terms of the Creative Commons Attribution License 4.0 (https://creativecommons.org/licenses/by/4.0/)

**Corresponding author (skobenko.o.v@nmu.one)*

associated displacements of the rock mass significantly affect the loading conditions of support systems. Under such conditions, conventional quasi-static approaches are often insufficient to describe the evolution of the stress-strain state of the "support-rock mass" system.

Recent studies indicate that floor heave remains one of the primary mechanisms of instability in deep underground excavations. Statistical analyses of underground transport tunnels demonstrated that floor uplift is controlled by geological structure, stress redistribution, and the mechanical properties of the surrounding rock mass. Modern support strategies therefore combine reinforcement of the floor zone with improvements in support-rock interaction in order to limit progressive deformation (Liu *et al.*, 2024). Additional investigations of deep soft-rock tunnels confirmed that deformation control requires not only strengthening of support systems but also pressure-relief measures and optimisation of excavation support schemes (Ling & Ying, 2024). M. Ma *et al*. (2022) investigated optimal support solutions for soft rock roadways using numerical modelling based on the Drucker-Prager yield criterion and demonstrated that appropriately designed combined support systems substantially reduce roadway deformation and improve excavation stability. Field investigations and numerical analyses conducted by Z. Tao *et al*. (2020) further showed that severe deformation in deep soft-rock tunnels results from the combined effects of high in situ stress, weak rock properties, and time-dependent behaviour, while integrated support systems comprising high-strength rock bolts, steel arches, and shotcrete provide the most effective deformation control. In addition to the immediate effects of stress redistribution, the long-term behaviour of deep underground excavations is strongly influenced by time-dependent deformation processes. Progressive deterioration of rock mass properties, creep, and stress relaxation may gradually bring the surrounding rock mass to a critical state even after excavation and support installation. K. Arora & M. Gutierrez (2021) demonstrated that viscous-elastic-plastic deformation mechanisms play a fundamental role in the evolution of squeezing ground conditions and significantly affect tunnel behaviour over time. Similar conclusions were reported by G. Li *et al*. (2020), who showed that deformation and failure processes in deep soft-rock roadways develop progressively and substantially influence support performance. The importance of time-dependent deformation was also confirmed by Q. Zhu *et al*. (2024), who demonstrated that creep significantly accelerates failure evolution in deep high-stress roadways and contributes to the progressive deterioration of surrounding rock stability. Recent studies have increasingly emphasised that excavation stability should be analysed within the framework of a coupled rock-support system rather than by considering support structures separately. T. Yang *et al*. (2023) demonstrated that instability development and support efficiency are strongly controlled by the interaction between reinforcement systems and the surrounding rock mass. Analytical investigations performed by K.-H. Ahn & A. Pouya (2023) further showed that contact interaction between tunnel support and surrounding rocks significantly affects load transfer mechanisms and stress redistribution around underground openings. Similarly, R.-C. Fu *et al*. (2024) developed an exact analytical solution for deep tunnels considering viscoelastic-plastic rock behaviour and the actual excavation loading path, demonstrating that loading history has a substantial influence on stress redistribution and tunnel deformation. Because direct observation of stress redistribution and support loading mechanisms in deep underground excavations is difficult, numerical modelling has become one of the principal tools for investigating geomechanical behaviour. Numerical studies conducted by I. Sakhno & S. Sakhno (2023) demonstrated the effectiveness of computational approaches in analysing floor heave development and evaluating reinforcement efficiency. Similarly, R. Fan *et al*. (2024) showed that numerical models provide valuable insight into deformation evolution and the identification of conditions leading to excavation instability. Geomechanical investigations by M. Kimour *et al*. (2023) likewise confirmed that numerical modelling integrated with rock mass classification methods provides a reliable basis for excavation design and stability assessment under complex geological conditions. Such approaches create a methodological basis for analysing the stress-strain state of the "support-rock mass" system and for developing advanced loading models. Another important feature of deep underground excavations is the possibility of abrupt changes in the stress-strain state during instability development. Experimental investigations performed by H. Shi *et al*. (2023) demonstrated that fractured rock masses exhibit complex mechanical behaviour under dynamic loading conditions, leading to significant changes in strength characteristics and failure mechanisms. Such observations indicate that instability development cannot always be adequately represented by conventional quasi-static approaches alone, particularly when critical deformation states are reached. Physical simulation experiments conducted by S. Zhang *et al*. (2026) further demonstrated that large deformation of surrounding rocks in deep high-geostress roadways develops through progressive damage accumulation, highlighting the importance of incorporating realistic deformation mechanisms into support design and stability assessment.

Despite significant advances in the investigation of floor heave mechanisms, deep roadway stability, support technologies, and support-rock interaction, existing studies are primarily focused either on gradual deformation processes or on individual manifestations of instability. Considerably less attention has been devoted to the transition between these states and its influence on the loading conditions of steel arch supports. In particular, the evolution of support loading from deformation-controlled behaviour to a regime characterised by rapid stress redistribution remains insufficiently formalised within existing geomechanical models. Therefore, the development of a two-phase approach capable of describing both gradual deformation accumulation and its subsequent transformation into intensified support loading remains an important scientific and engineering problem. The aim of this study was to develop and validate a two-phase loading model for steel arch supports in deep underground excavations that accounts for the nonlinear interaction between the support system and the surrounding rock mass.

Materials and Methods

The performance of underground excavations supported by steel arch systems was analysed taking into account the interaction in the "support-rock mass" system under increasing geostatic pressure and contour deformation. A two-phase loading scheme was adopted: a phase with controlled deformation, characterised by a gradual increase in the displacements of the excavation contour, and a phase of suddenly applied static load, which occurs after the loss of stability of the excavation bottom. The transition between the phases was governed by a predetermined critical displacement criterion corresponding to the onset of instability. The computational domain was represented as a fragment of the excavation under plane strain conditions, explicitly taking into account the geometry of the cross-section. The model dimensions were selected to eliminate the influence of boundaries in the central analysis zone. Anchor elements were located in accordance with the design configuration of the support system.

The research methodology was based on an integrated combination of analytical methods of deformable solid mechanics, numerical modelling using the finite element method (FEM) or the discrete element method (DEM), and comparative analysis with field observations. This approach ensured consistency between theoretical assumptions and field monitoring data. The analytical model of the steel arch support and its behaviour was described using the classical model of a curved beam on an elastic foundation (Winkler foundation model). Within this framework, the surrounding rock mass was represented as a system of distributed elastic springs, the stiffness of which characterised the resistance of the rock mass to deformation. The governing differential equation describing the deformation of the steel arch under the influence of external loading and the reaction of the rock mass was written in the following general form:

$$Id4u(x)/dx4 = R(x, t), \tag{1}$$

where $u(x, t)$ – the vertical displacement of the support element at point x and time t; EI – the bending stiffness of the steel element; $R(x, t)$ – the distributed load exerted by the surrounding rock mass The internal forces in the model are determined by the combined stiffness of the surrounding rock mass, the anchor reinforcement system, and the steel arch support, which is consistent with contemporary approaches to support-rock interaction modelling (Ahn & Pouya, 2023; Yang *et al.*, 2023). For rock bolt support:

$$N = k_a(u_n - u_{nop}) = E \cdot \varepsilon, \tag{2}$$

where k_a – the anchor stiffness; u_a and u_r – the displacements of the anchor and the surrounding rock mass, respectively; and ε is the anchor strain. For the steel arch support, the normal forces, shear forces, and bending moments are considered.

Normal force:

$$N = EA \cdot \frac{du}{ds}. \tag{3}$$

Shear force:

$$Q = \frac{dM}{ds}. \tag{4}$$

Bending moment:

$$M = -EI \cdot d^2w/ds^2, \tag{5}$$

where E – the modulus of elasticity of the arch; A – the cross-sectional area; I – the moment of inertia of the projected profile; u and w are the longitudinal and transverse displacements, respectively, and s – the coordinate along the arch. These expressions make it possible to describe the stress-strain state of the combined support system under complex external loading and to evaluate the interaction between support elements and the surrounding rock mass under varying geomechanical conditions (Ahn & Pouya, 2023). The analytical framework combines methods of deformable solid mechanics with numerical modelling based on the finite element and continuum approaches. Similar methodologies have been successfully applied in the analysis of floor heave development, support performance, and excavation stability in deep underground workings (Sakhno & Sakhno, 2023; Fan *et al.*, 2024). A comparative analysis was performed between the measured excavation contour displacements obtained from field monitoring and the corresponding analytical and numerical predictions, which is consistent with modern practices in geomechanical research.

Ensuring the stability of deep underground excavations remains a critical issue in modern geomechanics and geotechnical engineering. Studies of deep soft-rock roadways demonstrated that increasing depth is associated with higher stress concentrations, enhanced deformation of the surrounding rock mass, and deterioration of excavation stability conditions (Li *et al.*, 2020). Furthermore, investigations of floor heave mechanisms confirmed that deformation of the excavation floor represents one of the principal manifestations of instability and therefore should be explicitly considered in geomechanical calculations and numerical analyses (Mo *et al.*, 2020; Sakhno & Sakhno, 2023). The operational performance of underground excavations is ensured through the installation of steel arch support systems. Two loading phases are considered: a deformation-controlled phase under prescribed, gradually increasing displacements; a phase of impulsive distributed loading occurring after the loss of stability of the excavation floor. The proposed model is based on the concept of piecewise-continuous loading, with phase transition governed by a predefined critical displacement criterion.

The computational domain represents a fragment of the excavation under plane strain conditions, explicitly accounting for the geometry of its cross-section. The size of the modelling domain is selected to eliminate the influence of boundary conditions on results obtained in the central region. Anchor elements are positioned according to the design specifications. The geomechanical parameters of the support-rock system include rock mass mechanical properties, excavation depth, cross-sectional dimensions, support type, and steel profile characteristics. Rock mass properties are evaluated based on laboratory test results, field investigations, and numerical modelling. Key parameters include the elastic modulus, Poisson's ratio, uniaxial compressive strength, uniaxial tensile strength, internal friction angle, cohesion, and specific adhesion. These parameters govern the resistance of rocks to compression and shear and are critical for assessing the geomechanical conditions surrounding the excavation and for selecting a rational support system. The contact between the support and the surrounding rock mass is mathematically described as a nonlinear interaction between two structural elements. At the initial stage, load transfer occurs elastically, followed by a transition to plastic contact behaviour as deformation progresses. Consideration of contact friction characteristics, support stiffness, and non-uniform load distribution is essential in numerical simulations. These effects are modelled using specialised contact elements implemented in software packages such as FLAC3D, ABAQUS, or UDEC.

Depending on excavation depth and rock mass structure, the following primary failure mechanisms are considered: brittle failure with crack formation, plastic deformation, shear failure, and combined mechanisms. At great depths, elevated stress levels promote predominantly plastic and combined failure modes. Failure zones are identified using the Mohr-Coulomb criterion or alternative strength criteria, depending on the adopted material model and research objectives. During interaction with the rock mass, normal and shear forces develop within the steel arch elements and vary along the excavation perimeter. Their analysis is performed using limited equilibrium methods, the finite element method, or semi-analytical approaches. Internal forces-bending moments, shear forces, and axial forces-define the load-bearing capacity of the support elements and serve as key criteria for optimising support profiles. Three main stages of support performance during rock mass deformation are distinguished: an initial elastic stage, where the support operates within elastic limits; an intermediate stage, characterised by plastic deformation of the surrounding rock mass and partial load transfer to the arch; a critical stage, in which the contact zone fails, and the support operates under limit conditions. These stages describe the temporal evolution of loads acting on the support system.

The structural characteristics of the steel arch support, including the profile of steel sections, connection methods, and the presence of additional reinforcing elements, significantly influence its stiffness and stability. Analyses indicate that closed-loop systems reinforced with stiffening ribs provide a more uniform load distribution. The selection of support bearing points and support conditions is also crucial and depends on excavation width and lateral pressure characteristics. Accounting for secondary deformations during long-term operation of deep underground excavations is essential, as these are associated with rock creep and delayed settlements. Such processes may lead to additional loading of the support even after primary deformations have stabilised. To capture these effects, viscoelastic and rheological models must be employed, enabling prediction of the long-term evolution of the stress-strain state of steel arch support throughout the service life of the excavation. A necessary condition for implementing long-term prediction is the determination, through in situ investigations, of parameters describing the deformation characteristics of the rock mass, namely the time-dependent relationships of changes in the elastic modulus and Poisson's ratio.

Results and Discussion

The result of the study was the development and analytical study of a two-phase model describing the stress-strain state of a steel arch support in permanent underground workings. The model took into account the interaction with the surrounding rock mass, the transition from a quasi-static to an excited (impulse) state of loading, and separate mechanical mechanisms controlling each phase. The steel arch was modelled as an elastic curved beam with length L and bending stiffness EI. Hinged supports were provided at the base of the arch, where steel anchor bolts could be installed. The surrounding rock mass was represented as a solid medium capable of elastic-plastic behaviour with dilatancy after critical stress or deformation thresholds were exceeded. The interaction between the arch and the surrounding rock mass in both loading phases was analyses under plane deformation conditions.

The computational scheme considered a steel arch optionally reinforced with anchorage elements at the support points. In the first loading phase, the arch was subjected to a distributed displacement field $w(x)$ induced by the deforming surrounding rock mass. In the second phase, the loading was represented by a concentrated or distributed load $q(x)$ simulating the effects of roof instability or sudden stress redistribution. As an illustrative example, a standard double-track underground excavation supported by a steel arch made of SVP-27 special profile was analyses. The adopted parameters were: $L = 8.58$ m; $EI = 6 \times 10^5$ N/m^2; critical displacement $w_{cr} = 0.30$ m; the load distribution $q(x)$ is assumed to be piecewise constant. The modelling domain was defined so that the object of investigation was the steel arch support interacting with the surrounding rock mass deforming toward the excavation under in situ stresses and anthropogenic influences. The subject of investigation was the stress-strain state of the steel arch support. The surrounding rock mass was represented as a heterogeneous system including: a boundary zone of inelastic deformation; a fracture development zone; a direct contact zone where loosened rock interacted with the steel arch. The boundaries between modelling phases were determined based on field observations, geophysical measurements, and analytical assessment of critical displacement conditions.

The proposed loading model can be described as one of the options, as a time-dependent function that accounts for two distinct stages:

$$R(x, t) = (1 - \chi(t)) \cdot k(x)u(x, t) + \chi(t) \cdot (-q(x)), \quad (6)$$

where $k(x)$ – the modulus of the rock's elastic reaction; $q(x)$ – the intensity of the uniform vertical pressure from the collapsed mass; $\chi(t)$ – the Heaviside function, which defines the transition between the stages.

The transition between the loading regimes occurs when the critical vertical displacement in the floor rock mass is reached:

$$\chi(t)=\{0, \delta(t) < \delta cr1, \delta(t) \geqslant \delta kp, \quad (7)$$

where $\delta cr = 0.3$ m. The value $\delta cr = 0.3$ m was determined empirically for the geological and mining conditions of the Western Donbas coal basin based on field observations of floor heave processes and stability loss in deep excavations. This parameter should be considered as a calibrated value applicable to similar geomechanical environments. The critical displacement can be expressed in a generalised form as $\delta cr = f(H, \sigma c, E, S)$, where H – mining depth; σc – compressive strength of floor rocks; E – deformation modulus; S – support stiffness. However, for the considered case study, this relationship was simplified by adopting the empirically established value $\delta cr = 0.3$ m.

First regime: the displacements of the arch ends are prescribed. An approximate form of the displacement is used:

$$u(x) = u_{max}/2 \times (1 - cos(\pi x/L)), x \in [0, L]. \quad (8)$$

From this, the reaction of the rock mass can be determined:

$$R_1(x) = k(x) \times u(x), \quad (9)$$

and the bending moment:

$$M_1(x) = -EI \times (u_{max} \times \pi^2/(2L^2)) \times cos(\pi x/L). \quad (10)$$

Second regime: the load from the roof collapse is prescribed. This occurs after floor heave and the formation of roof falls:

$$R_2(x) = -q(x), q(x) = const = q_0. \quad (11)$$

A new form of $u(x)$ – determined, taking into account the boundary conditions, followed by the updated distribution of bending moments:

$$M_2(x) = -EI \times d^2u(x)/dx^2. \quad (12)$$

At the lower boundary of the digital model, fixed support conditions (zero displacement) are imposed. At the lateral boundaries, either symmetry or prescribed displacements are applied, depending on the symmetry of the problem. The upper boundary may be free or subjected to loading according to the depth of the excavation. The initial stress state is assumed to be hydrostatic or determined using justified empirical formulas.

Depending on the type of support, the boundary conditions for the steel arch are as follows:

hinged support: $u(0) = u(L) = 0$, $M(0) = M(L) = 0$; (13)

fixed support: $u(0) = u(L) = 0, du/dx|x=0 = du/dx|x=L = 0$. (14)

Anchors are represented as elements that transfer loads to the rock mass through a contact zone. Their behaviour is defined by elastic properties (stiffness) as well as the parameters of the ultimate force at which failure occurs. Nonlinear contact interaction is modelled between the anchor and the surrounding rock mass. The model accounts for adhesion, possible micro-movements, friction, and strength reduction due to loosening. Upon reaching the limit conditions, detachment or sliding is implemented. For long-term prediction of the support system's behaviour, rock creep is taken into account. Rheological models such as Norton-Bailey, Burger, or others, which describe the dependence of deformation on time and stress, are applied. This allows considering the relaxation of loads in the "rock mass-support" system. Analytical solutions are possible in simple cases (constant k, cosine-shaped displacement); numerical implementation is carried out using the finite element method (FEM). The mesh is constructed with adaptation in zones of expected stress concentration. Nonlinear solution procedures with incremental load application and convergence control are used. Load distributions $R(x)$, displacements $u(x)$, and bending moments $M(x)$ are constructed for both phases.

The stress-strain state of the support, as well as the distributions of loads and bending moments for both phases, are schematically presented in Figure 1a and Figure 1b, respectively. These figures are intended to illustrate the proposed mechanical concept rather than represent specific measured data. Figure 1a schematically presents the time-dependent response of the "support-rock mass" system $R(t)$ and illustrates the mechanism of phase transition. The first phase corresponds to the regime of prescribed deformations, in which the load increases proportionally to the excavation contour displacement up to the level level R_1 at time t_1. Point B denotes the attainment of a critical contour displacement associated with the onset of elastic-plastic stability loss in the floor rocks and the initiation of floor heave development. From this moment, the system transitions to the second phase, characterised by a change in the interaction mechanism and the formation of impulsive loading, reaching the level R_2. Figure 1b schematically illustrates the variation in bending moment distribution within the steel arch support during each phase. In the first phase (prescribed deformation regime), a classical bending moment diagram is formed, with maximum values concentrated at the arch crown. In the second phase (prescribed load regime), redistribution of internal forces occurs due to nonlinear contact interaction and changes in loading configuration. This effect is conditionally represented by the modified shape of the bending moment diagram. Analysis of these dependencies allows identifying key features of steel support behaviour in each phase.

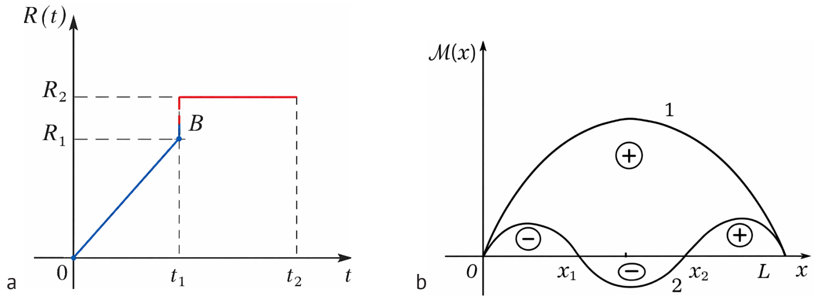

Figure 1. Conceptual schematic representation of the two-phase loading model of a steel arch support in deep underground workings

Notes: a) evolution of the load acting on the support during the first and second loading phases; b) distribution of bending moments in the support during the first and second loading phases

Source: developed by the authors based on the proposed theoretical model

In the first phase, under prescribed displacements from the rock mass, bending moments are a function of the deflection shape. The bending moment diagram has a sinusoidal form, with a maximum at the centre of the arch span. The maximum moment value is directly proportional to the displacement amplitude and the flexural stiffness of the support. The support state in this phase is considered quasi-static and controlled. In the second phase, the bending moment distribution assumes a classical form, transitioning from tensile forces along the contour to compressive forces. The combined moment diagram exhibits a complex shape depending on the parameters of the distributions in each phase. The presented calculations and diagrams illustrate changes in the deflection shape, moment distribution, and load nature in two fundamentally different phases. This allows clear differentiation of the support operation regimes, which is essential for designing reinforced structures adapted to real conditions at great depths.

Three main stages of the support's behaviour during rock deformation were identified: the first stage – the elastic stage-during which the support operated within the elastic range and load redistribution was moderate; the second is the transitional stage, characterised by plastic deformation of the surrounding rock and a gradual transfer of the load to the arch; and the third stage is the critical stage, during which contact deteriorated and the support approached its limit state under increased loading. These stages described the temporal evolution of loads acting on the support system and clarified the mechanism of transition from displacement-controlled behaviour to load-controlled response. The structural characteristics of the steel arch support-including profile geometry, connection methods, and the presence of reinforcing elements-were found to significantly influence stiffness and load distribution. Closed-loop systems reinforced with stiffening ribs provided a more uniform redistribution of internal forces along the perimeter. The selection of bearing points and boundary conditions was shown to depend on excavation width and lateral pressure characteristics. Secondary deformations associated with rock creep and delayed settlements were observed to produce additional loading of the support even after stabilisation of primary displacements. To capture these long-term effects, rheological and viscoelastic models were incorporated, enabling prediction of the long-term evolution of the stress-strain state throughout the service life of the excavation.

The results obtained were compared with studies of the last five years on the mechanisms of stability loss in deep underground excavations. The increase in plastic deformation with depth and the expansion of loosening zones identified in this study were consistent with the mechanisms of floor heave formation described by S. Mo *et al*. (2020). Their research confirmed that floor heave significantly influences support performance. The present results supported this conclusion and further specified the mechanical consequences of this influence through a displacement-based instability criterion. The change in stress distribution with increasing geostatic pressure was consistent with the deformation characteristics reported by G. Li *et al*. (2020), Y. Ling & X. Ying (2024). However, unlike their work, which primarily focused on empirical deformation observations, the present study introduced a formalised bifurcation-based transition criterion that defined the boundary between quasi-static and impulse phases.

The obtained results agree with the findings of I. Sakhno & S. Sakhno (2023) and R. Fan *et al*. (2024), who demonstrated that floor heave significantly influences excavation stability and support loading. The present study further develops this concept through a phase-dependent loading model. The numerical results regarding sharp increases in bending moments under instability conditions were consistent with the dynamic response patterns described by H. Shi *et al*. (2023). At the same time, the present model additionally demonstrated the migration of maximum bending moments from the arch crown toward the support zones during the impulse phase, which was not explicitly formalised in their analysis. The importance of nonlinear contact interaction confirmed in this research corresponded to the modelling results of K.-H. Ahn & A. Pouya (2023). Their conclusions indicated that neglecting contact nonlinearity led to an underestimation of internal forces. The present study supported this view and incorporated contact nonlinearity directly into the phase-dependent formulation.

The nonlinear mechanical behaviour of steel arches under high ground pressure described H. Shi *et al*. (2024) confirmed that geometric and material nonlinearities significantly influenced load-bearing capacity. The obtained results were consistent with these findings and demonstrated that such nonlinear effects became especially pronounced during the impulse loading stage. The time-dependent deformation processes identified in this work were comparable with the rheological behaviour reported by K. Arora & M. Gutierrez (2021), R.-C. Fu *et al*. (2024). Their results emphasised the significance of creep effects in deep roadways. The present study agreed with this interpretation and incorporated long-term deformation into the general stability framework. The effectiveness of reinforcement systems in controlling deformation of deep soft-rock roadways was confirmed by the numerical investigations of C. Zhang *et al*. (2026). Their results demonstrated that grouted rock bolting significantly improved the mechanical response of the surrounding rock mass and increased excavation stability under complex geomechanical conditions. The present study supports this interpretation and further extends it by demonstrating that support performance is strongly influenced by the phase-dependent evolution of loading conditions associated with floor-heave-induced instability.

The obtained results demonstrated that instability develops progressively and may be accompanied by substantial changes in the stress-strain state after reaching a critical deformation level. This interpretation is consistent with contemporary studies of deep roadway instability but extends them through the introduction of an explicit displacement-based transition criterion. The monitoring-based assessment of deformation development and support performance reported by S. Qin *et al*. (2026) confirmed that instability evolves progressively before reaching a critical state. The present findings are consistent with this interpretation and provide an analytical explanation of the observed deformation evolution within a unified mechanical framework. The probabilistic assessment of underground excavation stability proposed by F. de Silva *et al*. (2023) demonstrated the importance of accounting for uncertainty. Although the developed model remained deterministic, its structure allowed for further extension toward reliability-based analysis, which was considered a promising direction for future research.

The rock mass characterisation principles formulated by M. Kimour *et al*. (2023) confirmed that accurate mechanical parameterisation was essential for stability prediction. The present study supported this methodological position and applied compatible mechanical assumptions focused on phase evolution. In addition, the numerical investigations of nonlinear support-rock interaction conducted by T. Yang *et al*. (2023) demonstrated that coupled behaviour significantly influenced stress redistribution. The present results agreed with this conclusion and integrated the coupled interaction into the proposed framework. The mechanical representation of the support as a structural element interacting with an elastic foundation was conceptually consistent with the simplified finite element formulation. The beam-on-two-parameter-foundation model demonstrated that accounting for shear interaction within the foundation layer significantly affected bending moment distribution and displacement patterns. The present study agreed with this methodological approach and extended it to deep underground conditions by incorporating phase-dependent instability development and nonlinear contact interaction. Unlike the simplified elastic formulation adopted in their work, the current model additionally captured the transition to impulse loading and redistribution of internal forces after reaching the critical contour. Field observations of large deformation control presented by S. Zhang *et al*. (2026) confirmed that inadequate accounting for floor heave led to progressive loss of stability. The current findings supported this practical conclusion and provided a theoretical basis for interpreting such cases.

Overall, the reviewed studies confirmed the relevance of considering progressive deformation and failure evolution in deep underground workings. Most of the analysed works supported the key theses formulated in this article regarding the decisive role of stress redistribution, nonlinear interaction, and combined loading. However, unlike existing models, the present research formalised the impulse loading stage through a bifurcation-based displacement criterion and integrated nonlinear contact interaction, rheological effects, bending moment migration, and analytical load redistribution within a single consistent mechanical framework. This unified approach provided a comprehensive interpretation of support behaviour under deep geomechanical conditions and clarified the similarities and differences between the obtained results and contemporary scientific findings.

Conclusions

The necessity of considering the phased interaction between steel supports and the surrounding rock mass in deep underground excavations has been substantiated. It has been shown that the stress-strain behaviour of the "support-rock mass" system cannot be adequately described within a single loading regime due to fundamentally different mechanical responses before and after floor instability. A two-phase geomechanical model has been proposed and analytically justified. The model reflects the evolution of the stress-strain state during progressive rock mass deformation and formalises the transition between quasi-static and impulse loading stages. In the first phase, prescribed deformations of the surrounding rock mass are assumed. The support behaviour is governed by controlled bending, and its mechanical state is defined by the deflection geometry and stiffness of the arch elements. The bending moment distribution remains continuous and is primarily dependent on the imposed displacement contour. The transition to the second phase is triggered by the loss of elastic-plastic stability of the floor rock, leading to heave development, partial unloading of the surrounding mass, and local roof destabilisation. This transition results in an impulsive loading regime accompanied by rapid stress redistribution within the steel support.

The results demonstrate a fundamental difference in bending moment distributions between the two phases. After the onset of floor instability, the maximum bending moments shift from the arch crown towards the support zones, while stress concentration and internal forces increase significantly, raising the likelihood of reaching the ultimate load-bearing capacity. A bifurcation-based displacement criterion has been formulated to define the boundary between quasi-static deformation and impulse loading, providing a physically justified indicator of instability initiation. The analysis confirms that neglecting nonlinear contact interaction and phase transition effects leads to underestimation of internal forces and incomplete representation of support performance. The proposed model integrates nonlinear contact behaviour, stress redistribution, bending moment migration, and long-term deformation within a unified framework. The results are of both theoretical and practical significance, contributing to improved support design reliability and more accurate assessment of critical operational states. Future work should focus on experimental validation, three-dimensional modelling, probabilistic analysis, and the development of design-oriented software tools.

Acknowledgements

None.

Funding

None.

Conflict of Interest

None.

References

[1] Ahn, K.-H., & Pouya, A. (2023). Analytical solution of circular tunnel-lining interaction with elastic contact. *Tunnelling and Underground Space Technology*, 140, article number 105311. doi: 10.1016/j.tust.2023.105311.

[2] Arora, K., & Gutierrez, M. (2021). Viscous-elastic-plastic response of tunnels in squeezing ground conditions: Analytical modeling and experimental validation. *International Journal of Rock Mechanics and Mining Sciences*, 146, article number 104888. doi: 10.1016/j.ijrmms.2021.104888.

[3] de Silva, F., Ramondini, M., & Flora, A. (2023). Reliability-based evaluation of the stability of underground cavities in Naples. In A. Ferrari, M. Rosone, M. Ziccarelli & G. Gottardi (Eds.), *Geotechnical engineering in the digital and technological innovation era* (pp. 587-594). Cham: Springer. doi: 10.1007/978-3-031-34761-0_71.

[4] Fan, R., Chen, T., Wang, S., Jiang, H., & Yin, X. (2024). Study on influencing factors and prediction of tunnel floor heave in gently inclined thin-layered rock mass. *Applied Sciences*, 14(17), article number 7701. doi: 10.3390/app14177701.

[5] Fu, R.-C., Wang, H.-N., & Jiang, M.-J. (2024). Exact analytical solution for deep tunnels in viscoelastic-plastic rock considering the actual loading path. *Applied Mathematical Modelling*, 128, 370-391. doi: 10.1016/j.apm.2024.01.009.

[6] Kimour, M., Boukelloul, M.L., Hafsaoui, A., Narsis, S., Benghadab, K.M., & Benselhoub, A. (2023). Geomechanical characterization of rock mass rating and numerical modeling for underground mining excavation design. *Journal of Geology, Geography and Geoecology*, 32(1), 67-78. doi: 10.15421/112308.

[7] Li, G., Ma, F., Guo, J., Zhao, H.J., & Liu, G. (2020). Study on deformation failure mechanism and support technology of deep soft rock roadway. *Engineering Geology*, 264, article number 105262. doi: 10.1016/j.enggeo.2019.105262.

[8] Ling, Y., & Ying, X. (2024). Pressure relief for drilling (trenching) and support technology in deep soft rock tunnels. *Frontiers in Earth Science*, 12, article number 1501420. doi: 10.3389/feart.2024.1501420.

[9] Liu, Y., Tao, L., Zhao, S., Chen, W., & Ni, Y. (2024). Technology for treatment and reinforcement of soft rock tunnel floor using sealing material. *Buildings*, 14(12), article number 4004. doi: 10.3390/buildings14124004.

[10] Ma, M., Guo, Q., Pan, J., Ma, C., & Cai, M. (2022). Optimal support solution for a soft rock roadway based on the Drucker-Prager yield criteria. *Minerals*, 12(1), article number 1. doi: 10.3390/min12010001.

[11] Mo, S., Ramandi, H.L., Oh, J., Masoumi, H., Canbulat, I., Hebblewhite, B., & Saydam, S. (2020). A new coal mine floor rating system and its application to assess the potential of floor heave. *International Journal of Rock Mechanics and Mining Sciences*, 128, article number 104241. doi: 10.1016/j.ijrmms.2020.104241.

[12] Qin, S., Zhao, X., Song, J., Ma, S., Wang, F., Wang, C., & Wang, Y. (2026). Monitoring-based assessment of deformation behaviour and support effectiveness in a deep hard rock drift. *Applied Sciences*, 16(3), article number 1388. doi: 10.3390/app16031388.

[13] Sakhno, I., & Sakhno, S. (2023). Numerical studies of floor heave mechanism and the effectiveness of grouting reinforcement of roadway in soft rock containing the mine water. *International Journal of Rock Mechanics and Mining Sciences*, 170, article number 105484. doi: 10.1016/j.ijrmms.2023.105484.

[14] Shi, H., Chen, W., Zhang, H., Song, L., Li, M., Wang, M., & Lu, P. (2023). Dynamic strength characteristics of fractured rock mass. *Engineering Fracture Mechanics*, 292, article number 109678. doi: 10.1016/j.engfracmech.2023.109678.

[15] Shi, H., Zhang, H., Chen, W., Song, L., & Li, M. (2024). Pull-out debonding characteristics of rockbolt with prefabricated cracks in rock: A numerical study based on particle flow code. *Computational Particle Mechanics*, 11(1), 29-53. doi: 10.1007/s40571-023-00607-9.

[16] Tao, Z., Cao, J., Yang, L., Guo, A., Huang, R., Yang, X., Yuan, D., & Hou, L. (2020). Study on deformation mechanism and support measures of soft surrounding rock in Muzhailing deep tunnel. *Advances in Civil Engineering*, 2020, article number 9367916. doi: 10.1155/2020/9367916.

[17] Yang, T., Liu, J.Z., Luo, J.Q., Shen, Y.P., & Fu, P. (2023). Study on instability mechanism of soft rock roadway and pressure-relief bolt-grouting support technology. *Scientific Reports*, 13, article number 20667. doi: 10.1038/s41598-023-47451-8.

[18] Zhang, C., Wang, Y., Zhao, E., Fang, Y., Zhang, X., Li, L., & Binwal, S. (2026). Research on the large deformation mechanism of surrounding rocks in deep high geostress roadway through physical simulation tests. *Advances in Civil Engineering*, 2026, article number 4535876. doi: 10.1155/adce/4535876.

[19] Zhang, S., Jiang, F., Yang, M., Zhao, Y., Qiao, W., Wang, L., Zhang, X., & Wu, Y. (2026). Numerical simulation study on grouted rock bolting for surrounding rock masses in deep soft rock roadway. *Buildings*, 16(5), article number 1014. doi: 10.3390/buildings16051014.

[20] Zhu, Q., Li, T., Gao, X., Wang, Y., & Wang, B. (2024). Deformation characteristics and failure evolution in deep high-stress roadways under creep action. *Engineering Failure Analysis*, 157, article number 107689. doi: 10.1016/j.engfailanal.2023.107689.

Передумови дослідження двофазної моделі навантаження сталевого кріплення у виробках глибокого закладення

Олександр Скобенко

Кандидат технічних наук, доцент
Національний технічний університет «Дніпровська політехніка»
49005, просп. Дмитра Яворницького, 19, м. Дніпро, Україна
https://orcid.org/0000-0003-4606-4889

Любомир Куроп

Аспірант
Національний технічний університет «Дніпровська політехніка»
49005, просп. Дмитра Яворницького, 19, м. Дніпро, Україна
https://orcid.org/0009-0000-8121-8068

Анотація. Глибокі підземні виїмки на значних глибинах характеризуються підвищеним тиском гірської породи, підйомом дна та явищами нестабільності, що істотно змінюють умови навантаження на сталеві арочні опори. Традиційні квазістатичні розрахункові моделі не враховують у повній мірі перехід до імпульсного навантаження, пов'язаного з втратою пружно-пластичної стійкості навколишньої гірської породи. Метою даного дослідження було розроблення та обґрунтування двофазної моделі навантаження для сталевих арочних опор у глибоких підземних виїмках з урахуванням нелінійної взаємодії з гірською породою. Методологія поєднувала аналітичне моделювання на основі теорії вигнутої балки на пружному фундаменті, моделювання методом скінченних елементів та порівняння з даними моніторингу на місці. Цей інтегрований підхід дозволив проаналізувати еволюцію напружено-деформаційного стану системи «опора-гірська порода» та визначити критерій фазового переходу. Результати демонструють значні відмінності у стані напруження-деформації сталевої опори між квазістатичною та імпульсною фазами. Запропоновано та обґрунтовано критерій фазового переходу, заснований на критичному зміщенні контуру виїмки. У першій фазі максимальні згинальні моменти зосереджуються на вершині арки та залежать від амплітуди зміщення та жорсткості на згин. У другій фазі навантаження стає імпульсним, а пікові згинальні моменти зміщуються у бік зон опори залежно від конфігурації обвалу покрівлі. Проаналізовано перерозподіл внутрішніх сил за умов нелінійної контактної взаємодії, а також вплив жорсткості анкера. Показано, що імпульсне навантаження може призвести до переходу опори в граничний стан, навіть якщо квазістатичні умови здаються прийнятними. Отримані результати можуть бути застосовані при проектуванні та оцінці сталевих опор у глибоких гірничих виробітках, а також при розробці систем моніторингу для раннього прогнозування втрати стійкості

Ключові слова: напружено-деформований стан; пучення; геомеханічна взаємодія; модель біфуркації; згинальні моменти

Journal of Kryvyi Rih National University

Journal homepage: https://journal-knu.com.ua/en

Article's History: Received: 22.10.2025 Revised: 03.03.2026 Accepted: 28.04.2026 Published: 29.05.2026

Vol. 24, No. 1, 2026

ISSN 2306-5451

e-ISSN 2519-2736

UDC 331.45:62-5:631

DOI: 10.31721/2306-5451-2026-1-24-73-85

Occupational health and safety in the age of automated engineering solutions in agriculture

Oleg Ivanov*

PhD in Technical Sciences, Associate Professor
Poltava State Agrarian University
36003, 1/3 Hryhorii Skovoroda Str., Poltava, Ukraine
https://orcid.org/0000-0002-1761-9913

Nadiia Opara

PhD in Agricultural Sciences, Associate Professor
Poltava State Agrarian University
36003, 1/3 Hryhorii Skovoroda Str., Poltava, Ukraine
https://orcid.org/0000-0002-0128-8400

Abstract. The rapid implementation of automated engineering solutions in agriculture has significantly transformed occupational health and safety conditions. The purpose of this study was to analyse the impact of automation on occupational safety in the agricultural sector, identify emerging risks, and develop practical approaches to safety management. The research was based on a comprehensive methodological framework combining system analysis, comparative legal analysis, risk classification, and cases described in scientific literature involving automated systems. National regulatory frameworks were examined alongside international standards to assess their adequacy in addressing the challenges associated with agricultural automation. The results demonstrated that automation does not eliminate occupational risks but leads to their transformation, forming a multidimensional risk system in which traditional hazards are supplemented by new categories, including risks related to human–machine interaction, cybersecurity, and increased psychophysiological load. It was established that the transition from manual labour to supervisory and analytical functions reduces direct physical risks while increasing dependence on system reliability, data accuracy, and decision-making processes. The study also revealed significant regulatory gaps, particularly in liability distribution, software reliability, and safety requirements for autonomous systems. In addition, the results confirmed the transformation of labour functions, characterised by increased demand for digital competencies and the need for structured training and certification systems. The practical significance of the study lies in the development of applied safety management approaches, including scenario-based risk assessment, implementation of digital monitoring systems, and continuous personnel training. The application of these measures contributes to reducing occupational injuries, minimising downtime, improving process controllability, and enhancing the overall efficiency of agricultural enterprises. However, their effectiveness depends on overcoming regulatory, organisational, and financial constraints

Keywords: human-machine interaction; autonomous agricultural systems; industrial cybersecurity; precision farming technologies; risk transformation; robotics

Introduction

The integration of automated engineering solutions into the agricultural sector fundamentally transformed not only production processes but also the nature of occupational risks. Unlike traditional mechanisation,

Suggested Citation:
Ivanov, O., & Opara, N. (2026). Occupational health and safety in the age of automated engineering solutions in agriculture. *Journal of Kryvyi Rih National University*, 24(1), 73-85. doi: 10.31721/2306-5451-2026-1-24-73-85.

Copyright © The Author(s). This is an open access article distributed under the terms of the Creative Commons Attribution License 4.0 (https://creativecommons.org/licenses/by/4.0/)

*Corresponding author (oleg.ivanov@pdau.edu.ua)

which primarily altered physical workloads, modern automation introduced complex interactions between humans, autonomous machines, and digital infrastructures. This created a qualitatively new risk environment characterised by unpredictability, system interdependence, and increased reliance on software-controlled decision-making. This trend is also supported by a study by Z. Zhai *et al.* (2020) on decision support systems in Agriculture 4.0, which demonstrated that the increasing reliance on data-driven platforms enhances decision-making efficiency but simultaneously introduces new dependencies on data quality, system integration, and algorithmic reliability.

Under such conditions, occupational health and safety could no longer be limited to conventional hazard prevention approaches focused on mechanical or chemical factors but required a systemic model capable of addressing hybrid risks emerging at the intersection of human factors, robotics, and digital technologies. This challenge became particularly acute in contexts where external destabilising factors, such as military threats or labour shortages, accelerated the adoption of automation without the simultaneous development of adequate regulatory and safety frameworks.

Scientific research increasingly focused on various aspects of automation in agriculture and its implications for safety and labour transformation. J. Lincoln *et al.* (2025) investigated occupational safety challenges related to robotics and autonomous machines in agriculture and concluded that traditional safety models were insufficient for managing risks associated with human-robot interaction, particularly during maintenance and non-routine operations. Similarly, J.C. Mayoral Baños *et al.* (2023) developed a risk management framework for safe robotic navigation in agricultural environments, emphasising the importance of integrating human detection systems and fail-safe mechanisms to prevent collisions. Their findings highlighted that technological reliability alone did not guarantee safety without proper system design and operational protocols. In the context of technological development, S. Hossain *et al.* (2025) analysed autonomous navigation systems in agricultural machinery and demonstrated that environmental factors such as dust, uneven terrain, and sensor limitations significantly affected system performance, thereby increasing the likelihood of operational errors. At the same time, J. Lowenberg-DeBoer *et al.* (2021) examined the regulatory impact on autonomous agricultural equipment in Europe and concluded that legal uncertainty regarding liability distribution among stakeholders represented a major barrier to the safe implementation of such technologies. This indicated that safety issues extended beyond technical aspects and required institutional and legal solutions.

The transformation of agricultural production through digitalisation was also explored by V. Tankosić *et al.* (2024), who emphasised that Agriculture 4.0 technologies, including IoT and data-driven platforms, significantly improve operational efficiency while simultaneously introducing new categories of risks related to system reliability, data quality, and cybersecurity vulnerabilities. Similarly, K.G. Liakos *et al.* (2018) highlighted that the application of machine learning in agriculture enables advanced predictive analytics and optimisation of production processes, but increases dependence on data accuracy and model reliability, which may introduce additional operational risks. This perspective is further supported by S. Ballingall *et al.* (2023), who analysed safety standards for autonomous systems and demonstrated that cybersecurity becomes an essential component of operational safety, particularly in systems based on artificial intelligence and remote control technologies. From a labour perspective, automation does not eliminate jobs but transforms them, increasing demand for specialists capable of combining technical, analytical, and managerial competencies. At the same time, this shift creates new psychophysiological risks associated with increased cognitive load and responsibility (World Economic Forum, 2023).

L. Benos *et al.* (2023) demonstrated that the increasing integration of human–robot interaction systems in agriculture requires a transition from traditional reactive safety approaches toward more proactive risk management strategies based on continuous monitoring, operator supervision, and the implementation of structured safety protocols. In addition, A. Bechar & C. Vigneault (2016) analysed the fundamental concepts and components of agricultural robots, emphasising that their operational efficiency depends on the integration of mechanical systems, sensors, and control algorithms, which simultaneously creates multiple points of potential failure and risk. Despite the significant contributions of these studies, several important aspects remained insufficiently explored. Existing research tended to analyse technological, legal, or social factors separately, without considering their interaction within a unified risk system. In addition, the specific conditions of countries experiencing external stressors, such as armed conflict or large-scale labour shortages, were rarely incorporated into safety models, although these factors significantly influenced both the pace of automation and the nature of risks. Furthermore, there was a lack of comprehensive approaches that integrated cybersecurity, human–machine interaction, and regulatory frameworks into a single occupational safety management concept adapted to agricultural systems.

These research gaps determined the relevance of this study. The aim of the study was to provide a comprehensive analysis of the impact of automated engineering solutions and robotics on the occupational health and safety system in the agricultural sector, to identify emerging and transformed risks, and to develop practical, regulation-oriented recommendations for effective safety management under conditions of digitalisation and external challenges. To achieve this aim, the study addressed several interrelated objectives, including the analysis of traditional and emerging occupational risks in agriculture, the examination of trends in the implementation of automated and robotic systems, the classification of new risk categories associated with human–machine interaction, the comparative assessment of national and international regulatory frameworks, and the evaluation of labour market transformations and training requirements in the context of agricultural digitalisation.

Materials and Methods

The study was conducted as an independent research work and was not carried out within the framework of a specific funded scientific project. It was based on a comprehensive methodological framework that integrated analytical, comparative, and prognostic approaches to assess the impact of automated engineering solutions on occupational health and safety in the agricultural sector. The study relied on a combination of regulatory, scientific, and empirical data sources, which ensured the reliability and multidimensional nature of the analysis. The material base of the research included current national legislative and regulatory documents of Ukraine, in particular The Labour Code of Ukraine (1971), which established general occupational safety requirements for production processes and equipment, as well as DSTU 2293:2014 (2014), which defined the fundamental terminology related to occupational health and safety, including the concepts of risk, hazard, and safety management systems. These documents were used to evaluate the existing regulatory framework and to identify its limitations in the context of the implementation of automated technologies. In addition, international standards were analysed, including ISO 45001:2018 (2018), which provided a framework for occupational health and safety management systems, ISO 18497:2018 (2018), which specified safety requirements for highly automated agricultural machines, and UL 4600 (2020), which addressed safety evaluation principles for autonomous systems. These standards were selected due to their direct relevance to automation and robotics and were used as benchmarks for comparative analysis.

The methodological approach of the study was grounded in system analysis, which allowed occupational safety to be considered as a complex and dynamic system influenced by technological, organisational, and external factors. This method was applied to identify cause-and-effect relationships between the introduction of automation technologies and the transformation of occupational risks. Its selection was justified by the need to assess interdependencies between human factors, technical systems, and regulatory mechanisms within a unified analytical framework. Comparative legal analysis was employed to evaluate discrepancies between national legislation and international standards regulating the safety of automated and autonomous systems. This method enabled the identification of regulatory gaps, particularly in the areas of liability distribution, human–machine interaction, and cybersecurity. Its application was justified by the necessity to assess the degree of alignment of the national regulatory framework with contemporary technological developments. The method of classification and systematisation was applied to structure occupational risks into traditional and emerging categories. Traditional risks included physical, chemical, and biological hazards, while emerging risks were associated with human–machine interaction, cybersecurity threats, and increased psychophysiological load. This method ensured a consistent conceptual framework for risk identification and facilitated further analytical interpretation.

Empirical analysis was conducted through the examination of documented incidents involving automated and robotic systems in agricultural environments. Three representative cases were selected for analysis based on their relevance to the key categories of occupational risks associated with agricultural automation. The first case concerned human–robot interaction and operator supervision in agricultural tasks, highlighting challenges related to communication, safety protocols, and human presence detection (Benos *et al.*, 2023). The second case focused on autonomous navigation in a real agricultural environment and examined the influence of sensor performance and environmental conditions on navigation accuracy and system reliability (Fujinaga, 2025). The third case addressed safety, operational constraints, and risk factors associated with the deployment of autonomous agricultural systems, including issues related to human detection, collision prevention, and regulatory requirements (Spagnuolo *et al.*, 2025). These cases were selected because they represent complementary technological, environmental, and human-related dimensions of occupational risks in automated agricultural systems. The analysed cases included examples of human–robot interaction failures, such as unintended collisions caused by sensor misidentification, accidents during maintenance and testing procedures, and malfunctions of autonomous navigation systems under adverse environmental conditions. The identification of patterns was carried out using qualitative comparative analysis, which involved the systematic comparison of incident characteristics, including causal factors, operational conditions, and the presence or absence of safety protocols. This approach made it possible to identify recurring risk factors, such as insufficient personnel training, inadequate system design, and the lack of standardised safety procedures. In addition, forecasting methods were applied to assess trends in the transformation of the labour market and qualification requirements in the context of agricultural digitalisation. This involved the analytical review of current technological trends, scientific literature, and international reports to identify stable development patterns and potential future scenarios. The application of forecasting methods was justified by the rapid evolution of automation technologies and the need to anticipate emerging occupational risks. The research procedure was implemented through several sequential stages. Initially, traditional occupational risks in agriculture were identified based on regulatory documents and scientific literature. Subsequently, emerging risks associated with automation and robotics were analysed and classified. This was followed by a comparative assessment of regulatory frameworks to identify inconsistencies and gaps. Finally, the analytical findings were used to formulate recommendations aimed at improving occupational safety management in the context of automated agricultural systems.

Results and Discussion

Activities in the agricultural sector were traditionally associated with a wide range of occupational risks, including physical, chemical, and biological hazards. Physical risks arose from the operation of heavy machinery, such as tractors and harvesters, where workers were exposed to moving parts, rollovers, and mechanical injuries. Chemical risks were related to the use of pesticides, herbicides, and fertilisers, which could cause poisoning and occupational diseases, while biological risks included exposure to zoonotic infections. However, the introduction of automated engineering solutions did not eliminate these risks but fundamentally transformed their structure and interrelationships.

The transformation of risks was characterised by a clear cause-and-effect relationship between the implementation of automation technologies and changes in the role of workers within production systems. As automation replaced direct manual operations, workers transitioned from physically intensive tasks to supervisory and analytical functions. This transition altered the structure of occupational risks. Instead of being primarily exposed to direct mechanical hazards associated with operating machinery, workers became responsible for monitoring system performance, interpreting sensor information, supervising autonomous operations, and making corrective decisions when abnormal situations occurred. As a result, occupational safety increasingly depended on the quality of human–machine interaction, the reliability of communication channels, and the operator's ability to correctly interpret system feedback. In human-robot interaction environments, operators often perform supervisory functions remotely, requiring continuous situational awareness and timely intervention in the event of sensor errors, navigation failures, or unexpected system behaviour (Benos *et al.*, 2023). Consequently, the likelihood of direct physical injuries may decrease, while the importance of cognitive workload, decision-making quality, and system transparency increases. This shift reduced exposure to traditional mechanical hazards; however, it simultaneously increased dependence on the reliability and stability of digital systems and autonomous equipment. The use of autonomous machinery may reduce the likelihood of operator-related accidents by minimising direct human involvement in hazardous operations; however, it introduces new categories of risks associated with sensor failures, incorrect object recognition, communication disruptions, and unpredictable system behaviour. Perception-related failures, including sensor malfunctions and missed detections, are among the most frequently reported causes of operational errors in agricultural robotic systems. At the same time, navigation accuracy in such systems may vary within ±0.05 m depending on sensor performance, while communication latency in human–machine interaction systems can reach approximately 15-20 ms, which may affect system responsiveness under variable environmental conditions (Zhivkov *et al.,* 2023; Fujinaga, 2025). Thus, the reduction of direct physical risks resulted in the emergence of indirect, technologically mediated hazards, which required new approaches to risk assessment and management. This shift occurred because the increasing complexity and autonomy of technological systems reduced direct human involvement while simultaneously increasing dependence on system reliability, sensor accuracy, and real-time data processing, which, in turn, increased the probability of system-related errors and delayed responses. In the case of autonomous agricultural machinery, operators may perform remote supervision of field operations, which reduces the risk of direct physical injury but increases the likelihood of incidents related to communication delays, software failures, and incorrect sensor data interpretation under variable environmental conditions (Zhivkov *et al.*, 2023; Spagnuolo *et al.,* 2025).

The empirical analysis of documented incidents involving automated and robotic systems revealed several recurring patterns. Three representative cases were analysed to identify the principal sources of occupational risks in automated agricultural systems. The first case, based on the review of human–robot interaction applications in agriculture, highlighted challenges related to operator supervision, communication reliability, and the implementation of safety protocols in collabourative work environments (Benos *et al.*, 2023). The second case concerned autonomous navigation of an agricultural robot operating in a real cultivation environment, where navigation performance depended on LiDAR-based perception and the ability to maintain a positional accuracy of approximately ±0.05 m under changing environmental conditions (Fujinaga, 2025).

The third case focused on agricultural robotic systems operating in complex field environments and identified critical challenges associated with human detection, obstacle recognition, collision prevention, and regulatory compliance requirements (Spagnuolo *et al.*, 2025). The review emphasised that autonomous agricultural robots frequently operate in dynamic environments characterised by the simultaneous presence of workers, machinery, crops, and unexpected obstacles. Under such conditions, the effectiveness of safety functions depends on the reliability of perception systems, obstacle detection algorithms, and fail-safe mechanisms. The study further highlighted that operational safety cannot be ensured solely through technical performance, as safe deployment also requires appropriate regulatory frameworks, operator training, and compliance with established safety procedures. These findings support the results of the present study, which indicate that occupational risks in automated agricultural systems emerge through the interaction of technological, environmental, and organisational factors.

Collectively, these cases demonstrated that technical failures, perception errors, communication limitations, and insufficient safety measures represent the most common sources of operational risk in agricultural automation. The analysed cases demonstrated that incidents involving autonomous agricultural machinery were most frequently associated with sensor failures, communication disruptions, and incorrect object recognition under variable environmental conditions (Benos *et al.*, 2023; Spagnuolo *et al.*, 2025). In a number of cases, unsafe situations occurred during maintenance operations or in scenarios where the presence of a human operator was not correctly detected by the system, leading to near-miss events and potential collisions. These findings indicate that operational risks in automated agricultural systems are strongly dependent on system reliability, environmental adaptability, and the effectiveness of human detection mechanisms.

For example, T. Fujinaga (2025) reported the operation of an autonomous agricultural robot in a real strawberry production environment, where navigation accuracy depended on LiDAR-based perception and stable interpretation of environmental features. The robot maintained a distance accuracy of approximately ±0.05 m relative to cultivation beds; however, the study emphasised that sensor limitations and environmental variability could affect localisation accuracy and navigation stability. Such limitations are particularly important in agricultural environments where uneven terrain, vegetation density, and changing lighting conditions may reduce perception accuracy and increase the need for operator intervention. Similarly, studies reviewed by L. Benos *et al.* (2023) highlighted that communication quality, operator supervision, and the effectiveness of safety protocols are critical factors influencing the safe operation of collabourative agricultural robotic systems.

The qualitative comparative analysis made it possible to identify common patterns and differences in the causes of incidents across various operational contexts. The comparison was performed across three principal groups of factors: technical factors (sensor performance, software reliability, communication stability), environmental factors (terrain variability, obstacles, weather conditions, and changes in operating environments), and human-related factors (operator supervision, decision-making, and compliance with safety procedures). This classification made it possible to evaluate not only the direct causes of incidents but also the interactions between different categories of risk factors. It was established that the most significant causal factors included insufficient reliability of sensor systems, limited adaptability of autonomous equipment to changing environmental conditions, and the absence or incomplete implementation of safety protocols during maintenance and non-standard operations. Incidents occurring under standard operating conditions were primarily associated with technical failures, whereas incidents in complex or unpredictable environments were more likely to involve a combination of technical, environmental, and human-related factors. For example, a sensor malfunction occurring under controlled operating conditions may result only in a temporary reduction in navigation accuracy. However, the same malfunction in a dynamic agricultural environment characterised by uneven terrain, variable lighting conditions, or the presence of workers may significantly increase the probability of unsafe situations and require immediate operator intervention. Similarly, the consequences of communication disruptions depend on the operator's ability to recognise abnormal system behaviour and apply appropriate safety procedures. These observations indicate that incident outcomes are determined not by isolated technical failures but by the interaction of technical, environmental, and human-related factors (Benos *et al.*, 2023; Fujinaga, 2025; Spagnuolo *et al.*, 2025). This indicates that occupational risks in automated agricultural systems are systemic in nature and arise from the interaction of multiple interdependent variables rather than from isolated causes.

The comparative analysis revealed a clear differentiation of risk factors depending on operating conditions, with technical factors prevailing under controlled environments, while environmental and human-related factors became dominant in variable and unpredictable conditions. In the context of armed conflict, these transformations were further intensified. Traditional risks were compounded by external threats, including landmines and unexploded ordnance, as well as labour shortages caused by mobilisation and migration. These factors accelerated the adoption of automation technologies, which in turn increased the importance of managing complex, dynamic, and interdependent risks. As a result, occupational safety in agriculture evolved into a multidimensional system in which traditional, technological, and external risks coexisted and interacted, forming a unified risk environment (Pietrantoni *et al.,* 2024; Yang *et al.,* 2025). Automation in the agro-industrial complex includes several interconnected technological domains (Spagnuolo *et al.*, 2025). Intelligent management systems based on precision agriculture technologies enable real-time monitoring of soil conditions, crop status, and equipment performance, which improves decision-making and operational efficiency. At the same time, this increases dependence on data accuracy, system reliability, and cybersecurity. Autonomous ground machinery performs hazardous and labour-intensive tasks, reducing direct human exposure; however, it introduces risks related to machine autonomy, navigation errors, and interaction within shared workspaces. Unmanned aerial vehicles are used for monitoring and targeted application of crop protection products, which reduces chemical exposure but introduces additional risks associated with flight safety, communication failures, and regulatory constraints. These findings are consistent with the results of the present study.

The comparative analysis of regulatory frameworks, presented in Table 1, demonstrated that the national system of occupational safety regulation was primarily focused on traditional hazards, whereas international standards increasingly addressed challenges related to automation, robotics, and cybersecurity. In particular, international standards emphasised the implementation of human detection systems, fail-safe mechanisms, and risk-oriented design approaches for autonomous machines, while national regulations lacked specific provisions regarding liability distribution, software reliability, and human–machine interaction. This discrepancy created a regulatory gap that complicated the safe implementation of automated technologies and limited the effectiveness of existing safety management systems. A more detailed comparison indicates that national regulatory documents are primarily oriented toward general occupational safety requirements and the operation of conventional equipment. For example, The Labour Code of Ukraine (1971) establishes general obligations regarding workplace safety and the use of production equipment, while DSTU 2293:2014 (2014) standardises fundamental occupational safety terminology, including the concepts of risk and hazardous factors. However, these documents do not provide specific requirements for autonomous decision-making systems, human-machine interaction, software reliability, or cybersecurity. In contrast, ISO 18497:2018 (2018) contains dedicated provisions related to the safe operation of autonomous agricultural machinery, including human detection and collision prevention mechanisms. Similarly, UL 4600 (2020) and UL 4740 (2024) focus on safety assurance for autonomous systems through risk assessment procedures, cybersecurity requirements, and the verification of critical system components. Consequently, international standards provide more detailed mechanisms for addressing automation-specific risks, whereas the national framework remains focused on general occupational safety principles.

Table 1. Overview of regulatory acts and standards

Name of the act/standard	Type	Scope	Key provisions	Status in Ukraine
The Labour Code of Ukraine	Law	General occupational safety	Requirements for the design, manufacture, and commissioning of production equipment	Mandatory
DSTU 2293:2014 "Occupational Safety. Terms and Definitions of Basic Concepts"	Standard	Occupational safety terminology	Standardisation of terms "risk", "hazardous factor", "occupational safety"	Mandatory (recommended for use)
Temporary Procedure for the Use of Airspace	Regulatory Act	Use of drones	Prohibition of flights over certain objects, requirement for authorisation	Mandatory, but creates bureaucratic barriers
ISO 18497	Standard	Agri-robot safety	Safety requirements, human detection, collision prevention	Recommended
UL 4600, UL 4740	Standards	Autonomous systems safety	Risk assessment, cybersecurity, component testing	Recommended, but not integrated into the national legal framework

Source: compiled based on The Labour Code of Ukraine (1971), DSTU 2293:2014 (2014), ISO 18497:2018 (2018), UL 4600 (2020), UL 4740 (2024)

At the regulatory level, the results indicated the need for the development of targeted policy instruments aimed at bridging the gap between national legislation and international standards. This included the adaptation of ISO-based safety requirements for autonomous agricultural systems, the introduction of certification frameworks for digital and robotic equipment, and the establishment of clear liability models for human-machine interaction scenarios. The implementation of these measures required the development of practical regulatory tools, such as standardised risk assessment methodologies, guidelines for the certification of autonomous systems, and the integration of cybersecurity requirements into occupational safety regulations. The necessity of these instruments is directly linked to the risk categories identified during the empirical and comparative analyses. For example, certification procedures for autonomous agricultural equipment can help address risks associated with software failures, sensor malfunctions, and unreliable system behaviour by establishing minimum safety and performance requirements before deployment. Standardised risk assessment methodologies are particularly important for evaluating human–machine interaction scenarios, including situations involving remote supervision, operator intervention, and collabourative work environments. Likewise, the integration of cybersecurity requirements into occupational safety regulations is essential because communication disruptions, unauthorised system access, or data integrity failures may affect the reliability and safety of autonomous operations. These measures therefore provide regulatory mechanisms for mitigating the technological, environmental, and human-related risks identified in the study (ISO 18497:2018, 2018; UL 4600, 2020; Spagnuolo *et al.*, 2025). The adoption of such instruments would have a direct impact on agricultural enterprises by increasing the predictability of regulatory requirements and facilitating the safe deployment of automated technologies.

The emergence of new categories of risks represented one of the key results of the study and reflected the systemic transformation of occupational safety under conditions of automation. Risks related to human-machine interaction arose due to the absence of clearly defined physical and functional boundaries between workers and autonomous systems, which increased the probability of collisions, unsafe proximity, and unintended system responses. These risks became particularly significant during maintenance, calibration, and non-standard operations, where safety protocols were often insufficiently developed or inconsistently applied. Cybersecurity risks were associated with the integration of digital platforms, remote control systems, and data exchange networks into agricultural production processes. Unauthorised access, software failures, or disruptions in communication channels could result in uncontrolled equipment behaviour, which directly affected operational safety and increased the likelihood of hazardous situations. Thus, the growing dependence on digital infrastructure led to the emergence of a new category of technologically mediated risks requiring specialised control mechanisms.

Psychophysiological risks were linked to the increased cognitive load imposed on workers, who were required to monitor complex systems, analyse large volumes of data, and make decisions under conditions of uncertainty and time constraints. This shift in functional responsibilities contributed to fatigue, reduced attention, and a higher probability of human error. Consequently, automation not only reduced physical strain but also redistributed risk toward cognitive and psychological domains. These categories of risks formed an interconnected and hierarchical system in which human–machine interaction risks, cybersecurity threats, and psychophysiological factors were interdependent and could amplify each other, creating complex multi-layered risk scenarios. The transformation of professional roles and qualification requirements, presented in Table 2, confirmed a shift from physically oriented occupations to roles requiring digital competencies, analytical skills, and the ability to effectively interact with automated systems. This transition reduced exposure to traditional physical hazards; however, it simultaneously increased exposure to cognitive and technological risks. In addition, the absence of a unified certification system for operators of automated equipment created additional safety challenges related to insufficient training, inconsistent qualification levels, and variability in operational practices. These factors limited the effectiveness of safety management and increased the likelihood of incidents in automated agricultural environments.

Table 2. Changes in qualification requirements and skills of agricultural workers

Traditional roles	New roles	Required competencies	Main risks
Tractor operator / combine harvester operator	Autonomous equipment operator, Agronomist-analyst	Physical endurance and practical skills, knowledge of mechanisms, practical experience	Physical injuries, fatigue, exposure to vibration and noise
Field agronomist	Unmanned aerial vehicle operator, Precision agriculture specialist	Technological literacy, data analysis, software management	Cyber risks, psychophysiological load, fatigue
Technician / repair specialist	Mechatronics and robotics specialist	Knowledge of hydraulics, electricity, and mechanical systems	Physical injuries, overexertion, risk of electric shock
Manual labour worker	Weeding robot operator	Robot interaction, monitoring, and control	Collision risks, lack of clear interaction protocols

Source: compiled based on the analysis of V. Tankosić *et al.* (2024), J. Lincoln *et al.* (2025), S. Hossain *et al.* (2025)

The forecasting analysis enabled the formulation of three distinct development scenarios for occupational risks in agricultural automation, reflecting different levels of technological adoption and regulatory maturity. The scenarios were differentiated according to three principal criteria: the rate of technology adoption, the degree of regulatory development, and the level of organisational preparedness, including personnel training and safety management practices. These criteria were selected because the results of the empirical, comparative, and regulatory analyses indicated that they exert the strongest influence on the emergence and management of occupational risks in automated agricultural systems. In a baseline scenario, automated technologies are introduced gradually and under relatively controlled conditions, allowing organisations sufficient time to adapt operating procedures and train personnel. As a result, traditional physical risks are progressively reduced, while technological and cognitive risks increase at a manageable rate. In an accelerated automation scenario, driven by labour shortages, economic pressures, or technological incentives, autonomous systems are implemented faster than organisations can adapt regulatory procedures, training programs, and safety protocols. Under such conditions, the probability of incidents associated with software reliability, operator errors, communication failures, and inadequate risk management increases. In a regulated development scenario, technological deployment is accompanied by certification procedures, personnel training programs, internal safety protocols, and the harmonisation of national legislation with international standards. Under these conditions, the risks associated with autonomous systems become more predictable and controllable, contributing to improved system reliability and enhanced occupational safety outcomes. These scenarios demonstrate that the evolution of occupational risks in agriculture is directly dependent on the pace of technological adoption, the level of regulatory development, and the effectiveness of organisational safety measures. This conclusion is consistent with the empirical findings of the study, which demonstrated that occupational risks are influenced not only by technological factors but also by the adequacy of regulatory frameworks and the preparedness of organisations to manage human–machine interaction and autonomous system operation (Benos *et al.*, 2023; Spagnuolo *et al.*, 2025).

The generalised results of the applied methods indicate that the transformation of occupational risks in agricultural automation follows a consistent and interconnected pattern. The system analysis demonstrated that the implementation of automated technologies changes the role of workers and shifts the structure of occupational risks from direct mechanical hazards toward technology-dependent risks associated with autonomous systems, sensor reliability, software performance, and human–machine interaction. The analysis of documented incidents revealed recurring patterns related to perception errors, communication disruptions, and limitations of safety mechanisms. The qualitative comparative analysis further showed that the consequences of such failures depend not only on technical conditions but also on environmental variability and human-related factors, including operator supervision and compliance with safety procedures. The comparative assessment of regulatory frameworks indicated that existing national regulations only partially address automation-specific risks, while international standards provide more comprehensive approaches to risk management, human detection, and collision prevention. Finally, the forecasting analysis demonstrated that the future evolution of occupational risks depends on the interaction between technological adoption, regulatory development, and organisational preparedness. Collectively, these findings confirm that occupational risks in automated agricultural systems are not isolated phenomena but emerge through the interaction of technological reliability, environmental conditions, and human-related factors. This conclusion provides a structured basis for the development of integrated occupational risk management strategies in agricultural automation (Benos *et al.*, 2023; Fujinaga, 2025; Spagnuolo *et al.*, 2025).

The practical implementation of automated technologies required the development of structured safety management mechanisms at the enterprise level. Risk assessment procedures were adapted to include scenario-based analysis, the identification of human–machine interaction zones, and the evaluation of system reliability under variable environmental conditions. In practice, this was implemented through the integration of digital monitoring systems, automated risk analysis tools, and adaptive safety management protocols that enabled real-time identification and mitigation of potential hazards. Internal regulations defined operational protocols, including emergency response procedures, maintenance safety requirements, and safe operating modes for autonomous equipment. The implementation of digital monitoring systems enabled real-time tracking of equipment performance and worker activities, which facilitated the early detection of hazardous situations and supported more informed and timely decision-making. For employers, the implementation of automated technologies required the establishment of standardised safety management frameworks. These included clearly defined internal regulations, structured operational procedures, and the use of advanced digital tools for monitoring and control. Digital systems, such as real-time monitoring platforms and predictive analytics tools, enabled continuous assessment of operational conditions and supported proactive risk management. In addition, the effective use of automated systems required the implementation of structured training and certification programs, including simulation-based training and periodic qualification assessment of personnel working with autonomous equipment.

The application of these measures can positively influence the operational efficiency of agricultural enterprises by reducing the frequency of disruptions associated with human error, equipment malfunction, and delayed responses to abnormal operating conditions. Digital monitoring and control systems provide continuous information on machine status, navigation performance, and operational parameters, allowing operators to identify anomalies at an early stage and implement corrective actions before failures escalate into accidents or prolonged downtime. In addition, automated systems can reduce the need for direct human involvement in hazardous or repetitive tasks, thereby decreasing exposure to occupational risks and improving the continuity of field operations. Evidence from recent studies indicates that the implementation of robotic and automated technologies may contribute to measurable operational improvements. For example, agricultural automation has been associated with reductions in manual labour requirements of up to 58%, decreases in labour costs of approximately 22.5%, and reductions in pesticide exposure risks of up to 45% in selected agricultural applications (Anastasiou *et al.*, 2025). Furthermore, automated monitoring and control technologies improve process transparency, support more efficient resource allocation, and facilitate data-driven operational decision-making, which contributes to enhanced productivity and operational stability (Spagnuolo *et al.*, 2025). These findings indicate that the efficiency gains associated with automation result not only from technological improvements themselves but also from enhanced process control, reduced operational uncertainty, and more effective allocation of labour and technical resources.

However, the implementation of such technologies was constrained by regulatory barriers, high initial investment costs, and the lack of standardised training and certification systems. These barriers included regulatory uncertainty, limited harmonization with international standards, high capital investment requirements, and insufficient availability of qualified personnel. Furthermore, small and medium-sized enterprises faced additional constraints related to limited access to digital infrastructure and financial resources. These limitations had to be considered when developing strategies for the safe and effective integration of automation into agricultural production systems. Generalised implementation scenarios indicated that effective occupational safety management in automated agriculture required coordinated interaction between equipment manufacturers, agricultural enterprises, and regulatory authorities. Manufacturers integrated advanced safety features, including sensor redundancy, human detection systems, and fail-safe mechanisms, into system design. Agricultural enterprises implemented comprehensive risk assessment procedures, digital monitoring tools, and continuous personnel training and certification programs. Regulatory authorities ensured the harmonisation of national legislation with international standards and developed practical guidelines for certification, risk assessment, and safety validation of automated systems. The alignment of these elements enabled not only the reduction of occupational risks but also the improvement of operational efficiency, system controllability, and the overall sustainability of agricultural production.

The results of this study demonstrated that the implementation of automated engineering solutions in agriculture led to a transformation of occupational risks, shifting from traditional physical hazards to complex system-based risks associated with human–machine interaction, digitalisation, and cognitive load. These findings were further analysed in the context of recent scientific literature. L. Benos *et al.* (2023) conducted a systematic review of human–robot interaction in agriculture, focusing on safety incidents and operational conditions. They found that the lack of clearly defined interaction zones between humans and robotic systems significantly increases the likelihood of accidents, particularly during maintenance and non-standard operations. These findings are consistent with the results of the present study, which also identified human-machine interaction as a critical risk factor. The study supports this conclusion and further emphasises that in agricultural environments, characterised by variability and low standardisation, these risks are amplified. L. Pietrantoni *et al.* (2024) investigated the integration of collabourative robots in agriculture and other industries, with particular attention to human factors and safety. Their study demonstrated that increased automation is associated with higher levels of cognitive load and psychological stress among operators. These findings align with the present study, which identified psychophysiological risks as a key component of modern occupational safety. However, while L. Pietrantoni *et al.* (2024) primarily examined structured environments, the results of this study indicate that in agricultural contexts, environmental variability further intensifies these effects. Therefore, the conclusions of L. Pietrantoni *et al.* (2024) are supported and further extended by incorporating the influence of external conditions. M. Spagnuolo *et al.* (2025) conducted a technical review of agricultural robotics, focusing on sustainability and operational challenges. They found that automation improves productivity and reduces labour intensity, but introduces new risks related to system reliability and environmental interaction. These findings are strongly consistent with the present study. However, the obtained results expand this perspective by demonstrating that these risks form an interconnected system influenced by technological, organisational, and regulatory factors.

In their study, Y. Yang *et al*. (2025) analysed the application of blockchain and IoT technologies in agriculture, focusing on data management and system security. They found that digitalisation enhances transparency and operational efficiency but creates vulnerabilities related to cybersecurity and data integrity. These findings are consistent with the present study, which identified cybersecurity risks as an essential component of occupational safety. This conclusion is supported, and it is further emphasised that failures in digital systems can directly translate into physical safety risks in automated environments. A.J. Moshayedi *et al*. (2024) examined the role of robotics in transforming agricultural practices. Their study showed that robots reduce human exposure to hazardous tasks but introduce uncertainties related to system autonomy and decision-making processes. These findings align with the present study. However, this conclusion is extended by demonstrating that such uncertainties are exacerbated by environmental variability, including terrain complexity and sensor limitations. A.A. Mirani *et al*. (2021) reviewed the application of machine learning in agriculture, focusing on predictive analytics and decision-support systems. They found that data-driven technologies improve efficiency and decision-making accuracy. These findings partially correspond with the present study. While the benefits of such systems are acknowledged, the results of this study indicate that excessive reliance on algorithmic decision-making may introduce additional risks related to data inaccuracies and model bias. Therefore, these conclusions are partially supported, while emphasising the need for human oversight.

E. Anastasiou *et al*. (2025) reported that the implementation of agricultural automation and robotic technologies can contribute to reductions in manual labour requirements, lower labour costs, and decreased exposure to occupational hazards in selected agricultural applications. These findings are consistent with the results of the present study, which also identified the potential of automation to improve operational efficiency and reduce workers' exposure to hazardous tasks. However, the results of this study additionally demonstrate that the successful realisation of these benefits depends on the reliability of autonomous systems, the adequacy of safety protocols, and the effectiveness of regulatory and organisational measures governing their deployment. J. Ingram *et al*. (2022) analysed the development of digital agriculture and identified key research priorities, including system integration, data governance, and user adaptation. They found that increasing digitalisation enhances decision-making capabilities but also introduces systemic dependencies on data quality and infrastructure reliability. These findings align with the present study. This conclusion is supported, and it is further demonstrated that such dependencies create new categories of risks associated with system failures and data inconsistencies E. Anastasiou *et al*. (2025) conducted a systematic analysis of robotics and extended reality applications in agriculture. Their study showed that these technologies significantly improve operational efficiency and reduce manual labour, but require advanced safety frameworks to ensure reliable human-machine interaction. These findings are consistent with the present study. This conclusion is supported, and it is further emphasised that the lack of standardised safety protocols remains a critical limitation.

In their research, M.R. Endsley (2021) conducted a systematic review of objective measures of situation awareness, comparing methods used to assess human cognitive performance in complex systems. The study demonstrated that increased system complexity and information density reduce situational awareness and increase the likelihood of decision-making errors. These findings are consistent with the present study, which identified psychophysiological risks associated with monitoring automated systems. However, while M.R. Endsley (2021) focused on controlled environments, the present study demonstrates that in agricultural contexts, environmental variability further exacerbates cognitive load. Therefore, these conclusions are supported, with an emphasis on their amplified impact in real-world agricultural systems. Overall, the analysis of recent studies confirms that automation in agriculture does not eliminate occupational risks but redistributes them across technological, cognitive, and organisational domains. The present study contributes to the existing body of knowledge by demonstrating that these risks form a multidimensional and interconnected system influenced by environmental conditions, regulatory frameworks, and human competencies. This integrated perspective provides a more comprehensive understanding of occupational safety in automated agricultural systems and highlights the need for systemic and adaptive risk management approaches.

Conclusions

The study established that the implementation of automated engineering solutions in agriculture does not eliminate occupational risks but leads to their structural transformation. Traditional physical, chemical, and biological hazards are reduced in terms of direct human exposure; however, they are replaced by technologically mediated risks associated with system reliability, human–machine interaction, and digital infrastructure. As a result, occupational safety in the agricultural sector evolves into a multidimensional system characterised by the interaction of conventional, technological, and external risk factors.

A key driver of this transformation is the change in the role of workers within production processes. The transition from manual labour to supervisory and analytical functions decreases the likelihood of mechanical injuries but increases dependence on automated systems and the quality of decision-making. This shift contributes to the emergence of new categories of risks, including interaction-related hazards, cybersecurity threats, and increased psychophysiological load caused by the need to process complex information in real time. The results also demonstrate the existence of a significant gap between national regulatory frameworks and international safety requirements for automated and autonomous systems. This gap limits the effectiveness of safety management and complicates the implementation of advanced technologies. At the same time, the study confirms that effective risk management requires the integration of scenario-based risk assessment, digital monitoring systems, and structured training and certification programs for personnel. Overall, the findings indicated that ensuring occupational safety in the conditions of agricultural automation requires a systemic approach that combines technological, organisational, and regulatory solutions. Such an approach enables not only the reduction of occupational risks but also supports the sustainable and efficient development of agricultural production systems. From a practical perspective, the implementation of these measures contributes to improved operational performance, including reduced injury rates, minimised downtime, and enhanced process controllability. However, the effectiveness of such approaches depends on overcoming regulatory, financial, and organisational barriers, particularly in the context of limited resources and insufficient standardisation.

Acknowledgements

None.

Funding

None.

Conflict of Interest

None.

References

[1] Anastasiou, E., *et al.* (2025). Applications of robotics and extended reality in agriculture: A review. *Smart Agricultural Technology*, 12, article number 101521. doi: 10.1016/j.atech.2025.101521.

[2] Ballingall, S., Sarvi, M., & Sweatman, P. (2023). Standards relevant to automated driving system safety: A systematic assessment. *Transportation Engineering*, 13, article number 100202. doi: 10.1016/j.treng.2023.100202.

[3] Bechar, A., & Vigneault, C. (2016). Agricultural robots for field operations: Concepts and components. *Biosystems Engineering*, 149, 94-111. doi: 10.1016/j.biosystemseng.2016.06.014.

[4] Benos, L., Moysiadis, V., Kateris, D., Tagarakis, A.C., Busato, P., Pearson, S., & Bochtis, D. (2023). Human-robot interaction in agriculture: A systematic review. *Sensors*, 23(15), article number 6776. doi: 10.3390/s23156776.

[5] DSTU 2293:2014. (2014). *Occupational health and safety. Terms and definitions of basic concepts*. Retrieved from https://education.profiteh.kiev.ua/pluginfile.php/267/mod_page/content/132.pdf.

[6] Endsley, M.R. (2021). A systematic review and meta-analysis of direct objective measures of situation awareness: A comparison of SAGAT and SPAM. *Human Factors*, 63(1), 124-150. doi: 10.1177/0018720819875376.

[7] Fujinaga, T. (2025). Autonomous navigation method for agricultural robots in high-bed cultivation environments. *Computers and Electronics in Agriculture*, 231, article number 110001. doi: 10.1016/j.compag.2025.110001.

[8] Hossain, S., Rahman, M., Rahman, A., Kabir, M.M., Mridha, M.F., Huang, J., & Shin, J. (2025). Automatic navigation and self-driving technology in agricultural machinery: A state-of-the-art systematic review. *IEEE Access*, 13, 94370-94401. doi: 10.1109/ACCESS.2025.3573324

[9] Ingram, J., *et al.* (2022). What are the priority research questions for digital agriculture? *Land Use Policy*, 114, article number 105962. doi: 10.1016/j.landusepol.2021.105962.

[10] ISO 18497:2018. (2018). *Agricultural machinery and tractors – safety of highly automated agricultural machines – principles for design*. Retrieved from https://www.iso.org/standard/62659.html.

[11] ISO 45001:2018. (2018). *Occupational health and safety management systems – requirements with guidance for use*. Retrieved from https://www.iso.org/standard/63787.html.

[12] Liakos, K.G., Busato, P., Moshou, D., Pearson, S., & Bochtis, D. (2018). Machine learning in agriculture: A review. *Sensors*, 18(8), article number 2674. doi: 10.3390/s18082674.

[13] Lincoln, J., Gorucu, S., Khorsandi, F., Aby, G.R., Elliott, K., Shutske, J., & Issa, S.F. (2025). Occupational safety research needs in the field of robotics and autonomous machines in agriculture. *Journal of Agricultural Safety and Health*, 31(3), 217-230. doi: 10.13031/jash.16216.

[14] Lowenberg-DeBoer, J., Behrendt, K., Canavari, M., Ehlers, M.-H., Gabriel, A., Huang, I., & Zdráhal, I. (2021). The impact of regulation on autonomous crop equipment in Europe. In *Precision agriculture '21* (pp. 711-717). Leiden: Wageningen Academic. doi: 10.3920/978-90-8686-916-9_85.

[15] Mayoral Baños, J.C., From, P.J., & Cielniak, G. (2023). Towards safe robotic agricultural applications: Safe navigation system design for a robotic grass-mowing application through the risk management method. *Robotics*, 12(3), article number 63. doi: 10.3390/robotics12030063.

[16] Mirani, A.A., Memon, E.M.S., Chohan, R., Wagan, A., & Qabulio, M. (2021). Machine learning in agriculture: A review. *International Journal of Scientific & Technology Research*, 10(5), 229-234.
[17] Moshayedi, A.J., Sohail Khan, A., Yang, Y., Hu, J., & Kolahdooz, A. (2024). Robots in agriculture: Revolutionizing farming practices. *EAI Endorsed Transactions on AI and Robotics*, 3. doi: 10.4108/airo.5855.
[18] Pietrantoni, L., Favilla, M., Fraboni, F., Mazzoni, E., Morandini, S., Benvenuti, M., & De Angelis, M. (2024). Integrating collabourative robots in manufacturing, logistics, and agriculture: Expert perspectives on technical, safety, and human factors. *Frontiers in Robotics and AI*, 11, article number 1342130. doi: 10.3389/frobt.2024.1342130.
[19] Spagnuolo, M., Todde, G., Caria, M., Furnitto, N., Schillaci, G., & Failla, S. (2025). Agricultural robotics: A technical review addressing challenges in sustainable crop production. *Robotics*, 14(2), article number 9. doi: 10.3390/robotics14020009.
[20] Tankosić, V., Mirjanić, B., Prodanović, R., Lekić, S., & Carić, B. (2024). Digitalization in agricultural sector: Agriculture 4.0 for sustainable agriculture. *Journal of Agronomy, Technology and Engineering Management*, 7(1), 1036-1042. doi: 10.55817/geqw8736.
[21] The Labour Code of Ukraine. (1971, July). Retrieved from https://zakon.rada.gov.ua/laws/show/322-08#Text.
[22] UL 4600. (2020). *Standard for safety for the evaluation of autonomous products*. Retrieved from https://webstore.ansi.org/standards/ul/ul4600ed2020?ad_acct=0089&gad_source=1&gad_campaignid=23054412413&gbraid=0AAAADvqK-W-KghI2B9E1RGqVznV7xsyW&gclid=CjwKCAjw8uTQBhAdEiwAVvtJygADOEQ4iYwhdtqgKypy0oOzZiLf2mJvmuW7acuANAPYNfq4Ce5XMhoCdy4QAvD_BwE.
[23] UL 4740. (2024). *Lidar and lidar systems used in vehicles*. Retrieved from https://www.shopulstandards.com/ProductDetail.aspx?UniqueKey=47187.
[24] World Economic Forum. (2023). *Future of jobs report 2023*. Retrieved from https://www.weforum.org/reports/the-future-of-jobs-report-2023/.
[25] Yang, Y., Zhang, Y., & Liu, X. (2025). A survey of blockchain applications for management in agricultural and livestock internet of things. *Future Internet*, 17(1), article number 40. doi: 10.3390/fi17010040.
[26] Zhai, Z., Martínez, J.F., Beltran, V., & Martínez, N.L. (2020). Decision support systems for agriculture 4.0: Survey and challenges. *Computers and Electronics in Agriculture*, 170, article number 105256. doi: 10.1016/j.compag.2020.105256.
[27] Zhivkov, T., Sklar, E.I., Botting, D., & Pearson, S. (2023). 5G on the farm: Evaluating wireless network capabilities and needs for agricultural robotics. *Machines*, 11(12), article number 1064. doi: 10.3390/machines11121064.

Охорона праці в добу автоматизованих інженерних рішень в агросекторі

Олег Іванов

Кандидат технічних наук, доцент
Полтавський державний аграрний університет
36003, вул. Григорія Сковороди, 1/3, м. Полтава, Україна
https://orcid.org/0000-0002-1761-9913

Надія Опара

Кандидат сільськогосподарських наук, доцент
Полтавський державний аграрний університет
36003, вул. Григорія Сковороди, 1/3, м. Полтава, Україна
https://orcid.org/0000-0002-0128-8400

Анотація. Стрімке впровадження автоматизованих інженерних рішень в аграрному секторі суттєво трансформувало умови охорони праці. Метою цього дослідження було проаналізувати вплив автоматизації на безпеку праці в сільському господарстві, ідентифікувати нові ризики та розробити прикладні підходи до управління безпекою. Дослідження ґрунтувалося на комплексному методологічному підході, що поєднував системний аналіз, порівняльно-правовий аналіз, класифікацію ризиків та емпіричний аналіз інцидентів, пов'язаних із застосуванням автоматизованих систем. Національні нормативно-правові акти розглядалися у порівнянні з міжнародними стандартами з метою оцінки їх відповідності викликам автоматизації аграрного виробництва. Результати дослідження показали, що автоматизація не усуває професійні ризики, а призводить до їх трансформації, формуючи багатовимірну систему ризиків, у якій традиційні небезпеки доповнюються новими категоріями, зокрема ризиками взаємодії «людина-машина», кіберзагрозами та зростанням психофізіологічного навантаження. Встановлено, що перехід від фізичної праці до наглядових і аналітичних функцій зменшує безпосередній вплив механічних ризиків, водночас підвищуючи залежність від надійності систем, точності даних і якості прийняття рішень. Також виявлено суттєві регуляторні прогалини, зокрема щодо розподілу відповідальності, надійності програмного забезпечення та вимог безпеки для автономних систем. Крім того, підтверджено трансформацію трудових функцій, що характеризується зростанням потреби у цифрових компетентностях і необхідністю впровадження структурованих систем навчання та сертифікації персоналу. Практична значущість дослідження полягає у розробленні прикладних підходів до управління охороною праці, зокрема на основі сценарного оцінювання ризиків, впровадження цифрових систем моніторингу та безперервного навчання персоналу. Застосування цих заходів сприяє зниженню рівня виробничого травматизму, мінімізації простоїв, підвищенню керованості виробничих процесів та загальної ефективності діяльності аграрних підприємств, водночас ефективність їх реалізації залежить від подолання регуляторних, організаційних і фінансових обмежень

Ключові слова: людино-машинна взаємодія; автономні аграрні системи; промислова кібербезпека; точне землеробство; трансформація ризиків; робототехніка

Journal of Kryvyi Rih National University
Journal homepage: https://journal-knu.com.ua/en
Article's History: Received: 12.12.2025 Revised: 01.04.2026 Accepted: 28.04.2026 Published: 29.05.2026
Vol. 24, No. 1, 2026
ISSN 2306-5451
e-ISSN 2519-2736

UDC 621.3621.791.75:669.14-415.
DOI: 10.31721/2306-5451-2026-1-24-86-93

Improving the crack resistance of blast furnace skips

Ivan Kryvda*

Postgraduate Student
Dnipro State Technical University
51918, 2 Dniprobudivska Str., Kamianske, Ukraine
https://orcid.org/0009-0005-0724-853X

Abstract. The operation of the blast furnace lining is accompanied by intense abrasive and impact wear, which makes it necessary to develop iron-containing surfacing materials with a heterogeneous carbide microstructure to increase strength and wear resistance. The aim of the work was to increase the mechanical strength and durability of the lining of the blast furnace shop by optimising the structure of the deposited layers and establishing regularities between the microstructure, mechanical properties and wear resistance of the coatings. The research was carried out using electric arc surfacing on samples of 09G2S steel. Tests were conducted for hardness, impact toughness and abrasive wear, as well as microstructural analysis of the surfaced layers and assessment of the nature of crack formation after microindentation. The main results of the experimental studies show that the hardness of the deposited layers ranged from 52 HRC in SAS Global to 58 HRC in VELTEC, while the impact toughness varied from 18 J/cm^2 in Duroxite to 22 J/cm^2 in VELTEC, demonstrating an inverse relationship between hardness and impact toughness: harder layers are more prone to brittle fracture. Abrasive wear tests showed that VELTEC demonstrated the best wear resistance with a mass loss of 0.12 g and only one crack per 100 cm^2, while SAS Global had the highest number of cracks (4 per 100 cm^2) and a mass loss of 0.20 g, and Duroxite had intermediate values – 0.18 g mass loss and 3 cracks. As a result, it was found that the formation of a hypereutectic structure with an M_7C_3 carbide phase contributes to a reduction in the intensity of abrasive wear and limits the spread of microcracks. The obtained welded layers are characterised by a combination of increased hardness and sufficient impact toughness, which is critical for the operation of the lining under variable impact loads. The practical value of the results lies in the possibility of their use in the restoration and modernisation of blast furnace linings in order to increase the inter-repair resource and reduce operating costs

Keywords: welding; microstructure; wear; strength; residual stress; hardness

Introduction

In modern blast furnace production, one of the key elements of the transport system is a skip designed for the cyclical vertical movement of charge materials to the blast furnace charging device. Under operating conditions, the skip undergoes intense abrasive impact from agglomerate, coke and ore, which causes accelerated wear of its internal surfaces. To protect the skip body from premature destruction, lining in the form of removable or deposited wear-resistant elements is widely used.

One of the main reasons for the limited service life of the skip lining is crack development, which occurs due to a combination of thermal, mechanical and structural factors. As noted by S.V. Shchetynin *et al*. (2019), residual stresses generated during surfacing play a crucial role in the appearance of microcracks, which can later develop into macro-cracks and cause the deposited layer to detach. Their microstructure has a significant influence on the tendency of deposited layers

Suggested Citation:
Kryvda, I. (2026). Improving the crack resistance of blast furnace skips. *Journal of Kryvyi Rih National University*, 24(1), 86-93. doi: 10.31721/2306-5451-2026-1-24-86-93.

Copyright © The Author(s). This is an open access article distributed under the terms of the Creative Commons Attribution License 4.0 (https://creativecommons.org/licenses/by/4.0/)

**Corresponding author (kryvda.v@icloud.com)*

to crack development. High-chromium iron-containing alloys, typically used for wear-resistant surfacing, form eutectic structures with M7C3-type carbides, which provide high hardness but are also characterised by increased brittleness. An alternative approach to improving the operational reliability of linings is the use of modified surfacing alloys, in which hardening is achieved due to fine boride and carbide phases. According to the findings of O. Ivanov (2020), the development of a fine-dispersed structure with a uniform distribution of reinforcing phases helps to reduce the rate of crack propagation and increase resistance to destruction. In addition to the chemical composition of the deposited material, the surfacing technology has a significant impact on the crack resistance of the lining. The study by L. Zong *et al.* (2019) established that reducing the linear thermal energy and controlling the inter-pass temperature can reduce the level of residual stresses and form a more favourable structure of the deposited layer.

Similar conclusions were provided in the paper by A. Czupryński *et. al.* (2022), where the efficiency of optimised surfacing modes for parts of metallurgical equipment was shown. An additional factor in increasing the life of the lining is the use of buffer layers between the steel base and the wear-resistant surfacing. The study by T. Varis *et al.* (2023) explored the possibility of using iron-based (Fe-based) thermal spray coatings as an alternative to standard hard coatings to protect parts from abrasive and cavitation wear. Several commercial and experimental Fe coatings applied by high velocity Oxy-Fuel and High Velocity Air-Fuel (HVAF) methods were analysed and their microstructure, hardness, and wear resistance were compared with coatings based on WC-CoCr and Cr_3C_2-NiCr. The results showed that Fe coatings generally have a lower resistance to abrasive wear due to the lower content and size of solid phases, but in cavitation erosion tests they showed good, and sometimes better, results compared to standard coatings. The researchers concluded that cavitation wear resistance is largely determined by microstructure, cohesion between layers, and the material's ability to undergo plastic deformation, rather than just hardness, and that Fe-based coatings, especially those applied by HVAF, have significant potential for use under cavitation loading conditions.

Z.T. Öztürk (2021) investigated the effect of alloying elements such as Si, Cr, B, and Ni on the microstructure and abrasive wear resistance of FE-C-Si-Cr-B-Ni deposited layers. Hardness and abrasive abrasion tests of various alloy compositions were performed, including microstructural analysis using metallography. The results showed that the introduction of Ni and Cr promotes the generation of a denser boride and carbide structure, which increases the hardness and wear resistance of coatings. C. Okechukwu *et al.* (2024) developed new ferro alloy surfaced alloys for conditions of high abrasive wear under low impact loads. A comprehensive study of mechanical properties, including hardness, impact strength, and weight loss during abrasive wear, was conducted. The study showed that the optimal composition of the alloy provides a balance between high wear resistance and sufficient impact strength, which makes it suitable for industrial applications. The study by O. Skvortsov & O. Mikosianchyk (2023) considered the wear resistance of electric arc coatings under the action of abrasive wear. The researchers investigated the effect of coating technology and microstructure on the development of microcracks and material loss during abrasive wear tests. The results showed that coatings with a more uniform carbide phase show better wear resistance and less tendency to crack, highlighting the importance of controlling the microstructure during surfacing.

Despite a significant number of scientific papers devoted to wear-resistant surfacing, the issue of a comprehensive assessment of the influence of the microstructure, technological modes, and mechanical characteristics of the deposited layers on the operational reliability of the blast furnace skip lining remains insufficiently covered. In particular, it is necessary to clarify the relationship between the structure of the deposited layers, hardness indicators, impact strength, and the intensity of abrasive wear under conditions close to real operation. The purpose of this study was to comprehensively assess the influence of technological parameters of surfacing and structural features of deposited wear-resistant layers on the mechanical characteristics and operational reliability of the blast furnace skip lining.

Materials and Methods

The object of the study was deposited wear-resistant layers formed on a steel base, used for the manufacture and restoration of blast furnace skip linings. As a base material, low-alloy structural steel of the VELTEK brand was used, characterised by satisfactory weldability, stable structure, and wide application in metallurgical equipment operating under abrasive and impact loads (Pokhmurska *et al.*, 2017). The samples were welded using the arc method in a protective gas environment with semi-automatic direct current welding equipment. The chosen surfacing method ensured arc stability, heat investment control, and the development of a dense deposited structure that met advanced requirements for the restoration of wear-resistant parts for metallurgical purposes (Belik *et al.*, 2016).

To conduct experimental studies, low-alloy structural steel was used as the base material, which was typical for the lining elements of metallurgical equipment in terms of chemical composition, mechanical properties, and weldability. The choice of this material was conditioned by its wide application in blast furnace shops, and the possibility of forming deposited layers without the development of technological defects, which ensured correct modelling of real operating conditions of the skip lining. The samples were made in the form of rectangular plates measuring 100 × 50 mm with a base metal thickness of 10-15 mm, which provided sufficient rigidity during surfacing and geometry stability during subsequent mechanical tests. Before surfacing, the surface of the samples was subjected to mechanical cleaning and degreasing to minimise the influence of foreign factors on the development of the deposited layer. The actual surfacing modes were selected considering the technological recommendations for arc surfacing of wear-resistant materials and the need to reduce residual stresses. Surfacing was performed at a welding current of 220-260 A and an arc voltage of 24-28 V. The speed of movement of the burner was 18-22 cm/min, which ensured the development of a uniform roller without undercuts and pores. The inter-pass temperature was maintained at a level not exceeding 150°C to limit heat accumulation and reduce the risk of thermal cracks (Zong *et al.*, 2019).

The choice of these welding modes was based on the critical influence of linear thermal energy on the development of the microstructure of the deposited layer. Microstructural studies of deposited layers and thermal impact zones were performed by optical metallography methods. Preparation of metallographic grinds was carried out according to the standard method with mechanical grinding and polishing, after which chemical etching was performed to identify the phase structure. Microstructure analysis was aimed at evaluating the morphology of reinforcing phases, the nature of their distribution, and the relationship with possible crack propagation paths (Ivanov, 2020). The hardness of the deposited layers was determined by indentation with measurement in the deposited metal, the thermal impact zone, and the base metal. This approach allowed estimating the gradient of mechanical properties in a bimetallic system, which is an important factor in the crack resistance of deposited coatings (DSTU EN 14700:2008, 2008). Wear resistance was evaluated by laboratory tests for abrasive wear, which simulate the operating conditions of the lining of a blast furnace skip. The test method corresponded to generally accepted approaches to the analysis of deposited wear-resistant materials and allowed comparing the wear intensity of different deposited layers under the same load conditions (Czupryński *et al.*, 2022).

To ensure the reliability of the results, all mechanical tests were performed on at least three samples for each series. The results were presented as average values with an indication of the root-mean-square deviation (M ± SD), which allowed estimating the spread of experimental data and ensured the correctness of the comparative analysis of the obtained characteristics (Venkatesh *et al.*, 2015). To ensure statistical reliability of the results, the study was carried out on a series of samples formed under the same technological conditions of surfacing. The total sample size was at least 24 samples, which were divided into two experimental groups depending on the structural organisation of the deposited layers. Within each group, 12 samples were made, which allowed evaluating the reproducibility of the results and reducing the impact of random errors. For each type of deposited coating, at least three parallel measurements of hardness, impact strength, and abrasive wear indicators were used, followed by the determination of average values. This approach ensured sufficient statistical reliability of experimental data and allowed correctly comparing the results obtained with each other, and with the data given in the scientific literature.

Results and Discussion

Research results have shown that the operational reliability of blast furnace skip linings is determined by a combination of intense abrasive and impact wear and a complex stress-strain state that arises during equipment operation. Analysis of the design features of the lining shown in Figure 1 shows that the most loaded areas are direct contact with abrasive material, where a combined wear mechanism is implemented.

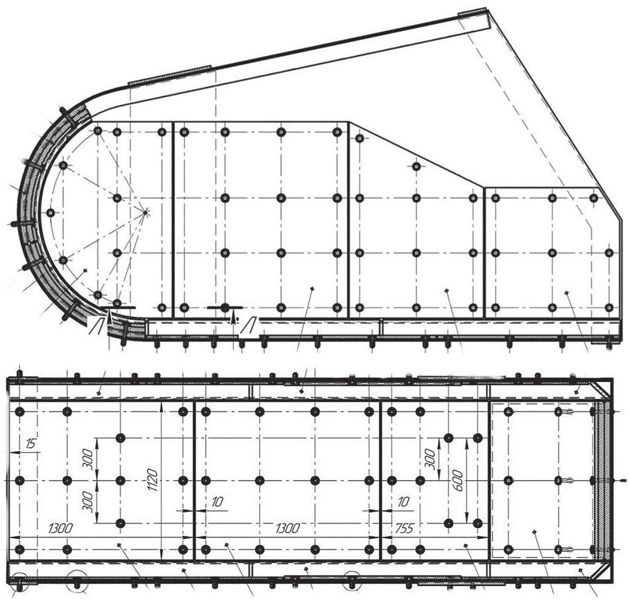

Figure 1. Drawings of the skip lining for the blast furnace

Source: created by the author

Experimentally determined values of hardness and impact strength of deposited layers are summarised in Table 1. The presented data were obtained as part of the author's experimental studies on a series of samples manufactured under the same technological conditions. Analysis of the results showed that with an increase in the hardness of the deposited layer, a decrease in impact strength is observed, which indicates an increase in the susceptibility of the material to brittle fracture. A similar relationship between hardness and impact strength is typical for wear-resistant deposited coatings and was noted by B. Venkatesh *et al*. (2015). The results of abrasive wear tests and crack resistance assessments are shown in Table 2.

Table 1. Hardness and impact strength of deposited layers of different types of materials

Brand	Hardness, HRC	Impact strength, J/cm^2	Notes
VELTEK	58	22	Optimal combination
Duroxite	55	18	High hardness, lower viscosity
SAS Global	52	20	Average indicators

Source: compiled by the author

Table 2. Abrasive wear and resistance to microcracks of modern deposited layers

Brand	Weight loss, g	Number of cracks per 100 cm^2	Notes
VELTEK	0.12	1	Best wear resistance
Duroxite	0.18	3	Moderate wear, high hardness
SAS Global	0.20	4	Largest number of cracks

Source: compiled by the author

All values were obtained in the course of experimental studies, which allows considering them as a reliable basis for analysing the operational behaviour of deposited layers. It is established that an increase in abrasive wear resistance is accompanied by a decrease in weight loss of material, but excessive rigidity of the structure increases the risk of local micro-destruction. Similar patterns were described by C. Fan *et al*. (2006), who emphasised the need for a comprehensive assessment of wear resistance and fracture resistance. Microstructural analysis of the deposited layers makes established a relationship between the phase composition and the mechanisms of crack development. Figure 2a shows the structure of a hypereutectic Fe-Cr-C alloy with a carbide phase of the M7C3 type, while Figure 2b illustrates the nature of crack propagation after microindentation. The results show that cracks are initiated mainly in the carbide phase and propagate along the interfacial boundaries, which is conditioned by the high brittleness of carbides. A similar mechanism of crack development was described in detail in the paper by R. Zahiri *et al*. (2014).

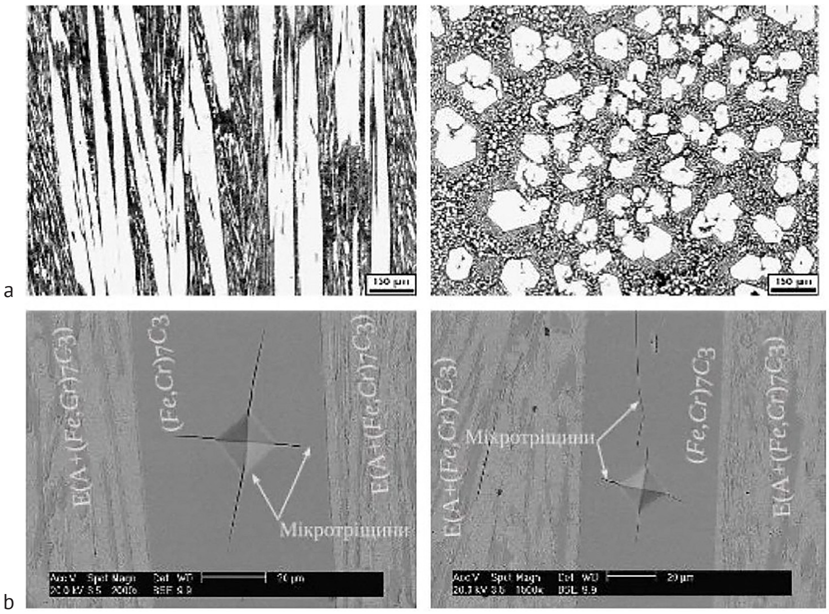

Figure 2. Structure of the hypereutectic Fe-Cr-C alloy and the nature of crack propagation after micro-indentation
Notes: a – carbide phase M7C3; b – crack propagation directions
Source: R. Zahiri *et a*l. (2014)

Comparison of microstructural observations with the mechanical characteristics given in Table 1 and Table 2 established that a more uniform distribution of the carbide phase helps to reduce the stress concentration and slow down the development of cracks. The results obtained indicate that the deposited layers are characterised by a combination of high hardness, sufficient impact strength, and increased resistance to abrasive wear, which is crucial for the operation of the blast furnace skip lining under abrasive and impact loads. The generalised mechanical characteristics of the deposited layers are shown in Table 1, and the results of tests for abrasive abrasion and crack resistance are shown in Table 2. As the analysis of the results shows, the increase in performance characteristics is conditioned by the development of a heterogeneous microstructure consisting of a metal matrix and solid carbide-type phases. Similar patterns were established by P.M. Prysyazhnyuk *et al*. (2022), who noted that the uniform distribution of carbide inclusions in the iron-containing matrix significantly increases the resistance to abrasive and erosion wear. The results obtained in this paper confirm this thesis, since samples with a more uniform structure show a lower intensity of weight wear.

The microstructural features of the deposited layers are confirmed by analysing the structure of the hypereutectic Fe-Cr-C alloy. As shown in Figure 2, the M7C3-type carbide phase forms a branched grid that effectively prevents local plastic deformation. C. Fan *et al*. (2006) noted that it is this morphology of carbides that contributes to an increase in the resistance to nucleation and propagation of microcracks under contact loading. The nature of crack development observed in this paper after microindentation is consistent with the above provisions. In the paper by L.F. Holovko *et al*. (2012), the use of laser-plasma surfacing for the development of wear-resistant surfaces of machine parts was considered. The researchers investigated a combined process in which the plasma supplies and heats the powder material, and the laser melts it together with the base, which increases the efficiency of surfacing and reduces energy costs. The main attention was paid to modelling temperature fields and selecting optimal process modes, and the conclusions showed that this approach is promising for obtaining high-quality wear-resistant coatings and reducing the volume of experimental studies. An important aspect is the ratio of hardness and impact strength of the deposited layers. According to the results presented in Table 1, an increase in hardness is not accompanied by a critical decrease in impact strength, which is fundamental for parts operating under variable impact loads. A similar effect was described by P.M. Prysyazhniuk (2024), proving that multilayer deposited coatings with an optimised structure exhibit more balanced mechanical properties compared to single-layer coatings.

The abrasive wear of the deposited layers (Table 2) decreases with increasing volume fraction of solid phases and increasing the microhardness of the matrix. B. Maroli *et al*. (2017) showed that in the case of iron-containing deposited alloys with high carbide content, wear occurs mainly by a micro-cutting mechanism, but the wear rate is significantly reduced by blocking the movement of abrasive particles. The results obtained in this paper correspond to this concept. The paper by Z.-H. Wang *et al*. (2014) investigated the microstructure and wear resistance of Fe-Cr-B-C hard-surfaced alloys produced by arc surfacing with a wire structure with flux to improve the abrasive wear resistance of the surface layers of parts. Using optical, scanning electron microscopy, and X-ray diffraction, they analysed the effect of boron content on phase development, size, and distribution of borides in the alloy, finding that as boron increases, the boride structure changes from a discontinuous to a continuous network, and at concentrations above ~3% by weight, the proportion of primary (Fe, Cr) B increases, and the distribution becomes more uniform. This leads to an increase in the hardness and abrasive wear resistance of alloys to a certain level of boron (<4%). The results showed that the controlled application of boron can significantly affect the microstructure and wear resistance of Fe-Cr-B-C deposited layers, making them promising for use under heavy friction and abrasion conditions.

Special attention should be paid to the effect of residual stresses formed during surfacing. L. Zong *et al*. (2019) emphasised that excessive structural rigidity without sufficient stress relaxation can contribute to brittle fracture. No signs of intense intergranular crack development were found in the studied samples, which indicates an acceptable level of thermal stresses formed during the surfacing process. B. Trembach *et al*. (2022) emphasised that the introduction of boron and chromium into iron-containing deposited alloys can significantly increase abrasive wear resistance without dramatically reducing ductility. The wear values obtained in this paper confirmed the feasibility of using such compositions to restore lining elements that are experiencing intense wear. The design features of the skip lining shown in Figure 1 substantiate the localisation of areas of increased abrasive and impact load. It is these zones that are critical from the standpoint of part loss, which is consistent with the conclusions of F. Franěk *et al*. (2009), who noted that the wear resistance of deposited layers should be evaluated considering actual contact conditions and element geometry. Thus, the results of experimental studies confirm the global trends established in the recent studies by foreign researchers regarding the effectiveness of the use of iron-containing deposited coatings to increase the service life of parts working in conditions of abrasive and impact wear. However, the obtained data complement the existing understanding of the relationship between the microstructure, hardness, impact strength, and mechanisms of destruction of deposited layers.

Conclusions

The paper examined the features of the development and operational behaviour of deposited wear-resistant layers designed to increase the reliability of the blast furnace skip lining. It was shown that the nature of lining wear is determined by a combination of abrasive and impact load and a complex stress-strain state formed in the most loaded zones of the structure. It was established that the mechanical and operational properties of deposited layers significantly depend on their microstructural organisation. The development of structures with a high content of the carbide phase contributes to an increase in hardness and abrasive wear resistance, but is accompanied by an increase in the tendency to brittle fracture. It was found that the uneven distribution of carbide inclusions is one of the main factors for the initiation and development of cracks in the deposited layers. The use of multilayer deposited systems helps to reduce hardness gradients and stress redistribution in the thermal impact zone, which positively affects the resistance to destruction of deposited coatings. The results obtained confirm the feasibility of a comprehensive approach to choosing the structure of deposited layers, which takes into consideration not only the hardness and wear resistance indicators, but also the ability of the material to counteract crack development under operating conditions. The results of the study are consistent with the situation as of 2025 and can be used to substantiate technological solutions for the restoration of blast furnace skip linings in order to extend their service life and improve operational reliability. A promising area of further research is an in-depth microstructural analysis of deposited layers and thermal impact zones using quantitative phase analysis to establish the relationship between the morphology of reinforcing phases and fracture resistance indicators. It is advisable to use methods of numerical modelling of the stress-strain state to assess the effect of residual and thermal stresses on the development of cracks in multilayer systems. Special attention should be paid to the study of the effect of heat treatment after surfacing on reducing the level of residual stresses and stabilising the microstructure of the deposited layers. Further research in this area will expand the practical application of the developed technological solutions and increase the efficiency of restoring blast furnace equipment elements.

Acknowledgements

The author expresses deep gratitude to the scientific supervisor, Doctor of Technical Sciences, Professor Valerii Viktorovych Peremityk, for constructive guidance, support, and inspiration that contributed to the successful completion of the research.

Funding

None.

Conflict of Interest

None.

References

[1] Belik, O.G., Yefremenko, V.V., &Cheiliakh, Ya.O. (2016). Methods of wide-layersurfacing of wear-resistant alloys. *Reporter of the Priazovskyi State Technical University. Section: Technical Sciences*, 33, 63-67.

[2] Czupryński, A., Poloczek, T., & Urbańczyk, M. (2022). Characterization of a new high-abrasion-resistant iron-based alloy for hardfacing applications. *International Journal of Modern Manufacturing Technology*, 14(1), 27-33. doi: 10.54684/ijmmt.2022.14.1.45.

[3] DSTU EN 14700:2008. (2008). *Welding consumables.Welding consumables for surfacing*. Retrieved from https://online.budstandart.com/ua/catalog/doc-page.html?id_doc=29730.

[4] Fan, C., Chen, M.-C., Chang, C.-M., & Wu, W. (2006). Microstructure change caused by $(Cr, Fe)_3C_6$ carbides in high chromium Fe-Cr-C hardfacing alloys. *Surface and Coatings Technology*, 201(3-4), 908-912. doi: 10.1016/j.surfcoat.2006.01.010.

[5] Franěk, F., Badisch, E., & Kirchgaßner, M. (2009). Advanced methods for characterisation ofabrasion/erosion resistance of wear protection materials. *FME Transactions*, 37(2), 61-70.

[6] Holovko, L.F., Bloshchytsyn, M.S., & Tretiak, V.A. (2012). Formation of wear-resistant surfaces by laser-plasma surfacing. *Mechanics and Advanced Technologies*, 64, 99-105.

[7] Ivanov, O. (2020). Investigation of structure and properties of wear-resistantcoatings obtained by surfacing with powder electrodes based on the Fe-Ti-B-Csystem. *Central UkrainianScientific Bulletin. Technical Sciences*, 3(34), 81-87. doi: 10.32515/2664-262X.2020.3(34).81-87.

[8] Maroli, B., Dizdar, S., & Bengtsson, S. (2017). Iron-based hardfacing alloys forabrasive and impact wear. In *International thermal spray conference* (pp. 1-7). Düsseldorf: ASM International.

[9] Okechukwu, C., Dahunsi, O.A., Oke, P.K., & Oladele, I.O. (2024). Development of ferro-alloy hardfacing for high abrasion and low impact wear applications. *Metallurgical and Materials Engineering*, 24(1), 71-81. doi: 10.30544/338.

[10] Öztürk, Z.T. (2021). Wear behavior and microstructure of Fe-C-Si-Cr-B-Ni hardfacing alloys. *Materials Testing*, 63(3), 215-223. doi: 10.1515/mt-2020-0033.
[11] Pokhmurska, H.V., Voitovych, A.A., & Dziubyk, A.R. (2017). Technology ofmanufacturing wear-resistant plates. *Design, Production and Operation ofAgricultural Machines*, 47(2), 215-220.
[12] Prysyazhniuk, P.M. (2024). *Scientific principles of formation of wear- and impact-resistant coatings of the "high-manganese steel – refractory compounds" system byelectric arc surfacing*. (Doctoral dissertation, Lviv Polytechnic National University, Lviv, Ukraine).
[13] Prysyazhnyuk, P., Ivanov, O., Matvienkiv, O., Marynenko, S., Korol, O., & Koval, I. (2022). Impact and abrasion wear resistance of the hardfacings based on high-manganese steel reinforced with multicomponent carbides of Ti-Nb-Mo-V-C system. *Procedia Structural Integrity*, 36, 130-136. doi: 10.1016/j.prostr.2022.01.014.
[14] Shchetynin, S.V., Shchetynina, V.I., Koval, O.V., Nikitenko, P.V., & Elsaed, Kh. (2019). Improvement of crack resistance and wear resistance during high-speed surfacing atlow heat input. *Reporter of the Priazovskyi State Technical University. Section: Technical Sciences*, 38, 72-79. doi: 10.31498/2225-6733.38.2019.181399.
[15] Skvortsov, O., & Mikosianchyk, O. (2023). Research of the wear resistance of electro-spark coatings under abrasive conditions. *Problems of Friction and Wear*, 3(100), 45-55. doi: 10.18372/0370-2197.3(100).17895.
[16] Trembach, B., Vynar, V., Trembach, I., & Knyazev, S. (2022). Comparison of two-body abrasive wear resistance of high chromium boron-containing Fe-C B-13wt.%Cr Ti alloy with incomplete replacement of Cr for Cu the Fe C B 4wt.%Cr 7wt.%Cu-Ti alloy. *Problems of Tribology*, 27(3(105)), 34-40. doi: 10.31891/2079-1372-2022-105-3-34-40.
[17] Varis, T., Lagerbom, J., Suhonen, T., Terho, S., Laurila, J., & Vuoristo, P. (2023). On the applicability of iron-based coatings against abrasion and cavitation erosion wear. *Journal of Thermal Spray Technology*, 32(2-3), 473-487. doi: 10.1007/s11666-022-01517-7.
[18] Venkatesh, B., Sriker, K., & Prabhakar, V.S.V. (2015). Wear characteristics of hardfacing alloys: State-of-the-art. *Procedia Materials Science*, 10, 527-532. doi: 10.1016/j.mspro.2015.06.002.
[19] Wang, Z.-H., Wan, G.-L., He, D.-Y., Jiang, J.-M., & Cui, L. (2014). Microstructures and wear resistance of Fe-Cr-B-C hardfacing alloys. *Journal of Materials Engineering*, 9, 57-62. doi: 10.11868/j.issn.1001-4381.2014.09.010.
[20] Zahiri, R., Sundaramoorthy, R., Lysz, P., & Subramanian, C. (2014). Hardfacing using ferro-alloy powder mixtures by submerged arc welding. *Surface and Coatings Technology*, 260, 220-229. doi: 10.1016/j.surfcoat.2014.08.076.
[21] Zong, L., Guo, N., Li, R., & Yu, H. (2019). Effect of boron content on microstructure and wear resistance of Fe-Ti-B-C hardfacing alloys. *Coatings*, 9(4), article number 265. doi: 10.3390/coatings9040265.

Підвищення тріщиностійкості футерівки скіпа доменного цеху

Іван Кривда

Аспірант

Дніпровський державний технічний університет

51918, вул. Дніпробудівська, 2, м. Кам'янське, Україна

https://orcid.org/0009-0005-0724-853X

Анотація. Експлуатація футірки скипа доменного цеху супроводжується інтенсивним абразивно-ударним зношуванням, через що актуально розробляти залізовмісні наплавні матеріали з гетерогенною карбідною мікроструктурою для підвищення міцності та зносостійкості. Метою роботи було підвищення механічної міцності та довговічності футірки скипа доменного цеху шляхом оптимізації структури наплавлених шарів і встановлення закономірностей між мікроструктурою, механічними властивостями та зносостійкістю покриттів. Дослідження виконано з використанням електродугового наплавлення на зразках зі сталі 09Г2С. Проведено випробування на твердість, ударну в'язкість і абразивне стирання, а також мікроструктурний аналіз наплавлених шарів і оцінку характеру тріщиноутворення після мікроіндентування. Основні результати експериментальних досліджень показують, що твердість наплавлених шарів коливалася від 52 HRC у матеріалу SAS Global до 58 HRC у ВЕЛТЕК, тоді як ударна в'язкість змінювалася від 18 Дж/см² у Duroxite до Дж/см² у ВЕЛТЕК, що демонструє обернену залежність між твердостю та ударною в'язкістю: більш тверді шари мають більшу схильність до крихкого руйнування. У випробуваннях на абразивне стирання встановлено, що ВЕЛТЕК проявив найкращу зносостійкість із масовою втратою 0,12 г та лише однією тріщиною на 100 см², тоді як SAS Global характеризувався найбільшою кількістю тріщин (4 на 100 см²) і втратою маси 0,20 г, а Duroxite мав проміжні значення – 0,18 г втрати маси та 3 тріщини. У результаті встановлено, що формування заевтектичної структури з карбідною фазою типу M_7C_3 сприяє зниженню інтенсивності абразивного зношування та обмеженню поширення мікротріщин. Отримані наплавлені шари характеризуються поєднанням підвищеної твердості та достатньої ударної в'язкості, що є критичним для роботи футірки в умовах змінних ударних навантажень. Практична цінність результатів полягає у можливості їх використання при відновленні та модернізації футірки скипів доменних печей з метою збільшення міжремонтного ресурсу та зниження експлуатаційних витрат

Ключові слова: наплавлення; мікроструктура; зношування; міцність; залишкові-напруження; твердість

Journal of Kryvyi Rih National University
Journal homepage: https://journal-knu.com.ua/en
Article's History: Received: 14.11.2025 Revised: 20.03.2026 Accepted: 28.04.2026 Published: 29.05.2026
Vol. 24, No. 1, 2026
ISSN 2306-5451
e-ISSN 2519-2736

UDC 622.235:622.341.1(477.63)
DOI: 10.31721/2306-5451-2026-1-24-94-106

Influence of the orientation of elongated shaped charges on the design of an optimal borehole pattern for the Kryvyi Rih Basin

Dmytro Brovko
Doctor of Technical Sciences, Professor
Kryvyi Rih National University
50027, 11 Vitalii Matusevych Str., Kryvyi Rih, Ukraine
https://orcid.org/0000-0001-9108-3857

Volodymyr Kononenko
PhD in Technical Sciences, Associate Professor
Kryvyi Rih National University
50027, 11 Vitalii Matusevych Str., Kryvyi Rih, Ukraine
https://orcid.org/0000-0002-5993-4268

Vasyl Khvorost*
PhD in Technical Sciences, Associate Professor
Kryvyi Rih National University
50027, 11 Vitalii Matusevych Str., Kryvyi Rih, Ukraine
https://orcid.org/0000-0002-9205-7797

Kostiantyn Haponenko
Postgraduate Student
Kryvyi Rih National University
50027, 11 Vitalii Matusevych Str., Kryvyi Rih, Ukraine
https://orcid.org/0009-0009-2068-9945

Abstract. The relevance of this study is driven by the need to improve the efficiency of drilling and blasting operations at iron ore open-pit mines in the Kryvyi Rih Basin through the application of elongated shaped charges spatially adapted to the structural characteristics of the rock mass in order to optimise borehole pattern parameters. The aim of the study was to determine the influence of the spatial orientation of elongated shaped charges on the geometric parameters of the borehole pattern and to develop engineering recommendations for its optimal design under the complex mining and geological conditions of surface mining. The research methodology was based on an integrated approach combining numerical modelling of wave propagation in continuous media using constitutive material behaviour models with nonlinear mathematical optimisation based on the Generalised Reduced Gradient (GRG) algorithm. The results demonstrated a nonlinear relationship between the dimensions of the intensive fragmentation zone and the rotation angle of the shaped cavity. Statistical analysis confirmed that the optimum rotation angle is 45°, provided that the shaped charge jet is oriented parallel to the strike of the principal fractures. Under these conditions, an elongated elliptical fracture zone is formed, enabling the transition from conventional square borehole patterns to rectangular spatial layouts. It was established that this configuration allows the spacing between boreholes to be increased to 7 m, while achieving a borehole convergence coefficient

Suggested Citation:
Brovko, D., Kononenko, V., Khvorost, V., & Haponenko, K. (2026). Influence of the orientation of elongated shaped charges on the design of an optimal borehole pattern for the Kryvyi Rih Basin. *Journal of Kryvyi Rih National University*, 24(1), 94-106. doi: 10.31721/2306-5451-2026-1-24-94-106.

Copyright © The Author(s). This is an open access article distributed under the terms of the Creative Commons Attribution License 4.0 (https://creativecommons.org/licenses/by/4.0/)

*Corresponding author (khvorost.v.v@knu.edu.ua)

of 1.52. Conversely, orienting the charge perpendicular to the fracture system produces an acoustic shielding effect, restricting the propagation of explosive energy and limiting the expansion of the borehole pattern. The practical significance of the study lies in the development of a differentiated methodology for the spatial positioning of explosive charges in ferruginous quartzites. The implementation of the proposed optimised borehole pattern parameters reduces specific drilling costs by 33% without compromising fragmentation quality. Furthermore, it decreases drilling tool wear, shortens the preparation cycle, and proportionally reduces the environmental impact through lower dust and gas emissions

Keywords: shaped cavity; ferruginous quartzite fragmentation; dynamic modelling; borehole convergence; drilling and blasting operations

Introduction

The efficiency of open-pit mining operations was largely determined by the quality of drilling and blasting preparation of the rock mass. One of the promising directions for intensifying the destruction processes was the application of elongated shaped charges (ESCs), capable of concentrating explosion energy in a specified direction. Globally, research on directed explosive action was actively developed, and increasing the efficiency of rock mass destruction through the directed concentration of detonation energy was considered one of the most urgent scientific and practical tasks for the modern mining industry.

The analysis of the current state of research in this field indicated significant interest from the scientific community in this issue. Furthermore, attention was focused on the mathematical and mechanical modelling of the stress field during an explosion by Q. Gao *et al.* (2020). In that study, the influence of the detonator's location on the efficiency of bench blasting was examined, and it was concluded that the correct spatial localisation of initiation was critically important. According to Y. Yao *et al.* (2021), an innovative approach using a bilateral slotted shaped charge was developed and investigated. The advantages of microsecond delays for the formation of directed cracks between boreholes were proven. Significant attention was also paid to the optimisation of the charge design itself. For instance, various shapes of shaped charge liners were investigated by K. Liu *et al.* (2023). Based on experimental data, it was concluded that the liner shape was the determining factor for the efficiency of directed rock destruction.

Despite significant progress in this field, the majority of research was focused on general principles, without proper adaptation to the specific mining and geological conditions of the iron ore open-pit mines in the Kryvyi Rih basin. The issue of mass blasts in the Kryvbas open-pit mines was studied by Ye.O. Nesmashnyi *et al.* (2022), whilst developing a method for the rapid determination of the flyrock distance. It was concluded that blast parameters required strict control to ensure safety. The variability of drilling and blasting parameters at local enterprises was analysed by H. Yeremenko *et al.* (2022). According to those researchers, there was an urgent need to improve the borehole pattern parameters, taking into account the spatial orientation of elongated shaped charges, to increase the quality of fragmentation and reduce the yield of oversized blocks.

A study by B. Andrieiev *et al.* (2026) was dedicated to a detailed analysis of the physical, mechanical, and hydrodynamic processes accompanying the detonation of elongated shaped charges during rock mass destruction under the conditions of iron ore open-pit mines. Attention was focused on the mechanisms of formation and interaction of shaped charge jets with high-strength ferruginous quartzites and ores. The redistribution of explosion energy during the application of the shaped charge effect was substantiated in the work, which allowed achieving directed crack formation and improving the quality of rock mass fragmentation. The scientific value of the study consisted in establishing the patterns of shock wave propagation and dynamic stresses in the rock mass upon detonation of elongated shaped cavities.

Consequently, the issue of developing scientifically substantiated methods for the optimal design of the borehole pattern, which would take into account the influence of ESC orientation on the efficiency of explosive breaking under the conditions of the Kryvyi Rih basin, remained unresolved. Within the scope of the conducted research, the aim was to determine the patterns describing the impact of the spatial orientation of elongated shaped charges on the formation of the borehole pattern, in order to create practical tools for its optimal design in the open-pit mines of the Kryvyi Rih basin. The realisation of the set objective encompassed the solution of three key tasks. Initially, global experience and theoretical foundations of using shaped charges for directed rock destruction were analysed. The subsequent step involved the construction of a mathematical model and the conduction of experimental studies on the influence of the ESC spatial orientation on fragmentation quality under the conditions of the Kryvyi Rih basin open-pit mines. The final stage of the work was the development and verification of a practical engineering methodology for calculating borehole pattern parameters.

Literature Review

The issue of increasing the efficiency of drilling and blasting operations was the subject of constant attention from researchers. A significant contribution to the development of the theory and practice of explosive rock destruction using shaped charges was made by various researchers. The influence of the design features of shaped charge liners on the nature of rock destruction was investigated by K. Liu *et al.* (2023) based on numerical modelling and laboratory experiments. Flat, arc-shaped, and triangular shapes of cavities were compared with each other. Based on the results of the work, it was concluded that the application of a triangular-shaped liner provided the best directed effect compared to other analogues.

According to Y. Yao *et al.* (2021), an innovative approach using a bilateral slotted shaped charge (BGSSC) was developed. The impact of microsecond initiation delays on the dynamics of crack development was investigated. It was concluded that precisely calculated time intervals allowed the formation of through cracks between boreholes, providing an even separation plane. The application of directed controlled blasting technology during the excavation of unstable rock slopes along the Konkan Railway was investigated by N. Bhagat *et al.* (2020). It was concluded that the proposed technology provided better control of the excavation contour, increased slope stability, and reduced undesirable rock destruction. The influence of the eccentric placement of a decoupled charge on the nature of rock destruction was investigated by C. Pan *et al.* (2022) using numerical modelling. It was established that such a design contributed to the concentration of explosion energy in a specified direction and improved the controllability of the destruction process. A numerical model based on the particle-based numerical manifold method for modelling crack development during explosive rock destruction was developed by X. Li *et al.* (2017). It was confirmed that the proposed approach reliably reproduced the crack propagation process and could be used for the optimisation of drilling and blasting parameters. The features of rock destruction when using a slotted cartridge with a decoupled charge were investigated by Y. Wang (2017). The results demonstrated that such a design provided a more efficient direction of explosion energy and the formation of controlled cracks. The mechanism of crack formation during shaped charge blasting was investigated, and a novel dual shaped charge technology was proposed by P. Xu *et al.* (2024). It was established that the use of two shaped charges increased the efficiency of directed rock destruction and improved the control of crack development. The mechanism of directed rock splitting under the action of a shaped charge jet was investigated by D. Liu *et al.* (2023). It was concluded that the shaped charge jet provided energy concentration in a specified direction, which facilitated the formation of main cracks and increased the efficiency of directed blasting.

A study by Q. Gao *et al.* (2020) was dedicated to the mathematical and mechanical analysis of stress field formation in an explosive charge. The main object of the research was the influence of the detonator's location on the overall explosion energy. It was concluded that the optimisation of the charge initiation point was capable of fundamentally changing the spatial distribution of energy and significantly improving the efficiency of bench blasting. Environmental and resource-saving aspects of blasting operations in open-pit mines were investigated in a study by O. Tverda *et al.* (2021). A new charge design with a radial gap completely filled with a chemically active substance was developed. It was concluded that such an approach allowed not only to reduce the seismic pressure on the rock mass but also to effectively neutralise harmful gases formed after detonation. The direct issue of designing and conducting drilling and blasting operations under the specific conditions of the Kryvyi Rih iron ore basin was also a subject of active research. Experimental studies on the variability of drilling and blasting parameters at the "Pivdennyi" open-pit mine of "Rudomain" LLC were conducted by H. Yeremenko *et al.* (2022). The impact of new materials on the final particle size distribution of the blasted ore was studied. Based on the results of the work, it was concluded that there was a necessity for the constant adaptation of borehole pattern parameters to the changing mining and geological conditions of the deposit.

It should be noted that despite the significant volume and depth of the aforementioned research, there were aspects of the topic to which insufficient attention was paid. In particular, the quantitative impact of the specific spatial orientation (angle of rotation) of elongated shaped charges on the rational distance between boreholes in the rock mass was practically unexplored in the analysed works. The absence of clear mathematical dependencies and a differentiated approach to the optimal design of the borehole pattern, taking into account the direction of the ESC action under the specific conditions of the iron ore open-pit mines of the Kryvyi Rih basin, formed a scientific gap, which served as the main prerequisite for conducting this research.

Materials and Methods

The general strategy of this research was based on a complex multiscale approach, which organically combined the analytical substantiation of gas-dynamic processes in the near-blast zone and the multivariant computer modelling of nonlinear continuum mechanics. Such a symbiosis of methods allowed overcoming the conceptual insufficiency of purely empirical or exclusively numerical approaches, verifying theoretical hypotheses regarding the spatial anisotropy of the stress-strain state of the rock mass caused by the directed action of the explosion, and obtaining reliable data for the further macroscale optimisation of drilling and blasting parameters. The limitation of this study was that the patterns of the formation of elliptical destruction zones were established for the conditions of hard ferruginous quartzites ($f = 16 - 18$). Changes in the properties of the rock mass or types of explosives would require further comparative analysis and calibration of mathematical models at other deposits.

The research logic involved a sequential transition from the micromodelling of shaped charge wave effects to the macroscopic engineering calculations of the geometric configurations of the borehole pattern. The mathematical and physical bridge in this transition was the energy focusing efficiency coefficient, obtained through the polynomial approximation of the volumes of the destroyed medium based on the results of a series of numerical calculations. The application of polynomial approximation in this context was a method of justified data dimensionality reduction, which allowed transforming redundant arrays of discrete parameters of the stress-strain state into a continuous analytical function. Since the volume of destruction was selected as an integral criterion accumulating energy expenditures on deformation, crack formation, and wave interference, the obtained polynomial dependence acted as a normalised response function of the geomedium. This allowed collapsing microscale dynamic effects into a weight coefficient, which was directly integrated into classical engineering methodologies for calculating blasting operations, ensuring the accurate transfer of fundamental patterns into applied design algorithms.

The experimental base of the research was formed with deep consideration of the specifics of the physical and mechanical properties of typical rocks of the Kryvyi Rih iron ore basin under conditions of intensive deepening of mining operations, where high tectonic stresses and changes in the nature of destruction began to play a dominant role. Unweathered primary magnetite quartzites of the basin's mine administrations were selected as the main media for studying the processes of fragmentation intensification. Magnetite quartzites were characterised by extremely high strength (strength coefficient on the M.M. Protodiakonov scale $f = 14 \div 18$, compressive strength $\sigma_c = 180 \div 220$ MPa, dynamic tensile strength $\sigma_t = 14 \div 18$ MPa), high density ($\gamma = 3{,}200 \div 3{,}400$ kg/m^3) and significant acoustic stiffness ($Z \approx 14 \div 16 \cdot 10^6$ kg/(m$^2 \cdot$ s)). The critical geomechanical feature of these ores was their structural anisotropy, caused by the complex folded block structure and the spatial orientation of the main systems of natural macrocracks. The presence of a network of subvertical and subhorizontal cracks with a distance between them from 0.2 to 0.8 m led to the spatial variability of the ultimate strength and a difference in the propagation velocity of elastic stress waves along and across the strike of the rock mass of up to 15-20%. Ferruginous quartzites of a schistose texture, as less strong host rocks, possessed a strength of $f = 8 \div 10$ (compressive strength $80 \div 120$ MPa, density $\gamma = 2{,}700 \div 2{,}900$ kg/m^3)). This texture formed an extremely high degree of mechanical and acoustic anisotropy (the structural anisotropy coefficient reached 1.4-1.6), which caused intensive dissipation of the kinetic explosion energy on the planes of weakness and required precise spatial alignment of the shaped charge axis with the dominant anisotropy vectors of the medium. This aspect was spatially formalised through the introduction of the azimuthal angle β, which determined the orientation of the shaped charge plane in the plan relative to the dominant system of natural cracks in the rock mass, which was a necessary condition for preventing energy losses. To initiate directed destruction and overcome the isotropic nature of the expansion of detonation products, specially designed elongated shaped charges were used, the structural diagram of which was presented in Figure 1.

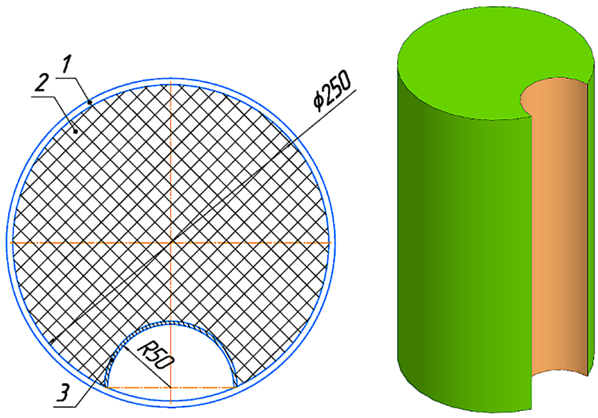

Figure 1. Cross-section of the elongated shaped charge
Notes: 1 – polymer shell; 2 – explosive; 3 – shaped cavity
Source: developed by the authors

According to the drawing, the total diameter of the charge (item 1) was 250 mm, which fully corresponded to the typical diameters of blast holes in Kryvbas open-pit mines when heavy roller cone drilling rigs of the SBSH-250 type were applied, which ensured the technological efficiency of implementation. The charge shell was manufactured from an extruded polymer material with a thickness of 2-3 mm. The choice of polymer was determined by its acoustic impedance, which was close to the parameters of industrial explosives, which minimised parasitic wave reflection at the media interface, and also provided the necessary geometric stability of the structure during loading into water-filled boreholes. The internal space (item 2) was filled with a pourable industrial explosive, for example, a water-resistant emulsion composition of the "Ukrainit" type with a linear density of about 40-45 kg/m. Along the charge formation line over its entire length, a semi-cylindrical shaped cavity (item 3) with a radius of 50 mm (R50) was formed. The choice of the semi-cylindrical geometry was determined by the necessity of forming not a classical thin shaped charge jet with high penetrating ability (the Munroe effect), but a massive explosively formed projectile with a flat front, capable of transmitting the maximum impulse of tensile stresses to the rock mass. Exclusively an air gap or a thin polyvinyl chloride film for waterproofing was used as the liner of the shaped cut. The rejection of the traditional metal liner was associated with the need to prevent the loss of detonation thermal energy on the plastic deformation of the metal and melting, focusing exclusively the gas-dynamic flow onto the borehole wall. The length of one charge module was 1-2 metres, with the structural possibility of their rigid axial connection by means of couplings into a continuous charge column of any required length.

To investigate the complex wave pattern, gas-dynamic shock parameters, and the initial stage of the micro- and macrocracking zone formation, a computer modelling methodology was applied in the high-performance ANSYS Autodyn software package, using the explicit method of integrating continuum dynamics equations over time. The computational domain was discretised by a detailed hexahedral finite-element mesh using a coupled formulation (Euler-Lagrange). In this setup, detonation products and the air medium were described by an Eulerian mesh to avoid problems with element degeneration under large gas deformations, and the rock mass was described by a Lagrangian mesh with built-in algorithms for geometric erosion of elements upon reaching critical values of plastic deformations or instantaneous destruction. The detonation of the explosive was modelled using the phenomenological Jones-Wilkins-Lee (JWL) equation of state, the parameters of which (A, B, R_1, R_2, ω, E_0) were precisely calibrated for emulsion explosives based on copper cylinder expansion tests. The behaviour of the rock mass under intensive dynamic loading was described by the complex Riedel-Hiermaier-Thoma (RHT) constitutive model. This model was critically important for the reliable reproduction of the behaviour of brittle media, since it took into account not only rock strength degradation due to the gradual accumulation of damage (parameter D), but also the nonlinear dependence of the yield strength on hydrostatic pressure, strengthening effects at high strain rates, and the influence of the Lode angle on the yield surface shape. Non-reflecting boundary conditions were set at the external boundaries of the computational domain to simulate an infinite rock half-space and level out errors from stress wave reflections from the artificial boundaries of the computational domain. A mesh sensitivity analysis was conducted until the convergence of results for peak pressures at the shock wave front with an error of less than 5% was achieved.

Since the direct search for optimal borehole pattern parameters by finite element methods at the level of the entire open-pit block was computationally impossible due to the gigantic number of degrees of freedom and the difference in scales (from millimetres in the borehole to tens of metres in the bench), the optimisation task was formalised in the form of a strict macroscale mathematical model of nonlinear programming (NLP). The general problem statement included an objective function of reduced economic costs and a complex system of nonlinear technological and geometric constraints:

$$F(X) = C_d \cdot \left(H + L_p\right) + C_e \cdot Q_a \cdot W \cdot H \cdot \gamma \to min$$
$$\begin{cases} A_0 \cdot K_f(\theta) \cdot \frac{a \cdot W \cdot H}{Q^{0.8}} \cdot Q^{1/6} - [d_{max}] \le 0 \\ K_s \cdot R \cdot Q^{-\alpha} \cdot K_{ppv}(\theta) - [PPV_{kr}] \le 0 \\ a_{min} \le a \le a_{max} \\ W_{min} \le W \le W_{max} \\ L_{p,min} \le L_p \le L_{p,max} \\ 0 \le \theta \le \frac{\pi}{2} \end{cases}, \qquad (1)$$

where C_d – the average cost of drilling one running metre of a borehole in hard quartzites; H – the height of the working bench; C_e – the cost of one kilogram of the manufactured explosive; Q_a – the design specific consumption; γ – the rock density. In the presented mathematical model, the following vector acted as the controlled vector of independent spatial variables:

$$X = [a, W, L_p, \theta, \beta]^T, \qquad (2)$$

where a – the distance between boreholes in a row; W – the line of least resistance (distance between rows); – the amount of subdrilling (which directly affected the toe breakage). The spatial orientation of the charge was described by two parameters: θ – the zenith angle of the shaped charge axis relative to the exposed plane in the vertical section (visualised in Fig. 2 as angle α); and β – the azimuthal angle of jet orientation in the horizontal plane relative to the strike of the dominant system of tectonic macrocracks.

The objective function $F(X)$ represented a mathematical expression for the minimisation of the total reduced costs for the basic processes of drilling and blasting operations. The first and most important inequality of the system formalised the critical technological condition for ensuring the required quality of rock mass fragmentation: it was the empirical Kuz-Ram equation, modified by the introduction of the surrogate energy focusing efficiency coefficient K_f (θ, β). The transition from microscale wave modelling in ANSYS Autodyn to macroscale optimisation calculation was realised through a sequential procedure of constructing a surrogate model (metamodel) based on interconnected stages. Initially, relying on a series of 45 basic numerical calculations in Autodyn for discrete spatial combinations of the zenith θ_i and azimuthal β_j angles, a step-by-step calculation of the degradation and strength fields of the rock mass was performed. In the subsequent step, the volume of the effective destruction V_{frac} (θ, β) zone was determined by numerical three-dimensional integration of those elements of the rock Lagrangian mesh for which the accumulated damage index in the RHT model reached the critical value $D \geqslant 0.85$, which corresponded to the complete exhaustion of the medium's bearing capacity and disintegration into separate fractions. Following this, the calculation of the normalised dimensionless energy focusing indicator relative to the baseline explosion of a cylindrical charge of similar mass without a shaped cavity (isotropic standard) was carried out as a ratio $\bar{V}_{frac}(\theta, \beta) = V_{frac}(\theta, \beta)/V_{iso}$. At the final stage, the obtained discrete data array $\bar{V}_{frac}(\theta_i, \beta_j)$ was approximated by a two-dimensional third-degree polynomial using the least squares method (LSM), which allowed obtaining the analytical expression of the coefficient as a smooth and differentiable function:

$$K_f(\theta, \beta) = c_0 + c_1\theta + c_2\beta + c_3\theta^2 + c_4\theta\beta + c_5\beta^2 + \\ + c_6\theta^3 + c_7\theta^2\beta + c_8\theta\beta^2 + c_9\beta^3, \tag{3}$$

where $c_0 \ldots c_9$ – empirical approximation coefficients calculated for a specific rock type. In particular, for magnetite quartzites, the values $c_0 = 1.08$, $c_1 = -0.32$, $c_2 = 0.54$, etc., were obtained, while ensuring a high quality of agreement with the coefficient of determination $R_2 = 0.94$. Due to the representation of the coefficient K_f (θ, β) in the form of a smooth polynomial, the GRG optimisation algorithm gained the capability of continuous calculation of the objective function and constraint gradients during the search for optimal drilling and blasting parameters without the need to use resource-intensive finite-element calculations at each iteration. The second inequality of the constraint system strictly limited the seismic effect on the boundary rock mass, where K_s and α – the structural attenuation coefficients of seismic waves, R – the distance to the object, and K_{ppv} (θ, β) accounted for the spatial redistribution of seismic energy vectors depending on the direction of the shaped charge impact. The subsequent block of inequalities determined the limit boundaries of the spatial search for geometric parameters.

The solution of this complex multi-parameter problem was performed by the iterative algorithm of the Generalized Reduced Gradient (GRG). The choice of exactly this advanced method was justified by the significant nonlinearity of the fragmentation quality and seismic action constraints. The GRG procedure was specially adapted to maintain strict solution feasibility at each iteration. At the first stage, the general vector of variables was algorithmically divided into a vector of dependent basic variables (variable α) and a vector of independent non-basic variables $X_N = [\theta, \beta, W, L_p]^T$. The reduced gradient was calculated using the matrix equation $\nabla_R F = \nabla_N F(X) - \nabla_N g(X)[\nabla_B g(X)]^{-1}\nabla_B F(X)$, which required the calculation of the Jacobian matrix of first partial derivatives. To compensate for the linearisation error, a rigid correction procedure using the Newton-Raphson method was initiated after each optimisation step. The strictness of finding the global minimum was verified by checking the classical Karush-Kuhn-Tucker (KKT) conditions for the extended Lagrange function $L(X, \lambda) = F(X) + \sum\lambda_i\, g_i\,(X)$ (Fig. 2).

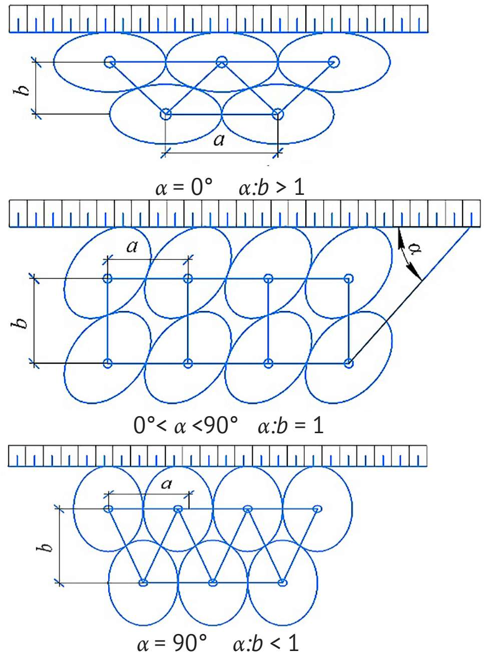

Figure 2. Orientation schemes of destruction ellipses from shaped charges for various topological configurations of the borehole pattern

Notes: *a*) $\alpha = 0°$; *b*) $0° < \alpha < 90°$; *c*) $\alpha = 90$^∘

Source: developed by the authors

Since the numerical experiments generated data arrays with a certain level of stochasticity, a rigorous statistical apparatus was applied for their processing and integration into the macromodel. The assessment of the reliability of the differences obtained between the series of data indicators with different angles θ and β was conducted using one-way and multi-way analysis of variance (ANOVA) with the testing of null hypotheses using Fisher's F-test. The construction of surrogate models and the approximation of response surfaces (in particular, the dependencies of the borehole utilisation factor and the average fragment diameter on W, θ and β) were carried out by methods of multiple nonlinear regression using least squares algorithms (LSM). The quality and predictive ability of the obtained regression equations were evaluated using the adjusted coefficient of determination ($R^2_{adj} \geqslant 0.85$), and the statistical significance of individual model coefficients was confirmed by Student's t-test at a given confidence probability level $P = 0.95$. The detection and exclusion of anomalous outliers in the measurements were performed according to

Chauvenet's criterion, which ensured the robustness of the final empirical dependencies.

Based on the in-depth synthesis of the numerical modelling results and statistically confirmed experiments, a unified applied methodology for designing an optimised borehole pattern was formalised. This algorithm was conceptually based on the determination of the equivalent elliptical radius of the destruction zone. The optimal line of least resistance (W) was calculated as a nonlinear function of the linear charge density, the dynamic strength limit of the rock, and the angles of the spatial orientation of the jet (θ and β). Such a sharply anisotropic energy distribution necessitated the transition to rectangular or elongated rhombic spatial structures. The borehole spacing ratio ($m = a/W$) was calculated iteratively for each of the presented schemes, ensuring a precise tangential or secant collision of the expanded destruction ellipses exactly at the boundary of the elastic deformation zones. This radically minimised the overexpenditure of explosive energy on overcrushing and maximised the borehole utilisation factor due to the complete elimination of toe formation at the bench floor. All the presented model parameters, mathematical boundaries, and physical-mechanical characteristics were clearly documented, which ensured the scientific reproducibility of computer simulations under the conditions of similar iron ore deposits.

Results

Based on the array of data obtained during a series of experimental blasts in the fractured ferruginous quartzites of the Kryvyi Rih basin, the patterns of destruction zone formation depending on the spatial orientation of ESCs were analysed. Considering the high strength and pronounced structural anisotropy of the investigated rocks, the spatial control of explosion energy acted as a key factor in the optimisation of drilling and blasting parameters. The analysis of the explosive destruction parameters revealed a nonlinear dependence between the inclination angle of the shaped charge liner (α) relative to the longitudinal axis of the borehole and the geometric dimensions of the deformation zones. An increase in the angle α was accompanied by a shift in the maximum stress concentration, which led to a change in the equivalent radii of the intensive fragmentation zone (R_d) and the radial crack zone (R_c). The geomechanical mechanism of this phenomenon consisted in a change in the action vector of the detonation products: with the inclination of the shaped charge jet, a more efficient shearing of the structural blocks of the rock mass occurred, which minimised energy losses on plastic deformations directly around the borehole walls. As evidenced by the data presented in Figure 3, the dimensions of both zones demonstrated a statistically significant increase with an increase in the angle α from 0° to 45°.

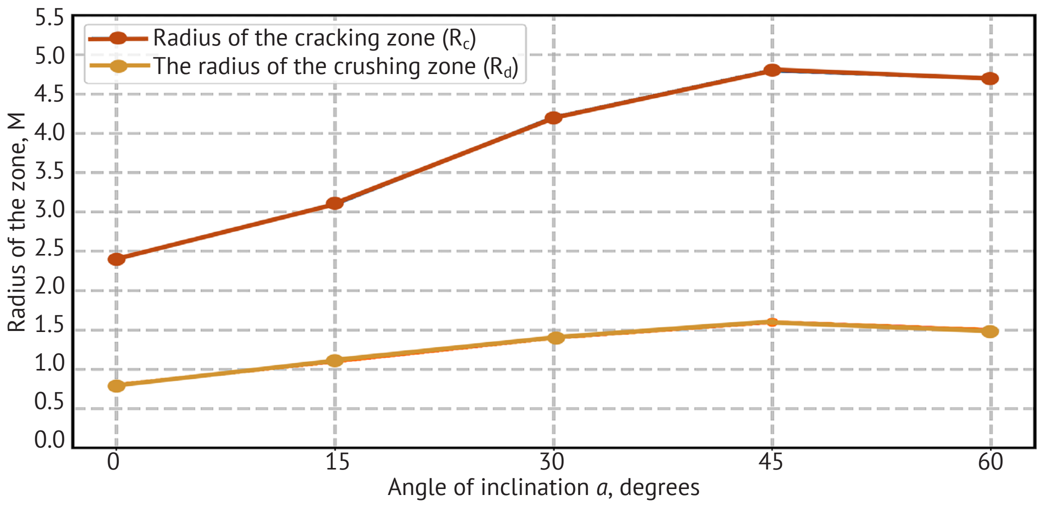

Figure 3. Dynamics of changes in the radii of the intensive fragmentation zones (R_d) and radial cracks R_c) depending on the inclination angle of the shaped charge liner

Source: developed by the authors

The results of the one-way analysis of variance (ANOVA) confirmed that the influence of the factor α on the size of the zone R_c was determining ($F = 42.6$; $p < 0.001$). At the same time, the post-hoc analysis using Tukey's test showed the absence of a statistically significant difference between the values of R_c and R_d in the range of angles of 45° and 60° ($p = 0.812$). This indicated the achievement of the limit of effective explosion energy redistribution in the rock mass. A further increase in the inclination angle (over 45°) led to the intensification of local rock overcrushing and the irrational expenditure of wave energy, which dissipated without the formation of new main cracks (Table 1).

Table 1. Statistical indicators of the sizes of destruction zones of ferruginous quartzites at various ESC orientations (n = 45)

ESC inclination angle (α),°	Radius of fragmentation zone (R_d), m	Radius of crack zone (R_c), m	Explosion energy utilisation factor (η), units
0 (baseline)	0.8 ± 0.1	2.4 ± 0.2	0.62 ± 0.04
15	1.1 ± 0.1	3.1 ± 0.2	0.68 ± 0.03
30	1.4 ± 0.2	4.2 ± 0.3	0.79 ± 0.05
45	1.6 ± 0.2	4.8 ± 0.3	0.86 ± 0.04
60	1.5 ± 0.2	4.7 ± 0.3	0.84 ± 0.05

Notes: data were presented in the format "mean value ± standard deviation"
Source: developed by the authors

As could be seen from the data in Table 1, the change in the spatial configuration of the charge directly influenced the explosive energy utilisation factor (η). In addition to the inclination angle, the influence of the azimuthal direction of the shaped charge jet (β) relative to the natural fracturing systems of the ore mass was quantitatively proven for the first time. Spearman's correlation analysis revealed a direct relationship (r_s = 0.84; p < 0.01) between the angle of the jet's encounter with the dominant crack system and the coefficient η. The maximum values η of were recorded provided that the ESCs were directed parallel to the strike of the rock mass or at an angle of up to 15° to the planes of weakness. In such a case, the "gas-dynamic wedge" effect was realised, where the detonation products penetrated into open natural cracks, expanding them and forming a continuous separation plane without additional energy losses on overcoming the resistance of the continuous medium. The established patterns of explosion energy redistribution served as a basis for adjusting the borehole pattern parameters. The directed increase in the radial crack zone (R_c) along the borehole row line allowed fundamentally changing the ratio between the line of least resistance (W) and the distance between the boreholes (α), designed in the rock mass. Due to the superimposition (superposition) of stress waves from adjacent charges oriented towards or parallel to each other, a single zone of guaranteed destruction was formed even with increased distances between the borehole axes. The data analysis (Table 2) demonstrated that the application of ESCs with an angle α in the range of 30-45° was accompanied by a proportional increase in the distance between boreholes a compared to traditional charges, whereas the value W of varied within the statistical error or demonstrated a tendency towards a slight decrease. The preservation or slight decrease W of was explained by the necessity of overcoming the rock resistance in the direction of the free bench surface to ensure high-quality separation and the formation of a rock pile with specified excavatability parameters.

Table 2. Design parameters of the borehole pattern for the Kryvyi Rih basin conditions depending on the ESC orientation

Charge type / Angle α,°	Line of least resistance (W), m	Distance between boreholes (a), m	Charge spacing ratio (m)	Specific drilling costs, m/m^3
Traditional (columnar)	5.0 ± 0.2	5.0 ± 0.2	1.00 ± 0.05	0.0024 ± 0.002
ESC, α = 15°	4.9 ± 0.2	5.6 ± 0.3	1.14 ± 0.06	0.0021 ± 0.001
ESC, α = 30°	4.8 ± 0.2	6.5 ± 0.3	1.35 ± 0.08	0.0018 ± 0.001
ESC, α = 45°	4.6 ± 0.3	7.0 ± 0.4	1.52 ± 0.09	0.0016 ± 0.002
ESC, α = 60°	4.3 ± 0.3	7.2 ± 0.4	1.67 ± 0.10	0.0016 ± 0.002

Source: developed by the authors

The application of Student's t-test for independent samples confirmed that the increase in the charge spacing ratio when using ESCs (α = 45°) compared to the baseline variant was statistically significant (t = 6.8; p < 0.001). As a result of the pattern expansion (increase a to 7.0 ± 0.4 to m) a significant reduction in specific drilling costs by 33.3% (from 0.024 to 0.016 m/m^3) was recorded. From an engineering perspective, this reduction not only reduced direct operational costs for rock mass preparation but also reduced the wear of drilling tools (roller cone bits), decreased the time equipment spent in the hazardous zone, and minimised the release of dust and gas clouds into the open-pit mine atmosphere. At the same time, the borehole utilisation factor (BUF) remained at the standard level 0.92 ± 0.03, which indicated the preservation of the full operability of the charges and the absence of negative phenomena in the form of "bootlegs". The economic feasibility of such an approach was justified by the fact that the additional costs for the shells themselves were statistically insignificant compared to the large-scale (by 33.3%) reduction in direct costs for drilling operations and the savings in tool life (Fig. 4).

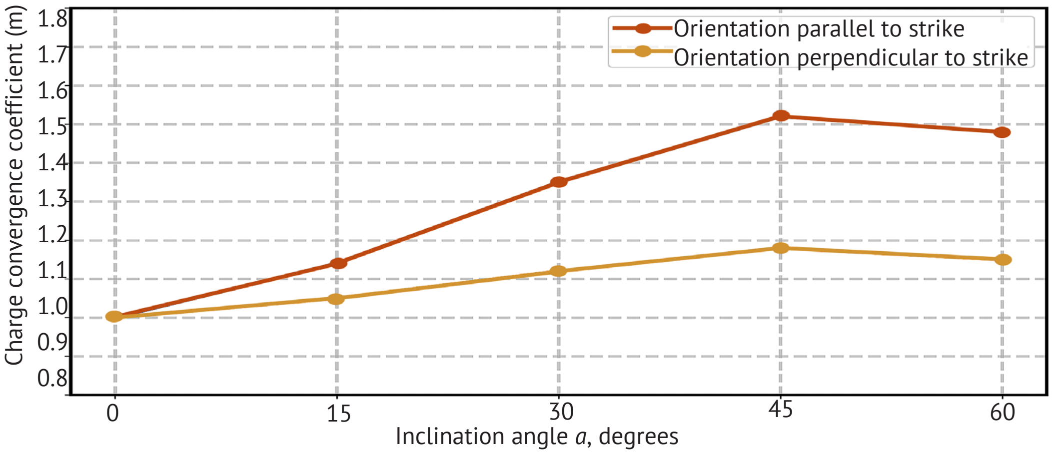

Figure 4. Empirical dependencies of the change in the charge spacing ratio (*m*) on the inclination angle (α) under the condition of jet orientation along (parallel) and across (perpendicular) the main fracture system of the rock mass

Source: developed by the authors

As reflected in Fig. 4, the maximum expansion of the borehole pattern was achieved exclusively under the condition of combined spatial orientation: an inclination angle of 45° with the simultaneous azimuthal direction of the shaped cavity parallel to the strike of the dominant crack system. In the case of directing the charge across the strike (perpendicularly), the increase in the coefficient *m* was levelled by the effect of energy shielding by open cracks. Due to the difference in acoustic impedance at the "rock – air or water-filled crack gap" boundary, a significant part of the compression wave energy was reflected in the form of a tensile wave, preventing the further propagation of the main crack in the specified direction. Under such conditions, the coefficient *m* reached an asymptotic maximum at the level of 1.18 ± 0.05. The obtained empirical dependencies $a = f(\alpha, \beta)$ and $W = f(\alpha)$ were a direct basis for the development of engineering nomograms. The process of practical utilisation of the results was envisaged as follows: relying on the data from the surveying and geological mapping of the structural blocks of the rock mass, the dominant azimuth of fracturing was determined. Furthermore, using nomograms, the spatial orientation of ESCs was established, which allowed maximising the destruction zone. At the final stage, the adjusted values of the distance between the boreholes and the line of least resistance were determined. Thus, designers under the conditions of the Kryvyi Rih basin open-pit mines received a substantiated toolkit for determining the optimal parameters of drilling and blasting operations, taking into account the structural and textural features of the local area.

Discussion

The physical understanding of the processes of targeted rock destruction using ESCs was significantly deepened by the obtained results, and conceptually new approaches to the design of drilling and blasting operations (DBO) were substantiated. A deep physical and mechanical explanation, associated with the focusing of liner elements and explosion products, was found for the identified increase in the radii of intensive fragmentation (R_d) and radial cracks (R_c) with an increase in the cavity inclination angle α to 45° with subsequent saturation of the effect. A study conducted by Z. Sun *et al.* (2024) was dedicated to the directed destruction of rocks using various liner materials and elongated slotted cavities. It was concluded by the authors that the application of such cavities allowed significantly reducing explosive energy losses on viscous destruction, which fully aligned with the identified 45% reduction of the plastic deformation zone radius in the hydrodynamic model. Furthermore, according to K.S. Ishchenko (2023), who investigated the blast parameters of charges with cavities of different cross-sectional shapes in the field of tensile stresses, it was established that the reduction of the peak pressure of detonation gases on the borehole walls in non-working directions prevented the transformation of rock into dust.

When comparing the obtained results regarding the mechanism of ESC action with the data dominating in modern literature, significant differences were observed. In particular, directed rock destruction using shaped charges with combined liners of various shapes was investigated by K. Liu *et al.* (2023), and it was pointed out that exactly the geometry of the shaped liner played a determining role in the formation of the shaped charge jet. In contrast to this, it was proven by the obtained results that for the conditions of mass blasts, not only the shape but also the density of the liner material was of critical importance. Since the use of expensive metals was economically unfeasible, the application of iron (pipe fragments) or aluminium allowed forming a high-speed "metal-gas-dynamic blade" that effectively cut through the rock.

The technological advantages of the proposed approach were emphasised by comparing the obtained results with modern methods of directed rock mass destruction. It was indicated by the results that the parallel orientation of the shaped cut to the crack system formed a sharply elongated elliptical destruction zone with a maximum energy utilisation factor ($\eta = 0.86$). During the research, it was established that the complex geometry of the open bench created exceptionally favourable conditions for the reflection of stress waves: the orientation of the shaped cavity strictly parallel to the line of least resistance maximised the synergetic effect of the interference of the direct compression wave and the oncoming unloading wave. Additionally, the mathematical and mechanical impact of the detonator's location on the bench blasting indicators was investigated by Q. Gao *et al*. (2020), and it was concluded that the optimisation of the initiation point was a critical factor in improving rock fragmentation quality due to the redistribution of stress wave directions. Also, a numerical study of an innovative shaped charge approach to rock destruction was conducted by Y. Yao *et al*. (2021), and a significant influence of microsecond delay intervals on the nature of crack formation was revealed, which confirmed the importance of the temporal and spatial positioning of charges.

The indisputable efficiency of the combined approach, where the solution of the mathematical programming problem ensured the transition from micro-models of destruction to open-pit macroparameters, was proven by an in-depth analysis of the obtained results. It was clearly demonstrated by the formulation of the nonlinear programming model with the objective function of reduced costs that the relationship between the direction of explosive energy and the pattern parameters could not be selected empirically without violating the system of technological constraints. It was mathematically proven by a detailed analysis of Lagrange multipliers that traditional technologies operated on the verge of acceptable fragmentation quality, whereas spatial energy control expanded this limit. Mathematical strictness in finding the parameters of the highest economic efficiency was provided by the use of gradient methods (Generalised Reduced Gradient – GRG) for problems of this class. In particular, according to M.N. Nawaz *et al*. (2022), the high efficiency and stability of the GRG method were proven in minimising costs under complex engineering and geological conditions. Also, the GRG method was applied for the approximation of dynamic coefficients in studies by H. Hasanudin *et al*. (2023), and its convergence was mathematically confirmed when searching for parameters in multifactorial models of a nonlinear nature.

The proven possibility of radical optimisation of the borehole pattern was the main result of such controlled formation of the destruction zone. The 18-22% increase in the pattern parameters obtained by the algorithm (в distance a increased to 7.0 ± 0.4 m at $W = 4.6 \pm 0.3$ m) fully confirmed the conclusions of international studies conducted by K. Bedri *et al*. (2023). Fragmentation during the blasting of fractured rock masses was analysed, and it was concluded that the spatial optimisation of drilling directions and pattern parameters allowed significantly reducing the total volume of drilling operations. However, as evidenced by the analysis of active constraints in the GRG algorithm, an extremely high sensitivity of the objective function to the charge installation angle was revealed: a deviation of more than 15 degrees from the optimal vector instantly activated the constraint on the ore fragment size, blocking the pattern expansion. This mathematical phenomenon was identical to the technological obstacles identified by J. Guo *et al*. (2024). The forecasting and optimisation of blasting parameters in open-pit mining operations using intelligent algorithms were investigated, and it was concluded that the failure to maintain charge positioning accuracy led to the instantaneous violation of technological constraints regarding the size of ore fragments. Shaped charge blasting technology for directed destruction was also studied by Q. Zhang *et al*. (2021), and it was found that this method provided high contouring accuracy and minimisation of explosive energy deviations, which confirmed the necessity of strict spatial control. Nevertheless, clear physical limitations were also revealed by the comparative analysis. The identified effect of rigid shielding when orienting the cavity across the cracks (spacing ratio $m \leqslant 1.18$) was consistent with classical results in the field of wave dynamics. Due to the sharp discrepancy in acoustic impedances at the "rock – empty crack" media boundary, the majority of the energy was reflected back into the rock mass, which made the artificial formation of an ellipse and pattern expansion under such conditions impossible.

When comparing the obtained results with the results of authors who investigated the optimisation of DBO in the Kryvyi Rih basin, a fundamental difference was observed. In particular, the experimental application of new materials and the variability of drilling and blasting parameters in a Kryvbas open-pit mine were studied by H. Yeremenko *et al*. (2022), and the focus was placed on the technological aspects of increasing blast efficiency. A methodology for the rapid determination of flyrock distance to ensure the safety of blasting operations was developed by Ye.O. Nesmashnyi *et al*. (2022). By comparing these works, it could be noted that none of the cited studies considered an integrated approach based on the synergy of mathematical programming, natural fracturing of the rock mass, and the shaped charge effect as a basis for the structural transformation of the pattern. In addition to the direct comparison of parameters, the 33.3% reduction in specific drilling costs without deterioration in fragmentation quality confirmed the conclusions published by O. Tverda *et al*. (2021). Resource-efficient and environmentally safe charge designs were proposed, and it was concluded that the implementation of such solutions proportionally reduced the technogenic load on the environment.

An in-depth analysis of scientific literature demonstrated that despite a significant number of publications dedicated to directed destruction and numerical optimisation methods, the majority of researchers analysed these issues in isolation. In particular, insufficient attention was paid to the mathematical modelling of conditions under which spatial control of explosive energy was directly integrated into borehole pattern parameters through nonlinear programming, taking into account the anisotropy of natural fracturing. Classical DBO design methods remained predominantly empirical, whereas existing nonlinear programming models did not account for the geodynamic influence of the shape and orientation of the shaped cavity on the elliptical destruction zone in hard ferruginous quartzites. Exactly these aspects of the topic, to which insufficient attention was paid by researchers in the analysed works, served as the motivation and direct impetus for conducting this study. Summarising, the comparison of the obtained results with research data proved that the integration of computational algorithms of nonlinear programming with the controlled spatial orientation of ESCs was a highly effective tool for DBO design. The empirical limitations of classical methodologies were overcome by the proposed combined approach, ensuring a mathematically rigorous and economically justified expansion of the borehole pattern.

Conclusions

As a result of the conducted research and computer modelling, the patterns of the influence of the spatial orientation of elongated shaped charges on the geometric parameters of the borehole pattern under the complex conditions of the Kryvyi Rih basin were established. It was proven that the development of the intensive fragmentation zones (R_d) and radial cracks (R_c) possessed a nonlinear dependence on the rotation angle of the shaped cavity (α) around the longitudinal axis of the borehole relative to the bench plane and the natural fracturing of the rock mass. Geomechanically, this was expressed in the formation of a destruction ellipse, where the change in the angle determined the orientation of its major axis, influencing the ratio between the distance in a row and the line of least resistance. The effect of structural "saturation" was confirmed by the analysis of variance (ANOVA): the rotation angle was optimal, at which a "gas-dynamic wedge" was formed, which most effectively opened the planes of weakness. A further increase in the angle (over 45°) did not provide a significant increase in the destruction zones, but only intensified local rock overcrushing and caused an irrational dissipation of wave energy.

The established patterns of energy redistribution substantiated the transition from square or triangular patterns to elongated rectangular or rhombic spatial structures, where the destruction zones of adjacent charges intersected at the boundary of elastic deformations, preventing the formation of intact rock pillars. Directing the shaped charge jet parallel to the strike of the main cracks (angle 45°) allowed increasing the distance between boreholes a to 7.0 ± 0.4 to m with an increase in the spacing ratio to 1.52 due to the superposition of oncoming stress waves. Conversely, the orientation of the charge across the strike caused acoustic energy shielding. Due to the difference in acoustic impedance at the "rock – crack" boundary, the compression wave was reflected in the form of a tensile wave back into the rock mass, which blocked the development of the destruction ellipse and limited the marginal spacing ratio at the level of 1.18. The prospects for further research consisted in the adaptation of optimisation algorithms for rocks with other physical and mechanical properties and types of anisotropy in the Kryvyi Rih basin. In particular, the behaviour of plastic rocks and rock masses with chaotic fracturing, where wave shielding was subject to other patterns, required investigation. A separate relevant direction was the investigation of the impact of the spatial orientation of charges under the conditions of multi-row short-delay blasting, where the interference of stress waves from the expanded borehole pattern would require the design of new initiation sequences and the adjustment of drilling and blasting parameters.

Acknowledgements

None.

Funding

None.

Conflict of Interest

None.

References

[1] Andrieiev, B., Brovko, D., Kononenko, V., Khvorost, V., & Haponenko, K. (2026). Analysis of physical processes in elongated shaped charges during rock mass destruction in iron ore quarries. *IOP Conference Series: Earth and Environmental Science*, 1630(1), article number 012015. doi: 10.1088/1755-1315/1630/1/012015.

[2] Bedri, K., Ould Hamou, M., Filali, M., Hadji, R., & Taib, H. (2023). Optimizing the blast fragmentation quality of discontinuous rock mass: Case study of Jebel Bouzegza Open-Cast Mine, North Algeria. *Mining of Mineral Deposits*, 17(4), 35-44. doi: 10.33271/mining17.04.035.

[3] Bhagat, N.K., *et al.* (2020). Innovative directional controlled blasting technique for excavation of unstable slopes along a busy transportation route: A case study of Konkan Railway in India. *Mining, Metallurgy & Exploration*, 37(3), 833-850. doi: 10.1007/s42461-020-00212-x.

[4] Gao, Q., Leng, Z., Yang, R., Wang, Y., Chen, M., Sun, P., & Luo, S. (2020). Mathematical and mechanical analysis of the effect of detonator location and its improvement in bench blasting. *Advances in Civil Engineering*, 2020, article number 6058086. doi: 10.1155/2020/6058086.

[5] Guo, J., Zhao, Z., Zhao, P., & Chen, J. (2024). Prediction and optimization of open-pit mine blasting based on intelligent algorithms. *Applied Sciences*, 14(13), article number 5609. doi: 10.3390/app14135609.

[6] Hasanudin, H., Zubaydi, A., & Aryawan, W.D. (2023). Roll dynamic coefficients approach of decay test using the generalized reduced gradient method (GRG). *Journal of Applied Engineering Science*, 21(2), 470-480. doi: 10.5937/jaes0-40421.

[7] Ishchenko, K.S. (2023). Study on explosion in different cross-sectional shape charge cavity in tensile stress field. *Scientific Bulletin of National Mining* University, 3, 32-38. doi: 10.33271/nvngu/20233/032.

[8] Li, X., Zhang, Q.B., He, L., & Zhao, J. (2017). Particle-based numerical manifold method to model dynamic fracture process in rock blasting. *International Journal of Geomechanics*, 17(5). doi: 10.1061/(ASCE)GM.1943-5622.0000748.

[9] Liu, D., Gu, Y., Sun, F., Li, F., Chen, S., & Liu, Q. (2023). Directional splitting mechanism of rock based on shaped charge jet. *Explosion and Shock Waves*, 43(8), article nimber 083303. doi: 10.11883/bzycj-2022-0496.

[10] Liu, K., Zhang, Y., Hou, T., Miao, Y., Zhao, X., & Zhang, M. (2023). Directional rock blasting using shaped charges using combined charge liners with different shapes. *Energy Science & Engineering*, 11(11), 4381-4393. doi: 10.1002/ese3.1587.

[11] Nawaz, M.N., Ali, A.S., Jaffar, S.T.A., Jafri, T.H., On, T.-M., Abdallah, M., Karam, S., & Azab, M. (2022). Cost-based optimization of isolated footing in cohesive soils using generalized reduced gradient method. *Buildings*, 12(10), article number 1646. doi: 10.3390/buildings12101646.

[12] Nesmashnyi, Ye.O., Tkachenko, H.I., & Mykhailenko, M.V. (2022). Operational determination of the rock fragments fly distance during mass blasts at the Kryvbas quarries. *Mining Journal*, 110, 161-168. doi: 10.31721/2306-5435-2022-1-110-161-168.

[13] Pan, C., Xie, L., Li, X., Liu, K., Gao, P., & Tian, L. (2022). Numerical investigation of effect of eccentric decoupled charge structure on blasting-induced rock damage. *Journal of Central South University*, 29, 663-679. doi: 10.1007/s11771-022-4947-3.

[14] Sun, Z., Li, X., Wang, Y., Chen, J., & Zhang, Y. (2024). Research on directional rock blasting based on different slotted pipe materials of the combined charge structure. *PLoS One*, 19(3), article number e0299614. doi: 10.1038/s41598-024-57957-4.

[15] Tverda, O., Kofanova, O., Repin, M., Kofanov, O., Tkachuk, K., Guts, N., & Cabana, E. (2021). A resource efficient and environmentally safe charge structure for mining in an open-pit. *Mining of Mineral Deposits*,15(4), 84-91. doi: 10.33271/mining15.04.084.

[16] Wang, Y. (2017). Study of the dynamic fracture effect using slotted cartridge decoupling charge blasting. *International Journal of Rock Mechanics and Mining Sciences*, 96, 34-46. doi: 10.1016/j.ijrmms.2017.04.015.

[17] Xu, P., Zhao, Y., & Yang, Z. (2024). Research on the crack formation mechanism of shaped charge blasting and the new dual-shaped charge blasting technology. *Mechanics of Advanced Materials and Structures*, 32(3), 374-390. doi: 10.1080/15376494.2024.2346810.

[18] Yao, Y., Sun, Q., Zou, B., & Mu, Q. (2021). Numerical study on an innovative shaped charge approach of rock blasting and the timing sequence effect in microsecond magnitude. *Rock Mechanics and Rock Engineering*, 54(9), 4523-4542. doi: 10.1007/s00603-021-02516-w.

[19] Yeremenko, H., Titov, D., Henkulenko, S., Zahorskyi, D., & Strilets, O. (2022). Experimental studies on the use of new materials and variability of drilling and blasting parameters at the "Pivdennyi" quarry of "Rudomain" LLC. *Mining Journal*, 56(1), 22-26. doi: 10.31721/2306-5435-2022-1-110-22-27.

[20] Zhang, Q., Wang, J., Guo, S., Gong, W., Feng, L., Wang, H., Ming, C., & Ma, Z. (2021). Shaped charge hydraulic blasting: An environmental, safe, and economical method of directional roof cutting. *Shock and Vibration*, 2021, article number 5511081. doi: 10.1155/2021/5511081

Вплив орієнтації подовжених кумулятивних зарядів на проектування оптимальної сітки свердловин для умов Криворізького басейну

Дмитро Бровко

Доктор технічних наук, професор
Криворізький національний університет
50027, вул. Віталія Матусевича, 11, м. Кривий Ріг, Україна
https://orcid.org/0000-0001-9108-3857

Володимир Кононенко

Кандидат технічних наук, доцент
Криворізький національний університет
50027, вул. Віталія Матусевича, 11, м. Кривий Ріг, Україна
https://orcid.org/0000-0002-5993-4268

Василій Хворост

Кандидат технічних наук, доцент
Криворізький національний університет
50027, вул. Віталія Матусевича, 11, м. Кривий Ріг, Україна
https://orcid.org/0000-0002-9205-7797

Костянтин Гапоненко

Аспірант
Криворізький національний університет
50027, вул. Віталія Матусевича, 11, м. Кривий Ріг, Україна
https://orcid.org/0009-0009-2068-9945

Анотація. Актуальність дослідження зумовлена необхідністю підвищення ефективності буровибухових робіт на залізорудних кар'єрах Криворізького басейну шляхом застосування подовжених кумулятивних зарядів, просторово адаптованих до структурних особливостей гірських порід задля оптимізації параметрів сітки свердловин. Метою роботи було встановлення закономірностей впливу просторової орієнтації подовжених кумулятивних зарядів на геометричні параметри сітки свердловин та розробка інженерних рекомендацій щодо її оптимального проектування в складних гірничо-геологічних умовах відкритого видобутку. Методи аналізу базувались на комплексному підході, що поєднує чисельне моделювання хвильової динаміки суцільних середовищ із використанням моделей поведінки матеріалів, математичне нелінійне програмування за алгоритмом узагальненого зведеного градієнта. Отримані результати доводять нелінійну залежність розмірів зон інтенсивного дроблення від кута повороту кумулятивної виїмки. Статистично підтверджено, що оптимальним є кут 45° за умови орієнтації струменя паралельно до простягання магістральних тріщин. Це дозволяє сформувати видовжену еліптичну зону руйнування та перейти від квадратних сіток до прямокутних просторових структур. Встановлено, що така конфігурація дозволяє збільшити відстань між свердловинами до 7 м і досягти коефіцієнта зближення зарядів на рівні 1,52. Водночас орієнтація заряду перпендикулярно до тріщин викликає ефект акустичного екранування енергії, що обмежує розширення сітки. Практична цінність досліджень полягає у розробці диференційованої методології просторового позиціонування вибухових зарядів у залізистих кварцитах. Впровадження запропонованих оптимізованих параметрів сітки свердловин забезпечує зниження питомих витрат на буріння на 33 % без погіршення якості дроблення. Це суттєво зменшує знос бурового інструменту, скорочує тривалість підготовчого циклу та пропорційно знижує екологічне навантаження на довкілля через зменшення обсягів пилогазових викидів

Ключові слова: кумулятивна виїмка; руйнування залізистих кварцитів; моделювання динаміки; зближення свердловин; буровибухові роботи

Journal of Kryvyi Rih National University
Journal homepage: https://journal-knu.com.ua/en
Article's History: Received: 21.08.2025 Revised: 25.02.2026 Accepted: 28.04.2026 Published: 29.05.2026
Vol. 24, No. 1, 2026
ISSN 2306-5451
e-ISSN 2519-2736

UDC 004.93:004.8:355.40
DOI: 10.31721/2306-5451-2026-1-24-107-119

Application of computer vision for target detection in multi-level military reconnaissance systems: Literature review

Denys Berkovskyi *

Postgraduate Student
National Aerospace University "Kharkiv Aviation Institute"
61000, 17 Vadym Manko Str., Kharkiv, Ukraine
https://orcid.org/0009-0004-0625-2839

Alina Artomova

PhD in Technical Sciences, Associate Professor
National Aerospace University "Kharkiv Aviation Institute"
61000, 17 Vadym Manko Str., Kharkiv, Ukraine
https://orcid.org/0000-0002-6761-2066

Abstract. The purpose of the research was to analyse modern computer vision methods for automatic detection and classification of targets in multi-level military intelligence systems, as well as to evaluate the effectiveness of deep learning algorithms in processing intelligence data under various observation conditions. To achieve this goal, the approach integrated a systematic literature review, the modelling of image processing architectures, and a comparative evaluation of neural network-based object detection models. Findings indicated that the deployment of state-of-the-art deep learning architectures specifically convolutional neural networks, YOLO (You Only Look Once) variants, and transformer-based models substantially improves the accuracy and robustness of automated military object detection in imagery acquired from unmanned aerial vehicles and satellite sources. Moreover, combining data from multiple sensors with multimodal processing techniques enhanced target recognition capabilities, particularly in scenarios characterised by low visibility, complex scene composition, or partial object occlusion. A comparative analysis of modern architectures has shown that the YOLO family models provide the best processing speed and are most suitable for real-time application on board unmanned aerial vehicles, while Faster Region-based Convolutional Neural Network demonstrates higher localisation accuracy for complex and small-sized objects, but requires higher computational costs. Convolutional neural network architectures provide a balanced ratio between accuracy and performance, while transformer-based models work more effectively in difficult observation conditions, in particular, with low spatial resolution, noise, partial overlap and masking of objects, but their use is accompanied by increased requirements for computational resources. In general, a compromise has been established between detection accuracy, processing speed and computational complexity of the models, which determines the feasibility of their application depending on the characteristics of the reconnaissance platform and the conditions for performing the task. Information was provided on the development of intelligent systems for automated analysis of intelligence data

Keywords: deep learning; computer vision; object detection; multisensory data fusion; real-time analysis; unmanned aerial vehicle

Suggested Citation:
Berkovskyi, D., & Artomova, A. (2026). Application of computer vision for target detection in multi-level military reconnaissance systems: Literature review. *Journal of Kryvyi Rih National University*, 24(1), 107-119. doi: 10.31721/2306-5451-2026-1-24-107-119.

Copyright © The Author(s). This is an open access article distributed under the terms of the Creative Commons Attribution License 4.0 (https://creativecommons.org/licenses/by/4.0/)

**Corresponding author (d.s.berkovskyi@khai.edu)*

Introduction

The effectiveness of reconnaissance in current military operations is contingent upon the rapid acquisition, processing, and interpretation of substantial volumes of diverse data originating from multiple sources. The escalating complexity of the battlefield environment, the extensive deployment of unmanned aerial systems, and the expanding volume of visual intelligence have notably impeded the timely identification of military targets. Conventional manual analysis methods are now inadequate to meet the requisite speed and accuracy for decision-making, thereby necessitating the adoption of automated approaches capable of processing reconnaissance data in near real time. Within this domain, computer vision and deep learning technologies have emerged as particularly promising due to their inherent capacity for object detection, classification, and tracking under demanding operational conditions.

Researchers N. Habash *et al*. (2025) noted that in contemporary combat settings, the prompt and accurate acquisition of information regarding the location, movement, and attributes of enemy assets is essential. Intelligence systems serve as the foundation of this process, typically integrating various components such as satellite observation platforms, unmanned aerial vehicles (UAVs), ground-based sensor arrays, and analytical centres responsible for processing and interpreting the collected data. According to W. Zhu & K. Chen (2026), the rapid advancement of digital technologies has led to a substantial increase in reconnaissance data volume, rendering manual analysis more challenging and time-intensive. The researchers emphasised that automated image and video analysis through computer vision techniques presents a viable solution to this problem. Similarly, researchers K. Elgamily *et al*. (2025) concluded that these methods can markedly enhance the efficiency of detecting and identifying military targets, particularly in aerial reconnaissance systems where large quantities of imagery require continuous and rapid assessment. Researchers C. Lee *et al*. (2024) demonstrated that deep learning algorithms have achieved notable success in object detection across diverse imagery types. Furthermore, researchers W. Hua & Q. Chen (2025) reported that contemporary neural network architectures are capable of identifying various military equipment classes even under conditions of image noise, low resolution, or complex backgrounds. These findings highlight the suitability of deep learning approaches for reconnaissance-related applications.

Researchers S. Mei *et al*. (2024) emphasised that the deployment of UAVs has become a key development in modern reconnaissance systems because they facilitate the collection of extensive visual data from operational zones, which can subsequently be analysed automatically by neural networks. In addition, researchers R. Sairam *et al*. (2023) concluded that this integration not only improves target detection accuracy but also reduces the cognitive load on human operators. Similarly, researchers V. Makarichev *et al*. (2025) investigated the influence of image noise on the performance of YOLO-based object detection in UAV imagery. The authors concluded that the application of modern denoising methods significantly improves localisation and classification accuracy, confirming the importance of image pre-processing for reliable computer vision deployment in practical reconnaissance systems. According to researchers Y. Wu & K. Tong (2025), current reconnaissance frameworks increasingly emphasise data fusion from multiple modalities, including optical imagery, infrared sensors, and radar systems. At the same time, researchers J. Leng *et al*. (2024) identified several persistent challenges, including the reliable detection of small objects, recognition of camouflaged equipment, adaptation to changing weather conditions, and limitations imposed by restricted onboard computational resources.

Despite advancements in military reconnaissance utilising computer vision, current research predominantly concentrates on the performance of isolated algorithms or specific use cases. A comprehensive evaluation of computer vision techniques within integrated military reconnaissance systems, which must account for diverse data sources, operational limitations, and varied mission demands, has received less attention. Moreover, comparative analyses of contemporary deep learning models under standardised evaluation metrics are infrequent. These shortcomings underscore the need for a thorough review and comparative assessment of existing methodologies. This study therefore sought to evaluate computer vision techniques for target detection in hierarchical military reconnaissance systems and to identify robust algorithms for the automated interpretation of reconnaissance imagery. To accomplish this purpose, a systematic literature review was undertaken to identify, analyse, and synthesise current research on computer vision applications in military reconnaissance. Relevant publications published primarily between 2021 and 2026 were sourced from the Web of Science, Scopus, IEEE Xplore, SpringerLink, and ScienceDirect databases. The literature search was performed using combinations of keywords including "computer vision", "deep learning", "object detection", "UAV", "remote sensing", "small object detection", "multisensory data fusion", "You Only Look Once (YOLO) models", "convolutional neural networks (CNN)".

Complementing the systematic literature review, comparative evaluation and modelling methodologies were employed to assess the suitability of current computer vision models for reconnaissance tasks. The comparative analysis encompassed metrics such as detection accuracy, precision, recall, F1-score, inference speed, computational complexity, resilience to environmental variations, and applicability for deployment on resource-limited UAV platforms. The quantitative values presented in Table 2 were derived from representative results reported in the reviewed studies and correspond to object detection performance evaluated using standard benchmark datasets and commonly reported metrics, primarily mean Average Precision (mAP). The qualitative ratings used in Table 2 for localisation quality, small object detection capability, and computational complexity were assigned based on a comparative analysis of the reviewed publications. localisation quality and small object detection capability reflect the reported detection performance of the models under challenging conditions, whereas computational complexity was determined according to the computational resources required for model inference, including model size, memory consumption, and processing speed on embedded and edge computing platforms. Conceptual architectural modelling was utilised to generalise identified approaches and evaluate their potential integration into hierarchical military reconnaissance systems. The functional levels of the model were distinguished according to the sequential stages of reconnaissance data processing and the functional responsibilities of system components, including data acquisition, transmission, preprocessing, intelligent analysis, data integration, and decision support, facilitating the development of recommendations for selecting computer vision techniques for automated reconnaissance image interpretation.

Features of Integrating Computer Vision Algorithms into Multi-Level Military Intelligence Systems

Multi-level military reconnaissance systems are designed to collect, process, and distribute information obtained from heterogeneous intelligence assets operating at different observation levels. Their effectiveness depends not only on the capabilities of individual reconnaissance platforms but also on the coordinated interaction between them. The integration of computer vision technologies has become one of the key factors enabling automated processing of large volumes of reconnaissance imagery and supporting timely operational decision-making within hierarchical intelligence architectures. According to researchers X. Bian & J. Ma (2025), multi-level military reconnaissance systems constitute complex information and analytical infrastructures. Similarly, researchers M. Soeleman *et al.* (2023) noted that these systems integrate various platforms for data collection, transmission, processing, and analysis. As shown in the work of researchers M. Vasishta *et al.* (2024), reconnaissance systems generally operate across several observational tiers, including space-based, aerial, and ground components, each characterised by different technical capabilities and operational constraints. Researchers Y. Yu & F. Da (2023) further emphasised that every level provides unique information sources, making effective integration a fundamental requirement for successful intelligence operations.

As noted by researchers Y. Yu & F. Da (2023), the growing volume of reconnaissance data has increased the importance of computer vision algorithms for automated information processing. One of the distinguishing characteristics of hierarchical reconnaissance architectures is the simultaneous use of multiple sensor types, including optical cameras, infrared sensors, radar systems, thermal imagers, and other observation devices. According to researchers L. Ramos & A. Sappa (2025), these sensors generate heterogeneous data with different spatial resolutions, noise characteristics, and acquisition frequencies. Consequently, computer vision algorithms must support multimodal data fusion while ensuring temporal and spatial consistency between information obtained from different reconnaissance platforms. The integration process typically begins with synchronising incoming data streams in both time and geographic coordinates. Satellite imagery usually provides strategic coverage over extensive areas, whereas UAVs supply high-resolution observations of selected regions, and ground-based sensors deliver detailed local information. Before computer vision algorithms are applied, these heterogeneous datasets require preprocessing, including geometric correction, coordinate transformation, temporal synchronisation, and sensor calibration. Such preprocessing enables data acquired from different sources to be represented within a unified reference framework, thereby improving the reliability of subsequent object detection and target tracking.

The location of data processing depends on operational requirements and available computational resources. According to L. Ramos & A. Sappa (2025), UAV platforms frequently perform preliminary image processing onboard to reduce communication latency and bandwidth consumption. Such onboard processing generally includes image enhancement, object localisation, and preliminary target classification using lightweight neural network models. More computationally demanding computer vision tasks are subsequently executed at edge-computing nodes deployed close to operational areas or within centralised intelligence processing centres, where more powerful computing resources allow comprehensive analysis, multisensory fusion, and long-term data storage. This distributed processing architecture balances real-time responsiveness with analytical accuracy. Computer vision techniques are extensively utilised for processing large reconnaissance data streams under near real-time conditions. As noted by L. Ramos & A. Sappa (2025), modern unmanned aerial vehicles continuously transmit high-resolution video requiring immediate analysis to identify potential threats. Researchers J. Leng *et al.* (2024) concluded that conventional image processing methods often struggle under dynamic battlefield conditions, whereas researchers J. Kang *et al.* (2022) demonstrated that deep learning approaches significantly improve both robustness and detection accuracy. Unlike traditional algorithms relying on manually engineered features, CNN automatically learn discriminative visual representations from training data.

J. Kang *et al*. (2022) also emphasised that effective interaction between reconnaissance levels represents one of the principal challenges of hierarchical intelligence systems. Satellite platforms provide extensive geographic coverage but update observations relatively infrequently. In contrast, UAVs deliver high-resolution imagery with greater temporal frequency while remaining constrained by flight endurance and operational range. Ground-based sensors complement these platforms by supplying highly detailed observations within local monitoring zones. Rather than competing, these platforms provide mutually complementary information, making data fusion an essential component of modern reconnaissance architectures. According to researchers Z. Li *et al*. (2022), computer vision algorithms play a central role in integrating information obtained from multiple reconnaissance platforms. Their functions include automated object detection, target classification, localisation, tracking, and feature extraction. The processed results are subsequently transmitted to intelligence management and decision-support systems, where they are combined with operational databases and additional intelligence sources. Decision-support systems utilise these outputs to generate alerts, prioritise detected objects, update the operational picture, and assist analysts and commanders during mission planning and execution.

As shown in the work of Z. Li *et al*. (2022), object detection remains one of the principal computer vision tasks within reconnaissance systems. The researchers classified modern object detection approaches into two-stage and single-stage architectures. Similarly, researchers Z. Cao *et al*. (2023) compared these approaches and concluded that two-stage models, such as Faster R-CNN, generally achieve higher detection accuracy, whereas single-stage models, including the YOLO and SSD families, offer considerably faster inference suitable for real-time aerial reconnaissance. Together, these studies demonstrate that selecting an appropriate detection architecture depends on the balance between computational efficiency and recognition performance required for a particular operational scenario. Researchers have also investigated computer vision performance under adverse observation conditions. Z. Cao *et al*. (2023) reported that low illumination, atmospheric interference, cluttered backgrounds, camouflage, and varying viewing angles significantly complicate target recognition. In agreement with these findings, researchers S. Paheding *et al*. (2024) demonstrated that deep learning models outperform traditional image processing techniques because they learn complex visual representations capable of generalising across challenging environments.

N. Habash *et al*. (2025) further identified small-object detection as one of the major challenges in reconnaissance imagery, particularly when vehicles, artillery systems, or military infrastructure occupy only a limited number of pixels. To address this limitation, the researchers proposed combining multi-scale feature extraction with specialised neural network architectures optimised for detecting small targets. These findings complement the work of Z. Cao *et al*. (2023), who likewise emphasised the importance of adapting detection models to operational battlefield conditions. Another important research direction concerns multimodal data fusion. According to N. Habash *et al*. (2025), combining observations obtained from different sensor modalities provides a more complete representation of the operational environment than relying on a single information source. Similarly, researchers T. Mouatassim *et al*. (2026) concluded that integrating optical, infrared, and radar imagery substantially improves target detection under night time conditions and limited visibility, where individual sensor types may exhibit reduced performance.

T. Mouatassim *et al*. (2026) additionally emphasised the necessity of optimising computer vision algorithms for deployment on resource-constrained reconnaissance platforms. Because UAVs possess limited computational power and energy reserves, researchers have investigated techniques including parameter quantisation, neural network compression, and hardware acceleration to enable efficient onboard inference without significantly degrading detection accuracy. The same researchers also highlighted that successful integration of computer vision requires reliable communication infrastructure. Data acquired by satellites, UAVs, and ground sensors must be securely transmitted through distributed communication networks to edge-processing nodes or centralised intelligence centres. After multisensory fusion and computer vision analysis, processed information is disseminated to command-and-control and decision-support systems, where it contributes to operational awareness, scenario modelling, threat prioritisation, and military planning.

Finally, researchers Y. Wu & K. Tong (2025) demonstrated that decision-support systems represent the final stage of the intelligence processing chain. Rather than replacing human analysts, computer vision technologies provide automatically generated situational information that accelerates decision-making while reducing operator workload. Overall, the reviewed studies consistently indicate that integrating computer vision into multi-level military reconnaissance systems extends beyond the application of object detection algorithms alone. It encompasses coordinated temporal and spatial synchronisation of multisensory data, distributed processing across onboard, edge, and centralised computing environments, multimodal information fusion, and seamless transmission of analytical results to decision-support systems. Continued research in these areas is expected to improve the effectiveness, responsiveness, and operational reliability of modern military intelligence architectures.

Deep Learning Methods for Automatic Detection of Military Objects in Reconnaissance Images

Recent advancements in artificial intelligence have substantially broadened the scope of automated visual data processing and analysis. According to researchers S. Gui *et al.* (2024), recent developments in artificial intelligence have significantly expanded the capabilities of automated image interpretation across various application domains. Similarly, researchers A. Jonnalagadda *et al.* (2024) emphasised that deep learning techniques have become one of the principal drivers of this progress. In military reconnaissance, these techniques enable enhanced automated detection, recognition, and classification of various objects within images and video streams, as also demonstrated by researchers V. Afifah (2026). According to A. Jonnalagadda *et al.* (2024), the visual data processed by modern reconnaissance systems originate from diverse platforms, including Earth observation satellites, unmanned aerial vehicles, stationary or mobile surveillance cameras, and other intelligence assets. These platforms continuously generate extensive volumes of visual information requiring efficient automated analysis. In operational military environments, however, image interpretation is further complicated by dynamic battlefield conditions, varying illumination, atmospheric effects, sensor noise, communication delays, electronic interference, and intentional camouflage. Consequently, computer vision algorithms must maintain high detection accuracy while satisfying strict latency requirements necessary for real-time decision-making.

As noted by A. Jonnalagadda *et al.* (2024), deep learning represents a specialised branch of machine learning that utilises multilayer artificial neural networks capable of identifying complex patterns in large datasets without relying on handcrafted feature descriptors. In contrast, N. Al-IQubaydhi *et al.* (2024) explained that traditional computer vision techniques depended primarily on manually engineered visual features, whereas contemporary neural networks automatically learn hierarchical feature representations during training. The researchers concluded that this capability enables deep learning models to perform effectively even under conditions characterised by substantial variations in object appearance, background complexity, and observation geometry.

According to V. Afifah (2026), CNNs remain among the most widely adopted deep learning architectures for image analysis. These networks are specifically designed for processing two-dimensional image data and employ successive convolutional layers to extract visual features with increasing semantic complexity. Their ability to learn discriminative representations has made CNNs particularly suitable for reconnaissance imagery acquired under heterogeneous operational conditions.

Recent research conducted by V. Makarichev *et al.* (2025) demonstrated that applying image pre-filtering and noise mitigation techniques significantly improves the performance of YOLO-family neural networks for vehicle and human localisation and classification in noisy UAV imagery. These findings suggest that detection performance depends not only on the neural network architecture itself but also on image quality and pre-processing procedures preceding inference. According to researchers M. Nikouei *et al.* (2025), neural network architectures used for automatic military object detection are generally divided into two principal categories: two-stage and single-stage detectors. Similarly, researchers E. Kırac & S. Özbek (2024) concluded that although two-stage detectors generally provide higher localisation accuracy, single-stage models offer considerably faster inference, making them particularly suitable for real-time reconnaissance applications where processing latency is critical. Nevertheless, the choice between these approaches depends on mission requirements, since faster processing often comes at the expense of detection accuracy for complex scenes or small targets.

Transformer-based architectures have recently attracted considerable research interest due to their capability to model long-range contextual relationships within images. According to M. Nikouei *et al.* (2025), this characteristic enables improved object detection in complex environments containing background clutter, camouflage, or significant viewpoint variation. However, compared with conventional CNN, transformer-based models generally require substantially greater computational resources, larger training datasets, and increased memory capacity. Consequently, although these architectures may achieve superior performance under certain conditions, their deployment on resource-constrained edge platforms, including onboard UAV computers, remains challenging. Table 1 presents a comparative analysis of deep learning algorithms, including their mathematical models and key computational principles.

Table 1. Comparative analysis of deep learning algorithms

Algorithm	Model type	Core idea	Strengths	Limitations
YOLO (v5/v8)	Single-stage detector	Direct object detection in one pass	Real-time performance, high speed	Lower accuracy for small objects
Faster R-CNN	Two-stage detector	Region proposal + classification	High detection accuracy	Slower processing speed

Table 1. Continued

Algorithm	Model type	Core idea	Strengths	Limitations
SSD	Single-stage detector	Multi-scale feature maps for detection	Good balance speed/ accuracy	Struggles with small objects
CNN (classification)	Feature extractor	Hierarchical feature learning	Strong feature extraction	Not designed for detection alone
Vision Transformer (ViT)	Transformer-based	Attention mechanism for image patches	High accuracy, global context	High computational cost

Source: developed by the author based on research by E. Kırac & S. Özbek (2024), M. Nikouei *et al*. (2025), A. Jonnalagadda *et al*. (2024) and V. Afifah (2026)

As noted by M. Nikouei *et al*. (2025), detecting small objects remains one of the most difficult tasks in automated reconnaissance image analysis. To address this limitation, researchers have proposed multi-scale feature extraction and feature pyramid architectures capable of preserving fine spatial information across multiple image resolutions, as summarised in Table 2. Nevertheless, detection performance is influenced not only by network architecture but also by the availability of high-quality annotated datasets. Small military targets frequently occupy only a limited number of pixels, while inaccurate or incomplete annotations may substantially reduce recognition accuracy even when advanced detection models are employed.

Table 2. The difficulty of detecting small objects

Detection method	Approach type	Working principle	Detection accuracy (%)	Localisation quality	Small object detection capability	Computational complexity
Single-scale detection	Single-scale	Processes the image at a single resolution	68	Low	Low	Low
Multi-scale detection	Multi-scale	Processes the image at multiple resolutions	81	Medium	Medium	Medium
Feature pyramid network	Hierarchical (FPN)	Uses feature pyramids across different scales	89	High	High	Above medium

Notes: detection accuracy values represent representative object detection performance reported in the reviewed studies and are based primarily on the mean Average Precision (mAP) metric evaluated on benchmark datasets for aerial and remote sensing object detection. The qualitative ratings were assigned through a comparative analysis of the reviewed publications, taking into account the ability of each method to accurately determine object positions, reliably detect small and weakly distinguishable targets, and maintain acceptable performance under different computational resource constraints
Source: developed by the author based on research by M. Soeleman *et al*. (2023), A. Jonnalagadda *et al*. (2024) and M. Niouei *et al*. (2025)

Beyond object detection, contemporary image analysis systems increasingly incorporate semantic and instance segmentation techniques. According to researchers Y. Wu & K. Tong (2025), these methods enable precise delineation of object boundaries and are particularly valuable in cluttered operational environments where overlapping or irregularly shaped objects frequently occur. Compared with conventional bounding-box detection, segmentation approaches provide richer spatial information that may improve subsequent target identification and scene understanding. Multisensory data integration has become another important research direction. According to researchers Z. Li *et al*. (2022), combining optical, infrared, and radar imagery enables more reliable target detection under varying operational conditions. Y. Wu & K. Tong (2025) similarly concluded that multimodal fusion enhances system robustness when individual sensors experience degraded performance due to weather conditions, smoke, poor illumination, or intentional concealment. Tracking detected objects across consecutive video frames constitutes another essential task in reconnaissance applications. According to Z. Li *et al*. (2022), following initial object detection, motion estimation and temporal feature propagation improve tracking continuity for moving targets. Y. Wu & K. Tong (2025) further emphasised that temporal analysis significantly reduces false detections while improving target trajectory estimation during prolonged surveillance missions. Military reconnaissance environments frequently involve deliberate countermeasures intended to reduce detection effectiveness, including camouflage, decoys, electronic interference, and rapidly changing operational conditions.

Another active research area concerns optimising neural network deployment on computationally constrained platforms. According to researchers J. Leng *et al*. (2024), techniques including model pruning, parameter quantisation, and lightweight network architectures are commonly applied to reduce computational complexity. However, the researchers also noted that increasing computational efficiency generally introduces trade-offs with recognition accuracy, requiring an appropriate balance between performance and resource consumption depending on operational requirements. Overall, the reviewed studies consistently demonstrate that deep learning techniques have become integral to automated processing of reconnaissance imagery. At the same time, the comparative analysis indicates that no single neural network architecture is universally optimal for all military reconnaissance scenarios. Instead, selecting an appropriate solution requires balancing detection accuracy, computational efficiency, robustness to adverse observation conditions, latency constraints, and compatibility with resource-limited deployment platforms.

Problems and Prospects for the Development of Intelligent Target Recognition Systems in Military Intelligence

Advancements in information technologies and artificial intelligence have opened new avenues for automating various aspects of military reconnaissance. According to researchers L. Ma *et al*. (2019), a key focus within this domain is the development of intelligent target recognition systems designed to autonomously process extensive volumes of visual data and identify objects of potential operational significance. The researchers also noted that, despite notable progress, the practical implementation of these systems within actual military information infrastructures remains constrained by a range of technical, methodological, and organisational challenges. One significant challenge stem from the complexity of the visual environments encountered during reconnaissance missions. As noted by researchers T. Mouatassim *et al*. (2026) and L. Jin *et al*. (2026), unlike many civilian computer vision applications where imaging conditions are relatively controlled, military reconnaissance images are frequently subject to noise, inconsistent illumination, intricate background textures, and atmospheric disturbances. Similarly, researchers G. Chen *et al*. (2022) emphasised that targets of interest may be partially or fully obscured by natural or artificial elements such as foliage, buildings, or camouflage installations.

According to G. Chen *et al*. (2022), the high variability in the visual appearance of military equipment and infrastructure further complicates automatic object recognition. The researchers concluded that an identical target could present substantially different visual features depending on factors such as viewing angle, lighting, sensor distance, or applied camouflage. Consequently, computer vision algorithms must exhibit robust generalisation capabilities to accurately detect objects despite significant deviations from training examples. Another impediment is the scarcity of labelled training data. According to researchers K. Wang *et al*. (2025), deep learning models typically demand large, annotated datasets comprising numerous examples from diverse object categories. However, in the military context, such datasets are often inaccessible due to security and confidentiality constraints. Therefore, the researchers proposed alternative strategies, including the synthesis of training data and the adoption of transfer learning methodologies. As noted by K. Wang *et al*. (2025), transfer learning entails leveraging models pre-trained on extensive publicly available datasets, such as ImageNet or COCO, subsequently fine-tuning them with smaller, domain-specific datasets containing military-relevant imagery. According to the researchers, this approach can mitigate the volume of labelled data required while maintaining satisfactory model performance.

High processing speed constitutes another crucial requirement for reconnaissance systems. According to researchers C. Lee *et al*. (2024), operational scenarios frequently necessitate real-time or near-real-time analysis. For instance, an unmanned aerial vehicle surveying an area may generate continuous video streams at dozens of frames per second, each demanding prompt analysis to reliably detect potential targets. In accordance with researchers J. Leng *et al*. (2024), both algorithmic efficiency and hardware capabilities must therefore meet stringent computational performance standards. To address these demands, researchers S. Johnson *et al*. (2026) reported that substantial efforts have focused on optimising neural networks by reducing parameter counts, designing compact architectures, and employing specialised accelerators such as graphics processing units or neural processing units. The researchers further noted that edge computing paradigms, in which data processing is partially executed onboard reconnaissance platforms rather than relying solely on centralised systems, have gained increasing prominence.

Reliability and robustness also represent critical attributes for computer vision systems in military applications, where misidentification can entail severe consequences. According to S. Johnson *et al*. (2026), recognition systems must sustain high accuracy and dependability under challenging environmental conditions. Similarly, researchers M. Nikouei *et al*. (2025) concluded that multisensory data fusion is one promising technique for enhancing reliability. By integrating data from multiple sensor modalities, such as combining optical imagery with infrared or radar inputs, the system can offset individual sensor limitations and achieve improved detection performance, especially under adverse weather or low-light scenarios. Another promising research direction is the exploration of self-supervised and semi-supervised learning approaches. According to researchers S. Gui *et al*. (2024), these methods enable training on extensive unlabelled image collections alongside limited annotated datasets, thereby expanding the effective training data pool and potentially enhancing model generalisation when labelled data are restricted.

S. Gui *et al.* (2024) also emphasised that integrating intelligent recognition systems into comprehensive military information architectures presents additional challenges. According to the researchers, outputs from computer vision algorithms must be seamlessly incorporated into command-and-control frameworks and decision-support tools, necessitating the development of specialised interfaces that facilitate operator interaction with detected object information for informed operational decision-making. In the same study, S. Gui *et al.* (2024) further highlighted that the technologies supporting big data processing and distributed computing play a vital role, since modern reconnaissance infrastructures may aggregate data from numerous observation sources concurrently, requiring software and hardware platforms capable of scalable, high-performance processing.

The development of autonomous reconnaissance systems that operate with limited human oversight is also gaining attention. As noted by S. Gui *et al.* (2024), in such systems, computer vision algorithms contribute not only to object detection but also to navigation, route planning, and tactical decision processes. Looking ahead, S. Gui *et al.* (2024) suggested that continued progress in artificial intelligence is expected to further enhance automated reconnaissance data analysis. The researchers identified the design of next-generation neural network architectures, multimodal data processing techniques, and the advancement of explainable AI systems capable of providing transparent and interpretable rationale for their outputs as particularly promising research directions. In summary, computer vision-based intelligent target recognition systems hold substantial promise for augmenting the effectiveness of military reconnaissance operations. While technical challenges persist, ongoing advancements in AI methodologies, computational resources, and data processing algorithms are progressively fostering conditions conducive to the broader adoption of these systems within contemporary military information infrastructures.

Architecture of an Intelligent Intelligence Image Processing System in Multi-Level Intelligence Complexes

The effective application of computer vision techniques in military intelligence largely depends on the proper design of the architecture of an intelligent system for processing reconnaissance data. According to researchers K. Gromada *et al.* (2022), such systems must not only enable automatic detection of objects within images but also integrate information from diverse sources, analyse it, and communicate results to decision support systems. The researchers further noted that contemporary multi-tiered reconnaissance complexes are constructed as intricate information systems comprising several interconnected levels for data collection, transmission, and processing.

According to researchers A. Howard *et al.* (2017), the overall architecture of an intelligent target recognition system in military reconnaissance can be conceptually divided into several primary functional layers: data acquisition, preliminary information processing, intelligent analysis, data integration, and decision support. Similarly, researchers F. Kadhum *et al.* (2026) emphasised that each layer performs specific functions while ensuring interaction with other system components. The initial stage involves collecting data from various observation sources. As noted by researchers V. Makarichev *et al.* (2025), key sources of reconnaissance information include satellite remote sensing systems, unmanned aerial vehicles, ground surveillance cameras, radar stations, and other sensor platforms. According to F. Kadhum *et al.* (2026), each of these sources generates substantial volumes of data, including both static images and high-resolution video streams.

Following data acquisition, preliminary information processing is conducted. According to F. Kadhum *et al.* (2026), the main objective at this stage is to prepare images for subs equent analysis by performing noise filtering, illumination normalisation, correction of geometric distortions, and image alignment. The researchers also noted that images may be transformed into different colour spaces or resised to optimise the performance of deep learning algorithms. Particular emphasis is placed on image georeferencing during this phase. Similarly, researchers R. Beard & T. McLain (2012) concluded that georeferencing represents a critical component of reconnaissance data integration because it allows information from multiple sources to be aligned within a unified coordinate system.

The subsequent stage is the intelligent analysis of images using computer vision algorithms and deep learning methods. According to researchers R. Sairam *et al.* (2023), this layer addresses automatic object detection, classification, and segmentation. The researchers explained that detection algorithms identify the presence and approximate localisation of objects of interest, while classification determines object categories, including military equipment, vehicles, engineering structures, or other infrastructural elements. In more complex scenarios, researchers G. Chen *et al.* (2022) reported that segmentation methods are employed to delineate precise object boundaries. R. Sairam *et al.* (2023) further emphasised that segmentation is particularly valuable when analysing scenes containing overlapping objects or irregular shapes because it provides detailed information regarding scene structure and spatial relationships.

After initial image analysis, results are transferred to the data integration layer. According to G. Chen *et al.* (2022), information obtained from disparate sources is consolidated at this stage. Similarly, R. Sairam *et al.* (2023) demonstrated that satellite image analysis may be combined with data from unmanned aerial vehicles or ground sensor systems to produce a more comprehensive and reliable situational overview. G. Chen *et al*. (2022) identified resolving inconsistencies between heterogeneous information sources as one of the principal challenges of data integration. According to R. Sairam *et al*. (2023), specialised data fusion algorithms evaluate the reliability of incoming observations and generate coherent results. For example, researchers J. Kang *et al*. (2022) explained that when one sensor detects an object while another fails to confirm it, the system must estimate the credibility of each source before assigning an appropriate confidence level to the integrated output.

J. Kang *et al*. (2022) further noted that object tracking modules constitute another essential component of intelligent reconnaissance architectures. Once an object has been detected, the system should continuously monitor its movement over time. According to the researchers, motion analysis algorithms estimate trajectories and predict future positions. Information processed at earlier stages is subsequently conveyed to decision support systems. G. Chen *et al*. (2022) concluded that these systems assist operators by generating notifications regarding newly detected objects, changes in their locations, or suspicious activities. Overall, J. Kang *et al*. (2022) described the architecture of an intelligent image processing system as an interconnected network of components supporting the continuous flow of intelligence data from acquisition to decision-making and adaptive control.

At the initial stage, data acquisition relies on various sensors and sources such as unmanned aerial vehicles, satellites, radar stations, optical cameras, and infrared detectors. Each source delivers raw data characterised by differing spatial resolutions, temporal frequencies, and spectral bands, necessitating careful coordination to facilitate compatibility and effective integration during subsequent processing. Once collected, the data is managed by a transmission and reception module responsible for linking distributed sensors with central processing units. According to J. Kang *et al*. (2022), this module maintains synchronisation across multiple data streams, buffers temporary data when necessary, and ensures secure and reliable communication channels. The researchers emphasised that these functions are essential for preventing data loss or temporal misalignment before downstream processing. The pre-processing module follows, preparing incoming data for further analysis through noise reduction, image stabilisation, normalisation, and georeferencing. As noted by the previously discussed studies, this stage harmonises heterogeneous sensor inputs to support direct data fusion and consistent analysis throughout the system. Subsequently, the intelligent analysis module receives pre-processed data to execute object detection, classification, tracking, multisensory fusion, and situational assessment. According to G. Chen *et al*. (2022), this module employs advanced machine learning methods, including CNNs and transformer architectures, to extract meaningful information from complex reconnaissance imagery. The structured analytical results produced then serve as input for the decision-making subsystem.

Recent research conducted by R. Tsekhmystro *et al*. (2025) suggests that applying pre-processing techniques such as image denoising can significantly improve the effectiveness of deep learning models for object localisation and classification in UAV imagery containing noise. The researchers demonstrated that denoising methods such as DRUNet improve image quality and consequently increase detection accuracy without requiring retraining of existing neural networks. According to G. Chen *et al*. (2022), the decision support module processes analytical outputs to generate actionable intelligence by evaluating operational scenarios, planning responses, and formulating recommendations for operators or command authorities. The researchers emphasised that close integration between the intelligent analysis and decision support modules enables timely and accurate operational decision generation. To facilitate human interpretation and response, researchers L. Jin *et al*. (2026) proposed a visualisation and user interface module that translates analytical outputs into intuitive displays. According to the researchers, these real-time visualisations include detected objects, trajectories, fused sensor information, and situational summaries, thereby bridging automated analysis with operator understanding. A. Rouhi *et al*. (2024) further noted that a feedback control mechanism interconnects the decision support and intelligent analysis components with the data acquisition subsystem. This feedback loop enables dynamic adjustment of sensor configurations, mission parameters, and data collection strategies according to analytical results and operational requirements, thereby improving the adaptability of reconnaissance systems.

Technologies for processing large volumes of data also play a significant role in the operation of modern reconnaissance systems. According to P. Sun *et al*. (2022), the continuously increasing amount of information originating from diverse observation sources requires efficient storage and analysis solutions. Similarly, researchers C. Li *et al*. (2025) concluded that distributed computing systems, cloud platforms, and specialised databases are widely employed to satisfy these computational requirements. L. Jin *et al*. (2026) additionally emphasised that security and reliability remain essential characteristics of military intelligence infrastructures because these systems process highly sensitive operational information. Accordingly, various cryptographic protection mechanisms, access control systems, and redundancy techniques are implemented to ensure resilience against unauthorised access and cyberattacks. Looking forward, L. Jin *et al*. (2026) suggested that future intelligent military reconnaissance architectures will increasingly incorporate artificial intelligence technologies and autonomous capabilities. According to the researchers, next-generation reconnaissance systems may independently analyse operational environments, identify potential threats, and formulate recommendations for subsequent actions with minimal human intervention. Overall, the architecture of an intelligent system for processing reconnaissance imagery constitutes a multi-layered structure comprising interconnected components responsible for data collection, processing, analysis, and integration, as shown in Figure 1.

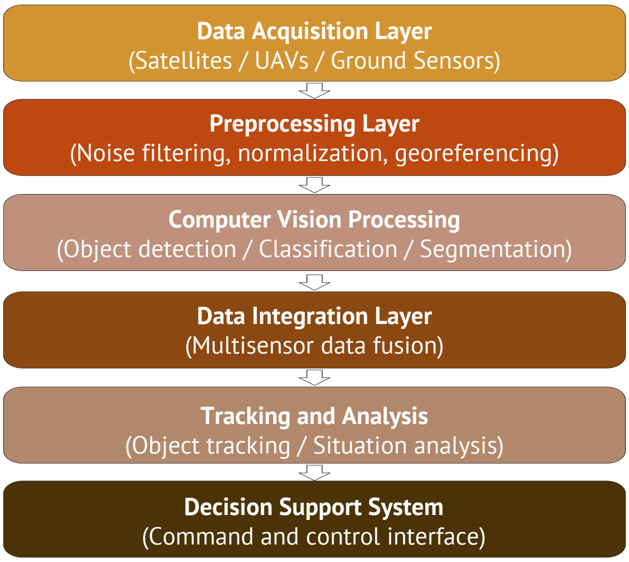

Figure 1. Image processing system architecture

Source: developed by the author based on research by G. Chen *et al.* (2022), P. Sun *et al.* (2022), A. Rouhi *et al.* (2024), C. Li *et al.* (2025) and L. Jin *et al.* (2026)

According to the reviewed studies, the combination of advanced computer vision and deep learning methods with an efficient computational infrastructure substantially enhances the operational effectiveness of contemporary military reconnaissance systems. The reviewed studies indicate that the effectiveness of intelligent reconnaissance architectures depends not only on the performance of individual computer vision algorithms but also on the coordinated interaction of all architectural layers. In practical deployments, several important architectural trade-offs must be considered. Processing data directly on edge platforms, such as UAVs, enables low-latency target detection but is constrained by limited computational resources, whereas centralised or cloud-based processing provides greater analytical capabilities at the cost of increased communication latency. Likewise, highly accurate deep learning models generally require more computational resources, creating a balance between recognition performance and real-time responsiveness. Multimodal data fusion substantially improves situational awareness and detection reliability; however, integrating heterogeneous sensor data increases algorithmic complexity and computational overhead. Finally, although autonomous computer vision systems can significantly reduce operator workload, human involvement in the decision-making loop remains essential for validating critical intelligence outputs and minimising the risks associated with false detections or incorrect classifications. These architectural compromises largely determine the practical effectiveness of modern military reconnaissance systems and should therefore be carefully considered during system design and deployment.

Conclusions

This study explored the application of computer vision and deep learning techniques for the automated detection of military objects within multi-level reconnaissance systems. A review of current scientific literature and existing technological frameworks indicated that advanced image processing algorithms are among the most promising approaches for enhancing the automated analysis of reconnaissance data. The investigation examined the fundamental principles guiding the design of multi-level reconnaissance systems, demonstrating that their operational effectiveness depends significantly on the capability to process large quantities of visual data generated by diverse sensor platforms. In this context, AI-driven computer vision algorithms enable automatic object detection, classification, segmentation, and tracking within video streams, thereby improving processing speed, reducing operator workload, enhancing target detection accuracy, and supporting more efficient decision-making in complex operational scenarios.

Particular emphasis was placed on assessing deep learning approaches for object recognition in reconnaissance imagery. Contemporary neural network architectures, including CNN, single-stage and two-stage detection models, as well as transformer-based frameworks, have exhibited robust performance in computer vision tasks. The analysis demonstrated that no single architecture is universally optimal for all reconnaissance scenarios. Instead, model selection should be based on operational requirements, balancing detection accuracy, inference speed, computational complexity, and suitability for deployment on resource-constrained reconnaissance platforms. Consequently, convolutional, transformer-based, and hybrid approaches should be regarded as complementary rather than competing solutions. The conducted analysis allowed the generalisation of the architectural organisation of multi-level reconnaissance systems. Their operation follows a hierarchical processing pipeline in which reconnaissance data are first collected from heterogeneous sources, including satellites, unmanned aerial vehicles, and ground-based sensors, then synchronised in time and geographic coordinates, pre-processed, analysed using computer vision algorithms, integrated through multisensory data fusion mechanisms, and finally transferred to decision-support systems. Feedback mechanisms subsequently allow analytical results to influence sensor tasking and subsequent data acquisition, forming a closed intelligence processing loop. The effectiveness of this architecture therefore depends not only on the performance of individual deep learning models but also on the efficient interaction between all functional layers.

The review also identified several common architectural principles characterising modern intelligent reconnaissance systems. Distributed processing architectures combining onboard, edge, and centralised computing environments provide the most effective balance between computational efficiency and operational responsiveness. Multisensory data fusion consistently improves situational awareness and target detection reliability by compensating for the limitations of individual sensing modalities. The integration of computer vision algorithms with decision-support systems significantly accelerates intelligence analysis while preserving human supervision during critical operational decisions. Modern deep learning algorithms notably improve object detection accuracy, classification performance, and support the near real-time processing of extensive datasets. This capability is especially critical in contemporary military contexts, where rapid information acquisition and analysis can decisively impact operational outcomes. Nonetheless, several challenges remain and warrant further research. These include difficulties in detecting small objects within high-resolution imagery, the scarcity of specialised training datasets for military applications, ensuring algorithm robustness under diverse observation conditions, and the limitations imposed by computational resources on mobile reconnaissance platforms. Prospective research directions involve devising more effective algorithms for small-object detection, enhancing methods for multisensory data integration, improving adaptive resource allocation between onboard, edge, and centralised processing infrastructures, and progressing toward autonomous intelligent reconnaissance systems capable of executing selected analytical tasks while maintaining reliable human oversight. Additionally, leveraging distributed computing and cloud-based platforms for managing large volumes of reconnaissance data presents a promising avenue for further exploration.

Acknowledgements

None.

Funding

The research has been funded by National Research Foundation of Ukraine (accessed on 24 June 2025) within Project No. 2025.06/0037 "A system for detecting and recognising camouflaged and small objects based on the use of modern computer vision technologies" (2025-2026).

Conflict of Interest

None.

References

[1] Afifah, V. (2026). YOLOv8 for object detection: A comprehensive review of advances, techniques, and applications. *International Journal of Advanced Computational Intelligence*, 2(1), 53-61. doi: 10.71129/ijaci.v2i1.pp53-61.

[2] Al-IQubaydhi, N., Alenezi, A., Alanazi, T., Senyor, A., Alanezi, N., Alotaibi, B., Alotaibi, M., Razaque, A., & Hariri, S. (2024). Deep learning for unmanned aerial vehicles detection: A review. *Computer Science Review*, 51, article number 100614. doi: 10.1016/j.cosrev.2023.100614.

[3] Beard, R.W., & McLain, T.W. (2012). *Small unmanned aircraft theory and practice*. Princeton & Oxford: Princeton University Press.

[4] Bian, X., & Ma, J. (2025). Deep learning based real time detection and localisation for targets in UAV remote sensing images. *International Journal of Advance in Applied Science Research*, 4(9), 8-13.

[5] Cao, Z., Kooistra, L., Wang, W., Guo, L., & Valente, J. (2023). Real time object detection based on UAV remote sensing: A systematic literature review. *Drones*, 7, article number 620. doi: 10.3390/drones7100620.

[6] Chen, G., Liu, S.-J., Sun, Y.-J., Ji, G.-P., Wu, Y.-F., & Zhou, T. (2022). Camouflaged object detection via context-aware cross-level fusion. *ArXiv*. doi: 10.48550/arXiv.2207.13362.

[7] Elgamily, K.M., Mohamed, M.A., Abou Taleb, A.M., & Ata, M.M. (2025). Enhanced object detection in remote sensing images by applying metaheuristic and hybrid metaheuristic optimisers to YOLOv7 and YOLOv8. *Scientific Reports*, 15, article number 7226. doi: 10.1038/s41598-025-89124-8.

[8] Gromada, K., Siemiątkowska, B., Stecz, W., Płochocki, K., & Woźniak, K. (2022). Real-time object detection and classification by UAV equipped with SAR. *Sensors (Basel, Switzerland)*, 22(5), article number 2068. doi: 10.3390/s22052068.

[9] Gui, S., Song, S., Qin, R., & Tang, Y. (2024). Remote sensing object detection in the deep learning era – a review. *Remote Sensing*, 16(2), article number 327. doi: 10.3390/rs16020327.

[10] Habash, N., *et al.* (2025). Recent real-time aerial object detection approaches, performance, optimisation, and efficient design trends for onboard performance: A survey. *Sensors (Basel, Switzerland)*, 25(24), article number 7563. doi: 10.3390/s25247563.

[11] Howard, A.G., Zhu, M., Chen, B., Kalenichenko, D., Wang, W., Weyand, T., Andreetto, M., & Adam, H. (2017). Mobilenets: Efficient convolutional neural networks for mobile vision applications. *ArXiv*. doi: 10.48550/arXiv.1704.04861.

[12] Hua, W., & Chen, Q. (2025). A survey of small object detection based on deep learning in aerial images. *Artificial Intelligence Review*, 58, article number 162. doi: 10.1007/s10462-025-11150-9.

[13] Jin, L., Wang, R., & Huang, B. (2026). A challenge-driven survey on UAV-based target tracking. *Computers, Materials & Continua*, 88(1), article number 2. doi: 10.32604/cmc.2026.080050.

[14] Johnson, S.L., Moore, H.D., & Porter, M.D. (2026). Toward resilient multi-modal drone detection in cluttered environments: A systems survey of EO/IR, radar, acoustic, LiDAR and RF modalities. *International Journal of Critical Infrastructure Protection*, 54, article number 100870. doi: 10.1016/j.ijcip.2026.100870.

[15] Jonnalagadda, A.V., & Hashim, H.A. (2024). SegNet: Segmented deep learning CNN approach for wildfire detection in UAV imagery. *Remote Sensing Applications: Society and Environment*, 34, article number 101181. doi: 10.1016/j.rsase.2024.101181.

[16] Kadhum, F.M., Abdulhameed, A.A., & Saud, J.H. (2026). Vision-based UAV detection methods using deep learning: A review. *Journal of Al-Qadisiyah for Computer Science and Mathematics*, 18(1), 281-301. doi: 10.29304/jqcsm.2026.18.12504.

[17] Kang, J., Tariq, S., Oh, H., & Woo, S.S. (2022). A survey of deep learning-based object detection methods and datasets for overhead imagery. *IEEE Access*. doi: 10.1109/ACCESS.2022.3149052.

[18] Kırac, E., & Özbek, S. (2024). Deep learning based object detection with UAV equipped with embedded system. *Journal of Aviation*, 8(1), 15-25. doi: 10.30518/jav.1356997.

[19] Lee, C., Son, J., Shon, H., Jeon, Y., & Kim, J. (2024). FRED: Towards a full rotation-equivariance in aerial image object detection. *Proceedings of the AAAI Conference on Artificial Intelligence*, 38(4), 2883-2891. doi: 10.1609/aaai.v38i4.28069.

[20] Leng, J., Ye, Y., Mo, M., Gao, C., Gan, J., Xiao, B., & Gao, X. (2024). Recent advances for aerial object detection: A survey. *ACM Computing Surveys*, 56(12), article number 296. doi: 10.1145/3664598.

[21] Li, C., Zhao, R., Wang, Z., Xu, H., & Zhu, X. (2025). RemDet: Rethinking efficient model design for UAV object detection. *Proceedings of the AAAI Conference on Artificial Intelligence*, 39(5), 4643-4651. doi: 10.1609/aaai.v39i5.32490.

[22] Li, Z., Wang, Y., Zhang, N., Zhang, Y., Zhao, Z., Xu, D., Ben, G., & Gao, Y. (2022). Deep learning-based object detection techniques for remote sensing images: A survey. *Remote Sensing*, 14(10), article number 2385. doi: 10.3390/rs14102385.

[23] Ma, L., Liu, Y., Zhang, X., Ye, Y., Yin, G., & Johnson, B.A. (2019). Deep learning in remote sensing applications: A meta-analysis and review. *ISPRS Journal of Photogrammetry and Remote Sensing*, 152, 166-177. doi: 10.1016/j.isprsjprs.2019.04.015.

[24] Makarichev, V., Tsekhmystro, R., Lukin, V., & Krytskyi, D. (2025). Performance improvement of vehicle and human localisation and classification by YOLO family networks in noisy UAV images. *Information*, 16(12), article number 1087. doi: 10.3390/info16121087.

[25] Mei, S., Lian, J., Wang, X., Su, Y., Ma, M., & Chau, L.-P. (2024). A comprehensive study on the robustness of deep learning-based image classification and object detection in remote sensing: Surveying and benchmarking. *Journal of Remote Sensing*, 4, article number 0219. doi: 10.34133/remotesensing.0219.

[26] Mouatassim, T., Airaj, M., & El Guarmah, E.M. (2026). Safeguarding the skies: The rise of machine learning approaches for cyberattack detection in unmanned aerial systems. *Cybersecurity* 9, article number 62. doi: 10.1186/s42400-025-00466-2.

[27] Nikouei, M., Baroutian, B., Nabavi, S., Taraghi, F., Aghaei, A., Sajedi, A., & Ebrahimi Moghaddam, M. (2025). Small object detection: A comprehensive survey on challenges, techniques and real-world applications. *Intelligent Systems with Applications*, 27, article number 200561. doi: 10.1016/j.iswa.2025.200561.

[28] Paheding, S., Saleem, A., Siddiqui, M.F.H., Rawashdeh, N., Essa, A., & Reyes, A.A. (2024). Advancing horizons in remote sensing: A comprehensive survey of deep learning models and applications in image classification and beyond. *Neural Computing and Applications*, 36, 16727-16767. doi: 10.1007/s00521-024-10165-7.

[29] Ramos, L.T., & Sappa, A.D. (2025). A decade of You Only Look Once (YOLO) for object detection: A review. *ArXiv*. doi: 10.48550/arXiv.2504.18586.

[30] Rouhi, A., Arezoomandan, S., Kapoor, R., Klohoker, J., Patal, S., Shah, P., Umare, H., & Han, D. (2024). An overview of deep learning in UAV perception. In *2024 IEEE international conference on consumer electronics (ICCE)*. Las Vegas: IEEE. doi: 10.1109/ICCE59016.2024.10444237.

[31] Sairam, R.V.C., Keswani, M., Sinha, U., Shah, N., & Balasubramanian, V.N. (2023). ARUBA: An architecture-agnostic balanced loss for aerial object detection. In *Proceedings of the IEEE/CVF winter conference on applications of computer vision (WACV 2023)* (pp. 3719-3728). Waikoloa, USA: IEEE Computer Society.

[32] Soeleman, M.A., Supriyanto, C., & Purwanto. (2023). Deep learning model for unmanned aerial vehicle based object detection on thermal images. *Revue d'Intelligence Artificielle*, 37(6), 1441-1447. doi: 10.18280/ria.370608.

[33] Sun, P., Liu, T., Chen, X., Zhang, S., Zhao, Y., & Wei, S. (2022). Multi-source aggregation transformer for concealed object detection in millimeter-wave images. *IEEE Transactions on Circuits and Systems for Video Technology*, 32(9), 6148-6159. doi: 10.1109/TCSVT.2022.3161815.

[34] Tsekhmystro, R., Lukin, V., & Krytskyi, D. (2025). UAV image denoising and its impact on performance of object localisation and classification in UAV images. *Computation*, 13(10), article number 234. doi: 10.3390/computation13100234.
[35] Vasishta, M.S.S.V., Amireddy, A.T.R., & Shrivastava, P. (2024). Small object detection for UAVs using deep learning models on edge computing: A comparative analysis. In *2024 5th international conference on circuits, control, communication and computing* (pp. 1-7). Bangalore: IEEE.
[36] Wang, K., Wang, Z., Li, Z., Su, A., Teng, X., Pan, E., Liu, M., & Yu, Q. (2025). Oriented object detection in optical remote sensing images using deep learning: A survey. *Artificial Intelligence Review*, 58, article number 350. doi: 10.1007/s10462-025-11256-0.
[37] Wu, Y., & Tong, K. (2025). Research advances on deep learning based small object detection in UAV aerial images. *Acta Aeronautica et Astronautica Sinica*, 46(3). doi: 10.7527/S1000-6893.2024.30848.
[38] Yu, Y., & Da, F. (2023). Phase-shifting coder: Predicting accurate orientation in oriented object detection. In *Proceedings of the IEEE/CVF conference on computer vision and pattern recognition (CVPR 2023)* (pp. 13354-13363). Vancouver: IEEE Computer Society.
[39] Zhu, W., & Chen, K. (2026). Real time object detection for unmanned aerial vehicles based on vision transformer and edge computing. *Scientific Reports*, 16, article number 6814. doi: 10.1038/s41598-026-37938-5.

Застосування комп'ютерного зору для виявлення цілей у багаторівневих системах військової розвідки: огляд літератури

Денис Берковський

Аспірант
Національний аерокосмічний університет «Харківський авіаційний інститут»
61000, вул. Вадима Манька, 17, м. Харків, Україна
https://orcid.org/0009-0004-0625-2839

Аліна Артьомова

Кандидат технічних наук, доцент
Національний аерокосмічний університет «Харківський авіаційний інститут»
61000, вул. Вадима Манька, 17, м. Харків, Україна
https://orcid.org/0000-0002-6761-2066

Анотація. Метою дослідження був аналіз сучасних методів комп'ютерного зору для автоматичного виявлення та класифікації цілей у багаторівневих системах військової розвідки, а також оцінювання ефективності алгоритмів глибокого навчання в обробці розвідувальних даних за різних умов спостереження. Для досягнення цієї цілі підхід інтегрує систематичний огляд літератури, моделювання архітектур обробки зображень та порівняльну оцінку моделей виявлення об'єктів на основі нейронних мереж. Результати дослідження показали, що розгортання найсучасніших архітектур глибокого навчання, зокрема згорткових нейронних мереж, варіантів YOLO та моделей на основі трансформаторів, суттєво покращує точність та надійність автоматичного виявлення військових об'єктів на зображеннях, отриманих з безпілотних літальних апаратів та супутникових джерел. Крім того, поєднання даних з кількох датчиків з мультимодальними методами обробки покращує можливості розпізнавання цілей, особливо в сценаріях, що характеризуються низькою видимістю, складним складом сцени або частковим перекриттям об'єкта. Порівняльний аналіз сучасних архітектур показав, що моделі сімейства YOLO забезпечують найкращу швидкість обробки та є найбільш придатними для застосування в режимі реального часу на борту безпілотного літального апарату, тоді як Faster R-CNN демонструє вищу точність локалізації складних і малорозмірних об'єктів, але потребує більших обчислювальних витрат. Архітектури згорткових нейронних мереж забезпечують збалансоване співвідношення між точністю та продуктивністю, тоді як моделі на основі трансформерів ефективніше працюють у складних умовах спостереження, зокрема за низької просторової роздільної здатності, наявності шуму, часткового перекриття та маскування об'єктів, однак їх використання супроводжується підвищеними вимогами до обчислювальних ресурсів. Загалом встановлено компроміс між точністю виявлення, швидкістю обробки та обчислювальною складністю моделей, який визначає доцільність їх застосування залежно від характеристик розвідувальної платформи та умов виконання завдання. Надано інформацію про розробку інтелектуальних систем для автоматизованого аналізу даних розвідки

Ключові слова: глибоке навчання; виявлення об'єктів; мультисенсорне об'єднання даних; аналіз у реальному часі; безпілотний літальний апарат

Journal of Kryvyi Rih National University
Journal homepage: https://journal-knu.com.ua/en
Article's History: Received: 19.12.2025 Revised: 24.03.2026 Accepted: 28.04.2026 Published: 29.05.2026
Vol. 24, No. 1, 2026
ISSN 2306-5451
e-ISSN 2519-2736

UDC 621.51
DOI: 10.31721/2306-5451-2026-1-24-120-137

Regenerative compressor machines: Overview of design parameters and factors affecting their efficiency (literature review)

Volodymyr Sitalo
Postgraduate Student
Sumy State University
40007, 116 Kharkivska Str., Sumy, Ukraine
https://orcid.org/0009-0005-0610-3320

Serhiy Vanyeyev
PhD in Technical Sciences, Associate Professor
Sumy State University
40007, 116 Kharkivska Str., Sumy, Ukraine
https://orcid.org/0000-0002-8205-0209

Stanislav Meleychuk
PhD in Technical Sciences, Associate Professor
Sumy State University
40007, 116 Kharkivska Str., Sumy, Ukraine
https://orcid.org/0000-0002-7507-6865

Oleh Chekh
Postgraduate Student
Sumy State University
40007, 116 Kharkivska Str., Sumy, Ukraine
https://orcid.org/0000-0003-2500-481X

Danylo Nikolaienko
Postgraduate Student
Sumy State University
40007, 116 Kharkivska Str., Sumy, Ukraine
https://orcid.org/0009-0009-6827-7691

Abstract. Increasing demands for energy efficiency in industrial equipment and the need to reduce operating costs highlight the relevance of research into regenerative compressors – a class of turbomachinery that combines the advantages of dynamic and positive-displacement machines and has significant potential for widespread industrial application. Study aimed to systematise and analyse current scientific research in the field of regenerative compressors and pumps to identify the key factors influencing their efficiency. The study was based on analysis and comparison of the results of experimental and numerical studies published in peer-reviewed scientific journals, as well as on the application of computational fluid dynamics (CFD) as a modern digital tool for engineering analysis. Study established that the efficiency of regenerative compressors is determined by a combination of geometric and design parameters. The type and shape of the impeller, as well as the number and profile of the blades,

Suggested Citation:
Sitalo, V., Vanyeyev, S., Meleychuk, S., Chekh, O., & Nikolaienko, D. (2026). Regenerative compressor machines: Overview of design parameters and factors affecting their efficiency (literature review). *Journal of Kryvyi Rih National University*, 24(1), 120-137. doi: 10.31721/2306-5451-2026-1-24-120-137.

Copyright © The Author(s). This is an open access article distributed under the terms of the Creative Commons Attribution License 4.0 (https://creativecommons.org/licenses/by/4.0/)

*Corresponding author (v.sitalo@kttf.sumdu.edu.ua)

influence the degree of pressure increase: the optimal number of blades lies within the range of 30-50, whilst blades of complex shape, despite their higher efficiency, complicate the manufacturing process. The dimensions and configuration of the working channel determine the intensity of circulation and the level of gas-dynamic losses – the height of the channel is a more decisive parameter than its cross-sectional area. The clearances in the flow path are critical: an increase in the axial and radial clearances from 0.15 mm to 0.2 mm leads to a reduction in performance of up to 50 %, which confirms the need to address them at design stage. CFD methods can be used to visualise complex spiral-like flow structures, identify sources of losses and optimise design solutions, thereby reducing costs of physical prototyping. The combination of analytical, experimental and CFD methods provides the basis for developing effective design approaches, which will ensure improved energy efficiency and expand the range of applications for these machines in industrial systems

Keywords: regenerative compressor; regenerative pump; regenerative hypothesis; numerical modelling; Ansys SFX; design optimisation

Introduction

Compressor equipment is an integral part of modern industrial systems and is central in supporting technological processes in the energy sector, the chemical industry, mechanical engineering and related sectors. At the same time, compressors are among the most energy-intensive pieces of equipment: their share of total electricity consumption at industrial enterprises can reach 30-40%. In this context, improving the energy efficiency of compressor equipment is not only an engineering necessity but also an economic and environmental one. A reduction in specific energy consumption by even a few percent can ensure significant resource savings at the level of an enterprise or an industry. Among the wide variety of compressor types, regenerative compressors occupy a special place, combining the characteristics of dynamic and positive-displacement machines. Their distinctive features include a simple design, the absence of surge, compactness and the ability to provide a relatively high degree of pressure increase with low working fluid flow rates. Despite these advantages, regenerative compressors have a comparatively low efficiency – typically in the range of 35-55% – which limits their wider industrial application. The complex flow structure in the flow path, significant sensitivity to geometric parameters and an insufficient methodological basis for comprehensive design optimisation highlight the need for further research in this field. Development of digital tools for engineering analysis, in particular computational fluid dynamics (CFD) methods, creates new opportunities for in-depth study of the operating processes of regenerative compressors and for identifying ways to improve their efficiency.

J.E. Adam *et al.* (2022) substantially contributed to research into the geometric parameters of regenerative compressors, studying the influence of various design parameters on the performance of a side-channel regenerative compressor stage. In particular, the researchers found that the shape of the blades and their angle of attack significantly affect the pressure ratio and isentropic efficiency. The results obtained highlight the significance of carefully selecting the impeller geometry at the initial design stage. Continuing this line of research, J.E. Adam *et al.* (2023) conducted a parametric study of the influence of the working channel geometry on the performance of a regenerative compressor. The authors varied the height, cross-sectional shape and length of the channel and found that the channel height is a more decisive parameter for mass flow than the cross-sectional area. At the same time, the study showed that the influence of individual channel parameters on isentropic efficiency is less pronounced and is mainly evident at high pressure values.

J. Nejadali (2021) applied the response surface method in combination with CFD to optimise the shape of aerodynamic-profile blades for a regenerative compressor. The results of the study showed that aerodynamic-profile blades can deliver higher efficiency compared to standard straight blades. However, the author noted that the complexity of manufacturing such blades may offset the performance advantages in terms of manufacturability and production costs. A. Salimi *et al.* (2023) conducted a multi-criteria optimisation of a regenerative pump with S-shaped blades using the response surface method. The researchers varied several geometric parameters simultaneously and found that the S-shaped blade configuration can provide a better balance between head and efficiency compared to traditional configurations. The results demonstrate the potential of applying multi-criteria optimisation methods to improve the design of regenerative machines. Q.-Q. Li *et al.* (2022) investigated the pressure pulsation characteristics in a regenerative pump as a function of the blade arrangement on the impeller. The authors found that an uneven blade arrangement can significantly reduce amplitude of pressure pulsations without a significant deterioration in head characteristics. This creates opportunities for reducing vibration and acoustic loads on the compressor's structural components under real-world operating conditions. L. Zhou *et al.* (2024) investigated, both numerically and experimentally, the effect of axial clearance on the performance of a regenerative pump. The researchers found that an increase in axial clearance leads to an increase in the intensity of bypass flows and a significant drop in the unit's head characteristics. The results of this study confirm that the axial clearance is one of the most critical parameters in the design of regenerative machines and requires careful monitoring both during manufacture and in operation. J. Zhang *et al.* (2024) conducted a quantitative analysis of energy losses in a regenerative compressor and developed an approach to predicting its operating characteristics. The researchers identified the main sources of losses in the flow path and determined their relative contribution to the machine's overall inefficiency. The proposed methodology can be used for targeted optimisation of design elements with the greatest potential for improving efficiency. W. Li (2025) investigated the effect of wall roughness on the performance of a regenerative pump using CFD modelling. Study determined that increasing the roughness of the internal surfaces of the flow path leads to an increase in hydraulic losses and a reduction in efficiency. The results obtained are of direct practical significance for the selection of materials and manufacturing technologies for the casing components of regenerative compressors, with the aim of minimising friction losses.

An analysis of the studies cited indicates that most of the research focuses on investigating the influence of individual geometric parameters on the performance of regenerative compressors and pumps. At the same time, issue of simultaneous optimisation across multiple parameters remains understudied: most authors vary the parameters sequentially, which prevents them from incorporating their mutual influence and finding the global optimum design. Furthermore, the comprehensive consideration of clearances in conjunction with other geometric parameters in CFD modelling remains an under-researched aspect. These gaps formed the basis for this study. Study aimed to conduct a comprehensive study and systematisation of scientific achievements in the field of regenerative compressors and pumps, to identify the key geometric and design parameters that determine their energy performance, and to justify promising avenues for improving these machines.

Study was conducted in the form of a systematic review. The international scientometric databases Scopus and Web of Science were used to compile the information base, and the search was conducted primarily using English-language queries based on the following key terms: "regenerative compressor", "side channel pump", "vortex compressor", "CFD optimisation" and "impeller geometry". The main criterion for selecting sources was that they had been published between 2020 and 2026, ensuring the relevance of the material considered. In addition, selected fundamental works from an earlier period were included – in particular, classic works on the theory of the regenerative hypothesis and the basic principles of flow component design – without which it is impossible to correctly interpret modern results and trace the evolution of approaches to the design of regenerative machines. A total of 51 scientific publications were analysed, including articles in peer-reviewed journals, proceedings of international conferences and institutional repositories. Sources were selected based on criteria of thematic relevance, scientific novelty and citation frequency in related research.

The study employs a range of general scientific and specialised methods. The method of systems analysis was used to organise the body of literature and identify interrelationships between design parameters and machine characteristics. Comparative analysis was used to compare the results of different research groups and to identify similarities and contradictions in the conclusions regarding the optimal values of geometric parameters. The method of generalisation was applied to formulate comprehensive conclusions based on the body of publications considered. A quantitative analysis of scientific publications determined level of scientific development in specific subject areas and identified gaps in existing research. The material has been organised into thematic sections: impeller design, channel geometry, separator, clearances and CFD modelling – which was used for a systematic coverage of the key aspects of regenerative compressor operation. The evolution of calculation methods has been analysed separately – from one-dimensional analytical models to three-dimensional CFD modelling verified on test benches – to assess their accuracy and limits of applicability at various stages of design.

Design Diagram and Classification of Regenerative Compressors

The design of a single-stage regenerative compressor (Fig. 1) comprises an impeller with blades evenly spaced around its circumference, as well as suction, discharge and working channels. A partition – known as a separator or baffle – is situated between the suction and discharge channels, ensuring they are kept separate. As noted by S. Vanyeyev *et al.* (2010), this design remains the basis for most modern regenerative machines. Despite its structural simplicity, the internal gas-dynamic processes in a regenerative compressor are complex: the working fluid moves along a spatial spiral trajectory, and each cycle between the blades and the channel is accompanied by momentum transfer, mixing and turbulent losses. This physical complexity explains why the accurate analytical prediction of the performance characteristics of regenerative machines remains an open scientific problem to this day. Notably, despite the significant volume of accumulated experimental and numerical data, a single, unified calculation methodology for regenerative machines of various types has not yet been developed – this is one of the key scientific gaps in this field.

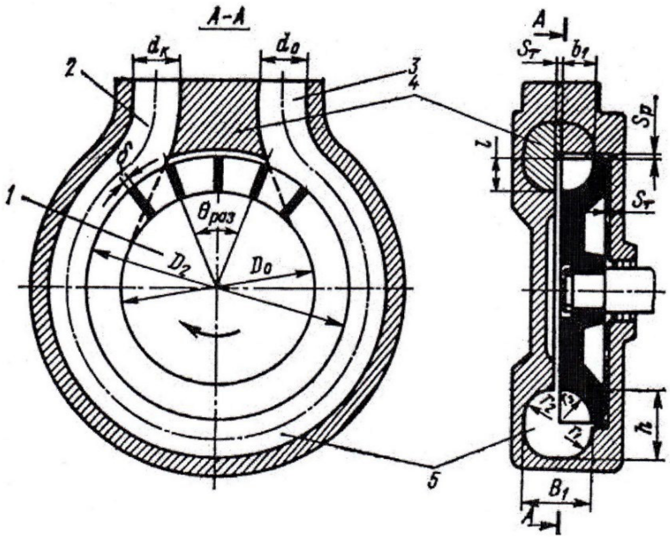

Figure 1. Schematic diagram of a regenerative compressor stage
Notes: 1 – impeller; 2 – discharge channel; 3 – suction duct; 4 – splitter; 5 – operating channel
Source: S.M. Vanyeyev *et al.* (2010)

Depending on the position of the casing's working channel in relation to the impeller blades, the flow paths of regenerative compressors are classified as peripheral, peripheral-lateral and lateral (Fig. 2). Compressors with a lateral channel arrangement have relatively high efficiency but low pressure. Peripheral channels provide higher pressures, although their efficiency is significantly lower. Peripheral-lateral channel arrangement is a compromise option, achieving an efficiency of up to 55% and a pressure coefficient ψ_{ad} = 1.6...3. M. Sreekanth *et al.* (2021), in their systematic review covering over 80 publications spanning 70 years, confirm this conclusion: the authors methodically compared the performance of different types of flow passages and concluded that the peripheral-lateral channel is the most balanced solution for a wide range of industrial applications. This conclusion is relevant: the advantage of the peripheral-lateral channel lies in the fact that the centrifugal effect is actively utilised in the peripheral section, resulting in a significant increase in pressure, whilst the lateral component facilitates the effective re-entry of the working fluid into the inter-blade space – thus ensuring that the entire channel area is utilised more uniformly in the energy exchange. At the same time, there is an absence in the literature of systematic comparative studies in which all three types of channels would be analysed under identical conditions using a single geometry; this complicates the quantitative justification of the advantages of the peripheral-lateral variant and represents a promising area for further research.

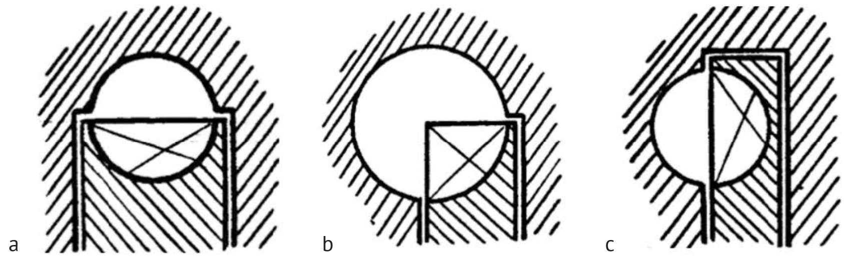

Figure 2. Main types of flow components in regenerative compressors
Notes: a – peripheral canal; b – peripheral-lateral canal; c – lateral canal
Source: S.M. Vanyeyev *et al.* (2010)

The shape of the flow section's profile in the meridional cross-section can be rectangular, circular or curved (Fig. 3). A rectangular cross-section is the simplest to manufacture, but is characterised by increased losses in the corner regions, where stagnation zones form. A circular cross-section ensures a smoother redistribution of velocities and a lower tendency for separation zones to form, which, according to W. Li (2025), has a positive effect on the level of hydraulic losses when operating under high-pressure conditions. A curved profile is an attempt to combine the advantages of both options. Thus, a common pattern emerges regarding the choice of cross-sectional shape: an increase in the aerodynamic efficiency of the channel shape is accompanied by greater manufacturing complexity, and each of the three options occupies a specific niche depending on the priorities: efficiency, manufacturability or compactness. M.M. Raheel & A. Engeda (2005), in their systematic study on the design of radial-bladed regenerative turbomachines, emphasise that the number of channels is increased primarily to boost capacity and flow rate, as well as to increase power output in turbine modes. Multi-channel flow sections are most easily implemented using a stage with an external peripheral channel; however, as the number of channels increases, the design of the separator becomes significantly more complex and the risk of cross-flow increases. It is worth noting the limited availability of quantitative data in the literature regarding the impact of the number of channels on performance – most publications focus on single-channel configurations, which represents a gap for applications with high performance requirements.

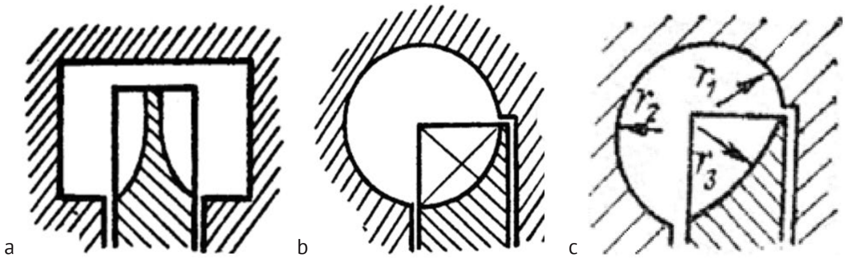

Figure 3. Shapes of the flow section profile in a meridional cross-section
Notes: a – rectangular duct; b – circular duct; c – curved duct
Source: S.M. Vanyeyev *et al.* (2010)

Regenerative turbomachines can be designed as single-flow, double-flow or multi-flow types. N.D. Karlsen-Davies & G.A. Aggidis (2016), in their fundamental review of regenerative annular pumps based on an analysis of over 120 sources, established that the use of double or multi-flow configurations makes it possible to relieve the rotor of radial forces and reduce the vibration load on the bearings. S. Münsterjohann *et al.* (2017) expanded on this idea by applying psychoacoustic evaluation criteria to the design of a low-noise side blower: the authors demonstrated that a symmetrical multi-flow blower configuration not only balances the force load but also significantly reduces the tonal components of noise, which is critical for medical and laboratory equipment. M. Raheel *et al.* (2003), whilst investigating the characteristics of single- and multi-stage regenerative compressors for natural gas transport, demonstrated that regenerative machines are competitive with centrifugal compressors in the range of low flow rates and high pressures: the measured pressure, for the same geometric parameters, increases proportionally with the number of stages in a multi-stage configuration, whilst efficiency decreases due to the accumulation of losses. Comparing the findings of these three research groups, a common pattern emerges: the transition from single-flow to multi-flow and multi-stage configurations expands the machine's functional capabilities, but is inevitably accompanied by either a reduction in efficiency or increased design complexity. This trade-off between productivity and efficiency in multi-stage designs remains unresolved and requires targeted research using multi-criteria optimisation methods. Thus, the choice of flow configuration and the number of stages is a complex design decision that simultaneously affects the mechanical reliability, hydraulic efficiency and acoustic characteristics of the machine.

The amount of energy transferred depends on the geometry and design parameters of the impeller and the casing components. M. Badami & M. Mura (2011), in the study on the development and validation of a one-dimensional model of a regenerative compressor for various devices, established that accurate consideration of geometric parameters – including the shape, arrangement and number of blades, as well as the dimensions of the annular channel – is crucial for adequate prediction of performance characteristics. The 1D model they developed demonstrated satisfactory agreement with experimental data for a wide range of geometries, confirming the validity of using simplified models in the early stages of design. At the same time, the authors note that the model exhibits systematic deviations at low flow rates, where non-linear effects become dominant. In the authors' view, this highlights the need to use three-dimensional CFD modelling to verify the results, particularly under non-standard operating conditions. To summarise the findings of this section, it should be emphasised that the structural layout and the type of flow path are the primary design decisions that determine the entire scope for further optimisation: the choice of channel type, cross-sectional shape and flow configuration effectively sets the upper limit of achievable efficiency, which cannot be significantly exceeded solely by optimising the geometry of the blades or clearances.

Effect of Impeller Geometry on Compressor Performance

Type and geometry of the blades directly affect the compressor's efficiency and determine the degree of pressure increase, as energy is transferred specifically from the impeller to the gas or liquid. G. Grabow (1975) established a fundamental relationship between the number of blades, their angle and the suction characteristics of regenerative pumps. Despite the age of these studies, the patterns identified by G. Grabow (1975) remain relevant and are used by contemporary researchers as a starting point. This indicates that the basic physics of momentum transfer in a regenerative machine is relatively stable and has not undergone any fundamental revision over the past five decades. It is worth noting that most contemporary studies of impeller geometry are highly specialised – they optimise one or two parameters for a specific geometry, without establishing generalised patterns suitable for use at the conceptual design stage.

Blade shape is one of the most debated parameters in the literature. J.E. Adam *et al.* (2022), using a systematic numerical experiment design that varied several geometric parameters simultaneously, found that blade geometry significantly influences the shape of the pressure characteristic: backwards-curved blades provide a more uniform pressure distribution and a wider range of stable operation, whilst straight blades have a steeper characteristic curve with a higher peak head at the design point. J. Nejadali (2021), using the response surface method in combination with three-dimensional CFD modelling to optimise airfoil-type blades, achieved an increase in isentropic efficiency of up to 8% compared with the baseline design featuring straight blades. The author systematically varied the angle of attack, profile thickness and curvature, and found that the angle of attack is the dominant parameter compared to the other variables. A. Salimi *et al.* (2023), building on this approach, applied multi-objective optimisation using the response surface method to a compressor with S-shaped blades and concluded that a simultaneous increase in pressure and efficiency is possible but requires a trade-off: maximum pressure is achieved at installation angles that slightly reduce efficiency, and vice versa. A common finding in the studies by J. Nejadali (2021), J.E. Adam *et al.* (2022) and A. Salimi *et al.* (2023) is that all three studies confirm the dominant role of the blade installation angle amongst the geometric parameters of the blade shape – this is a sufficiently reliable conclusion, as it has been obtained using three independent methods.

S.-Y. Jeon *et al.* (2019) adopted a different approach and developed a fundamentally new type of S-shaped blade, optimised for a microbubble pump. The research methodology was based on a combination of CFD modelling with an optimisation algorithm and verification using a physical prototype. The authors demonstrated that the S-shaped form helps to reduce cavitation and extend the operating range, although it does decrease the peak efficiency at the design point slightly compared with standard blades. Comparing the results of S.-Y. Jeon *et al.* (2019) and A. Salimi *et al.* (2023), a contradiction can be observed: both studies demonstrated the advantages of the S-shaped profile, but in different aspects – S.-Y. Jeon *et al.* (2019) addressed cavitation resistance, whilst A. Salimi (2023) emphasised simultaneous increase in head and efficiency. This is explained by the different operating conditions: the first study focused on pumping applications with a liquid medium, whilst the second focused on compressor applications with a gaseous medium. It is reasonable to assume that a direct comparison of these results is not valid without covering differences in Reynolds and Mach numbers. This circumstance highlights a significant scientific gap: the literature lacks studies that systematically compare the efficiency of different blade profiles under identical dimensionless similarity parameters, which makes it impossible to directly transfer results between applications.

K. Chen *et al.* (2022) investigated the effect of the blade tip undercut angle using three-dimensional unsteady CFD modelling, verified on a test bench. The researchers found that an increase in the undercut angle from 0° to 30° leads to a redistribution of high-velocity zones within the side channel and a change in secondary vortex structures. At angles of 15-20°, an optimal balance is observed between the level of turbulent losses and energy transfer efficiency, manifested in a 3-5% increase in isentropic efficiency. Although complex-shaped blades are generally more efficient, one of the main advantages of regenerative compressors – their structural simplicity – should be considered. Q.-Q. Li *et al.* (2022), based on an analysis of the match between the impeller and the duct, emphasise the need for a balance between geometric complexity and manufacturability; consequently, from a practical design perspective, the straight blade (Fig. 4) remains a sensible choice for most industrial applications, where manufacturability and cost take precedence over maximising efficiency. In the authors' view, the optimal strategy for selecting the blade shape should be determined as early as the technical specification stage: if maximum efficiency is the priority, the use of profiled blades verified via CFD is justified; if cost and service life are the priorities, straight blade with an optimised installation angle should be preferred.

The number of impeller blades is another key parameter. Q.-Q. Li *et al.* (2022), using unsteady CFD modelling and analysis of pressure pulsations via the fast Fourier transform, found that increasing the number of blades from 24 to 48 leads to a significant reduction in the amplitude of the dominant pressure pulsation frequencies, which is beneficial in terms of vibration reliability. At the same time, the contact surface area increases and, consequently, so do friction losses. J. Nejadrajabali *et al.* (2016), using flow pattern analysis and comparative CFD modelling, recommend a range of 30-50 blades as the optimal compromise. J. Pei *et al.* (2019), in their study of the effect of the side channel wrap angle, arrived at a similar optimum – 36 blades for the geometry under investigation. The agreement between the recommendations of these two independent research groups regarding the optimal range of blade count provides significant confirmation of the reliability of the results obtained, although it should be noted that the specific optimal number of blades depends on the wheel dimensions, channel height and operating mode. Notably, Q.-Q. Li *et al.* (2022) approached this issue from the perspective of dynamic characteristics, whilst J. Nejadrajabali *et al.* (2016) and J. Pei *et al.* (2019) – from perspective of static efficiency, and all three groups converge on the same range. This is one of the most reliable quantitative results in this field, suitable for direct application in engineering practice.

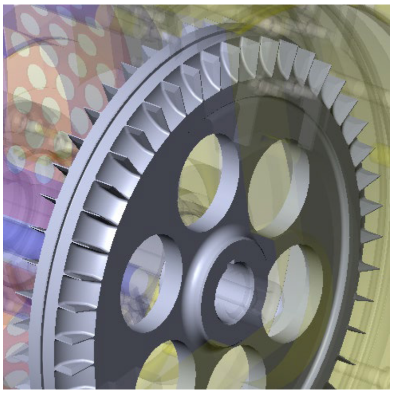

Figure 4. Straight peripheral-lateral blades
Source: compiled by the authors

The size of the impeller (outer diameter) determines the pressure increase within the machine via the tip speed of the blades. M.-W. Heo *et al.* (2016), using multi-objective optimisation that simultaneously accounts for aerodynamic and aeroacoustic criteria, demonstrated that increasing the diameter increases the pressure head but simultaneously increases the level of broadband noise due to the rise in circumferential velocity. In their study, the optimal diameter was determined as a compromise between these two criteria. F. Zhang *et al.* (2021), applying vortex identification methods to the results of CFD modelling, showed that reducing the impeller diameter whilst keeping other parameters constant leads to a decrease in the intensity of circulation vortices in the side channel, which reduces the efficiency of mass transfer between the impeller and the channel. Thus, the impeller size affects not only the kinematics but also the qualitative structure of the internal flow. When comparing studies by M.-W. Heo *et al.* (2016) and F. Zhang *et al.* (2021), it is worth noting that both studies reveal a mutually reinforcing effect: an increase in diameter simultaneously improves the hydraulic characteristics and worsens the acoustic characteristics; that is, diameter is a parameter with a clearly defined conflict of objectives. This makes it a natural candidate for multi-criteria optimisation rather than single-parameter tuning.

Methods for the systematic optimisation of impeller geometry are becoming increasingly widespread. H. Quan *et al.* (2020), applying an orthogonal design of experiments method to a regenerative pump, simultaneously varied the blade angle, the number of blades and the impeller diameter, and determined their relative importance: the number of blades is the most influential parameter (42% contribution), followed by the blade angle (35%) and the impeller diameter, which has the least influence (23%). The orthogonal approach can significantly reduce the number of CFD calculations required compared with a full factorial design, whilst maintaining the statistical validity of the conclusions. Building on this methodology, J. Yang *et al.* (2025) applied the orthogonal method to the numerical optimisation of a regenerative pump impeller design and found that the optimal combination of geometric parameters increases head by 7.3% and efficiency by 4.1% compared with the original design. When comparing the two studies, it is worth noting the methodological continuity and convergence of conclusions regarding the priority of parameters, which enhances confidence in the recommendations obtained. Notavly, the hierarchy of parameter influence established by H. Quan *et al.* (2020) – number of blades, angle, diameter – is consistent with the general conclusion regarding the dominant role of the number of blades, as derived from an analysis of the works by J. Nejadrajabali *et al.* (2016) and J. Pei *et al.* (2019). Such consistency in the results obtained using different methods and by different research groups suggests that this hierarchy has been reliably established. At the same time, it is worth noting that all the optimisation studies considered were conducted for specific geometries and operating conditions, and the question of whether the optimal values obtained can be extrapolated to other scales and conditions remains open.

Geometric Parameters of the Working Channel and Their Impact on Efficiency

The working fluid enters the impeller housing's working channel via the suction pipe and then flows into the inter-blade channels of the impeller. In the inter-blade channels, the mechanical energy of the drive is converted into the kinetic and potential energy of the gas. Centrifugal forces direct the gas particles predominantly in a radial direction from the inter-blade space into the working channel of the casing, where the kinetic energy of the flow is subsequently converted into pressure energy. The blade suction angle significantly influences the degree of symmetry of the secondary vortex motion in the channel: at angles close to 90°, the most uniform velocity distribution and the lowest losses in the recirculation zone are observed. This result is a substantial guideline for design; however, it is worth noting that there is a lack of studies in the literature that systematically vary the suction angle over a wide range for different types of channels, which limits the possibility of generalising this conclusion.

Mechanism of the spiral trajectory of the working body is a defining feature of the regenerative compressor, distinguishing it from all other classes of dynamic machines. W. Li (2025), in a CFD modelling of a regenerative pump taking into account the roughness of the channel walls, quantitatively assessed the influence of this mechanism: the repeated interaction of the blades with the same working fluid particles results in the regenerative compressor developing 3-5 times greater pressure than a centrifugal compressor of the same dimensions at the same rotational speed. This result is consistent with the classical theoretical estimates by W.A. Wilson *et al.* (1955); however, W. Li (2025) further demonstrated that the roughness of the channel walls can reduce this effect by 10-18%, depending on the Reynolds number and relative roughness. This is a substantial practical finding for manufacturers, as it highlights the significance of the quality of the channel surface finish. Despite practical significance of this parameter, the influence of roughness on the performance of regenerative machines remains under-researched in the literature – W. Li (2025) is, in fact, the only modern publication on this topic, indicating a significant scientific gap.

The parameters of the working channel – height, cross-sectional shape, length and curvature – directly influence the intensity of the working fluid circulation and the level of gas-dynamic losses. J.E. Adam *et al.* (2022), applying a systematic Design of Experiments (DoE) approach to a regenerative compressor and simultaneously varying the height, width and cross-sectional shape of the channel, established that the influence of channel geometry on performance is complex and non-linear: individual parameters exhibit significant interaction with one another, meaning that the optimal value of one parameter depends on the value of another. In particular, the authors found that the optimal channel height is a function of the number of blades: as the number of blades increases, the optimal channel height also increases. This interaction explains why attempts to optimise the channel geometry by varying just one parameter often yield conflicting results across different studies. This conclusion is substantial from a methodological point of view: it means that single-parameter studies of channel geometry, which constitute most publications in this field, are of limited value for practical design.

Working channel height is more substantial in determining mass flow rate than its cross-sectional area. J. Zhang *et al.* (2024), whilst conducting a quantitative analysis of energy losses in a regenerative compressor using the entropy production method, found that reducing the channel height whilst maintaining the cross-sectional area leads to an increase in local entropy dissipation in the secondary circulation zone, which is the primary mechanism of energy transfer. This is explained by the fact that a reduction in the duct height increases the velocity gradient in the vertical direction and, consequently, increases viscous losses. The authors quantitatively established that losses in the secondary circulation zone account for 35-45% of the compressor's total losses, confirming their dominant role. This result is substantial from a design perspective, as it indicates that optimisation efforts should primarily be directed towards minimising losses specifically in the secondary circulation zone. J. Wang *et al.* (2023) independently confirm this conclusion: in their comparative study, the lowest efficiency values are also observed for configurations with the minimum channel height. The consistency of the results obtained by J. Zhang *et al.* (2024) and J. Wang *et al.* (2023) – using different methods and for different machine configurations – suggests that the channel height is the most critical geometric parameter of the flow section among all those considered.

Cross-sectional shape of the working channel affects the compressor's performance through the distribution of velocities and the structure of secondary vortices. W. Li (2025) found that a circular cross-section provides more favourable flow conditions due to a more uniform velocity distribution and reduced local losses compared to a rectangular channel; the difference in efficiency between these two cross-sectional shapes, for the same channel height, is 2-4% at the design point. Q. Li *et al.* (2024), applying the Proper Orthogonal Decomposition (POD) method to the results of unsteady CFD simulations, demonstrated that the cross-sectional shape significantly influences the spatial structure of the dominant pressure pulsation modes: in channels with a circular cross-section, the dominant modes are more symmetrical and have a lower amplitude, which helps to reduce the vibration load. Comparing these results with the data from J.E. Adam *et al.* (2023), a general conclusion can be drawn: the cross-sectional shape is a substantial parameter, but its influence on static efficiency is less significant than that of the duct height, whilst it has a more significant impact on dynamic characteristics (pressure pulsations, noise). Thus, the choice of cross-sectional shape should be made addressing priorities of the specific application: if noise or vibration levels are critical, a circular cross-section is preferable; if manufacturability and production cost are the priority, a rectangular cross-section remains a reasonable choice.

The isentropic efficiency of a regenerative compressor exhibits a more complex dependence on the geometric parameters of the channel. J. Wang *et* *al.* (2023), comparing single- and multi-stage configurations of side-channel pumps at different channel heights, confirmed that the lowest efficiency values are observed for variants with the minimum side-channel height, whilst an increase in height leads to an increase in efficiency. Notably, in multi-stage configurations this effect is amplified, as losses in each stage accumulate. M. Badami & M. Mura (2012), based on a comparison of 1D and 3D CFD models of a regenerative blower for fuel cells, noted that three-dimensional modelling is relevant for accurate prediction of performance characteristics under non-design operating conditions. This highlights the fundamental limitations of one-dimensional models when analysing the influence of channel geometry – they may yield satisfactory results at the design point, but systematically fail at low and high flow rates, where three-dimensional effects are dominant. To summarise the findings of this section, a key pattern should be emphasised: of all the channel's geometric parameters, height has the greatest influence on static characteristics, whilst the cross-sectional shape determines the machine's dynamic behaviour. This hierarchy of parameter influence serves as a substantial guide for setting priorities when designing and optimising regenerative compressors; however, it must be acknowledged that most existing studies were conducted for a limited range of geometries and do not provide a complete picture of the interaction of all channel parameters simultaneously.

Design Features of the Separator and Their Impact on the Working Process

The separator (Fig. 5) is an essential structural component of the flow path in a centrifugal compressor; its function is to separate the discharge zone from the suction zone and to prevent the compressed gas from flowing in the opposite direction. However, a certain amount of gas inevitably penetrates the suction zone through the gaps between the rotor and the casing and through the inter-blade space, which is a source of volumetric losses. An analysis of existing research identified three interrelated areas of study concerning the separator: the influence of the wrap angle on hydraulic characteristics, the physics of "dead zone" formation, and the effect of the separator on transient force loads. These areas have developed to some extent in parallel and have only begun to be considered comprehensively in the latest studies. F. Zhang *et al.* (2020), using the entropy production method to quantitatively analyse energy losses in a side-channel pump at different channel wrap angles, found that the amount of leakage through the separator decreases as the radial clearance between the separator and the impeller decreases and as the separator wrap angle increases. However, the authors also demonstrated that increasing the separator angle simultaneously reduces the effective working section of the channel and leads to an 8-12% drop-in mass flow rate for every 15° increase in the angle. Thus, optimisation of separator angle is a problem with two mutually conflicting objectives.

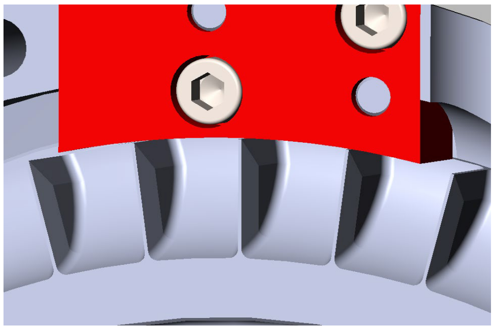

Figure 5. Separator (cutter)
Source: compiled by the authors

J. Pei *et al.* (2019), in a study of effect of the side channel coverage angle, modelled three geometric variants of the pump with separator angles of 15°, 30° and 45°, using unsteady three-dimensional CFD modelling with the results verified on a test bench. A comparative analysis showed that a 15° angle ensures the most intense mass transfer throughout the flow path: the authors quantitatively measured the intensity of secondary circulation by analysing the velocity vector field and found that at a 15° angle it is 18% higher than at a 45° angle. The 15° and 30° configurations demonstrate higher static pressure values in the outlet region – by 6-9% respectively – due to the greater length of the side channel and a longer duration of energy exchange. These results can be considered reliable and well-founded, as the authors conducted parallel measurements on a physical test rig, and the discrepancy between the CFD results and the experiment does not exceed 4%. A comparison of the approaches by F. Zhang *et al.* (2020) and J. Pei *et al.* (2019) reveals methodological complementarity: the former work quantitatively describes the mechanism of losses using the entropy method, whilst the latter quantitatively determines the optimum by comparing specific geometric variants. Together, they provide a sufficiently comprehensive picture to inform practical recommendations regarding the choice of the separator angle.

A. Fleder & M. Böhle (2012), based on the results of a systematic study of the internal flow structure in a side-channel pump using particle image velocimetry (PIV) and CFD, confirmed that minimum static pressure values are recorded in the separator zone for all geometric variants. The authors explained this phenomenon by the fact that, in the separator zone, the exchange of kinetic and potential energy between the blade channels and the annular channel is interrupted, with the result that energy which was not transferred in the preceding zone is irretrievably dissipated. A substantial contribution by A. Fleder & M. Böhle (2012) was that they were the first to quantitatively describe the minimum-pressure zone as a "dead zone" with zero net energy exchange – this is conceptually relevant for determination of why reducing the separator angle generally increases the machine's efficiency. Notably, study by A. Fleder & M. Böhle (2012) is one of the few studies in which the PIV method has been applied to the investigation of regenerative machines, which was used for verification of CFD results at the level of the velocity field, rather than merely integral characteristics. Expanding the use of such verification is a substantial methodological task for future research.

K.A. Adu-Poku *et al.* (2022), whilst investigating the internal flow mechanisms and transient force distribution in a side-channel pump using transient CFD with regenerative structure analysis, demonstrated that the design of the separator significantly influences the transient hydrodynamic forces acting on the impeller. In particular, the authors found that sharp pressure gradients arise in the separator region, which are the source of variable forces with a frequency that is a multiple of the number of blades and the rotational frequency. These forces can cause resonant phenomena if their frequency matches the natural frequencies of the structure. A. Javadi *et al.* (2026), using the Large Eddy Simulation (LES) method – which is a significantly more accurate but also much more resource-intensive approach compared to RANS – confirmed and elaborated on this result: the separator is a zone of heightened turbulent activity, where the kinetic energy of large eddies is actively transferred to smaller scales and dissipated as heat. According to estimates by A. Javadi *et al.* (2026), between 15 and 22% of the compressor's total losses are dissipated in the separator zone, depending on the operating mode. A comparison of the results of K.A. Adu-Poku *et al.* (2022) and A. Javadi *et al.* (2026) reveals complete qualitative agreement, whilst LES modelling provides a more detailed picture of the distribution of dissipation within the separator zone. A gap in the research remains: there are no studies dedicated to the targeted profiling of the separator edges as a means of reducing turbulent losses; although the physical nature of the losses in this zone has already been well described, the question of the optimal shape of the edges is scarcely addressed in the literature.

According to the authors, combination of the results of these studies provides a substantial design conclusion: the angle of the separator should be selected as the minimum permissible from a structural point of view (2-3 blade pitches), whilst the geometry of the separator's leading and trailing edges must be carefully profiled to reduce the intensity of separation phenomena and the associated losses. Reducing the wrap angle from 45° to 15° results in more intense flow exchange, higher static pressure values and lower hydraulic losses, which ultimately improves the machine's hydraulic performance. The findings of K.A. Adu-Poku *et al.* (2022) raise a substantial point: an excessive reduction in the separator angle without corresponding profiling of its edges may exacerbate transient force loads on the wheel due to the sharpening of pressure gradients at the boundary of the "dead zone". Consequently, the final choice of angle must be made addressing overall impact on all characteristics, including vibrational and acoustic ones.

Effect of Clearances in the Flow Path on Compressor Performance

Clearances in the flow path of a regenerative compressor are among the most sensitive design parameters, significantly affecting performance, compression efficiency and energy losses. Analysis of existing research has identified three main areas of focus: the quantitative determination of the proportion of losses due to clearances in the overall loss balance; the influence of clearances on the machine's dynamic characteristics; and the specific characteristics of clearances in hydrogen applications. It is noteworthy that all three areas have developed in parallel and are only now beginning to be considered in relation to one another. L. Zhou *et al.* (2024), using a combination of three-dimensional unsteady CFD modelling and experimental measurements on a test bench for a regenerative pump with five different axial clearance values in the range of 0.1-0.5 mm, demonstrated that the relationship between performance and clearance is non-linear: in the range of small clearances (0.1-0.2 mm), the increase in performance as the clearance decreases is significant (up to 15% for every 0.05 mm), whilst for large clearances (over 0.3 mm) this sensitivity decreases. The authors also found that a change in the axial clearance affects not only the volumetric efficiency but also the shape of the pressure characteristic: as the clearance increases, the steepness of the characteristic decreases, which may lead to unstable operation in a parallel configuration with other blowers.

J. Zhang *et al.* (2024), in a quantitative analysis of energy losses in a regenerative compressor using entropy method for various values of axial and radial clearances, found that losses due to clearances account for 28-40% of total hydrodynamic losses depending on the operating mode, and that this proportion increases with rising rotational speed. Notably, the authors were able to quantify the contributions of the axial and radial clearances: the axial clearance accounts for 70-75% of the total losses due to clearances, whilst the radial clearance contributes only 25-30%. This result provides a substantial practical guideline: during design and manufacture, the axial clearance must be controlled as the dominant factor. W.-Y. Zhang & Z.-H. Li (1991) established an analytical relationship between the magnitude of the axial clearance and the characteristics of a regenerative pump, which is generally consistent with modern CFD results, indicating the reliability of classical analytical approaches as a first approximation.

J. Wang *et al.* (2023), when comparing single-stage and multi-stage configurations of side-channel pumps, found that in multi-stage configurations the effect of clearances on head pulsations is significantly more pronounced than in single-stage ones: for the same clearance value, the amplitude of pulsations in a two-stage configuration is 40-60% higher than in a single-stage one. This is because, in a multi-stage configuration, flow through the clearances of the first stage disturbs the inlet field of the second stage, amplifying transient phenomena. Z.C. Zhu *et al.* (2001), in their early theoretical and experimental study of low-flow regenerative pumps, reached a similar conclusion regarding the significant influence of the gap on external characteristics, confirming that this pattern is not specific to a particular type of machine or operating mode, but is common to the class of regenerative machines. When comparing the results of J. Wang *et al.* (2023) and Z.C. Zhu *et al.* (2001), it is worth noting a substantial pattern: despite differences in methodology and a gap of more than twenty years between the publications, both studies confirm the general nature of the effect of clearances, which gives this conclusion the status of a well-established fact, suitable for direct use in design.

V.S. Sitalo & S.M. Vanieiev (2025) conducted a comprehensive analysis of the effect of the magnitude of the axial and radial clearances along the entire length of the flow path between the impeller and the compressor casing, which had an outer diameter of 250 mm, using three-dimensional CFD modelling in ANSYS CFX. The authors modelled two clearance options – 0.15 mm and 0.2 mm – and compared them with an idealised case with no clearances. The results are revealing: with a clearance of 0.15 mm, the compressor's performance decreases by 23% compared with the idealised case, and with a clearance of 0.2 mm, by 50% (Fig. 6). Such a sharp drop in performance with an increase in the clearance of just 0.05 mm is evidence of high sensitivity of regenerative machines to manufacturing precision. A comparison with the results of L. Zhou *et al.* (2024) shows qualitative agreement – both studies reveal a non-linear dependence with increased sensitivity at small clearances – which confirms the general nature of this pattern regardless of the type of working medium (liquid or gas). Notably, both studies – L. Zhou *et al.* (2024) and V.S. Sitalo & S.M. Vanyeyev (2025) – were conducted for specific geometries and do not cover the full range of impeller diameters, which limits the generalisability of the results. The development of generalised dimensionless relationships between the relative clearance and the relative reduction in performance is a promising area for further research.

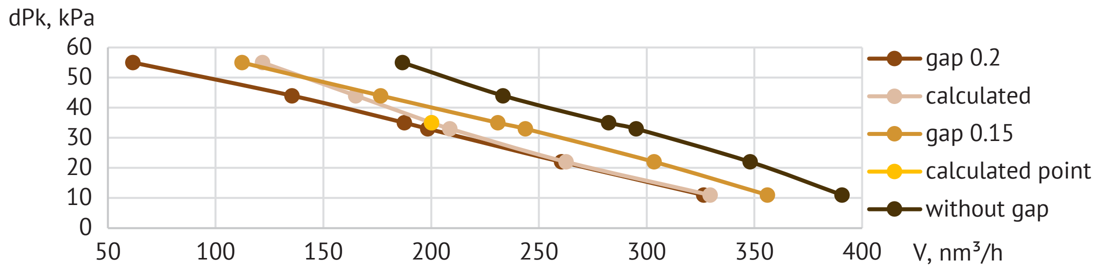

Figure 6. Compressor performance at different clearances in the flow path

Source: V.S. Sitalo & S.M. Vanyeyev (2025

Studies on regenerative machines for fuel cell systems emphasise issue of clearances. X. Yu *et al.* (2022), whilst conducting an experimental study into the effect of hydrogen recirculation on the performance of a PEMFC fuel cell, found that the accuracy with which the recirculation blower maintains the set hydrogen flow rate is critical for stable stack operation: a deviation in the recirculation flow rate of more than 8% from the calculated value leads to a significant reduction in fuel cell efficiency and an uneven distribution of membrane moisture. Since cross-flow through the gaps is the main source of flow instability, the results of X. Yu *et al.* (2022) indirectly confirm the need for strict control of the gaps in hydrogen pumps. Y. Chen *et al.* (2024), investigating the influence of the geometric parameters of a regenerative hydrogen pump in a PEMFC system using three-dimensional CFD with variations in the axial gap, quantitatively confirmed this conclusion: an increase in the axial clearance of 0.05 mm reduces the hydrogen recirculation coefficient by 11-15%, which is unacceptable for fuel cell systems with stringent stability requirements. Comparing the results of Y. Chen *et al.* (2024) with the data from V.S. Sitalo & S.M. Vanyeyev (2025) for an air compressor, it was found that hydrogen blowers are twice as sensitive to the gap size, which further justifies the need to establish separate, stricter tolerances for this class of machines.

X. Liang *et al.* (2024), whilst investigating the influence of design parameters on the efficiency of a regenerative blower for hydrogen recirculation in PEMFC fuel cells using transient CFD simulations verified on a test bench, found that the issue of clearances is particularly critical in hydrogen blowers: due to low dynamic viscosity of hydrogen (14 times lower than that of air), flow through gaps is proportionally greater for the same absolute gap values. Y. Chen *et al.* (2025) confirmed this finding, demonstrating that when switching from air to hydrogen, the efficiency of a regenerative compressor decreases by 8-12% with the same design clearances, and recommended reducing the permissible axial clearance for hydrogen blowers to 0.05-0.08 mm. The convergence of the findings by X. Liang *et al.* (2024) and Y. Chen *et al.* (2025), obtained independently and using different methods, lends these recommendations a high degree of credibility. It is appropriate to regard this result as substantial from a practical point of view: it means that design standards for clearances developed for air compressors cannot be automatically applied to hydrogen applications without revision. This is a fundamental caveat for design engineers in the field of hydrogen energy.

Thus, optimisation of clearances in the flow path is a complex task exceeding the scope of clearance reduction. It is necessary to address type of working medium, operating mode, design constraints on manufacturing accuracy, thermal deformation due to heating, as well as the risk of jamming at small clearances. To summarise the findings of this section, it is worth noting that clearances are the only parameter among those considered where the effect on the machine's performance is both the most significant and the least controllable in practice – due to the influence of wear, thermal deformations and manufacturing tolerances. Incorporation of clearances is an essential step in the creation of CFD models: calculations without clearances consistently yield overly optimistic results and cannot be used to quantitatively predict the performance of a real machine.

CFD Studies of Regenerative Flow Machines

Research into the operation of regenerative compressors began with a theoretical analysis of their gas dynamics. W.A. Wilson *et al.* (1955) proposed a theoretical model of the fluid-dynamic mechanism of regenerative pumps based on a pulsation approach, which became the first mathematically rigorous attempt to describe the circulation of the working fluid between the blades and the channel. Despite its age, this work is still cited in contemporary literature as a conceptual foundation, which attests to its fundamental significance. T. Meakhail *et al.* (2003), continuing this line of research, conducted a systematic study of the circulation flow in a regenerative pump using the PIV method and steady-state CFD modelling. The authors were the first to quantitatively describe the three-dimensional structure of the circulation and established that the actual trajectory of fluid particles is more complex than predicted by the simple spiral model proposed by W.A. Wilson *et al.* (1955): within a single blade pitch, the fluid undergoes not one but 1.5-2 complete circulations, which explains the more efficient energy transfer compared with theoretical estimates. In parallel, one-dimensional models based on the theory of angular momentum were developed – M. Badami & M. Mura (2011) demonstrated that such models are capable of reproducing the general shape of the pressure-flow characteristic with acceptable accuracy (an error of up to 10% at the design point), but systematically deviate in non-design operating conditions. The fundamental limitation of one-dimensional approaches is determined by the fact that they are unable to reproduce the three-dimensional structure of secondary circulation and, consequently, cannot quantitatively assess the influence of the channel's geometric parameters on local losses. Thus, the evolution of computational methods from the impulse theory of W.A. Wilson *et al.* (1955) through 1D models to three-dimensional CFD represents a sequential increase in the level of physical detail, whereby each new approach does not supersede previous one, but rather defines the limits of its applicability.

F.J. Quail *et al.* (2010; 2011) were among the first to systematically apply CFD to regenerative pumps. In their 2010 paper, the authors used three-dimensional CFD to analyse the flow structure and verified the results by comparing them with PIV measurements of the circulation. They found that CFD modelling qualitatively reproduces the main regenerative structures, but quantitative agreement depends on the choice of turbulence model. In their paper, F.J. Quail *et al.* (2011) developed a one-dimensional analytical model of torque exchange and compared it with three-dimensional CFD: the one-dimensional model showed satisfactory accuracy at the calculation point (a deviation of 5-8%) but was significantly inaccurate at low flow rates. M. Insinna *et al.* (2018) expanded on this comparison, demonstrating that for engineering design at the conceptual stage, the one-dimensional model is appropriate due to its speed, whilst at the detailed design stage, three-dimensional CFD is relevant. It is worth agreeing with this conclusion: a rational design strategy lies in the sequential application of both approaches – 1D for rapid parametric analysis and 3D CFD for final verification and optimisation. Notably, conclusion regarding the appropriateness of a two-stage approach has been confirmed by three independent research groups – F.J. Quail *et al.* (2011), M. Badami & M. Mura (2012), and M. Insinna *et al.* (2018) – which lends it the status of a sufficiently reliable methodological recommendation.

M. Badami & M. Mura (2012) conducted an in-depth comparison of 1D and 3D approaches for a regenerative blower for fuel cells. The methodology involved developing a proprietary 1D model, comparing it with three-dimensional CFD simulations, and verifying both approaches on a test bench. The authors emphasised that 3D CFD is essential for accurately predicting performance at low flow rates, where separation phenomena and reverse flows determine the behaviour of the machine. D. Griffini *et al.* (2015), using CFD to develop the design of a regenerative flow compressor, made a substantial observation: the Mach numbers in various elements of the compressor are around 0.5, and neglecting the compressibility effect leads to a systematic error of up to 7% in predicting the pressure rise. This is a fundamental caveat for researchers using incompressible CFD solvers to model regenerative compressors, a common practice due to its simplicity. Notably, despite the obviousness of this caveat, a significant proportion of publications appearing since the work by D. Griffini *et al.* (2015) continue to apply incompressible models without proper justification – this is a systemic methodological problem within the field that requires the attention of peer reviewers and journal editors.

C.-M. Jang & H.-J. Jeon (2014), whilst investigating the effect of blade pitch angle and tip thickness using steady-state CFD with bench testing, examined three different angles (14°, 18° and 22°) and found that an angle of 18° provides the best compromise between pressure increase and efficiency. Regarding tip thickness: 1 mm provides a better pressure increase than 2 mm and 3 mm. C. Lee & H.G. Kil (2014), whilst investigating a regenerative blower for a fuel cell system using CFD, found that when designing such machines, it is necessary to align the blower's aerodynamic characteristics with the dynamics of the fuel cell: the blower must provide the required flow rate across a wide range of back-pressure values, which is a more stringent requirement than in conventional industrial applications. The authors demonstrated that standard geometric recommendations for industrial blowers are not always optimal for fuel cell applications, and recommended separate CFD optimisation for each type of application. M. Sreekanth *et al.* (2021), in their comprehensive review, systematised the results of CFD studies and emphasised that the existing CFD data set for regenerative machines is heterogeneous: different research groups use different turbulence models, meshes and boundary conditions, which complicates a direct comparison of results.

One substantial area of application for regenerative blowers is life support systems. M.G. Izenson *et al.* (2011) developed and investigated a regenerative blower for ventilating an EVA (extravehicular activity) spacesuit, where a regenerative machine is the only technically viable option due to the combination of requirements for low mass, compactness and the ability to operate in microgravity conditions. The methodology included analytical design, CFD verification and testing of the prototype under conditions simulating extravehicular activity. It was established that the developed blower provides the required flow rates of CO_2 and O_2 across the range of mission conditions, whilst weighing less than 0.5 kg. M.G. Izenson *et al.* (2012) continued this research and conducted endurance and parametric tests on the EVA blower, establishing that the unit maintains satisfactory performance after 500 hours of operation without maintenance. Comparing the two studies, it is noted that they cover the full cycle from design to endurance validation – this is an example of a methodologically comprehensive study that provides a reliable basis for the implementation of regenerative blowers in mission-critical systems. Together with the findings of C. Lee & H.G. Kil (2014) and M. Badami & M. Mura (2012), these studies convincingly demonstrate that regenerative compressors are a competitive solution not only for industrial applications but also for systems with heightened requirements for reliability and compactness. At the same time, it must be acknowledged that research into the resource characteristics of regenerative machines is limited in the literature – studies by M.G. Izenson *et al.* (2011; 2012) remain only publications presenting a full cycle of reliability validation, which constitutes a significant gap for applications with heightened reliability requirements.

A. Javadi *et al.* (2026) improved the accuracy of CFD modelling by applying the Large Eddy Simulation (LES) method to a side-channel pump under several operating conditions. Compared with traditional RANS models (SST k-ω), LES modelling yielded significantly more accurate results in non-design operating conditions: the deviation from the experimental data for head did not exceed 2% (compared with 8-12% for RANS). The authors demonstrated that RANS models systematically underestimate the level of turbulent kinetic energy in flow separation zones (the separator zone and the outlet of the blade channel), which is the cause of their systematic errors. At the same time, the authors note that LES modelling requires 50-100 times more computational resources than RANS, which limits its practical application in engineering calculations. Q. Li *et al.* (2024), applying the POD method to the results of unsteady CFD simulations of a regenerative pump, found that the first three eigenmodes account for over 85% of pressure pulsation energy. This information is beneficial for design of active pulsation damping systems and for fault diagnosis. K.A. Adu-Poku *et al.* (2022), applying vortex identification methods (Q-criterion, λ2-criterion) to the results of unsteady CFD simulations, found that the structure of vortex formations in a side-channel pump depends significantly on the blade shape and directly determines the nature of the unsteady forces. T.-G. Lim *et al.* (2015) combined CFD modelling with aeroacoustic noise analysis and established a link between the vortex structures arising in the separator region and the dominant frequencies of the blower's acoustic noise. This study is one of the few to establish a quantitative correlation between CFD results and acoustic characteristics, which is relevant for applications with stringent noise requirements. M. Kumar *et al.* (2022), in a coupled fluid-structure interaction (FSI) analysis of a regenerative compressor and pump, demonstrated that the regions of maximum mechanical stresses in the impeller correlate with the regions of elevated hydrodynamic pressure identified by CFD modelling. This highlights the need to address FSI effects when designing compressors for applications with stringent service life requirements.

A general analysis of the evolution of CFD research into regenerative compressors formed several relevant conclusions. Firstly, CFD methods have progressed from qualitative visualisation of the flow to quantitative prediction of performance characteristics with an accuracy approaching that of physical experiments. Secondly, the choice of turbulence model is critical: RANS models are acceptable for steady-state conditions, but LES or hybrid RANS-LES approaches are necessary for unsteady conditions and the accurate analysis of transient phenomena. Thirdly, accounting for compressibility is essential even for subsonic flows at Mach numbers above 0.3. Fourthly, lack of standardised CFD verification protocols for regenerative machines significantly limits the ability to accumulate generalised knowledge in the field – since results obtained under different boundary conditions, meshes and turbulence models are fundamentally incomparable. According to the authors, further progress in CFD research into regenerative compressors lies in the application of machine learning methods to accelerate parametric optimisation and in the development of hybrid models that combine the accuracy of LES with acceptable computational costs.

Conclusions

An analysis of scientific research in the field of regenerative compressors and pumps systematised key factors determining their efficiency and formed following conclusions. The geometry of the impeller is a determining factor in energy transfer. The optimum number of blades lies within the range of 30-50: fewer blades reduce circulation intensity, whilst more blades increase friction losses. Complex blade profiles (airfoil, S-shaped) provide a 3-8% increase in isentropic efficiency compared with straight blades, but complicate the manufacturing process. For most industrial applications, the straight blade remains a sound choice in terms of manufacturability and production cost. Orthogonal optimisation methods confirm that the number of blades is the most influential parameter among the impeller's geometric characteristics.

Geometry of the working channel determines the intensity of secondary circulation and the level of irreversible losses. The height of the channel is a more significant parameter than its cross-sectional area: reducing the height whilst maintaining the area increases local entropy dissipation in the secondary circulation zone, which accounts for 35-45% of total losses. The optimum channel height depends on the number of blades, confirming the non-linear nature of the interaction between geometric parameters. The separator angle has a dual effect on performance: reducing the angle from 45° to 15° increases the mass transfer rate by 18% and the static outlet pressure by 6-9%, but at the same time reduces the effective working length of the channel. The separator zone accounts for 15-22% of the compressor's total losses, and incorrect profiling of this zone leads to resonant vibration phenomena.

The clearances in the flow path proved to be the most critical design parameter: increasing the axial clearance from 0.15 mm to 0.2 mm reduces performance by up to 50%. The axial clearance dominates the radial clearance, accounting for 70-75% of losses due to bypass flow. In hydrogen blowers for fuel cells, this sensitivity is twice as high as in air-driven machines, requiring the establishment of separate, tighter tolerances. CFD methods have evolved from qualitative visualisation to quantitative prediction of performance characteristics with an error of less than 2% when using the LES approach. RANS models are acceptable in design operating conditions but systematically produce errors in non-design regions. Compressibility must be addressed for Mach numbers above 0.3. The optimal design strategy involves a sequential combination of 1D analysis at the concept stage and 3D CFD at the detailed design stage. Further research should address development and verification of proprietary CFD models of a regenerative compressor, covering clearances and the actual properties of the gas; the parametric optimisation of the flow path geometry using machine learning methods; and experimental investigation of the effect of clearances on compressor performance when operating with different working fluids, in particular hydrogen.

Acknowledgements

None.

Funding

None.

Conflict of Interest

None.

References

[1] Adam, J.E., Heinrich, M., & Schwarze, R. (2022). Influence of different design parameters on side channel compressor performance *Engineering Research*, 86, 819-827. doi: 10.1007/s10010-022-00594-y.

[2] Adam, J.E., Heinrich, M., & Schwarze, R. (2023). Design of experiment on the influence of channel design onto regenerative compressor In *Proceedings of 15th European conference on turbomachinery fluid dynamics & thermodynamics*. Budapest: European Turbomachinery Society. doi: 10.29008/ETC2023-139.

[3] Adu-Poku, K.A., Zhang, F., Appiah, D., Chen, K., Osman, F.K., & Acheaw, E. (2022). Study on the inner flow mechanisms and unsteady force distribution of side channel pump. *Proceedings of the Institution of Mechanical Engineers, Part A: Journal of Power and Energy*, 236(6), 1109-1128. doi: 10.1177/09576509221081618.

[4] Badami, M., & Mura, M. (2011). Setup and validation of a regenerative compressor model applied to different devices. *Energy Conversion and Management*, 52(5), 2157-2164. doi: 10.1016/J.ENCONMAN.2010.10.044.

[5] Badami, M., & Mura, M. (2012). Comparison between 3D and 1D simulations of a regenerative blower for fuel cell applications. *Energy Conversion and Management*, 55, 93-100. doi: 10.1016/J.ENCONMAN.2011.10.003.

[6] Chen, K., Zhang, F., Appiah, D., Yuan, S., Hong, F., Zhu, L., & Song, M. (2022). Effect of blade tip cutting angle on energy conversion mechanism of side channel pumps. *Physics of Fluids*, 34(2), article number 025107. doi: 10.1063/5.0082671.

[7] Chen, Y., Ling, Y., Liu, A., Wang, L., Feng, J., & Peng, X. (2024). Effects of geometrical parameters on the performance of hydrogen regenerative pumps in proton exchange membrane fuel cell systems. *International Journal of Hydrogen Energy*, 77, 732-741. doi: 10.1016/J.IJHYDENE.2024.06.191.

[8] Chen, Y., Lv, H., Li, R., Liu, X., Wang, L., Feng, J., Peng, X., & Cao, F. (2025). Effects of operating parameters and fluids on the performance of a hydrogen regenerative flow compressor in a proton exchange membrane fuel cell system. *Applied Thermal Engineering*, 271, article number 126326. doi: 10.1016/j.applthermaleng.2025.126326.

[9] Fleder, A., & Böhle, M. (2012). A study of the internal flow structure in a side channel pump. In *Proceedings of the 14th international symposium on transport phenomena and dynamics of rotating machinery*. ISROMAC: Honolulu.

[10] Grabow, G. (1975). Influence of the number of vanes and vane angle on the suction behaviour of regenerative pumps. *Conference on Fluid Machinery*, 1, 351-364.

[11] Griffini, D., Salvadori, S., Carnevale, M., Cappelletti, A., Ottanelli, L., & Martelli, F. (2015). On the development of an efficient regenerative compressor. *Energy Procedia*, 82, 252-257. doi: 10.1016/j.egypro.2015.12.030.

[12] Heo, M.-W., Seo, T.-W., Shim, H.-S., & Kim, K.-Y. (2016). Optimization of a regenerative blower to enhance aerodynamic and aeroacoustic performance. *Journal of Mechanical Science and Technology*, 30(3), 1197-1208. doi: 10.1007/s12206-016-0223-5.

[13] Insinna, M., Salvadori, S., Martelli, F., Peroni, G., Simon, G., Dipace, A., & Squarcini, R. (2018). One-dimensional prediction and three-dimensional CFD simulation of the fluid dynamics of regenerative pumps. In *Proceedings of the ASME turbo expo 2018: Turbomachinery technical conference and exposition. Volume 2C: Turbomachinery*. Oslo: ASME. doi: 10.1115/GT2018-76416.

[14] Izenson, M.G., Chen, W., Hill, R.W., Phillips, S.D., & Paul, H.L. (2011). Design and development of a regenerative blower for EVA suit ventilation. In *41st international conference on environmental systems*. Portland: American Institute of Aeronautics and Astronautics.

[15] Izenson, M.G., Chen, W., McCormick, J., Paul, H.L., & Jennings, M.A. (2012). Performance and life tests of a regenerative blower for EVA suit ventilation. In *42nd international conference on environmental systems*. San Diego: American Institute of Aeronautics and Astronautics. doi: 10.2514/6.2012-3460.

[16] Jang, C.-M., & Jeon, H.-J. (2014). Performance enhancement of 20kW regenerative blower using design parameters. *International Journal of Fluid Machinery and Systems*, 7(3), 86-93. doi: 10.5293/IJFMS.2014.7.3.086.

[17] Javadi, A., Kumar, V., & Aidun, C.K. (2026). Large eddy simulations of side channel pump in different operating conditions. *Engineering Applications of Computational Fluid Mechanics*, 20(1), article number 2587723. doi: 10.1080/19942060.2025.2587723.

[18] Jeon, S.-Y., Yoon, J.-Y., & Jang, C.-M. (2019). Optimal design of a novel 'S-shape' impeller blade for a microbubble pump. *Energies*, 12(9), article number 1793. doi: 10.3390/en12091793.

[19] Karlsen-Davies, N.D., & Aggidis, G.A. (2016). Regenerative liquid ring pumps review and advances on design and performance. *Applied Energy*, 164, 815-825. doi: 10.1016/j.apenergy.2015.12.041.

[20] Kumar, M., Venkateshwaran, A., Kumar, M.S.S.P., Sreekanth, M., Jebaseelan, D., & Sivakumar, R. (2022). Strength analysis of a regenerative flow compressor and a pump based on fluid-structure coupling. *Materials Today: Proceedings*, 51(3), 1619-1624. doi: 10.1016/J.MATPR.2021.10.477.

[21] Lee, C., & Kil, H.G. (2014). The design, performance and CFD analyses of regenerative blower used for fuel cell system. In *SIMULTECH 2014 – proceedings of the 4th international conference on simulation and modeling methodologies, technologies and applications* (pp. 751-755). Setúbal: SciTePress.

[22] Li, Q., Tang, D., Lou, X., Zhao, G., Wu, P., Bie, F., & Lu, Y. (2024). Investigation of the unsteady pressure fluctuation mechanism in a regenerative flow pump based on proper orthogonal decomposition. *Physics of Fluids*, 36(2), article number 025111. doi: 10.1063/5.0190481.

[23] Li, Q.-Q., Zhu, D.-S., Luo, M.-H., Chang, A.-L., Wu, P., & Guo, C.-L. (2022). Investigation on the pressure fluctuation characteristics for a regenerative flow pump under different blade arrangements. *Journal of Fluids Engineering, Transactions of the ASME*, 144(10), article number 101208. doi: 10.1115/1.4054536.
[24] Li, W. (2025). Performance of vortex pump in CFD simulations with rough walls. *International Journal of Fluid Engineering*, 2, article number 013902. doi: 10.1063/5.0237732.
[25] Liang, X., Kang, H., Zeng, R., Pang, Y., Yang, Y., Qiu, Y., Tao, Y., & Shen, J. (2024). Impact of the structural parameters on the performance of a regenerative-type hydrogen recirculation blower for vehicular proton exchange membrane fuel cells. *Sustainability*, 16, article number 1856. doi: 10.3390/su16051856.
[26] Lim, T.-G., Lee, S.-M., Jeon, W.-H., & Jang, C.-M. (2015). Characteristics of unsteady flow field and aeroacoustic noise in a regenerative blower. *Journal of Mechanical Science and Technology*, 29, 2005-2012. doi: 10.1007/s12206-015-0421-6.
[27] Meakhail, T., Seung, O.P., Lee, D.A., & Mikhail, S. (2003). A study of circulating flow in regenerative pump. In *Proceedings of the KSAS 1st international session* (pp. 19-26). Seoul: KSAS.
[28] Münsterjohann, S., Zenger, F., & Becker, S. (2017). Efficient and noise reduced design of a side channel blower considering psychoacoustic evaluation criteria. *Applied Mechanics and Materials*, 856, 174-180. doi: 10.4028/www.scientific.net/AMM.856.174.
[29] Nejadali, J. (2021). Shape optimization of regenerative flow compressor with aero-foil type blades using response surface methodology coupled with CFD. *Structural and Multidisciplinary Optimization*, 64, 2653-2667. doi: 10.1007/s00158-021-03020-z.
[30] Nejadrajabali, J., Riasi, A., & Nourbakhsh, S.A. (2016). Flow pattern analysis and performance improvement of regenerative flow pump using blade geometry modification. *International Journal of Rotating Machinery*, 2016(1), article number 8628467. doi: 10.1155/2016/8628467.
[31] Pei, J., Zhang, F., Appiah, D., Hu, B., Yuan, S., Chen, K., & Asomani, S.N. (2019). Performance prediction based on effects of wrapping angle of a side channel pump. *Energies*, 12(1), article number 139. doi: 10.3390/en12010139.
[32] Quail, F.J., Scanlon, T., & Strickland, M. (2010). Development of a regenerative pump impeller using rapid manufacturing techniques. *Rapid Prototyping Journal*, 16(5), 337-344. doi: 10.1108/13552541011065731.
[33] Quail, F.J., Stickland, M., & Baumgartner, A. (2011). A one-dimensional numerical model for the momentum exchange in regenerative pumps. *Journal of Engineering for Gas Turbines and Power*, 133(9), article number 093001. doi: 10.1115/1.4002890.
[34] Quan, H., Guo, Y., Li, R., Su, Q., & Chai, Y. (2020). Optimization design and experimental study of vortex pump based on orthogonal test. *Science Progress*, 103(1). doi: 10.1177/0036850419881883
[35] Raheel, M., Engeda, A., Hamrin, D., & Rouse, G. (2003). The performance characteristics of single-stage and multistage regenerative flow compressors for natural gas compression application. *Proceedings of the Institution of Mechanical Engineers, Part C: Journal of Mechanical Engineering Science*, 217(11), 1221-1239. doi: 10.1243/095440603771665250.
[36] Raheel, M.M., & Engeda, A. (2005). Systematic design approach for radial blade regenerative turbomachines. *Journal of Propulsion and Power*, 21(5), 884-892. doi: 10.2514/1.1426.
[37] Salimi, A., Hooshdar Rostami, H., Riasi, A., & Nejadali, J. (2023). Multi-objective optimization of a regenerative pump with S-shaped impeller using response surface methodology. *International Communications in Heat and Mass Transfer*, 143, article number 106734. doi: 10.1016/j.icheatmasstransfer.2023.106734.
[38] Sitalo V.S., & Vanyeyev, S.M. (2025). Investigation of the influence of flow passage clearances of a regenerative compressor on its performance using the ANSYS CFX software package. In *Modern technologies in industrial production: Proceedings of the 12th all-Ukrainian scientific and technical conference* (pp. 163-164). Sumy: Sumy State University.
[39] Sreekanth, M., Sivakumar, R., Sai Santosh Pavan Kumar, M., Karunamurthy, K., Shyam Kumar, M.B., & Harish, R. (2021). Regenerative flow pumps, blowers and compressors – a review. *Proceedings of the Institution of Mechanical Engineers, Part A: Journal of Power and Energy*, 235(8), 1992-2013. doi: 10.1177/09576509211018118.
[40] Vanyeyev, S.M., Meleychuk, S.S., & Olada, Y.M. (2010). *Research on regenerative compressors*. Sumy: Sumy State University.
[41] Wang, J., Zhang, F., Zhang, J., Chen, K., & Hong, Q. (2023). Internal flow characteristics of single-stage and multi-stage side channel pumps. *Paiguan Jixie Gongcheng Xuebao/Journal of Drainage and Irrigation Machinery Engineering*, 41(2), 132-138. doi: 10.3969/j.issn.1674-8530.21.0190.
[42] Wilson, W.A., Santalo, M.A., & Oelrich, J.A. (1955). A theory of the fluid-dynamic mechanism of regenerative pumps. *Journal of Fluids Engineering*, 77(8), 1303-1311. doi: 10.1115/1.4014671.

[43] Yang, J., Li, X., Cheng, D., Ji, J., Zhao, M., Guo, W., & He, L. (2025). Numerical simulation for impeller structure optimization for vortex pump based on orthogonal design method. *Applied Sciences*, 15, article number 2265. doi: 10.3390/app15052265.

[44] Yu, X., Fan, J., Zhou, Y., Hao, D., Chen, J., Yu, T., & Zhang, C. (2022). Experimental investigation of the effect of hydrogen recirculation on the performance of a proton exchange membrane fuel cell. *International Journal of Hydrogen Energy*, 47(2), 1183-1191. doi: 10.1016/j.ijhydene.2021.10.063.

[45] Zhang, F., Appiah, D., Chen, K., Yuan, S., Adu-Poku, K.A., & Zhu, L. (2021). Investigation on the flow behavior of side channel pumps based on vortex identification. *Chinese Journal of Mechanical Engineering*, 34(1), article number 120. doi: 10.1186/s10033-021-00649-1.

[46] Zhang, F., Appiah, D., Hong, F., Zhang, J., Yuan, S., Adu-Poku, K.A., & Wei, X. (2020). Energy loss evaluation in a side channel pump under different wrapping angles using entropy production method. *International Communications in Heat and Mass Transfer*, 113, article number 104526. doi: 10.1016/j.icheatmasstransfer.2020.104526.

[47] Zhang, J., Li, S., Wu, P., Ye, H., Qi, Z., & Wu, D. (2024). Quantitative analysis of energy loss and performance prediction of regenerative compressor. *Applied Thermal Engineering*, 246, article number 122930. doi: 10.1016/j.applthermaleng.2024.122930.

[48] Zhang, W.-Y., & Li, Z.-H. (1991). The axial clearance of vortex pump. *Pump Technology*, 1, 15-17.

[49] Zhou, L., Zhou, C., Bai, L., & Agarwal, R. (2024). Numerical and experimental analysis of vortex pump with various axial clearances. *Water*, 16(11), article number 1602. doi: 10.3390/W16111602.

[50] Zhu, Z.C., Wang, L.Q., Huang, D.H., & Jin, Q.M. (2001). Theoretical design and experimental study of small-flow high-head vortex pumps. *Journal of Engineering Thermophysics*, 22(4), article number 450.

Вихрові компресорні машини: огляд конструктивних параметрів та чинників, що визначають їх ефективність (огляд літератури)

Володимир Сітало

Аспірант
Сумський державний університет
40007, вул. Харківська, 116, м. Суми, Україна
https://orcid.org/0009-0005-0610-3320

Сергій Ванєєв

Кандидат технічних наук, доцент
Сумський державний університет
40007, вул. Харківська, 116, м. Суми, Україна
https://orcid.org/0000-0002-8205-0209

Станіслав Мелейчук

Кандидат технічних наук, доцент
Сумський державний університет
40007, вул. Харківська, 116, м. Суми, Україна
https://orcid.org/0000-0002-7507-6865

Олег Чех

Аспірант
Сумський державний університет
40007, вул. Харківська, 116, м. Суми, Україна
https://orcid.org/0000-0003-2500-481X

Данило Ніколаєнко

Аспірант
Сумський державний університет
40007, вул. Харківська, 116, м. Суми, Україна
https://orcid.org/0009-0009-6827-7691

Анотація. Зростання вимог до енергоефективності промислового обладнання та необхідність зниження експлуатаційних витрат актуалізують дослідження вихрових компресорів – класу турбомашин, що поєднують переваги динамічних та об'ємних машин і мають значний потенціал для широкого промислового застосування. Метою роботи були систематизація та аналіз сучасних наукових досліджень у галузі вихрових компресорів і насосів з метою визначення ключових чинників, що впливають на їх ефективність. Дослідження базувалося на аналізі та порівнянні результатів експериментальних і чисельних робіт, опублікованих у реферованих наукових виданнях, а також на застосуванні методів обчислювальної гідродинаміки (CFD) як сучасного цифрового інструменту інженерного аналізу. Встановлено, що ефективність вихрових компресорів визначається комплексом геометричних та конструктивних параметрів. Тип і форма робочого колеса, кількість і профіль лопаток впливають на ступінь підвищення тиску: оптимальна кількість лопаток перебуває в діапазоні 30-50, а лопатки складної форми, попри вищу ефективність, ускладнюють виготовлення. Розміри та конфігурація робочого каналу визначають інтенсивність циркуляції та рівень газодинамічних втрат – висота каналу є більш визначальним параметром, ніж площа його поперечного перерізу. Критичними є зазори в проточній частині: збільшення торцевого та радіального зазору з 0,15 мм до 0,2 мм призводить до зниження продуктивності до 50 %, що підтверджує необхідність їх обов'язкового врахування на етапі проектування. Застосування CFD-методів дозволяє візуалізувати складну спіралеподібну структуру потоку, виявляти джерела втрат та оптимізувати конструктивні рішення, скорочуючи витрати на фізичне прототипування. Поєднання аналітичних, експериментальних і CFD-методів створює основу для формування ефективних підходів до проектування, що забезпечить підвищення енергетичної ефективності та розширення галузей застосування цих машин у промислових системах

Ключові слова: вихровий компресор; вихровий насос; регенеративна гіпотеза; чисельне моделювання; Ansys SFX; оптимізація конструкції

Вісник Криворізького національного університету

Том 24, № 1
2026

Заснований у 2003 р.
Виходить два рази на рік.

Відповідальний редактор:
С. Тіхлівець

Підписано до друку з оригінал-макета 30.06.2026
Ум. друк. арк. 16,1
Наклад 100 прим.

Контактна адреса:
Криворізький національний університет
50027, вул. Віталія Матусевича, 11, м. Кривий Ріг, Україна
Тел.: +38 (056) 409-06-06
E-mail: info@journal-knu.com.ua
https://journal-knu.com.ua/uk

Journal of Kryvyi Rih National University

Volume 24, No. 1
2026

Founded in 2003.
Published 2 times per year.

Managing Editor:
S. Tikhlivets

Signed to the print with the original layout 30.06.2026
Conventional Printed Sheet 16.1
Circulation 100 copies

Address for contacts:
Kryvyi Rih National University
50027, 11 Vitalii Matusevych Str., Krivyi Rih, Ukraine
Tel.: +38 (056) 409-06-06
E-mail: info@journal-knu.com.ua
https://journal-knu.com.ua/en